

Luigi Coppola

Hydrogeological Instability in Cohesive Soils

Techniques for Prediction, Prevention
and Control

 Springer

Hydrogeological Instability in Cohesive Soils

Luigi Coppola

Hydrogeological Instability in Cohesive Soils

Techniques for Prediction, Prevention
and Control

Linguistic Review by Dante Valerio Tedesco

 Springer

Luigi Coppola
University of Basilicata
Potenza
Italy

ISBN 978-3-319-74330-1 ISBN 978-3-319-74331-8 (eBook)
<https://doi.org/10.1007/978-3-319-74331-8>

Library of Congress Control Number: 2017963998

© Springer International Publishing AG, part of Springer Nature 2018

This work is subject to copyright. All rights are reserved by the Publisher, whether the whole or part of the material is concerned, specifically the rights of translation, reprinting, reuse of illustrations, recitation, broadcasting, reproduction on microfilms or in any other physical way, and transmission or information storage and retrieval, electronic adaptation, computer software, or by similar or dissimilar methodology now known or hereafter developed.

The use of general descriptive names, registered names, trademarks, service marks, etc. in this publication does not imply, even in the absence of a specific statement, that such names are exempt from the relevant protective laws and regulations and therefore free for general use.

The publisher, the authors and the editors are safe to assume that the advice and information in this book are believed to be true and accurate at the date of publication. Neither the publisher nor the authors or the editors give a warranty, express or implied, with respect to the material contained herein or for any errors or omissions that may have been made. The publisher remains neutral with regard to jurisdictional claims in published maps and institutional affiliations.

Printed on acid-free paper

This Springer imprint is published by the registered company Springer International Publishing AG part of Springer Nature

The registered company address is: Gewerbestrasse 11, 6330 Cham, Switzerland

*To my students and to all those ones who
want to continue along this route*

Preface

The *natural environment* is a perfect body, ruled by chemical–physical laws highly appropriate to the overall functionality of planet Earth. In such an environment, hydrogeological instability has its own function which is not always perceived as necessary and inescapable within the evolutive cycle of nature by anthropic communities. It is realised about the existence of landslides only during the mournful hydrogeological disasters so frequent along the orogenic ranges subjected to occasional and/or persistent rainfalls. Can we, as a consequence, attribute to hydrogeological disasters the simple function of accidentality or fortuity? The processes or events which actually give life to *inorganic matter* are not casual neither even less accidental. It is particularly ingenuous thinking that a natural phenomenon like landslides, so much complex and at the same time so much repetitive, can exist due to simple fortuity. There is no place in nature for the indetermination of functions, even if it derives from biological or geological bodies, otherwise the *Environment* could degenerate in *Chaos*.

Hydrogeological disasters are actually considered as such only when the relationship between anthropic activity and local environment is considered, which seems to be the only factor making landslides a natural calamity. If such perspective, in facts, is addressed to the vulnerability, often very high, of human settling systems to which the intensive exploitation of forested areas is added, the environmental imbalance assumes such a relevance to change in deep the arrangement of torrential waterways, furthermore very dynamic, which represent a further cause of the erosional process of orogenic ranges.

Starting from this assumption, is it possible to *predict* and *prevent* the triggering of a landslide in cohesive soils?

The approach to the study and analysis of a rotational landslide is currently confined within the limited scope of a numeric model; this limits the adequate comprehension of the real mechanisms which rule strains at failure. In fact, numerous are the uncertainties on the mechanical behaviour of soils subjected to thrusting stresses and to the evolution of the technical characteristics of moving masses and on the strain level during time. The problem of the stability of natural slopes in clay is currently considered as if the sliding mass was rigid along the

whole sliding surface. The failure effect is valued by means of methods of calculation which schematise the nature and the characteristics of the soil. The sliding mass is then subdivided in a limited number of simple elements which do not represent the intrinsic complexity of the body of the mass itself. No account is taken, furthermore, of the heterogeneity and of the natural discontinuities which every soil type has in situ, which insert in the failure process by means of a scaling factor and which demonstrate to vary from place to place. The sliding mass is then modelled regardless to its condition as a living being, to its function as an environmental entity, to its relationship with the surrounding territorial units, to its order and to the discipline which its own nature obliges to respect, to the kinematics which it shows during and after the failure and from which the hydrogeological hazard depends on.

Unfortunately, mathematics does not succeed in connecting to this reality and neither with whatever else complex reality regarding the physics of evolutionary processes of the Environment. Why?

When complex natural phenomena are explained through a series of equations, built up with the techniques of logical processes, mathematics does not perceive the reality of life because its rules cannot evolve, on the contrary of the laws of Nature. Nature, in fact, is founded on a *dualistic language* which is at the base of human mental reasoning. Natural physical processes instead are based upon a *monistic ratio*. Parts of the natural truth are therefore *indescribable* through the language of oppositions or of equalities of calculations and, very often, inaccessible to mental reasoning because this is outside of the potential scope of physical reality. Our mind can also perceive, within the scope of the normal possibilities of senses experience, a natural physical process but is not often able to describe it in numeric terms. Notwithstanding this, some physical phenomena can be subjected to a dualistic interpretation. The most evident example is the one of Albert Einstein's (1879–1955) theory of restricted relativity ($E = mc^2$), awarded of the Nobel Prize in 1921, which established the equivalence between the concepts of mass and energy; or when the quantum physicist Eugene Wigner (1902–1995), awarded of the Nobel Prize in 1963, wrote a fundamental paper on the relationships among mathematics, physics and sciences observing that it was possible, by using *abstract mathematical groups*, to create models of natural phenomena through the calculation of symmetries. The genius of Wigner, joined to the one of Hermann Weyl (1928), was to formulate a purely dualistic reasoning by using quite complex mathematical processes in order to interpret physical phenomena expressed by the Nature in monistic terms. The fact that the *mathematical theory of groups* produced such important predictions of a natural physical system does not mean, however, that it interacts with the system itself in each and every condition. A number of modern physicists consider in fact that such a link is likely to represent a spurious relationship established over space and time and which seems to exist only in function of how the human mind designed the experiment. The casual and statistical character of quantum physics, in fact, has never been satisfactory in determining the instant of the failure of a slope neither has ever been able to evaluate where along the slope the hydrogeological disruption could take place and how it could likely be but after

the triggering; only at that point quantum physics is able to provide a response to the natural phenomenon. It is undeniable, however, that our mind is able to perceive Nature even if it is not always able to express the mode of perception by means of mathematical calculations. But, if so, how can it be possible to pursue the *prediction* and the *prevention* of landslides?

In problems of geological nature, the dichotomy between the dualism of human thinking and the monism of natural processes is exasperated by the number of unknowns necessary to the mathematical process. The perception of the physical aspects of each natural process involving soils or subsoils is certainly more truthful if supported by in situ validation tests using instruments for scientific investigations. As a consequence, if the prediction and prevention of landslides is wanted to be carried out, the three-dimensional and surely ingenuous viewing on the use of numerical models, which reduces landslides to a set of distinct elements, tangible and independent, must be abandoned to pass to the alternative of the becoming of an indivisible totality of natural phenomena (Bohm 1955), which comprises, obviously, the time factor. *Yes, time!* Another great unknown impossible to evaluate mathematically in order to define those processes. So, what? A. Einstein, in the meanwhile, convinced us, about one century ago, that space and time are inseparable and curved. Quantum physics, furthermore, tells us that time begins when begins an interaction among quanta. Time, thus, emerges, like space, from the quantum gravitational field; *“every object in the Universe has its own time flowing and what determines this time is the gravitational field”* (Rovelli 2014). However, at a local level when the quantic nature of environmental phenomena is taken into account, the relative time does not work anymore. Does this mean that time has no longer value in natural processes? On the contrary, it means that time is variable from point to point and therefore it cannot be defined within the mathematical process on the evolution of the *Environment*, neither as an ordered elementary entity in a common succession of instants ... *“The dance of the Nature does not develop to the rhythm of the baton of a single conductor who beats the universal time: every process dances independently from the neighbouring ones, following its own rhythm. The flowing of time is internal to the world, begins in the world itself, from the relationships among quantic events which are the world and generate themselves their own time.”* Is it possible therefore to introduce the time factor into a deterministic equation to define the evolutive process of a landslide? Apparently not!

The alternative can be uniquely to rely on direct analytical methods devoted to measure in locum the totality of mechanisms which rule the processes of deformation at failure of a soil and interpret their developments. The logic is to obtain from the slope itself or from the mountainside itself a deformational response as the result of all the components, variable or not, which act on the effect of ground failure in order to overtake a certain theoretical vision of the behaviour of the soil and to assume the in situ experience as the direct proof of hydrogeological hazard.

By means of a radical renovation of the methodology of analysis, the present book individuates, thus, the analytical elements able to lead to the delimitation of the areas under hydrogeological hazard and provides practical methods to obtain

the resolutive values for the early evaluation of the deformation at failure. The book, furthermore, contains numerous practical examples on the observation and analysis of the territory correspondent to the theoretical discussion.

The field of interest is related to cohesive soils or predominantly cohesive soils. The type of failures considered are rotational and translational, according to the classification given by Varnes (1978), which represent circa 70% of the landslides occurring on the Earth.

Potenza, Italy

Luigi Coppola

Curriculum vitae

Prof. Luigi Coppola

Full Professor of Applied Geology–University of Basilicata

Retired since 1st January 2011

Email: luigicoppola2742@gmail.com

A1) Chair of *Applied Geology and Georesources*–University of Basilicata from 01.10.1984 to 30.09.2010.

A2) Head of the *Department of Geological Sciences*–University of Basilicata from 01.10.2002 to 31.12.2010.

B1) Author of 82No. scientific papers on national and international journals; 18No. summaries presented to conferences; 2No. didactic educational books.

C1) *School of Civil Engineering–Kingston Polytechnic–UK*

Referent: Full Prof. Edward Nicholas Bromhead

- Climate changes, landslides and erosion in the semiarid region of the Mediterranean areas subject to recent uplift.
- Risk from the stability of coastal landslides (ris.co.la).
- Fossil landslide dams and their exploitation for hydropower in the Italian dolomites.

C2) *Department of Civil Engineering–Aristotle University of Thessaloniki–Greece*

Referent: Associate Prof. Dr. S.C. Bandis

- Environment technologies to forecast, prevent and reduce natural risks (Hydrological and Hydrogeological risks).

C3) *Department of Geology–National Taiwan University–Taipei*

Referent: Full prof. Hongey Chen

- Geohazards in a neotectonic terrain.
- Fluvial dynamics for protection from water courses and the protection of water courses.

C4) *School of Geology–National University of Salta–Argentina*

Referent: Prof. Victor Omar Viera

- Geoenvironmental risks and territorial arrangement of the geoenvironmental and morphoclimatic unit of the eastern cordillera of the Province of Salta.

D1) *Ministry of the Interiors–Services for the self-management*

Head of the teaching and training activities on geological-environmental topics in the period January–July 2003 for the Nautilus Cooperative Company in Vibo Valentia, Italy.

D2) *Superior Council of Public Works*

Participant Member to the Superior Council of Public Works, 4th Section, Ministry of Public Works, Rome, from 29.11.2003 to 25.7.2008.

D3) *Council of Marche Region*

Member of the Committee of Inquiry on the “*Mining activity in the Marche region and in particular for the quarries of Gorgo a Cerbara and of Torno di Fano*”; year 2006.

E1) Industrial Patent for industrial invention named “***A method for the Forecast and the Prevention of Landslides in cohesive soils***” deposited at C.C.I.A.A. of Pisa–Italy on 31st May 2011 with ref. n. ITPI2011A000059. Approved by the Ministry for Economics Development–Italian Patent and Brands Office on 13th February 2012 with ref. n. IO 23902.

E2) The Patent has been deposited to the Ministry of Economics Development in Rome on 1st August 2012 with ref. n. PCT/IT/2012/000242 for the Worldwide International Extension.

Contents

Part I Preparatory Aspects of the Methodology of Analysis

| | | |
|----------|-----------------------------------------------------------------------------------------------------------------------------------------------------|----|
| 1 | Genesis and Structures of Cohesive Soils | 5 |
| 1.1 | Introduction | 5 |
| 1.2 | Mineralogic Composition of Clays | 5 |
| 1.3 | Electrostatic Characteristics of Clays | 18 |
| 1.4 | Genesis of Clayey Soils | 22 |
| | References | 25 |
| 2 | Causes of Landslides in Cohesive Soils | 27 |
| 2.1 | Introduction | 27 |
| 2.2 | The Principle of Effective Stresses | 27 |
| 2.3 | Equilibrium Conditions | 33 |
| 2.3.1 | Passive Thrust | 37 |
| 2.3.2 | Active Thrust | 39 |
| 2.4 | The Failure Process (from Bles and Feuga 1981) | 42 |
| 2.4.1 | Failure of Rocks Under Tension | 42 |
| 2.4.2 | Failure of Rocks Under Compression | 45 |
| 2.5 | The Influence of Pore-Water Pressure | 54 |
| | References | 56 |
| 3 | The Dating of Landslides | 59 |
| 3.1 | Introduction | 59 |
| 3.2 | General Overview of Quaternary Subdivisions in Marine Environment | 59 |
| 3.3 | Chronostratigraphic Evaluations of Landslide Units | 64 |
| 3.4 | Analytical Procedure for the Chronological Evaluation of Pre-Existing Landslides by Means of Tables 3.1 and 3.2—Example Referring to Würm | 66 |
| 3.5 | The Importance of a Correct Site Analysis | 71 |
| | References | 89 |

| | | |
|----------|------------------------------------------------------------------------|-----|
| 4 | The Pre-failure Deformation | 91 |
| 4.1 | Introduction | 91 |
| 4.2 | Development of Cracks Under Compression | 95 |
| 4.3 | Analysis of Brittle Deformation | 98 |
| 4.4 | Definition and Description of the Various Types of Fractures | 100 |
| 4.4.1 | Diaclases and Joints | 101 |
| 4.4.2 | Extension Fractures (Fentes) | 102 |
| 4.4.3 | Faults | 102 |
| 4.5 | Interpretation of the Mechanisms of Fractures Formation | 105 |
| 4.5.1 | Introduction | 105 |
| 4.5.2 | Formation of Diaclases and Joints | 106 |
| 4.5.3 | Formation of Extension Fractures and Fentes | 107 |
| 4.5.4 | Formation of Faults | 111 |
| 4.6 | The Stress Field | 118 |
| 4.6.1 | Identification of the Stress Field | 118 |
| 4.6.2 | Stress Field in a Continuous Medium | 120 |
| 4.6.3 | Stress Field in a Discontinuous Medium | 121 |
| 4.6.4 | Method of the Minimum Dihedral (or Quick Method) | 131 |
| 4.7 | The Analysis Process | 132 |
| | References | 134 |

Part II Methodological and Analytical Aspects

| | | |
|----------|---------------------------------------------------------------------------------------------------|-----|
| 5 | The Dynamics of Disruptions | 139 |
| 5.1 | Introduction | 139 |
| 5.2 | Dynamics of Recent Landslides | 139 |
| 5.2.1 | First Environment | 140 |
| 5.2.2 | Second Environment | 148 |
| 5.2.3 | Third Environment | 163 |
| 5.3 | Pre-existing Landslides | 171 |
| 5.3.1 | Relation Between Stress and Strain | 172 |
| 5.3.2 | Causes of Deformation at Failure | 179 |
| 5.3.3 | Reactivation of Pre-existing Landslides | 180 |
| | References | 188 |
| 6 | The Role of the Coefficient of Permeability K | 191 |
| 6.1 | Introduction | 191 |
| 6.2 | The Effect of Ground Anisotropy on Permeability | 191 |
| 6.3 | Consequence of Slopes Erosion on the Variations of the Coefficient of Permeability K | 197 |
| 6.4 | The North-Eastern Slope of Tricarico | 204 |
| 6.4.1 | Location | 204 |
| 6.4.2 | Lithology of the Slope | 204 |
| 6.4.3 | Morphological Processes in Place | 205 |

| | | |
|--------------|------------------------------------------------------------------------------------------------|------------|
| 6.4.4 | Instrumental Monitoring | 213 |
| 6.4.5 | Discussion | 215 |
| 6.5 | Hydraulic Conductivity and Hydraulic Potential at Failure | 216 |
| | References | 223 |
| 7 | Landslides Types and Their Failure Mechanisms | 225 |
| 7.1 | Introduction | 225 |
| 7.2 | Monotype Landslides | 226 |
| 7.3 | Composite Landslides | 229 |
| 7.4 | The Great Ancona Landslide | 232 |
| 7.4.1 | Chronicle Notes (from Carciofi 1983) | 232 |
| 7.4.2 | Summary of Damages (from Carciofi 1983) | 234 |
| 7.4.3 | Geological-Structural Framework of the Landslide | 234 |
| 7.4.4 | Morphological Aspects of the Slope | 238 |
| 7.4.5 | The Landslide | 240 |
| 7.4.6 | Technical Analysis of the Slope | 252 |
| 7.4.7 | Landslide Dynamics | 254 |
| 7.5 | Conclusions | 256 |
| | References | 257 |
| 8 | The Prediction and Prevention of Landslides | 261 |
| 8.1 | Introduction | 261 |
| 8.2 | Control of the Areas at Hydrogeological Risk | 262 |
| 8.3 | Notes on the State of the Art | 265 |
| 8.4 | Identification of Areas Subjected to Hydrogeological Risk | 266 |
| 8.5 | Analytical Procedure for Achieving the Prediction of Landslides in Cohesive Soils | 267 |
| | References | 274 |
| Index | | 277 |

Part I

Preparatory Aspects of the Methodology of Analysis

Introduction

On planet Earth, the conditions of hydrogeological instability are mainly conditioned by the structural arrangement of the local orogeny; in effects, the Earth's crust, by means of repeated translational tectonic events, has been subjected to compression and shear processes which today constitute the orogenic ranges of our planet. It can be well comprised, then, the status of failure and sometimes chaoticity in which the rock masses of the slopes currently are and what was the destruction of lithic elements (either composed by grains, laminations, clastic fragments and crystals) as well as the loss in their overall characters.

To such a peculiarity is associated, furthermore, the very high vulnerability of the settling systems induced by fluvial erosion morpho-evolutive processes.

An example of the geological-structural conditions related to the hydrogeological instability is provided by the Apennine chain which, mainly in south-central Italy, is affected by a number of landslides challenging the stability of historical settlements still inhabited. The territory is subdivided into multiple high-seismicity hydrographical basins, with a pluviometric regime characterised by intense rainfall alternate to long periods of absence of atmospheric precipitations to which corresponds an equally fragmented distribution of human settlements, configured, due to well-known historical events, during the course of a long period starting with the Early Middle Ages. The intensive exploitation of forested areas, both for the use of wood and for the creation of new agricultural areas and pasturelands, progressively assumed such a relevance to change deeply the arrangement, moreover very dynamic, of torrential watercourses which represent a further cause of the erosional process of the Apennine chain. Whatever are, thus, the mechanical processes which lead a slope to failure and their implications, they are not, generally, the object of the evaluation by means of the simple theorems of limit analysis. In fact, in soil mechanics the use of equations of the state of equilibrium is highly complicated, because it is needed to consider the soil as a single-phase material under drained

conditions, that is in the absence of interstitial pore-water pressures. Soils instead belong to a multi-phase system, where the knowledge of the initial conditions of the medium and of the boundary conditions, of applied stresses, of saturation state and of the behaviour at failure is a necessary and preliminary condition for the set-up of a credible system for the protection from hydrogeological hazard. Unfortunately, the overview on the mechanisms for the triggering of hydrogeological instability shows multiple difficulties deriving from problems of different orders which are encountered within the analysis process.

A **first problem** is derived from the formulation itself of the Method of Limit Equilibrium, also known in engineering as the Criterion of Thrust Wedges of Coulomb (1773), then perfected by Terzaghi (1923–1925) through the formulation of the Principle of Effective Stresses. Though such a method could be considered satisfactory because of the utility of obtaining solutions regarding excavation works and retaining structures in clayey soils, it cannot be considered as valid, instead, in slope stability problems. In fact, the procedure of analysis of the global limit equilibrium considers the mechanical behaviour of the soil as if it is a rigid body along the whole sliding surface; it is supposed therefore that under sliding conditions the stress state is constant, independently from strain and from time.

A **second problem** derives from the need to schematise the nature and the structural characteristics of the soil and to represent the intrinsic complexity of a natural volume of soil with a limited number of simple elements. The *Method*, then, does not take into account heterogeneity and natural discontinuities which every soil presents in situ and which are introduced in the failure process through a scaling factor which is demonstrated to be different from place to place. Furthermore, the *Method* itself requires the identification *a priori* of a hypothetical critical sliding surface by means of successive iterations.

A **third problem** is encountered in the definition of the constitution of the ground, which derives from the intrinsic limitations of investigation instruments.

Depending on these observations, it is derived that the *Method of Limit Equilibrium* can be applied only to those forms of hydrogeological instability which already assumed their own physiognomy within the context of a disaster already accomplished. When pursuing the purposes of landslides *prediction* and *prevention*, having as their target the protection of public safety, instead, if the stress conditions within the failure zone are not yet defined, it is impossible to demonstrate that the conditions of equilibrium at the boundaries and of soil shearing are satisfied and therefore none of the boundary conditions can be considered as correct or satisfactory. On the contrary, significant uncertainties remain on the behaviour of the individual lithological units subjected to deformational actions, neither are known the transition modes from the static equilibrium of a lithotype to the dynamic equilibrium at shearing, neither, even less, it is understandable the role of the lithic component at failure, that exerts notable influence on the damages induced by landslides. Even if it represents a useful investigation instrument, the *Method of Limit Equilibrium* schematises in an excessive way the complex geological reality and takes not always into account the hydraulic conditions at the boundaries, mostly

variable with time. It is necessary, therefore, that every comprehension effort is given to analytical methods devoted to measure *in-situ* the factors governing the mechanisms of strain at failure of a soil and to interpret the related developments.

References

- Coulomb, C. A. (1773). *Essai sur une Application de Regles de Maximis et Minimis a Quelques Problemes de Statique Relatifs a l'Architecture* (Vol. 7). Mem. Div. Sav. Acad.
- Terzaghi, K. (1923). *Die Berechnung der Durchlassigkeitsziffer des Tones aus dem Verlauf der Hydrodynamischen Spannungserscheinungen* Akademie der Wissenschaften in Wien (Vol. 132, No. 3/4, pp. 125–138). Mathematisch – Naturwissen – Schaffliche Klasse. Sitzungsberichte. Abteilung II.
- Terzaghi, K. (1925). *Erdbaumechanik auf Bodenphysikalischer Grund Lage*. Vienna: F. Denticke.

Chapter 1

Genesis and Structures of Cohesive Soils

1.1 Introduction

The knowledge of structure and mineralogic characteristics of cohesive soils is fundamental for undertaking the study of the reduction in free energy of a clay deposit as well as of the increase in its entropy. The evaluation of the energy released by a spontaneous reaction, like the alteration of a cohesive rock due to the interaction with the water seeping through the ground, represents the measure of the degree of disorder of the system leading a slope to hydrogeological instability. It is therefore necessary to discuss the reticular bonds of clay minerals that break down because of alteration, giving rise to simple molecules and ions, some of which are washed out or escape as gas producing fractures in the ground.

1.2 Mineralogic Composition of Clays

The crystalline nature of clays was ascertained in 1930 using X-ray diffractometry. They are made up of mono-mineral lamellae of silica (SiO_2), alumina (Al_2O_3) and water (H_2O) with variable amounts of iron, alkali and alkaline-earth substances (Fig. 1.1).

The majority of clay minerals has a structure derived from the superposition of ionic layers where, in the simplest form, a layer with positive ionic charge is interposed between two layers, above and below, with negative charge (Fig. 1.2). In the sketch of a clay crystal, in addition, spaces between ionic sheets exist, called *inter-basal spaces*, that were measured just by means of X-ray diffractometry. The composition of mono-mineral lamellae was, instead, deduced from the analysis of elements. Due to their characteristic structure in platelets, clays were defined *phyllosilicates*, name deriving from the ancient Greek *phyllon* = leaf. Other

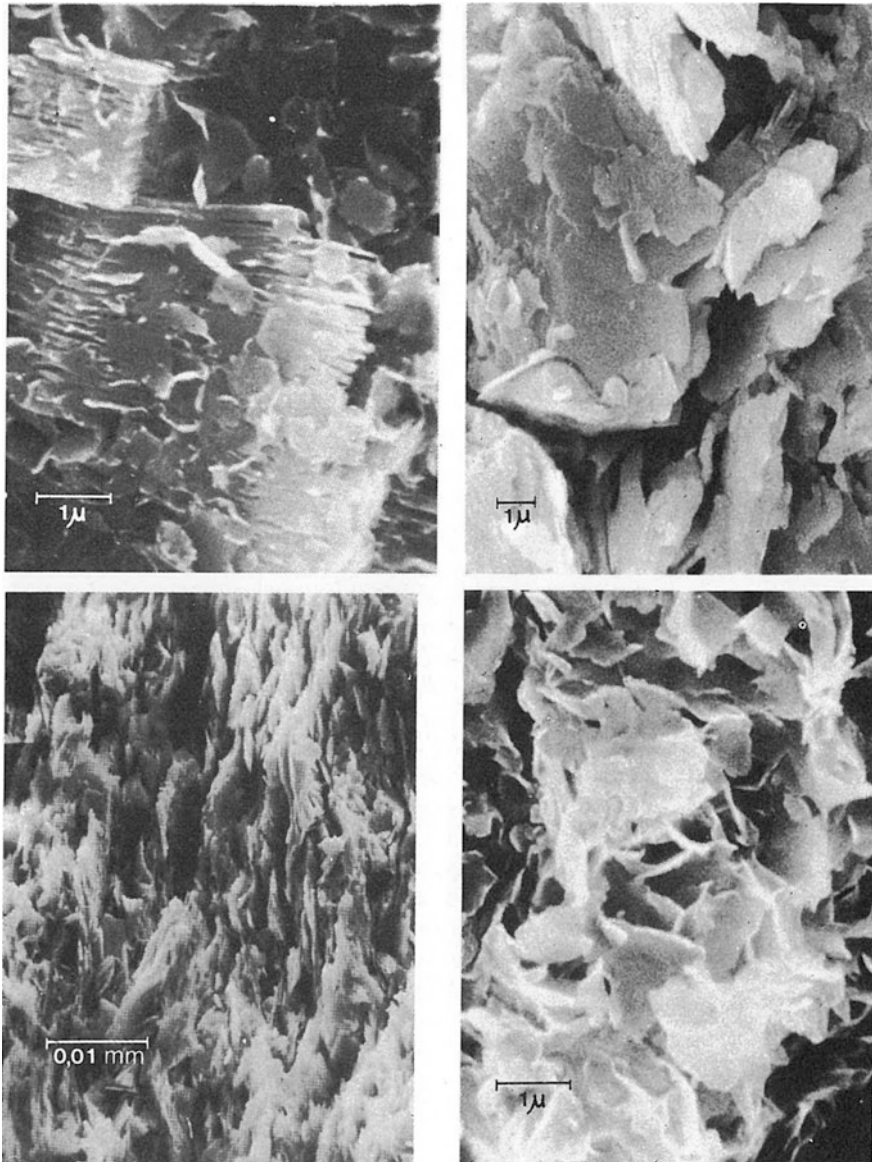


Fig. 1.1 Images of clay samples at the scanning electron microscope. To the top left: kaolinite, with structure of stacked lamellae; to the top right: illite, with front view of lamellae. To the bottom, right: illite, with side view of the lamellae; to the bottom, left: montmorillonite (from Heller 1969)

minerals, like quartzite, gypsum, pyrite, rock salt, carbonates, feldspars, mica, etc., are contained within the clay fraction as impurities and are altered residuals of strong primary minerals, often reduced to colloidal dimensions. Clay generally

contain also, even if as traces, a number of other materials (i.e. barium, manganese, titanium, etc.) or anions, sulphides, chlorides and, in considerably smaller amounts, fluorine compounds in the form of fluorides or fluorosilicates.

Mineral clays come from the slow decomposition of primary minerals like feldspars, micas, amphiboles, pyroxenes, which represent the basis of an “*aggregative complex*”. They are made up of aluminium silicates, more or less hydrated, with a general formula of $nSiO_2Al_2O_3mH_2O$. Depending on the amount of silica with respect to the alumina, the molecular ratio $R = SiO_2/Al_2O_3$ varies between 2 and 5; the molecular arrangement characterises the type of clay. These present a crystalline structure in thin sheets (phyllosilicates) and a characteristic beehive like pattern, with edges in touch with faces (Fig. 1.3). Although presenting this micro-crystalline structure, clays are characterised by colloidal properties because of the thinness of the particles, of their electrostatic charge and, somehow, of their pattern, that allow the adsorption of water molecules and/or of different ions in the inter-platelets spaces (Fig. 1.3); therefore, they are able to swell because of excessive hydration exactly as colloids.

Depending on the modes they are created, clays can be distinguished in *residual* and *transported*.

The first ones were created in the same place they lie by the chemical and physical alteration of pre-existing rocks. The composition of these clays varies depending on the type of minerals they derive from and from local climate. In wet climates, they undergo an enrichment in aluminium hydroxide and ferric hydroxide, alkali and magnesium, with removal of calcium carbonate. In dry climates, a

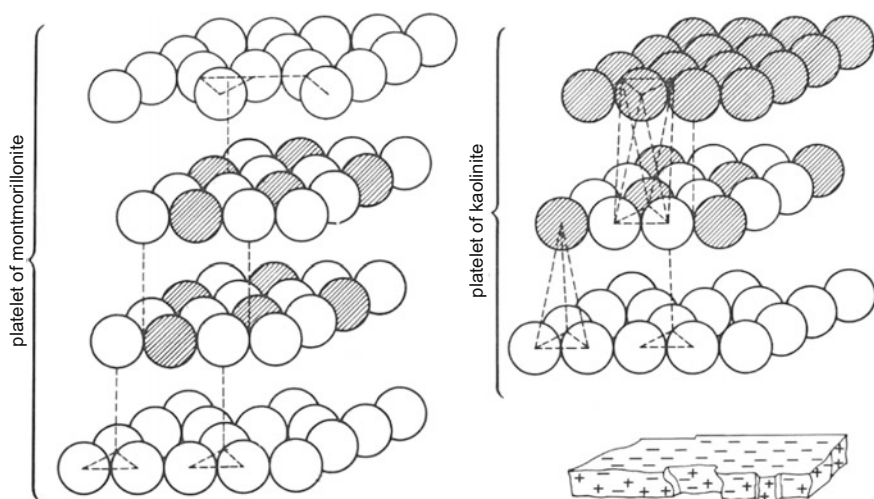


Fig. 1.2 Structure, in distinct layers, of montmorillonite (left) and of kaolinite platelets (right). Below: scheme of the distribution of electric charges on the surface of clay platelets. (Vertical dashed segments, to the bottom of the figures, must be intended as originating from the centre of the equilateral triangles at the base) (from Cavazza 1981)

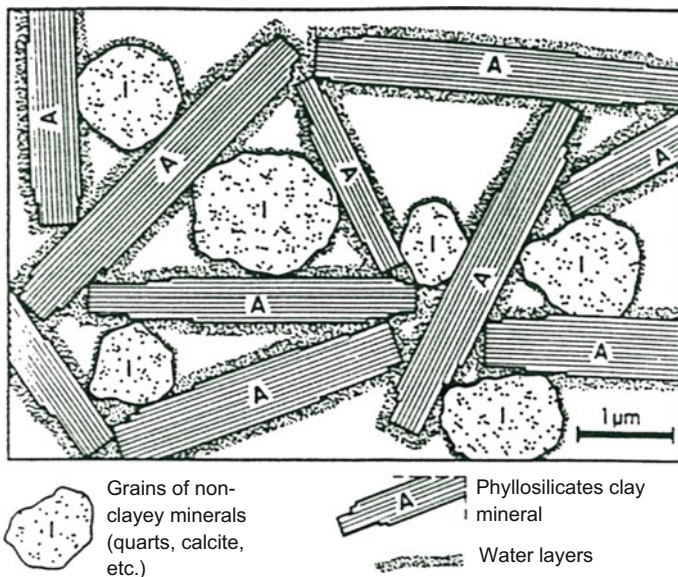


Fig. 1.3 Schematic representation of the fabric of clay materials

surface hardening is obtained, with an enrichment in calcium carbonate due to the rise to the surface of the underlying solutions. A typical residual clay is fireclay, whose main component is kaolinite.

Transported clays are formed by various types of debris (also comprising residual clays) transported into a sedimentary basin. They divide into:

Glacial clays: they are the fine fraction produced by the action of glaciers. They do not present a homogeneous composition, given that the content in limestone varies considerably also within the same deposit. Typical of these clays are the absence of organic residues and the lack in whatever selection in grain size distribution, unless carried out by the action of rivers.

Fluvial or alluvial clays: they have undergone a remarkable selection in grain size distribution but are irregularly deposited in fluvial sediments and change vertically and laterally into other types of deposits (arenaceous or pebbly). They are found in lenses, sometimes of large dimensions, made up almost exclusively of kaolinite and quartz debris. In dry climate conditions, they enriched in carbonates.

Lacustrine clays: they are exceptionally fine deposits, characterised by rhythmic sediments; they are essentially made up of calcite and illite (but rich in potassium).

Marine clays: they are the most diffused and varied in terms of particle size distribution and structure. Generally, they are grey-blue in colour and sometimes present numerous inclusions of organogenic shells.

Lagoon clays: they are characterised by their constant association to deposits of salt, chalk and of sulphur. They are found in generally very large deposits, often

variable and interbedded with deposits of chalk or sulphur. Their main component is illite. Of lagoon origin are smectite and bentonite.

Clay fabric, as observable, for example, at the scanning electron microscope (SEM), is sketched in Fig. 1.3.

Under the mineralogic point of view it is possible to distinguish four large groups of clays with different properties (Duchaufour 1970):

a. **Group of Kaolinites.** Hydrated Aluminium Silicate: $(2 \text{ SiO}_2 \text{ Al}_2\text{O}_3 \cdot 2 \text{ H}_2\text{O})$

This is the group with the lowest content in silicon and presents very pronounced colloidal properties; every sheet is organised into a very simple structure, made up of a tetrahedron of oxygen with silica (Si_2O_3) in the centre.

“The basic structure of this group is a 1:1 succession, formed by the sharing of oxygen atoms between a sheet of silica and a Gibbsite sheet $[\text{Al}(\text{OH})_3]$ (Fig. 1.4). Kaolinite has a fixed basal space H-O of adjacent layers. Layers superpose in a rather regular manner along the C axis to form crystals of thickness ranging between 0.05 and 2 μm ; the largest crystals have been found in clay deposits in China. They are hexagonal (if observed on the horizontal cross-section) and usually with a diameter greater than 0.2 μm ; this is visible on the electronic micrograph in Fig. 1.5a, b. Halloysite has the same structure of kaolinite, but differs for 2 or 4 molecules of water (for unit cell) located among the layers. The presence of this water bonded through hydrogen atoms, alters the distribution of forces inside the crystalline lattice: layers bend forming a tubular structure.

Isomorphic substitutions between Si_2 and Al are not frequent, with subsequent very low net negative charge: 0.005 equivalent for unit cell. Other than this, it is possible to develop a negative charge due to valences not saturated in oxygen and hydroxyl at the vertices of the crystal (Fig. 1.6)”.

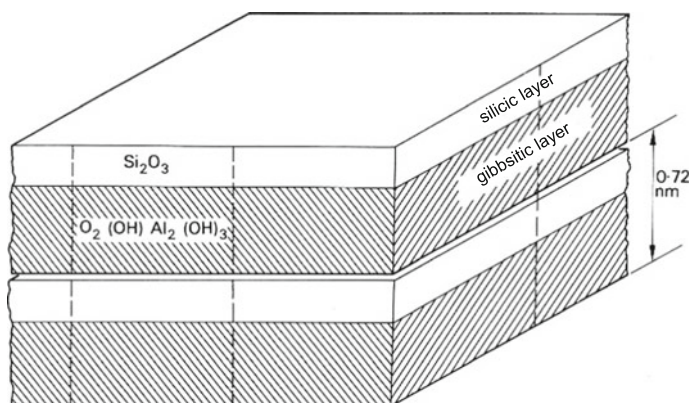


Fig. 1.4 Sketch of the structure of kaolinite—layered mineral 1:1 with hydrogen bonds among the layers (from White 1979)

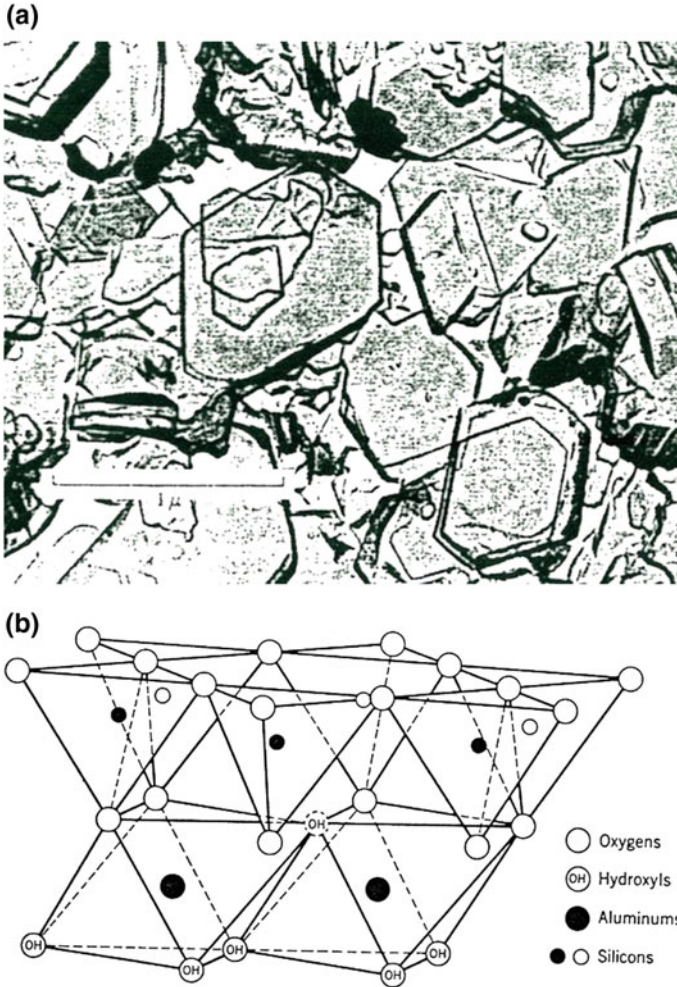


Fig. 1.5 a Electronic micro-photography of particles of kaolinite terraces. b Diagrammatic sketch of the structure of kaolinite layer

Kaolinites have lamellae rather fixed reciprocally and do not present free charges at their boundaries; therefore, they cannot attract molecules of water or cations within their inter-atomic interval; their property of structural modification is very low as well as reduced are the possibilities of swelling and adsorption. The thickness of kaolinite sheets remains constant (7 Å) whereas the one of halloysite is variable (interbedments of H₂O).

- b. **Group of Smectites.** Hydrate Aluminium Silicate: (4 SiO₂ Al₂O₃ 2 H₂O), richer in silica than the previous group.

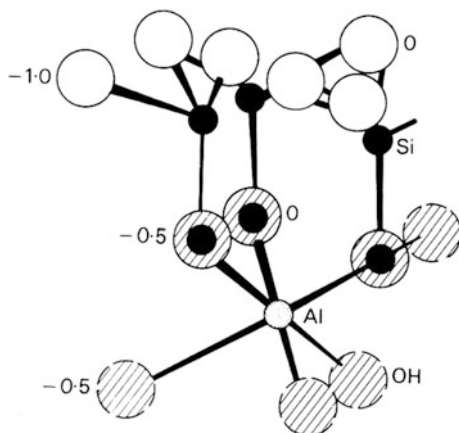


Fig. 1.6 Electric charges on the edge surface of kaolinite with high pH (from Hendricks 1945)

The colloidal properties, that absorb water and fix cations, are highly marked; the oxygen tetrahedron with Si in the centre forms a more spaced structure (2:1) similar to hydromicas but present a higher variability in composition, with isomorphous substitutions both in the octahedral and tetrahedral sheets (Fig. 1.7a). *Montmorillonite*, amongst the most important minerals of this group, presents two tetrahedral layers of silica containing an octahedral layer of *Gibbsite*.

The aluminium in octahedral position can be replaced by Mg^{++} , creating a deficit in valence balanced by an external ion, more often Na^+ , sometimes K^+ or Ca^{++} . Ions Na^+ and Ca^{++} show to have a weaker bond than K^+ , are located within the interlayer spaces and are not much orientated. The interlayer bond is weak and depends on the degree of hydration of the existing cations, that allow the increase in volume of the sheets. The basal space can range between 1 and 4 nm (Fig. 1.7b). The forms containing Ca^{++} present a basal space of 1.9 nm if at the maximum degree of hydration.

The most important smectite clays are *montmorillonites* (predominantly aluminised pole), *saponites* (predominantly magnesian pole) and *noutronites* (predominantly ferric pole). This group of clays presents the characteristic of an expandable lattice because the interlayers are easily accessible to hydrated cations. The thickness of the sheets is variable; 14.2 Å on the average, but can get to a maximum of 19 Å

- c. **Group of Illites.** Present a complex structure, similar to montmorillonites, constituted by two tetrahedral layers of silica containing an octahedral layer of *Gibbsite* (Fig. 1.8a, b); the formula of this composition of sheets is:



The molecular ratio SiO_2/Al_2O_3 is equal to 4.

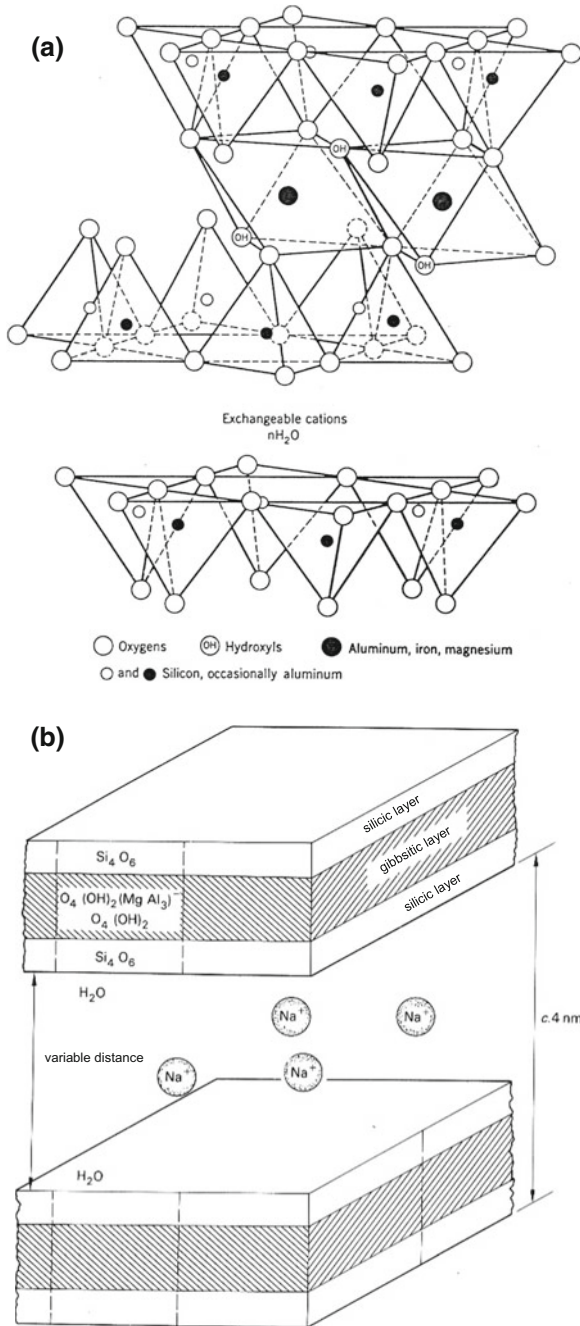


Fig. 1.7 **a** Diagrammatic sketch of the structure of smectite according to Hofmann, Endell, Wilm, Marshall and Hendricks. **b** Sketch of montmorillonite with variable inter-basal space with the dominating cationic species (from White 1979)

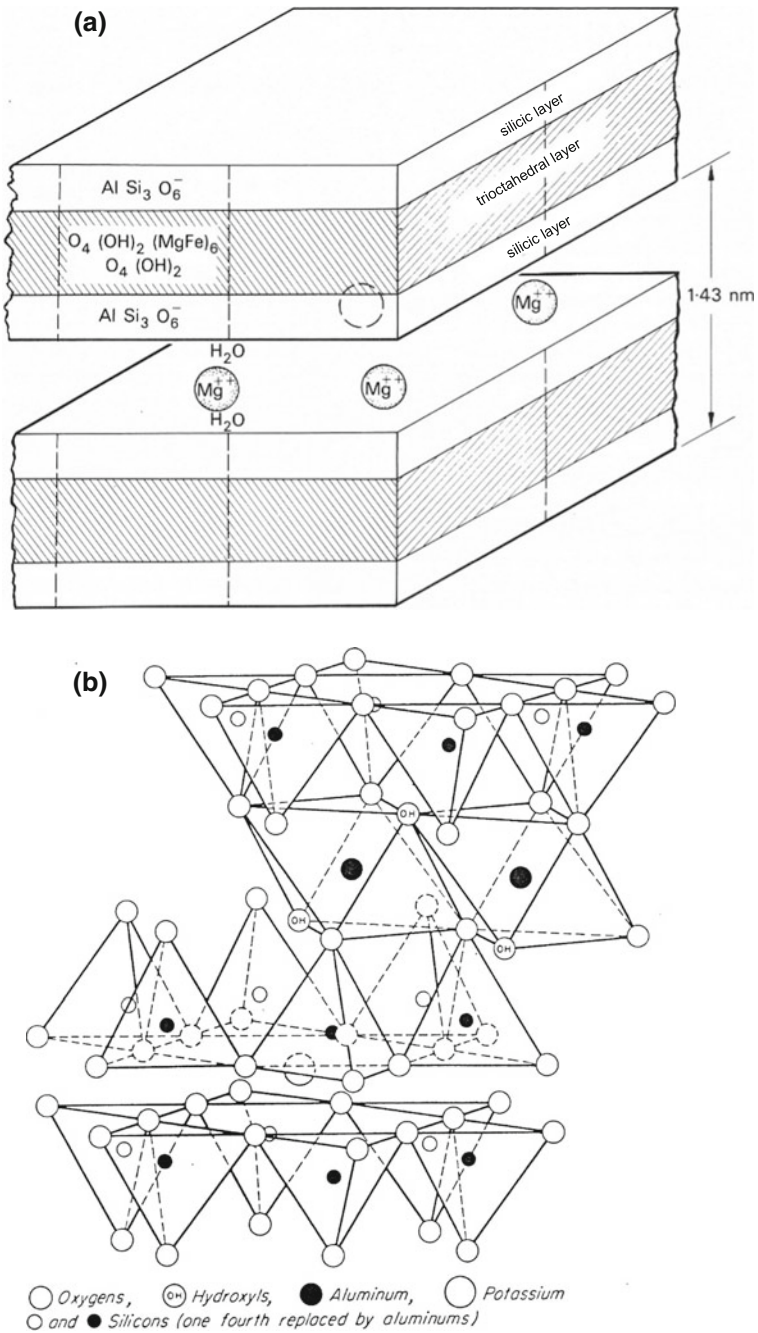


Fig. 1.8 **a** Sketch of vermiculite with fixed inter-basal space due to the presence of partially hydrated Mg²⁺ ions (from White 1979). **b** Diagrammatic sketch of the structure of muscovite (from Grim 1968)

The clays of this group are defined as hydromicas and are in close relationship with *micas*, also belonging to the same group. Hydromicas, however, have less atoms of silicon Si that are replaced by aluminium Al for *micas*. *Vermiculites* are analogous to *biotite* and *illites* to *Muscovite*. In particular, the first ones present a certain swelling potential whereas *illites*, in the strict sense, have a practically fixed structure. For *vermiculites*, in fact, the interlayer potassium K^+ is replaced by Ca^{++} and Mg^{++} . These cations are more hydrated than K^+ and therefore the interlayer space is occupied by a bi-molecular layer of oriented water molecules that widens the basal space from 1 nm, typical of mica, up to 1.4–1.5 nm (Fig. 1.8a). By means of the application of heat the structure shrinks to 1 nm and thus vermiculites present a reversible expandability.

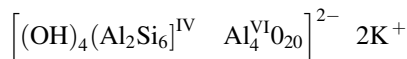
For *illites*, in the strict sense, K^+ ion remains as the main cation and the content in H_2O , generally greater than the one of *micas*, acts on K^+ which is replaced by ions of H_3O^+ . In this case the bonds among the layers are considerably weaker than the ones in *muscovite* and thus overlap in an unordered manner. However, *illites* have always a non-expandable structure, with basal space of 1 nm. They come directly from materials of phyllosilicate origin that undergoes minimal transformations because of the loss of the most degradable elements.

Illites are typical of mild climates and associated to lightly acidic and biologically active materials.

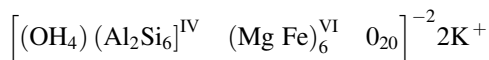
The thickness of *illite* sheets is practically fixed (10 Å), whereas in *vermiculites* can be as large as 14 Å.

- d. **Group of Chlorites.** *Micas* and *chlorites*, in the strict sense, belong to this group presenting a chain-like structure with two-dimensional extension. The lamellae present a structure with hexagonal voids (Fig. 1.9) deriving from an *octahedral chain of aluminium* (Fig. 1.10). When the atoms of aluminium occupy just $2/3$ of the octahedral positions available, the structure of *Gibbsite* is obtained $[Al_2(OH)_6]_n$. If, instead, Al is replaced by Mg, the structure of *Brucite* is obtained $[Mg_3(OH)_6]_n$.

The complete lattice with two-dimensional structure (Fig. 1.9) constitutes a single crystalline layer; the superposition, or the packing, of these layers according to the vertical axis generates a three-dimensional crystal (Fig. 1.11). In *muscovite*-like and *biotite*-like clays an atom of silicon out of four is replaced by aluminium; therefore, a net negative charge of two equivalent units per cell comes out: for *muscovite* the formula is



for *biotite*,



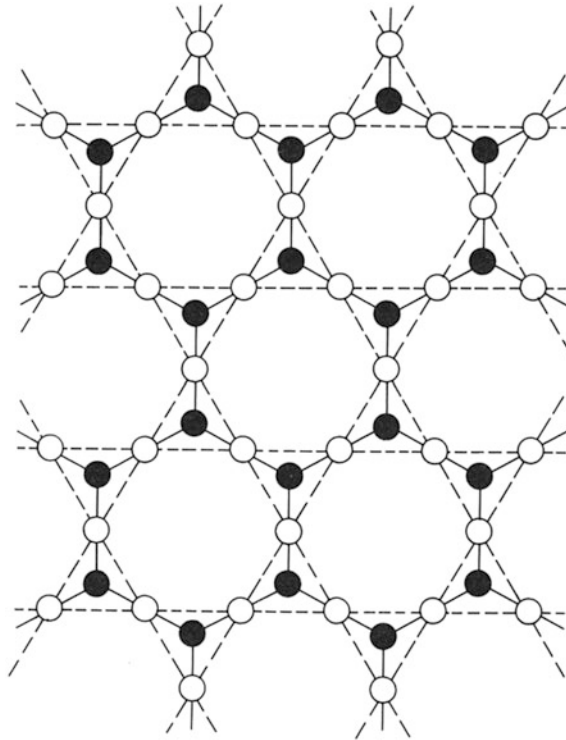


Fig. 1.9 Sheet of tetrahedrons of silicon in horizontal projection: the formation of exagonal holes can be observed (from Fitzpatrick 1971)

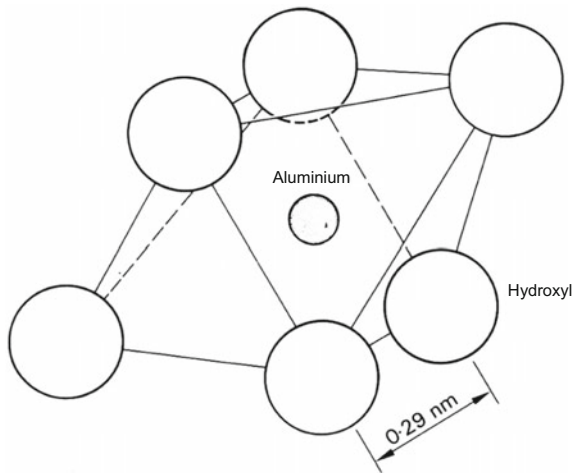


Fig. 1.10 Model of the octahedron of aluminium (from White 1979)

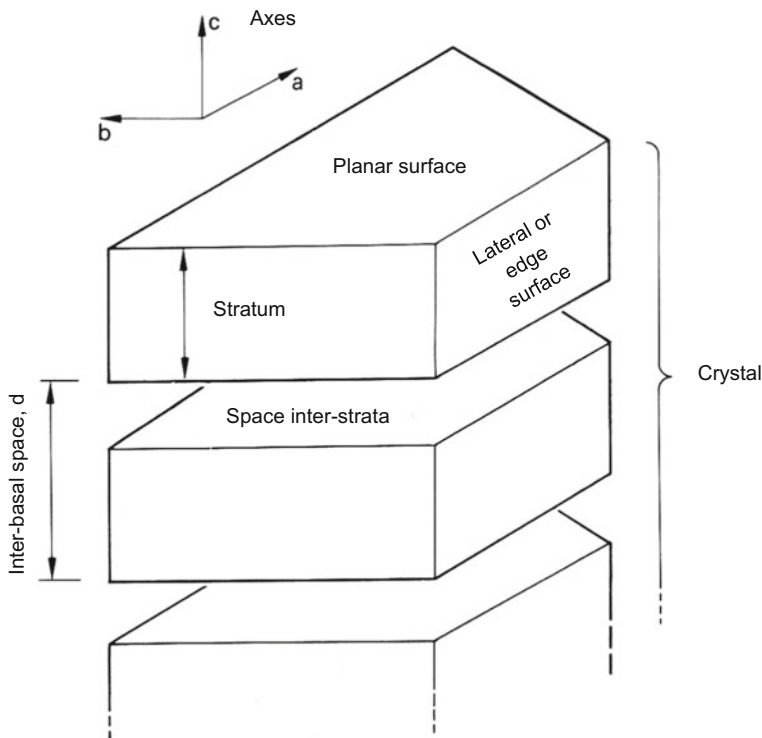


Fig. 1.11 Scheme of a crystal of chloritic clay (from White 1979)

In *muscovite* the negative charge is neutralised by K^+ ions retained in the superposed hexagonal spaces (Fig. 1.12). The presence of K^+ ions makes the bond among the layers very firm. Between the two-dimensional structures with superposed layers the one of *chlorites* is the most complex because has a *brucitic* layer interposed within the *muscovitic* sequence (silicon-gibbsite-silicon), as $2/3$ of the atoms of magnesium are replaced by aluminium (Fig. 1.13).

Chlorites are abundant in magnesiferous type of parent rocks (with layers of *brucite*), but do not preserve as such when getting in touch with water or in an acid environment rich in calcium ions.

Biotite is also not much stable in acid environments because of its content in ferrous iron, but less than *muscovite*.

The thickness of the platelets of *muscovite*, 2:1 scheme, is generally constant and equal to 10 \AA . Three-octahedral *biotite* (Mg^{++}) has a practically constant thickness of 10 \AA , as in *muscovite*. 2:2 chlorite, instead, has a platelets thickness of 14 \AA .

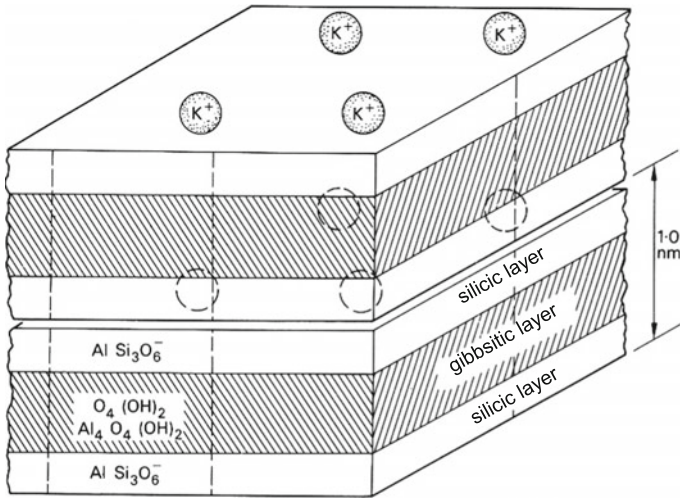


Fig. 1.12 Scheme of a muscovitic mica, 2:1 layered mineral (from White 1979)

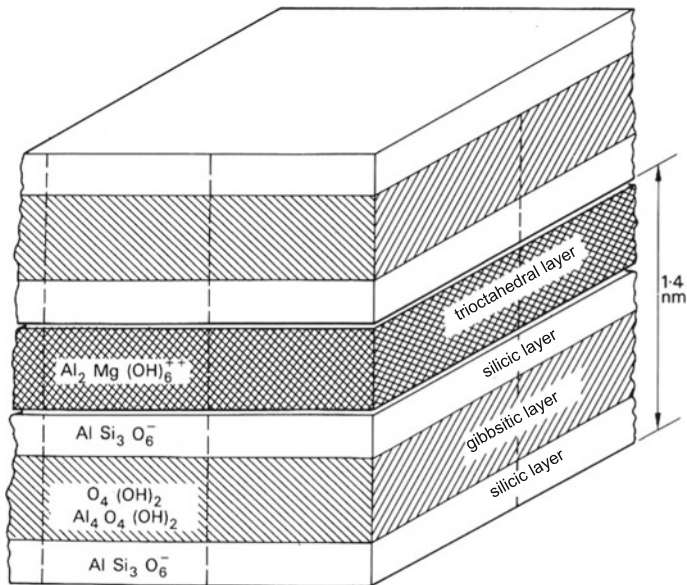


Fig. 1.13 Scheme of a chlorite, 2:2 mixed layers mineral (from White 1979)

1.3 Electrostatic Characteristics of Clays

It has been observed that phyllosilicates are characterised by an indefinite arrangement of tetrahedrons on two directions across a plane (Fig. 1.9). Tetrahedrons are bonded via three vertices and the ratio Si/O is equal to 1/2.5 and $(\text{Si}_4 \text{O}_{10})^{4-}$ constitutes the radical element. They exist in the form of laminations or platelets (Figs. 1.1 and 1.5a) surrounded by a layer of water (*zeolitic water*); furthermore, within their fabric are often present grains of non-clay materials, such as silt (silty clays) or sand (sandy clays) (Fig. 1.3).

This layout allows to derive several important indications, even if just at a qualitative level:

- Plasticity can be intended as the reciprocal sliding of the various components and depends on the amount of clay minerals, to which water layers are bonded that act as a “lubricant”.
- The greater the content in clay minerals, the greater the plasticity; the latter can be opportunely modified by adding grains of non-clayey materials.
- Upon drying, shrinkage is obtained because of the elimination of water layers; shrinkage is greater when larger is the amount of clay minerals.

For the purpose of the technical characterisation of a clayey soil it is important, therefore, to know the content (percentage in weight) in phyllosilic material with respect to the granular one.

- The electric characteristics of the surfaces of laminations depend on the crystalline structure, typical of each mineral.
- The greater the number of ions exchanged in the clay mineral during the modification, in situ or during the transport (isomorphic substitutions), the more the deposit results electrically not in equilibrium and tends to interact mainly with the water surrounding the single platelet until the complex becomes electrically neutral, with balanced attraction and repulsion forces. The platelets of clay minerals are therefore identified as water-active, in order to distinguish them from elements of similar dimensions, but usually granular and water-inert, and the interaction among them originates cohesion. Each platelet has a well-defined thickness, while the other dimensions are variable.

Attraction forces among clay particles are essentially of two types:

- a. *Electrostatic*, of the type of the ones taking place between the interlayer faces, characterised by negative charge, and the edge faces, presenting positive charge; or between K^+ ions and the adjacent layers in illite crystals; or, also, between partially hydrated Ca^{2+} and Mg^{2+} and vermiculite layers;
- b. *Van der Waals Forces* between atoms belonging to two particles. For pairs of atoms, the force reduces with the seventh power of the interatomic distance, but given that the total force acting between two particles is the sum of all the interatomic forces, the distance assumes a different influence.

The source of attractive forces is such that they have low variability with the changes in the solution phase, whereas, on the contrary, repulsion forces, developing because of the interaction with the double layer, are independent from the composition of the soils and from the concentration of solution within themselves. This is reasonably true for diluted suspensions of clay within saline solutions; in concentrated suspensions, however, and in natural soils particles are close enough to allow the interaction among diffuse layers and repulsion and attraction forces induce a *net attraction force* between two micelles. If the net force is of attraction, the particles stay close and in a *flocculated* status. Therefore, the aggregates to which the clays belong can stay stable. On the contrary, if the net force is repulsive, the particles stay distant to reach a new condition of equilibrium or depart enough to exist as single entities in solution and, therefore, to assume a de-flocculated status.

An excess in ions in the space between two particles able to interact induces, within the inter-layer solution, an *osmotic or swelling pressure*. This pressure can be as up to 10–20 bar, induces a deviation of about 1 nm or more and depends on the type of clay mineral, on the type of the cation in the inter-layer and on the concentration of the solution.

If K^+ is the dominant cation within the layer, the layers of hydromicas stack up with a face to face sequence, bonding opposite faces through K^+ : well oriented crystals are obtained in this way. Similar units form with montmorillonites when the predominant cations are Ca^{2+} and Mg^{2+} , even if the resulting structures are not perfectly oriented as in micas, so that it is preferred to consider them as quasi-crystals (Fig. 1.14). The superficial area of a fully dispersed montmorillonite is of about 750–800 m²/g, suggesting that each crystal is made up of 5–8 layers. The anions are completely excluded from the inter-layer regions and the diffused double layer is developed only on the external surfaces of the crystal. The inter-layer cations, with their attractive forces, stop the layers independently from the concentration of the solution. If the ground has relative humidity >50%, calcium-montmorillonite retains at least two layers of water molecules within the interlayer space (cations hydration). The basal space becomes, in this way, 1.5 nm. When the solution in the soil becomes more diluted, further water can be included only to the development of a basal space of about 20 nm, distance that is kept also when in distilled water. This is typical of the *intra-crystal* swelling of 2:1 calcium clays. The crystals of 2:1 clays, in fact, can arrange to form units with a thickness of up to 5 μm, called *domains*. Water can be adsorbed on the external surfaces of the crystals inside the major units and induce swelling and the formation of spaces and pores that retain it because of the surface tension of water. This kind of swelling is defined as *inter-crystalline* (Fig. 1.14); they cause the realignment of the particles that left the positions they had when the soil was dry, so that they are considered the cause of hysteresis of the soil-water retention curves at high suction levels.

A different swelling is obtained when divalent cations are replaced by monovalent Na^+ and Li^+ cations (Table 1.1). If the saline concentration falls under 0.3 N of NaCl, repulsive forces start prevailing and the swelling pressure moves particles to the typical distance of the thickness of the diffuse layer. Kaolinite crystals are larger than the ones of montmorillonite and hydromicas and present a face to face

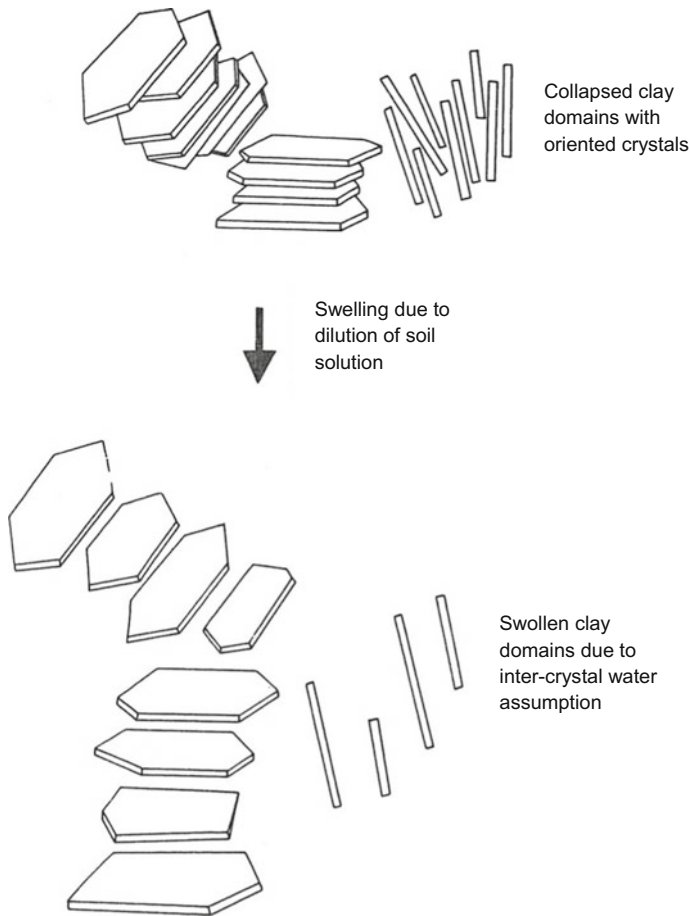


Fig. 1.14 Inter-crystal or inter-clay domain swelling (2:1 clay) (from Russel 1973)

flocculation (Fig. 1.14) in concentrated solutions and at high values of pH. Water run-off and the reduction in the concentration of the solution of the soil can induce the expansion of the diffuse layer and, therefore, a swelling pressure able to destroy the face to face arrangement. If, furthermore, a reduction in pH takes place, the edge faces obtain a positive charge and the attraction between them and the inter-layer faces induces the development of edge to face flocculation (Fig. 1.15).

Of the two mechanisms, face to face flocculation is typical of montmorillonitic clay and depends on the prevalence of divalent and trivalent exchangeable cations or on the precipitation of sesquioxides films forming “electrostatic bridges” between opposite surfaces. Flocculation edge to face is more common, instead, for kaolinite, because of positive charge on the edges in a greater number. This flocculation is independent from variations in the concentration of solutions, but is weakened by the adsorption of anions such as H_2PO_4 on the edge. In the same manner, chemical

Table 1.1 Inter-crystal swelling for saturated 2:1 clays with different cations

| Clay mineral | Charge for unit cell | Exchangeable cation | Swelling in diluted solution (nm) |
|-----------------|----------------------|-----------------------------|------------------------------------|
| Mica | -2.0 | K, Na | none |
| Vermiculite | -1.3 | Ca, Mg, Na K Cs Li | 1.4-1.5 1.2 1.2 ≥4.0 |
| Montmorillonite | -0.67 | Ca, Mg K Cs Na, Li | 1.9 1.5 and ≥4.0 1.2 ≥4.0 |

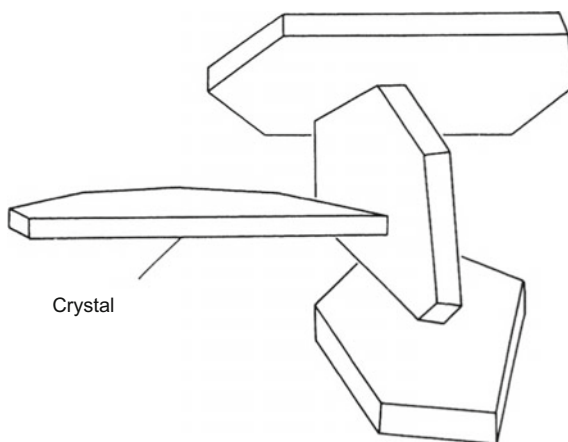


Fig. 1.15 Electric charges on the edge surface of kaolinite with high pH (from Hendricks 1945)

adsorption of phosphate and organic anions on sesquioxides can invert the superficial charge and make oxides negative, by deactivating them as clay flocculants.

In all the practical problems and especially in the ones regarding hydrogeological disruption, clay particles are in contact with water and the stability of natural slopes and/or of versants in cohesive soils depends on the interactions taking place among the particles themselves, water and the substances dissolved into it.

Water molecules are defined as dipolar because, even if neutral overall, have the two hydrogen atoms both arranged on the same side with respect to the oxygen atom. The surface of water particles, negatively charged, therefore, tend to absorb the hydrogen of water molecules, that are arranged according to a certain structure determined by the position of absorbed cations. The water in immediate contact with the particles, given that it is influenced by bonds of such a strength to be unable to be divided from them just by means of mechanical actions, must be considered as an integral part of the structure of the particles themselves and is defined as *absorbed water* as it is no longer free to move.

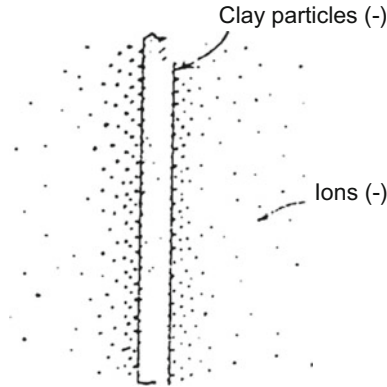


Fig. 1.16 Distribution of cations in the proximities of a clay particle with surface characterised by negative charges (from Terzaghi and Peck 1967)

The ensemble of the negatively charged electric layer of the surface of a particle and the positively charged electric layer of the absorbed water is indicated as double electric layer; its thickness varies considerably depending on the type of the clay mineral and of the characteristics of the cations. *Adsorbed water exerts a noticeable influence on the mechanical properties of the clay mass.*

The cations adsorbed by clay particles are in continuous movement because of the thermal agitation and are arranged statistically in the proximity of the surface of the particle, according to a decreasing density when increasing the distance from the surface itself, as observable in Fig. 1.16. Therefore, the water is less subjected to the electrostatic bonds when getting far from the particle, getting back to the condition of free water.

When hydrodynamic phenomena are considered, ruled by the conditions at the boundaries, it will be referred solely to free water, also identified as *pore-water*.

1.4 Genesis of Clayey Soils

When clay platelets, electrically active, are in suspension within the water, almost stationary in the sedimentary environment, they contrast the gravitational field and do not sediment. They, in fact, are in chemical equilibrium because of the alteration process, which took place at the origin and during the transport; therefore, only an electric change in the environment, even in very long times, allows the platelets to precipitate into clay sediments.

Attraction and repulsion electric forces and the factors causing their variations rule the sedimentary phenomenon and characterise the solid skeleton of clays.

The particular arrangement clay particles take during sedimentation is consequence of the aforementioned surface forces. In distilled water, the negative charge of each particle applies a repulsive force to the others that does not allow them to

bind each other; gravity force is minimal. The particles, therefore, precipitate very slowly or even remain in suspension because of Brownian motions.

In natural waters containing a sufficient concentration of electrolytes, like the ones flowing in calcareous soils, the surface of clay particles often attracts and adsorbs ions of opposite charge, therefore they can mutually attract and aggregate into flocculated masses, heavy enough to sediment because of the effects of gravity. In certain circumstances, especially if the edges of the platelets forming the particles present positive charge, the particles themselves are arranged, within the flocculated mass, according to an edge to face arrangement (Figs. 1.17 and 1.18a), while in other cases are arranged according to a substantially parallel arrangement (Fig. 1.18b).

The sediments made up exclusively of clay minerals are generally aggregates of these arrangements, with the latter also able to assume a loose fabric. Within each flocculated mass, then, particles have edge to face or parallel arrangements or also an intermediate scheme.

Marine clays are particularly of interest, with predominantly illitic clay minerals. The materials transported by rivers once entering the seas encounter, suddenly, a saline electric environment which is different from the previous one, especially in the concentration of electrolytes. Attractive forces, of colloidal nature, therefore, prevail among the particles in comparison to the repulsive ones and therefore they group into flocks (micelles) usually around inert grains. The flocks achieve, in this case, a size that can be subjected to the action of gravity and the particles sediment, forming an open structure solid skeleton, “*honeycomb-like*”, with a relatively small specific weight (Figs. 1.2 and 1.19a). Usually marine clays are also silty, including inert grains of a size with sedimentation velocity equal to the one of the flocks. If the deposit is in fresh water, platelets tend to create a system of electric dipoles that tend to neutralise reciprocally because of the bond between the edge of a particle

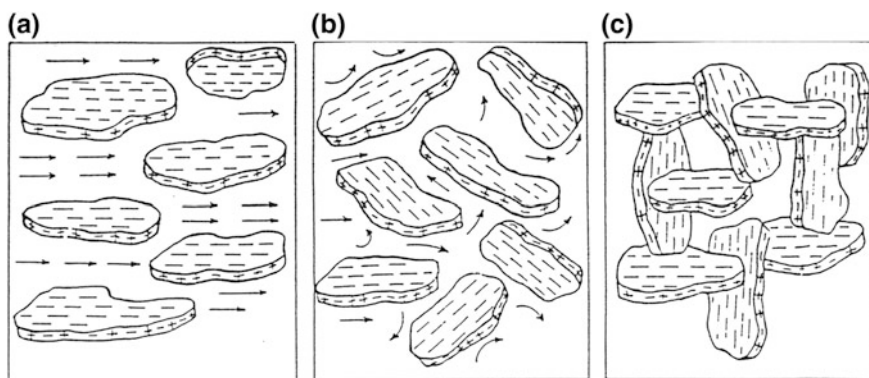


Fig. 1.17 a Parallel arrangement of platelets dispersed in water and subjected to a flow (“sol” status); b isotropic arrangement of platelets: flow is interrupted (“sol” status); c for a system in a steady state, platelets are orientated to obtain a “house of cards”-like structure, incorporating water within the cavities (“gel” status)

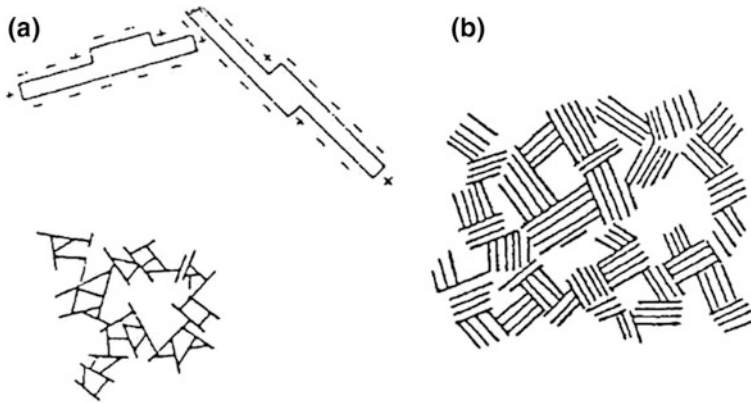


Fig. 1.18 **a** Edge-to-face arrangement of clay platelets and their combination in flakes. **b** Flakes of clay particles with parallel arrangement (from Terzaghi and Peck 1967)

with the centre of another one (Fig. 1.19b). In the case the repulsive forces, of colloidal nature, overtake the attractive ones, such as in an environment where the temperature or the concentration of electrolytes reduces considerably, like in lacustrine clays, the depositional arrangement of the platelets is dispersed (Fig. 1.19c). The particles in it tend to arrange in a parallel pattern: this happens also when remoulding a flocculated structure.

The formation process can be, sometimes, influenced by a variation in the electric environment, as, for example, it happens for clays emerged from the sea in regression and then infiltrated by fresh water. These sediments, during geological times, present an unstable solid skeleton, because in equilibrium only with the original electric environment.

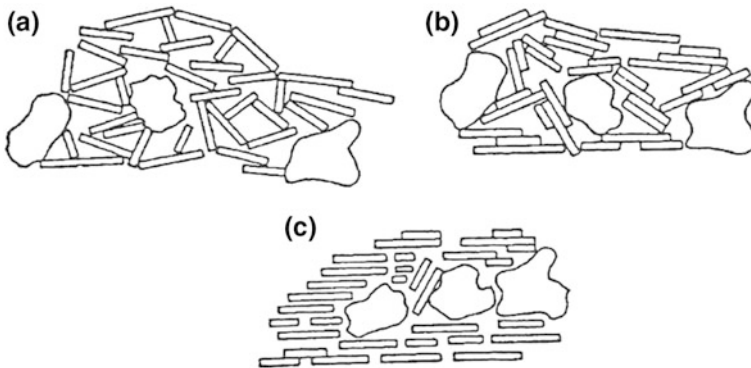


Fig. 1.19 Structures of clay in the natural state: **a** in brackish water environment; **b** in fresh water environment; **c** disperse structure (from Lambe 1960)

A further phase of the formation of clays is represented by the mutations, also artificial, that clays undergo with time, both in terms of stress state and both of chemical environment, that represent the chemical history of the clay.

Clays are defined as overconsolidated if the entire mass, further to the natural increase in the size of the deposit, underwent the action of additional pressures applied by surcharges (for example by glaciers) during their geological history. The related loads increased the compactness of the clay by reducing the water content.

If the loads that induced the overconsolidation are removed (for example by erosion), the clay undergoes a reduction in the applied stress (decompression) that can still be under development, with sensible effects. Other noticeable effects can be mainly obtained after manmade excavations.

A sensible progressive consolidation can develop when deposits emerge from water and are put in contact with air. They undergo a slow evaporation and water rises within the pores because of the action of capillarity: consolidation is caused in this way but, usually, is less important than the one induced by the removal of pre-existing loads.

It is evident, therefore, that the overconsolidation ratio of clay deposits is linked to the water content.

When overconsolidation is induced by tectonic actions metamorphic phenomena take place. Shaley clays are soils that underwent slight metamorphic actions, due to fragments of rock masses, rich in clay fractions, in a slightly competent matrix. These soils are usually prone to swelling and make difficult every type of work taking place within them, especially the excavation of tunnels.

Consolidation changes gradually to crystallisation when the effects of dynamic metamorphism increase. Clay shales, therefore, are obtained and characterised by sub-planar discontinuity surfaces. When the overconsolidation pressure is large enough to induce the crystallisation of clays, they become unable to rehydrate and therefore the swelling phenomenon becomes irreversible; for example, the change from marls to slates, phyllites or to mica-schist is observed. If, instead, the phenomenon is reversible, at least in part, clay swells while rehydrating; this process is defined clay *activity*.

References

- Basso, F. (1995). *Difesa del suolo e tutela dell'ambiente*. Bologna: Pitagora Editrice.
- Cavazza, L. (1981). *Fisica del terreno agrario*. Torino: UTET.
- Ciavatta, C., & Vianello, G. (1989). *Bilancio idrico dei suoli: applicazioni tassonomiche, climatiche e cartografiche*. Bologna: Editrice Clueb.
- Comel, A. (1937). *Elementi di Pedologia climatica*. Udine: Istituto delle Edizioni Accademiche.
- Duchaufour, P. (1970). *Précis de pédologie*, Paris, VI^e: Masson et C^{ie}, Éditeurs 120, Boulevard Saint-Germain.
- Erhart, H. (1967). *La genèse des sols en tant que phénomène géologique*. Paris: Masson.
- Fitzpatrick, E. A. (1971). *Pedology*. Edimburgh: Oliver and Boyd.
- Giordano, A. (1999). *Pedologia*. Torino: UTET.

- Gisotti, G. (1983). *Geologia e pedologia nell'assetto del territorio*. Bologna: Edagricole.
- Grim, R. E. (1968). *Clay mineralogy*. New York: McGraw-Hill Book Company.
- Heller, L. (1969). *Proceedings of the International Clay Conference, Tokyo* (Vol. 1), Jerusalem: Israel University Press.
- Hendricks, S. B. (1945). Base exchange of crystalline silicates. *Industrial and Engineering Chemistry*, 37, 62–630.
- Kezdi, A. (1972). *Stability of Rigid Structures, Proceedings 5th European Conference of SMFE* (Vol. 2, pp. 105–130).
- Lambe, T. W. (1960). *A Mechanistic Picture of Shear Strength in Clay, Proceedings Research Conference on Shear Strength of Cohesive Soils, ASCE* (pp. 555–580).
- Magaldi, D., & Ferrari, A. G. (1984). *Conoscere il suolo, introduzione alla pedologia*, Gruppo Editoriale Fabbri, Etas S.p.A.
- Russel, E. W. (1973). *Soil conditions and plant growth* (10th ed.). London: Longmans.
- Terzaghi, K., & Peck, R. B. (1967). *Soil mechanics in engineering practice*. New York: Wiley.
- Università degli Studi della Basilicata (1996). *Dispense di Mineralogia*, a cura di G. Piccarreta, A. Caggianelli, S. Fiore, Potenza.
- White, R. E. (1979). *Introduction to the principles and practice of soil science*. Oxford: Blackwell Scientific Publication.

Chapter 2

Causes of Landslides in Cohesive Soils

2.1 Introduction

Landslides represent the element of greater geomorphological danger for hillsides and mountainous areas; the knowledge of them in terms of delimitation progressively improved in recent years, due to the sensitivity to the problem, to the need to take census of the damages as well as for the adoption of ever more advanced surface survey technologies and surface analysis methods that derive from techniques for positioning and survey (GPS, LASER, RADAR, etc.) developed for military and space exploration purposes. This approach, that contributes specifically to delineating surface movements and effects on the soil, does not provide, however, enough information on internal causes and on the factors predisposing the triggering that remain to date often uncertain and not univocal.

2.2 The Principle of Effective Stresses

The prediction and prevention of a landslide cannot be measured based on the effects or on the kinematics of the event on the ground surface but, based on a more rigorous geological and geotechnical process, must be based on the internal mechanical behaviour of the slope and on its hydrogeological conditions. For this purpose, in order to identify the causes of landslides in cohesive soils, it is first necessary to distinguish the fields of research and focus on those of relevance.

Within a mountain range, *the neotectonics* are responsible for the processes of structuration of the slopes while *the lithological and structural characteristics of the outcropping soils associated with local climatic conditions* govern the distribution of areas under erosion; *the deepening of watercourses* controls the hydrogeological instability of the slopes.

When in a region the hydrographic network undergoes a rejuvenation due to the lowering of the base level of the main watercourse, the predominantly clayey and

silty-clayey soils undergo an unloading phase with a decrease in the consolidation stress, while the slope is subjected to a seepage motion due to a particularly high hydraulic gradient between the upslope and the valley resulting in an increase in the piezometric head in the proximity of the erosional scarps (Fig. 2.1).

In effects, a gradient in water potential can also develop because of rainfall events, because the water infiltrating the soil upslope has a greater potential energy than the one infiltrating at the toe of a slope generated by the erosional action of a river. Consequently, the combination of the renewed slope acclivity, due to the primary engraving action of the superficial hydrographic system, the decay of the mechanical properties of the soils, consequence of the geological-structural history of deformations and fluctuations of groundwater, due to the abundancy of precipitations, are the most frequent causes of instability of natural slopes. These are therefore environmental causes that produce hardly foreseeable changes in the boundary conditions and in soil properties themselves and which make the instability of natural slopes a very complex issue.

Seismic and anthropic activities result to be contributory causes only, sometimes determinant but occasional, in the genesis of the state of hydrogeological instability of the slopes.

In order to understand the causes of landslides in cohesive soils, it is therefore necessary to refer to some fundamental concepts that define their behaviour, because clays are anisotropic, with non-linear and viscous elastic properties. The starting point is a mechanism of interaction between the various phases that constitute a pelitic unit known as the Principle of Effective Stresses, introduced by Terzaghi (1936) at the 1st International Conference on Soil Mechanics and Foundation Engineering.

“The stresses in a certain point can be determined by the knowledge of the main total stresses $\sigma_1, \sigma_2, \sigma_3$. If the inter-granular space is filled with water at a pressure u , the total stresses can be divided into two contributions. One of them, called neutral pressure u , acts on water and on the grains in every direction with equal intensity. The differences $\sigma'_1 = \sigma_1 - u, \sigma'_2 = \sigma_2 - u, \sigma'_3 = \sigma_3 - u$, represent the contribution of pressure, in excess of “ u ”, which is entirely applied to the solid phase.

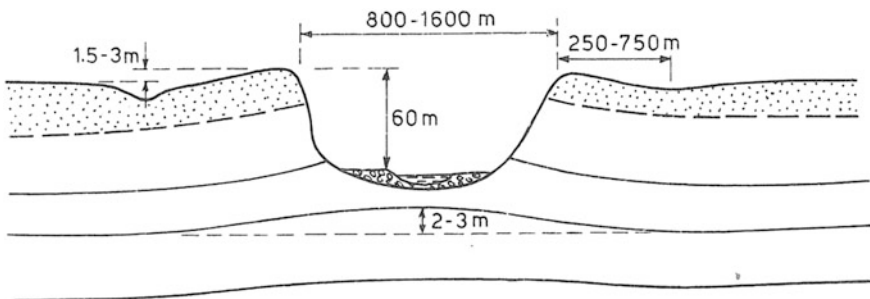


Fig. 2.1 Typical effects of erosion in some valleys of Canada (from Matheson and Thomson 1973). Swelling phenomena due to fluvial erosion: uplifting and rotation of the scarps; deposits with anticlinal configuration; development of cracks and faults

This fraction of the total stress is called effective stress. A change in neutral pressures does not induce changes in the volume; porous materials (such as sand, clay, and concrete) react to a change of u likewise uncompressible materials and with null internal friction angle.

All the effects induced by a change in stress, such as compression, distortion and a change in shear strength are solely due to a change in effective stresses.

Consequently, any stability assessment of a saturated medium requires the knowledge of both total and neutral stresses.”

The evaluation and distribution of pore-water pressures in the soil are primarily important for the knowledge of the intrinsic causes of landslide triggering and constitute the primary target for the prediction and prevention of hydrogeological instability in cohesive soils. This is much more important when the analysis is devoted to the recovery and preservation of the building heritage as well as to allowing the urban expansion, which has to take place following a common line of interventions that goes beyond the municipal boundaries and assesses the evolutionary phenomena interesting the whole territory within a single physiographical unit, which corresponds to the basin.

The principle of effective stresses (Terzaghi 1936) can be illustrated by the following example (Fig. 2.2).

A container is filled with granular materials to level h_2 and with water to level $(h_2 + h_1)$. At the bottom of the container is attached a pipe connected to a tank where the water is at the same level as the granular material. There is therefore no flow of water. On section AA, at depth $(h_1 + z)$ from the free surface of water, the vertical pressure p is given by:

$$p = h_1\gamma_a + z\gamma_{sat}$$

where γ_a is the specific weight of water and γ_{sat} the unit weight of the saturated soil.

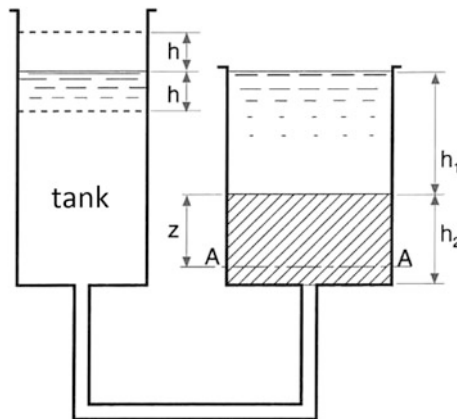


Fig. 2.2 From Colombo (1978)

Given that p depends on the weight of all the overlying materials (water + soil) it is called total pressure and Terzaghi demonstrated that is linked to the effective pressure p' and to the neutral pressure u from the equation:

$$p = p' + u$$

that, in terms of stresses, becomes:

$$\sigma = \sigma' + u$$

This equation describes the principle of effective stresses by Terzaghi, where

- σ total stress
- σ' effective stress
- u neutral stress

The total stresses are therefore defined as

$$\sigma_1 = \sigma'_1 + u \quad \sigma_2 = \sigma'_2 + u, \quad \sigma_3 = \sigma'_3 + u,$$

where $\sigma'_1, \sigma'_2, \sigma'_3$ represent the *effective stresses* related to the sole solid phase.

It can therefore be assessed that all the effects produced by a change in shear resistance are solely due to a change in effective stresses. Consequently, *the main cause of the failure of a slope and/or of the deformation that it can undergo is due to the shearing actions that the solid particles of the soil exchange among them.*

The flow of water through a medium is ruled by Darcy's Law (Darcy 1856),

$$Q = K \cdot S \cdot i$$

where

- Q flow of water in m^3/s
- K coefficient of permeability, dependent on soil characteristics
- S area of the cross section for the flow of water, in m^2
- i hydraulic gradient (Fig. 2.3).

$$\frac{H_1 - H_2}{L}$$

A flow of water or a seepage of water through a certain medium is induced wherever a hydraulic gradient (i) develops.

If u is the hydraulic head generating the flow and H the thickness of the aquifer layers, it can be obtained:

$$i = \frac{u}{H}$$

therefore $u = i \cdot H$ (in terms of water column) and $u = \gamma_a \cdot i \cdot H$ (in terms of pressure)

The neutral stress (u) in a medium is given by the hydraulic gradient (i) multiplied by the hydraulic head (H) corresponding to the *piezometric level*.

On a predominantly clayey slope, a hydraulic gradient can easily develop between contiguous areas because the circulation of seeping water within them is influenced by the anisotropy and the heterogeneity of the porous medium. In fact, seepage must take into account the interaction between solid particles and interstitial fluid, the principle of conservation of mass (if the mass remains constant over time), the three state parameters (pressure-density-temperature) and the second Newton's Law, according to which a fluid is forced to move by surface forces (resulting from the pressures applied to the boundary) and the mass forces due to gravity. It follows that along a slope the water infiltrating to the upstream takes on more potential energy than the one infiltrating downstream and, along the path, the piezometric surface is extremely irregular so to develop hydraulic gradients (i), sometimes relevant, from point to point (Fig. 2.3).

The variation in neutral stress (u) along a slope is mainly due to the local variation of voids index (e) of the soil.

Within granular soils, drained conditions take place; as a consequence, seepage provides a continuous flow and therefore the hydraulic gradient (i), as well as neutral pressure (u), are equal to 0, indicating a stable soil condition. It can be therefore summarised that the circulation of water within permeable soils does not induce any water potential ($i = 0$) and therefore does not trigger landslides. In drained conditions, a slope is not subjected to landslides, and therefore spring water cannot be the cause for landslides unless the underground water circulation has a greater flow than the one at the outlet point. In cohesive soils, instead, undrained conditions take place. This is due to electrostatic effects within the clay (see Chap. 1); water molecules, in fact, are imprisoned in the inter-particles voids until the saturation

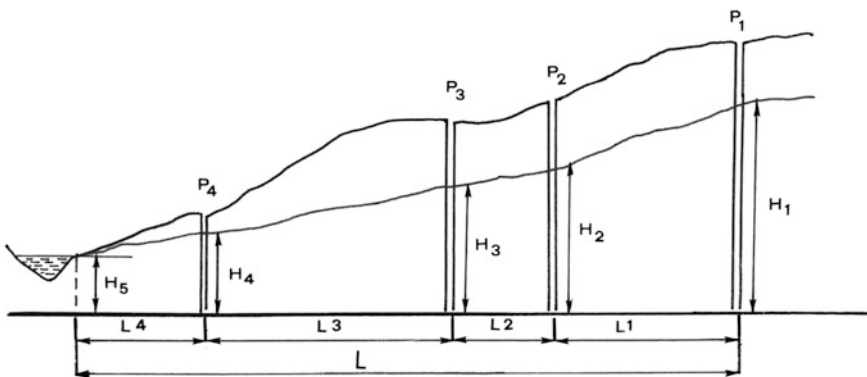


Fig. 2.3 Evaluation of the hydraulic gradient by means of wells. Example $i_1 = H_1 - H_2 / L_1$

develops. This, in confined conditions, becomes perfectly impermeable and maintains its solid state until it is preserved from expanding. In these conditions, furthermore, the clay mass undergoes an increase in unit weight and, at the same time, an increase in the lateral thrust pressure. The failure due to shearing is therefore governed by the Terzaghi equation, based on the principle of effective stresses:

$$\tau = c' + (\sigma_n - u) \operatorname{tg} \varphi'$$

where

- τ shear stress at failure;
- σ_n normal stress to the failure surface;
- c' effective cohesion;
- φ' effective friction angle

The cause of landslides in cohesive soils, therefore, is mainly attributed to the neutral pressure u . When u assumes a value equal to σ_n (this happens in saturated soils under undrained conditions), the strength of cohesive soils becomes very low as $(\sigma_n - u) = 0$ and therefore the Terzaghi equation becomes

$$\tau = c_u \quad \text{and} \quad \varphi' = 0$$

where c_u represents the undrained cohesion.

The lithostatic load is taken solely by water molecules and since interstitial water does not withstand static shear stresses, any increase in loading on the saturated confined mass results in shear strain.

If, on the other hand, the saturated cohesive soil is free to expand, an increase in saturation results in a change of clay state, from solid to plastic state with an increase in the volume of the mass. However, this only occurs if there are conditions at the boundary characterised by σ'_v (normal vertical effective stress) and σ'_h (normal horizontal effective stress) lower than σ_u (neutral stress)

$$\sigma'_u > \sigma'_v, \sigma'_h$$

If, on the other hand, the saturated cohesive soil is free to expand, an increase in saturation results in a change of clay state, from solid to plastic state with an increase in the volume of the mass. However, this only occurs if there are conditions at the boundary when σ'_v (normal vertical effective stress) and σ'_h (normal horizontal effective stress) are lower than σ_u (neutral stress).

In that case, the over-saturated clay expands to the plastic or fluid-plastic state in the direction of the lower confining pressure, often occupying the voids due to the tectonic cracking of the deposit.

2.3 Equilibrium Conditions

Let us consider within a half space of cohesive soil, bounded above by a horizontal plane, a generic soil element at a depth z , as on Fig. 2.5. Such element is in a state of rest if no shear stresses are applied to its faces, therefore the normal vertical σ_{vo} and horizontal σ_{ho} stresses are principal stresses.

Once the value of K_o is known, it is possible to calculate the horizontal stress σ_{ho} . In fact, we know that there is a relationship between the effective horizontal stress σ'_{ho} and the effective vertical σ'_{vo} that is expressed by the coefficient of thrust at rest K_o .

$$K_o = \frac{\sigma'_{ho}}{\sigma'_{vo}} \quad \text{or} \quad \sigma'_{ho} = K_o \cdot \sigma'_{vo}$$

where:

- the total vertical stress at the generic depth z , in the case of homogeneous clays with unit volume equal to γ , is given simply by the equation (Fig. 2.4):

$$\sigma'_{vo} = \gamma \cdot z$$

- in the case of layered soils, this can be calculated as the sum of the contribution of n layers with unit weight γ_i and thickness Δz_i :

$$\sigma'_{vo} = \sum \gamma_i \cdot \Delta z_i$$

- vertical stress σ'_{vo} is an effective stress and is calculated, once is known the value of pore-water pressure u_o , using the equation:

$$\sigma'_{vo} = \sigma_{vo} - u_o$$

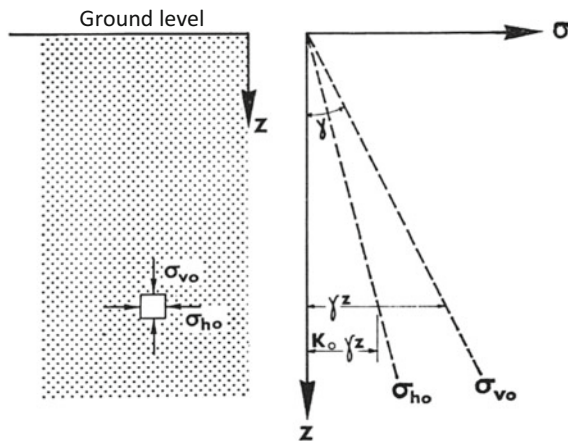


Fig. 2.4 Geostatic stresses in the absence of groundwater (from Cestelli Guidi 1987)

In this situation, if the cohesive deposit remains at rest for a sufficiently long time:

- the stresses equalise towards a constant value at every depth;
- no deformation is under development;
- each vertical section can be considered as of symmetry, therefore no shear stresses can exist on vertical and horizontal planes;
- vertical σ_{vo} and horizontal σ_{ho} stresses are principal stresses and the principal planes of the stress system are vertical and horizontal.

This condition of the effective stresses is called “ K_0 condition”.

The evaluation of the horizontal stress σ'_{ho} , despite to what observed for σ'_{vo} , represents one of the most complicated issues in Soil Mechanics, as the current value of σ'_{ho} , depends on the particular stress history of the deposit; therefore also the value of the coefficient of thrust at rest K_0 depends on the stress history of the soil, i.e. on the magnitude and duration, in the right sequence, of the stresses to which the deposit has been subjected from the formation to the current saturation.

This original state of stress, however, is generally altered by other phenomena: variations in groundwater level, capillarity and tectonic movements. Other phenomena, that are not by themselves stresses, but have a major influence on soil behaviour, have to be considered, like elements belonging to the stress history of the deposit: chemical cementation, thixotropic hardening, drained creep (aging) and dissolution due to changes in the chemical environment of deposition.

The evaluation of the coefficient of thrust at rest K_0 , therefore, varies with each load increment $\Delta\sigma'_v$, which produces noticeable variations Δe (where e represents the voids index). In these conditions, the value of the K_0 coefficient, indicated in the following as $K_0(NC)$ for all the times it is referred to the normally consolidated state, depends solely on the nature of the soil and can be estimated by means of empirical formulas. One of the most well known and most widely used formula is the one proposed by Jaky (1944), which links the $K_0(NC)$ coefficient to the angle of shearing resistance φ' :

$$K_0(NC) = \left(1 + \frac{2}{3} \sin \varphi'\right) \left(\frac{1 - \sin \varphi'}{1 + \sin \varphi'}\right)$$

often simplified as:

$$K_0(NC) \cong 0.95 - \sin \varphi' \quad \text{for cohesive soils.}$$

A further equation linking this coefficient to the plasticity index of clays was proposed by Massarsch (1979) (Fig. 2.5).

In the case of normally consolidated soils ($OCR = 1$), Bishop (1966) carried out numerous tests on sands and clays, under different compaction conditions and measured the values of the coefficient at rest (Table 2.1).

The table shows that the greater is the value of the friction angle, the more competent is the soil and, therefore, characterised by reduced values of lateral

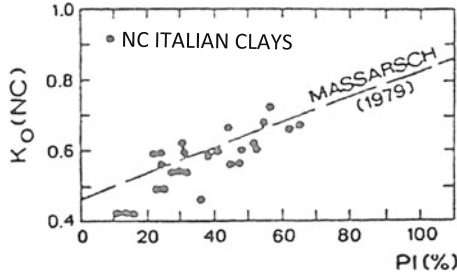


Fig. 2.5 Variation of K_0 coefficient with the plasticity index (from Massarsch 1979)

Table 2.1 Values of the coefficient of thrust at rest K_0 for loose NC soils

| | φ | K_0 |
|-------------------------|-----------|-------|
| Dense sand, saturated | 39° | 0.36 |
| Loose sand, saturated | 34° | 0.46 |
| Sandy clay, undisturbed | 33° | 0.43 |
| Silty clay, undisturbed | 27° | 0.57 |
| Clay, remoulded | 20° | 0.70 |

stresses; the range of variability of K_0 reduces. Cestelli Guidi (1987) deduced from this that “if the soil is saturated and undrained, as lateral deformation was denied, it is obtained that $\Delta\sigma_{vo} = \Delta u$ and, therefore:

$$\frac{\Delta\sigma_{ho}}{\Delta\sigma_{vo}} = 1$$

i.e. under fluid state conditions, where stresses are the same in all the directions, $\sigma_{vo} = \sigma_{ho} = 1$; but, if the soil experiences drained conditions, meaning $\Delta u = 0$,

$$\frac{\Delta\sigma_{ho}}{\Delta\sigma_{vo}} = K_0$$

From the previous equation it can be observed that a reduction in pore-water pressure, due for example to a lowering in groundwater level, induces a reduction in the total horizontal stress that, if the vertical load remains constant, is equal to:

$$\Delta\sigma_{ho} = (1 - K_0)\Delta u$$

In the proximities of the ground surface (where σ_{vo} assumes low values) this phenomenon could lead to tensile stresses that appear, sometimes, as small cracks in the soil (along the principal planes of failure).

It is therefore clear that in cohesive soils the lateral pressure σ_{ho} depends not only on the type of soil and on the stress history, as previously mentioned, but also on the magnitude of pore-water pressures.

In Fig. 2.6 it can be observed the range of variation of K_o in function of the overconsolidation ratio $OCR > 1$. It ranges from active limit values K_a to passive limit ones K_p depending on the stress state induced by phases of geological loading or unloading (a) and on the plasticity index correlated to different values of the overconsolidation ratio (b).

It can be noted that during a depositional phase it is always $\sigma_v > \sigma_h$ therefore $K_o < 1$ until it reaches the K_a minimum limit value, while upon unloading (during an erosional phase, glaciers melting, etc.), as the vertical stress reduces, the horizontal stress stay “locked”, in principle, in correspondence of the previous values, therefore $K_o > 1$ until it reaches the $K_o \cong 3$ maximum value, beyond which the failure is achieved. The range of variation of the coefficient of thrust at rest, therefore, is $K_o = 0.4 - 2.5$ and it can be simulated with the oedometric test.

In the case of overconsolidated cohesive soils, if geologically predictable on the basis of the pre-consolidation stress, or, on the basis of the extrapolation of soil profile, the thickness of the eroded layer, it can be evaluated, in principle, the resulting increase of K_o .

For example, if in the past the thickness of a layer with a unit weight of $\gamma = 2 \text{ t/m}^3$, assumed dry for reasons of simplicity, was 100 m with $K_o = 0.5$ a horizontal stress of $\sigma_{ho} = 0.5 \cdot 2 \cdot 100 = 100 \text{ t/m}^2$ was obtained at the base; if the current thickness is 25 m, it is obtained $K_o \cong 100/2 \cdot 25 = 2$, if assuming σ_{ho} constant prior to unloading.

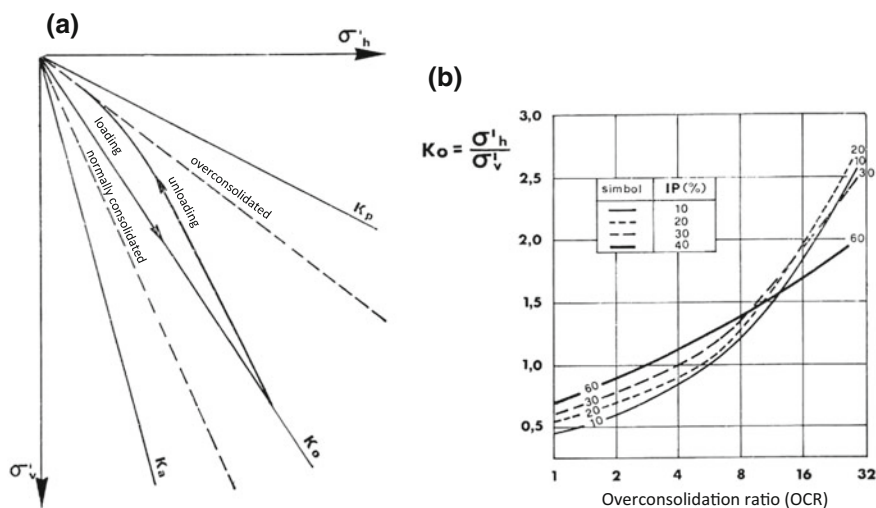


Fig. 2.6 Variability of $K_o = \sigma'_h/\sigma'_v$ in function of the degree of saturation. The zone comprised between K_o and K_a is representative of normally consolidated clays and the zone comprised between K_o and K_p of overconsolidated clays; **a** geological unloading effect (Henkel 1960); **b** plasticity index effect (from Cestelli Guidi 1987)

As a consequence, in overconsolidated soils, the coefficient $K_o(OC)$ increases and is evaluated via empirical formulas such as (Schmidt 1966; Alpan 1967):

$$K_o(OC) = K_o(NC) \cdot OCR^\alpha$$

where for the exponent α it can be suggested a value of 0.46 ± 0.06 and it seems that such value is applicable also to every further unloading starting from the normally consolidated condition (NC). If the overconsolidation ratio is modest ($OCR = 4-5$), the value of $K_o(OC)$ is close to unity and the unloading, considered as linear, can be interpreted in terms of theory of elasticity (Wroth 1975).

2.3.1 Passive Thrust

If, starting from the state of equilibrium at rest, in particular of hydrostatic type ($K_o = 1$), a deformation is applied to the soil volume, inducing compression on the horizontal direction, such as in an element of volume like the one reported on Fig. 2.7, it induces the two vertical faces, a-c and b-d, to get closer, an increase in the horizontal stresses is derived such that $K_o > 1$; in fact, $K_o = \frac{\sigma_{ho}}{\sigma_{vo}}$ for $\sigma_{ho} > \sigma_{vo}$, K_o is > 1 . When the horizontal stresses achieve the maximum value compatible with the static equilibrium, then $\sigma_1 = \sigma'_h$ and $\sigma_3 = \sigma'_{vo}$.

It is possible to check by means of the Mohr's diagram (Fig. 2.8) that, at failure, a well-defined relationship exists between the maximum principal stress σ_1 and the minimum one σ_3 .

From the geometry

$$\sigma_1 + d = OA + AB \quad \text{being } AB = OA \text{ sen } \varphi$$

$$\sigma_3 + d = OA - AB$$

$$\sigma_1 + d = OA + OA \text{ sen } \varphi = OA (1 + \text{sen } \varphi)$$

$$\sigma_3 + d = OA - OA \text{ sen } \varphi = OA (1 - \text{sen } \varphi)$$

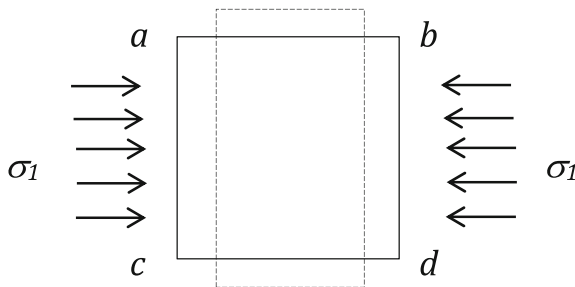


Fig. 2.7 Lateral compression

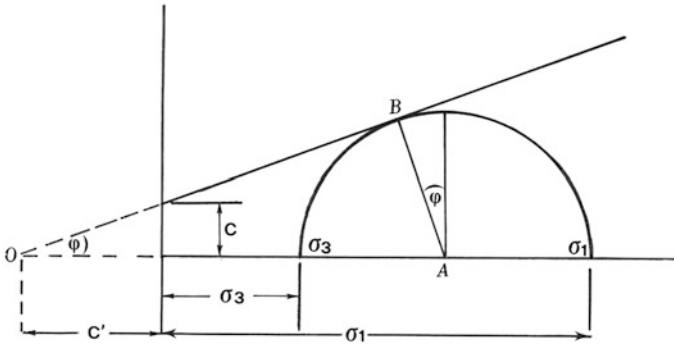


Fig. 2.8 Failure condition in terms of Mohr's circle

therefore, given that the unknown is $\sigma_1 = \sigma_{hp}$ = passive thrust or limit strength

$$OA = \frac{\sigma_1 + d}{1 + \text{sen } \varphi} = \frac{\sigma_3 + d}{1 - \text{sen } \varphi} \sigma_1 + d = \frac{\sigma_3 + d}{1 - \text{sen } \varphi} (1 + \text{sen } \varphi)$$

$$\sigma_1 = \sigma_3 \frac{1 + \text{sen } \varphi}{1 - \text{sen } \varphi} + d \left(\frac{1 + \text{sen } \varphi}{1 - \text{sen } \varphi} - 1 \right)$$

because

$$d = \text{cotg } \varphi = c \frac{\cos \varphi}{\text{sen } \varphi} = c \frac{\sqrt{1 - \text{sen}^2 \varphi}}{\text{sen } \varphi}$$

putting

$$\sigma_1 = \sigma_3 \frac{1 + \text{sen } \varphi}{1 - \text{sen } \varphi} + 2c \sqrt{\frac{1 + \text{sen } \varphi}{1 - \text{sen } \varphi}}$$

therefore

$$\sigma_1 = \sigma_3 \text{tg}^2 \left(45 + \frac{\varphi}{2} \right) + 2 \text{ctg} \left(45 + \frac{\varphi}{2} \right)$$

considering

$$N_\varphi = \text{tg}^2 \left(45 + \frac{\varphi}{2} \right)$$

$$\sigma_1 = \sigma_3 N_\varphi + 2c \sqrt{N_\varphi}$$

then

$$\sigma'_{hp} = \sigma'_{vo} N_\varphi + 2c\sqrt{N_\varphi} \quad \text{passive thrust or limit strength.}$$

The element achieved the upper limit equilibrium state.

From this, assuming $c = 0$ or drained conditions, it is obtained:

$\sigma_1 = \sigma_3 N_\varphi$ and the limit equilibrium coefficient K_p is

$$K_p = \frac{\sigma'_{hp}}{\sigma'_{vo}} = \frac{\sigma_1}{\sigma_3} = N_\varphi = \text{tg}^2 \left(45 + \frac{\varphi}{2} \right) = \frac{1 + \text{sen } \varphi'}{1 - \text{sen } \varphi'}$$

defined as *upper limit equilibrium coefficient* or *upper limit strength coefficient* or *passive thrust coefficient*.

In the case of saturated cohesive soils, or for $\varphi_u = 0$, it is obtained:

$$\sigma_{hp} = \sigma'_{vo} + 2c_u$$

then $\sigma_1 = \sigma_3 + 2c_u$ and $K_p = 1$ that physically corresponds to the fluid plastic state.

2.3.2 Active Thrust

If, instead, starting from the equilibrium state at rest $K_o = \frac{\sigma'_{ho}}{\sigma'_{vo}}$ a motion of expansion of the volume in the horizontal direction is activated, with the faces a–c and b–d of the elementary volume moving away (Fig. 2.9), a reduction in the horizontal stress σ_h is obtained, starting from the value σ_{vo} ; in that case, K_a is defined as *lower limit equilibrium coefficient* or *lower limit strength coefficient* or *active thrust coefficient* and is a value lower than 1 ($K_a = \frac{\sigma'_{ha}}{\sigma'_{vo}} < 1$).

Mohr's circle falls to the left of σ_{vo} on Fig. 2.8 because, in conditions of active thrust is obtained that (Fig. 2.10).

$$\sigma'_{vo} = \sigma_1 \quad \text{and} \quad \sigma'_{ha} = \sigma_3$$

In the condition of limit equilibrium, or when the boundary of the Mohr's circle touches the limit lines, the horizontal stress ($\sigma_{ha} = \sigma_3$) lowers to its minimum value and, therefore:

$$\begin{aligned} \sigma_1 + d &= OA' + A'B' \\ \sigma_3 + d &= OA' + A'B' \end{aligned}$$

being $A' B' = OA' \text{ sen } \varphi$, then:

$$\begin{aligned}\sigma_1 + d &= OA' + OA' \text{ sen } \varphi = OA' (1 + \text{sen } \varphi) \\ \sigma_3 + d &= OA' + OA' \text{ sen } \varphi = OA' (1 - \text{sen } \varphi)\end{aligned}$$

$$OA' = \frac{\sigma_1 + d}{1 + \text{sen } \varphi} = \frac{\sigma_3 + d}{1 - \text{sen } \varphi}$$

From which

$$\sigma_3 + d = \frac{\sigma_1 + d}{1 + \text{sen } \varphi} (1 - \text{sen } \varphi)$$

$$\frac{\sigma_3(1 + \text{sen } \varphi) + d(1 + \text{sen } \varphi)}{1 + \text{sen } \varphi} = \frac{\sigma_1(1 - \text{sen } \varphi) + d(1 - \text{sen } \varphi)}{1 + \text{sen } \varphi}$$

$$\sigma_3 \frac{(1 + \text{sen } \varphi)}{1 + \text{sen } \varphi} = -d \frac{(1 + \text{sen } \varphi)}{1 + \text{sen } \varphi} + \sigma_1 \frac{(1 - \text{sen } \varphi)}{1 + \text{sen } \varphi} + d \frac{(1 - \text{sen } \varphi)}{1 + \text{sen } \varphi}$$

$$\sigma_3 = \sigma_1 \frac{1 - \text{sen } \varphi}{1 + \text{sen } \varphi} + d \left(\frac{1 - \text{sen } \varphi}{1 + \text{sen } \varphi} - 1 \right)$$

$$\sigma_3 = \sigma_1 \frac{1 - \text{sen } \varphi}{1 + \text{sen } \varphi} - 2c \sqrt{\frac{1 - \text{sen } \varphi}{1 + \text{sen } \varphi}}$$

Being

$$\frac{1 - \text{sen } \varphi}{1 + \text{sen } \varphi} = \text{tg}^2 \left(45 - \frac{\varphi}{2} \right)$$

$$\sigma_3 = \sigma_1 \text{tg}^2 \left(45 - \frac{\varphi}{2} \right) - 2c \text{tg} \left(45 - \frac{\varphi}{2} \right)$$

because

$$N_\varphi = \text{tg}^2 \left(45 + \frac{\varphi}{2} \right) \text{tg}^2 \left(45 - \frac{\varphi}{2} \right) = \frac{1}{N_\varphi}$$

it is obtained

$$\sigma_3 = \sigma_1 \cdot \frac{1}{N_\varphi} - 2c \frac{1}{\sqrt{N_\varphi}}$$

then $\sigma_{ha} = \sigma_{vo} \cdot \frac{1}{N_\varphi} - 2c \frac{1}{\sqrt{N_\varphi}}$ Active thrust

From this, for $c = 0$ or under drained conditions it is obtained:

$$\sigma_{ha} = \sigma_{vo} \cdot \frac{1}{N_\phi} \text{ Active thrust in drained soils}$$

And the K_a *limit equilibrium coefficient* is:

$$K_a = \frac{\sigma_{ha}}{\sigma_{vo}} = \frac{1}{N_\phi} = \text{tg}^2 \left(45 - \frac{\phi}{2} \right) \text{ in drained soils}$$

In the case of saturated cohesive soils, or for $\phi_u = 0$, undrained conditions, it is obtained:

$$K_a = \text{tg}^2 45^\circ = 1 \text{ that physically corresponds to } K_p, \text{ or to fluid plastic state,}$$

and $\sigma_{ha} = \sigma'_{vo} - 2c_u$ *active thrust* in undrained saturated soils.

2.4 The Failure Process (from Bles and Feuga 1981)

During a simple compression test on a generic rock, to each stress σ corresponds a strain ε such that it is possible to define a stress-strain curve σ - ε (Fig. 2.11).

The stress-strain curves of various rocks show two distinct states of strain. On the first stage, the strain is minimum if compared to the increase in stress and when the load decreases the rock gets back to its initial shape. This stage corresponds to the *elastic domain*.

Once is overtaken the elastic threshold, strain becomes irreversible and the rock can provide two different limit behaviours:

- (a) failure is immediately achieved (*brittle deformation domain*, Fig. 2.12);
- (b) strain develops without relevant increments of the stress, identifying the *plastic deformation domain* (Fig. 2.13a-c).

In the first case, it is stated that the rock as an *elastic-brittle* behaviour and in the second case the behaviour is defined as *elastic-plastic*. The two behaviours are independent from the time factor. If the strain is influenced by time, the strain velocity results to be a function of stress and the behaviour is defined as *viscous*.

The tectonic cracking generally corresponds to an elastic-brittle behaviour of the rocks.

2.4.1 Failure of Rocks Under Tension

Tensile tests can be carried out in direct or indirect manners, depending on how the forces are applied.

In the *direct tensile test*, a stress- σ_1 is applied to parallel faces of the rock sample (the test can be carried out by applying the σ_3 stress or not) (Fig. 2.14).

In the *indirect tensile test* (also called *the Brazilian test*) a compression is applied to two opposite generative lines of a cylindrical rock sample (Fig. 2.15).

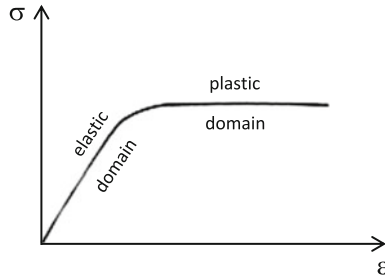


Fig. 2.11 Plastic type behaviour

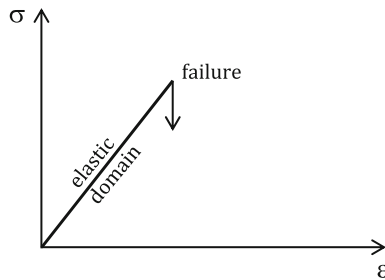


Fig. 2.12 Brittle type behaviour

In all the cases, the failure is induced on a plane perpendicular to the tensile stress.

In the Brazilian test, the theory of elasticity establishes that a uniform tensile stress is generated on the plane containing the two generative forces according to which the compression is exerted.

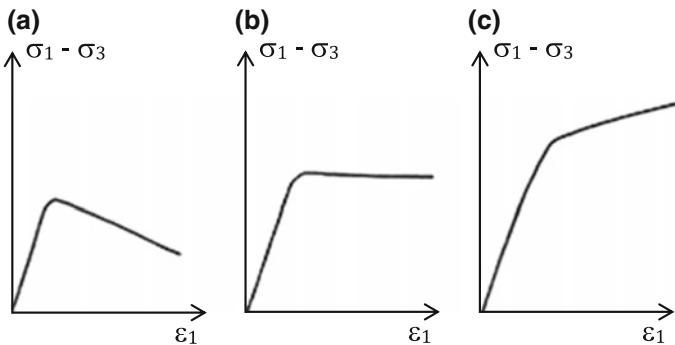


Fig. 2.13 **a** Plastic with strain softening or ductile type behaviour; **b** moderate plastic behaviour; **c** plastic behaviour with strain hardening

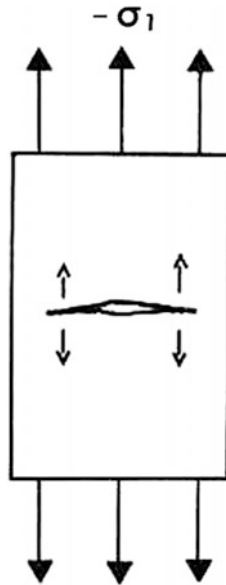


Fig. 2.14 Tensile failure

The failure is induced on this plane. The principal stress σ_1 lies on the same plane, producing a *tension crack* parallel to F and normal to the tensile stress.

In the direct tensile test, the plane of failure is not imposed and, therefore, the position of cracks is induced by the presence of micro-cracks on the sample.

The induced stress is concentrated on the sides of the micro-crack located perpendicularly to the stress and, when the limit strength is achieved, a brutal failure is obtained due to the propagation of the crack at its ends (Fig. 2.15. b2).

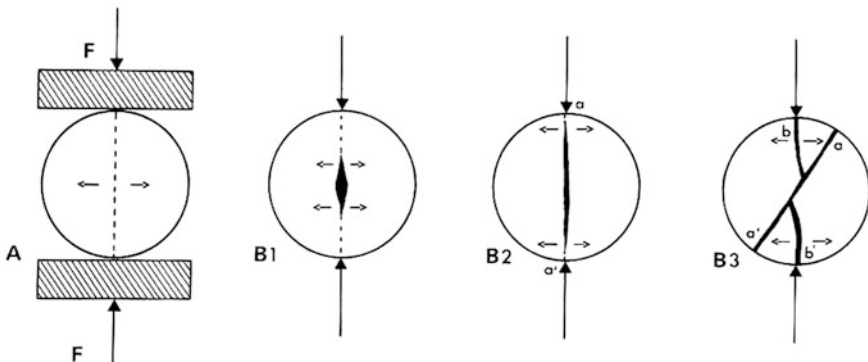


Fig. 2.15 Sample cracking after a Brazilian test

The tensile strength is inversely proportional to the squared root of the length of the crack

$$\rho = \frac{1}{\sqrt{l}}$$

The tensile strength of rocks is significantly lower than the compressive strength. This means that in a triaxial stress field, while σ_1 exerts a strong compression for achieving the limit strength of the rock, σ_3 (minimum stress) induces the generation of tension cracks because of its tensile nature.

In both the cases of tensile conditions, the cracks that are produced are always normal to the tensile stress. Thus, generalising, all the tension cracks are normal to the tensile stress and parallel to the principal compressive stress (Fig. 2.15).

From Fig. 2.15, b3, by rotating the plane in which crack a–a' is contained in a way that this becomes oblique to the diametric plane F–F, a new crack b–b' is obtained after the closing of the first one with a penetration line corresponding to the level of intersection of the two cracks.

This crack allows to understand that it's development is subsequent to the formation of a–a'.

2.4.2 Failure of Rocks Under Compression

The most intuitive method for measuring shear strength is to submit the samples to triaxial compression, extending the use of techniques developed for loose soils. This is what is done, in practice, taking into account the specific issues of lithoid materials.

– Theoretical failure in the absence of σ_3

When a cylindrical sample is subjected to a compressive stress σ_1 the failure is produced in general along one or two planes oblique to σ_1 . This means that σ_1 breaks up, within the samples, in two components: σ_n normal to the failure plane and τ , tangential to the plane of failure (Fig. 2.16). In the absence of σ_3 (unconfined compressive test) the values of σ_n and τ can be easily calculated.

Being ab the trace of the failure plane; bb' is perpendicular to ab' and assumed equal to 1; be θ the angle between the direction of σ_1 and the failure plane. It is obtained

$$bb' = ab \sin \theta \quad \text{da cui } ab = 1 / \sin \theta.$$

At failure plane ab , because of tilting, is larger than plane bb' ; given that σ_1 applies a force on the surface (bb'), the components of σ_1 (σ_n and τ) do not act on the same unit surface, but on a surface greater than the unit one because of the

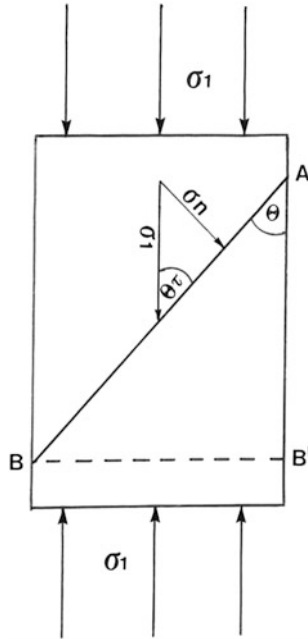


Fig. 2.16 Theoretical failure in the absence of σ_3

coefficient $1/\sin\theta$ (dimensionless factor). As a consequence, the components of σ_1 on plane ab are:

$$\sigma_n = \frac{\sigma_1 \sin \theta}{\frac{1}{\sin \theta}} = \sigma_1 \sin^2 \theta$$

$$\tau = \frac{\sigma_1 \cos \theta}{\frac{1}{\sin \theta}} = \sigma_1 \sin \theta \cos \theta = \frac{1}{2} \sigma_1 \sin 2 \theta$$

For a given θ , σ_n and τ can be thus calculated. The maximum value of the shear stress (τ) is obtained for $\theta = 45^\circ$; in facts, $\sin 2\theta = \sin 90^\circ = 1$ and therefore

$$\tau = \frac{1}{2} \sigma_1 \quad \text{and} \quad \sigma_n = \sigma_1 \cdot 0.5 = \frac{1}{2} \sigma_1$$

so

$$\sigma_n = \tau = \frac{\sigma_1}{2}$$

Drawing the Mohr's circle (Fig. 2.17), when $\sigma_3 = 0$, it is obtained that the circle has the origin at the intersection of the axes. It can be observed that for $\theta = 45^\circ$ $\sigma_n = \frac{1}{2} \sigma_1$ and $\tau = \frac{1}{2} \sigma_1$.

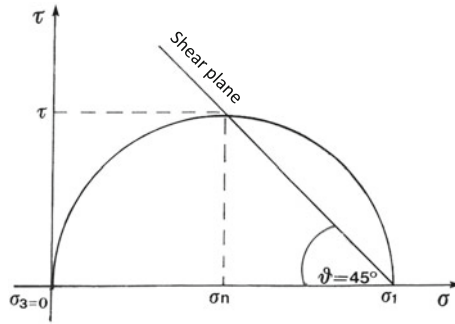


Fig. 2.17 Mohr's circle for $\sigma_3 = 0$

– Theoretical failure in presence of σ_3

It must be pointed out that in the nature a rock is subjected to a state of triaxial compression and that its behaviour depends on the relative values of $\sigma_1, \sigma_2, \sigma_3$.

A sketch of two-dimensional compression for σ_1 and σ_3 on a plane of failure shows that the effects due to the normal components σ_{n1} and σ_{n3} derived from σ_1 and σ_3 sum up when shear stress τ_3 , due to σ_3 , acts on the opposite direction of shear stress τ_1 , due to σ_1 (Fig. 2.18). Actually, given that the effective stresses control the stress-strain behaviour of the rock, a failure criterion is better defined when it is expressed in terms of effective stresses. As a consequence, peak resistance is of the type:

$$\sigma_1 = f(\sigma_2, \sigma_3)$$

i.e. σ_1 is a function of σ_2 and σ_3 .

Given that data from laboratory tests indicate that the intermediate principal stress σ_2 has less influence on peak resistance than the minimum stress σ_3 , the criteria generally used reduce to the form:

$$\sigma_1 = f(\sigma_3)$$

Therefore σ_3 plays a very important role on the cracking of rock. This stress condition can be easily represented in terms of Mohr's circle. The construction derives from the failure conditions. Reporting τ and σ on the Cartesian plane, putting the values of σ_1 and σ_3 from the test on the abscissa and the Mohr's circle is drawn (Fig. 2.19a). The angle θ , then, defines the tilting of the failure plane with respect to σ_1 (Fig. 2.19b).

Reporting this relationship in terms of shear stress τ and of normal stress σ_n is obtained what described on Fig. 2.20.

$$\tau = f(\sigma_n)$$

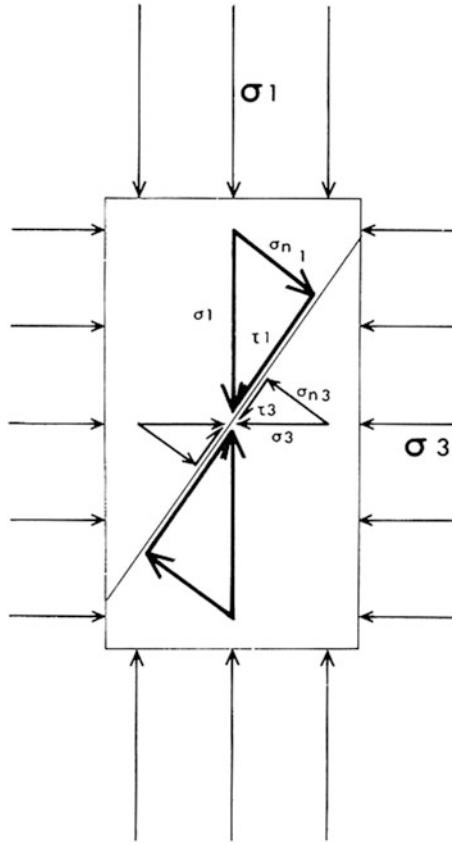


Fig. 2.18 Influence of σ_3 confining pressure on brittle failure (from Bles and Feuga 1981)

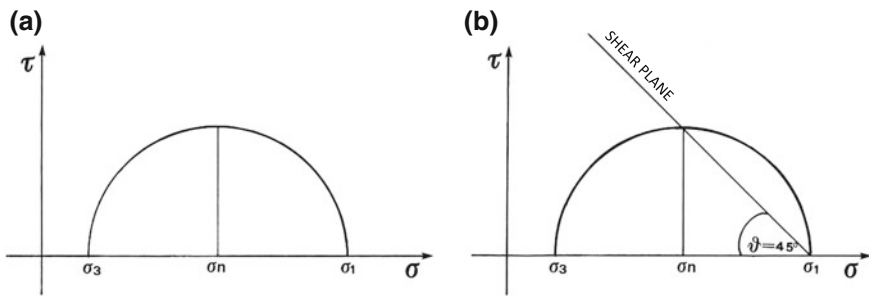


Fig. 2.19 Mohr's circle for $\sigma_3 > 0$

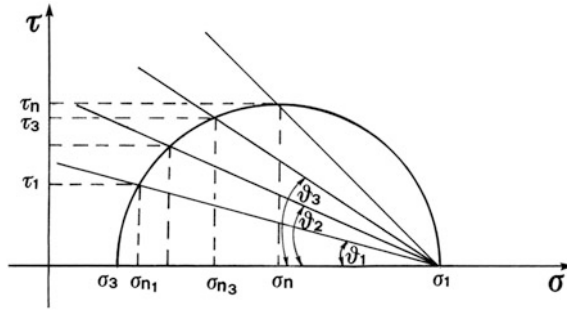


Fig. 2.20 Reduction of angle θ in function of σ_n .

In facts, from the Mohr's circle can be observed that θ reduces in function of the reduction in σ_n and vice versa. From this it can be also observed that by reducing σ also σ_n and τ reduce.

Using the Mohr's circle, the values of σ_n and τ , normal and shear stresses respectively can be easily calculated, as derived from σ_1 . From the graph in Fig. 2.21 it is obtained:

$$\sigma_n = OC - PC \quad \text{being } PC = R \cos 2\theta = \frac{\sigma_1 - \sigma_3}{2} \cos 2\theta$$

$$\sigma_n = \frac{\sigma_1 + \sigma_3}{2} - \frac{\sigma_1 - \sigma_3}{2} \cos 2\theta$$

$$\tau = R \sin 2\theta = \frac{\sigma_1 - \sigma_3}{2} \sin 2\theta$$

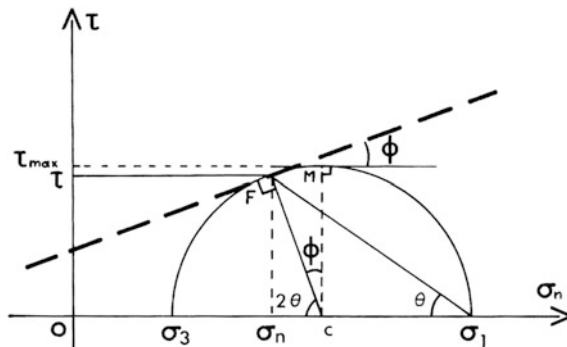


Fig. 2.21 Bi-dimensional representation of tensors σ_1 and σ_3 by means of the Mohr's circle (from Bles and Feuga 1981)

Also in this case, shear is maximum for $\theta = 45^\circ$; in facts:

$$\begin{aligned}\cos 2\theta &= \cos 90^\circ = 0 \\ \sin 2\theta &= \sin 90^\circ = 1\end{aligned}$$

therefore, the maximum value at failure is:

$$\tau = \frac{\sigma_1 - \sigma_3}{2}$$

in this case

$$\sigma_n = \frac{\sigma_1 + \sigma_3}{2}$$

It must be considered, however, that for $\theta = 45^\circ$, i.e. in correspondence of τ_{max} , it is obtained that $\varphi = 0$.

This means that τ is maximum only when $\varphi = 0$, condition that can be observed in the tensile test when the whole shear strength is provided by the effective cohesion only or when dealing with a saturated cohesive soil in undrained conditions.

Notwithstanding this, in laboratory compression tests the angle θ is always lower than 45° . This is due to the shear strength typical of the rock considered; this strength considers in every rock the presence of a friction angle

$$\begin{aligned}\varphi &= \frac{\pi}{2} - 2\theta \\ \varphi &= 90^\circ - 2\theta\end{aligned}$$

As a consequence, by having knowledge of the value of θ (from the site) it is possible to evaluate the friction angle of the material.

By carrying out additional shear tests with variable values of σ_1 and σ_3 (positive, negative or null), a Mohr's circle can be defined for every test representing the values of the stresses at the condition of limit equilibrium, i.e. immediately before the failure. The envelope of the Mohr's circles is called intrinsic curve and defines the stable domain, where it is not possible to achieve the failure, from the instable domain, where the failure is achieved (Fig. 2.22).

If, after achieving the failure condition, on the same sample it is increased the applied deformation, the shear strength reduces until it reaches a minimum value, corresponding to the "residual" shear strength (Fig. 2.23). Figure 2.24 reports the envelope curve for the maximum and minimum values of the shear stress obtained on the same sample. The vertical distance between the two envelopes indicates the loss in shear strength undergone by increasing the deformation.

The equation of the enveloping line was defined by Coulomb (1773), who postulated that the shear strength is due to the sum of two components: a *cohesion*, constant, and a strength due to the internal friction depending on the normal stress (σ_n). Coulomb developed his theory in terms of stresses on the shear plane *ab* and

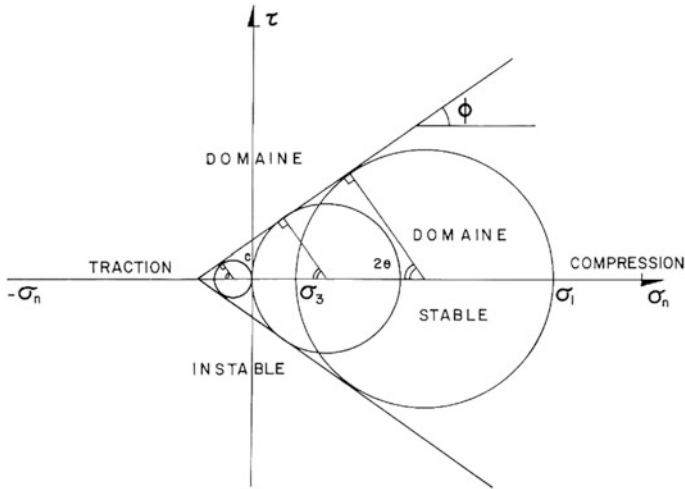


Fig. 2.22 Mohr's circles at failure with the corresponding intrinsic curves (from Bles and Feuga 1981)

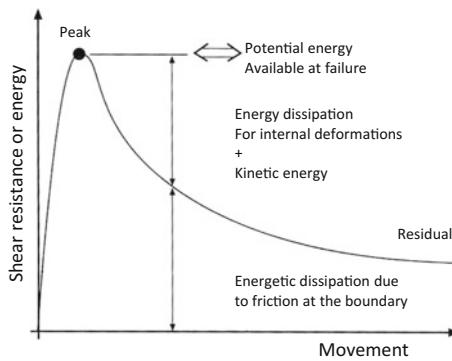


Fig. 2.23 Peak shear strength and energy dissipation mechanism until reaching a value of shear stress at failure correspondent to the residual shear strength (from Leroueil et al. 1996, modified)

found the relationship between shear stress τ and normal stress σ_n by assuming the enveloping curve as a straight line:

$$\tau = \tau_o + \sigma_n \text{tg } \varphi$$

The equation establishes that the shear strength τ available on a sliding plane is a function of the normal stress σ_n acting on the plane and of the characteristics of the material τ_o and $\varphi \cdot \tau_o$ which was later called as cohesion “c”; this represents the shear strength when $\sigma_n = 0$.

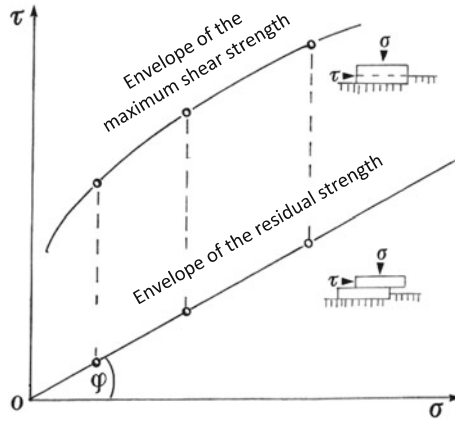


Fig. 2.24 Envelope of the maximum and minimum shear stresses of a cohesive rock sample

The intrinsic curve, or the envelope of Mohr’s circles, can assume different shapes according to the different types of rocks; in facts, the Mohr’s circle (Figs. 2.20 and 2.21) shows that by increasing θ the angle φ reduces and this means that when φ reduces the cohesion increases, meaning that there is a passage from granular materials to predominantly cohesive materials.

- (a) In the case of saturated clays, the envelope curve is parallel to the axis of the abscissa (Fig. 2.25). The shear strength is independent from normal stress σ_n and is always equal to cohesion c_u , short-term behaviour for $\varphi = 0$.

Saturated clays $\tau = c$ and $2\theta = \frac{\pi}{2} = 90^\circ$

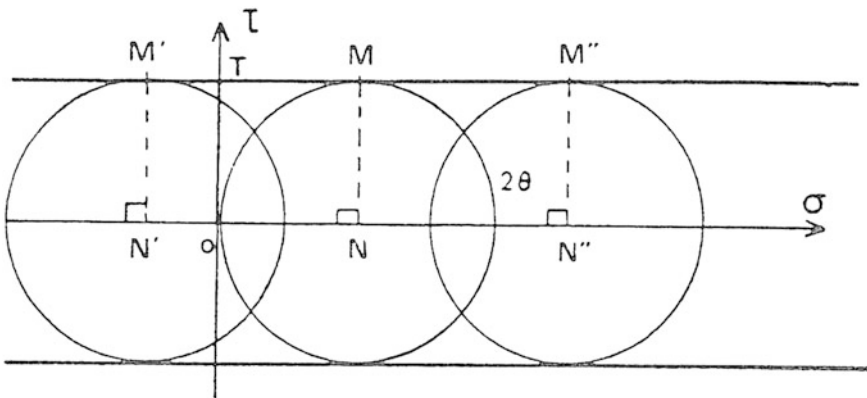


Fig. 2.25 Undrained behaviour of a compact clayey soil

- (b) In the case of granular materials, cohesion is absent and the friction angle is constant. The envelope curve is a straight line passing through the origin of the axes (Fig. 2.26). Cohesion $\tau_o = c$ is null. The shear strength is indirectly linked to the normal stress σ_n .
- (c) For rocks, the cohesion is not null, but the internal friction angle varies in function of the normal stress σ_n ; τ_o and ϕ vary in function of the applied principal stress (Fig. 2.27).

The envelope curve, or intrinsic curve, provides therefore a certain number of information:

- (a) It defines the domains where, for different values of σ_1 and σ_3 , a rock is stable, meaning that it strains without failing, or is unstable, therefore it deforms with failure.
- (b) It allows immediately to understand the angle θ , which defines the shear plane with σ_1 , or the angle 2θ , which defines the two conjugated failure planes.

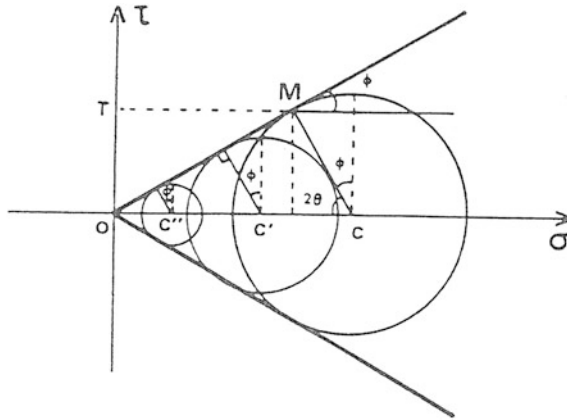


Fig. 2.26 Intrinsic curve of a sand

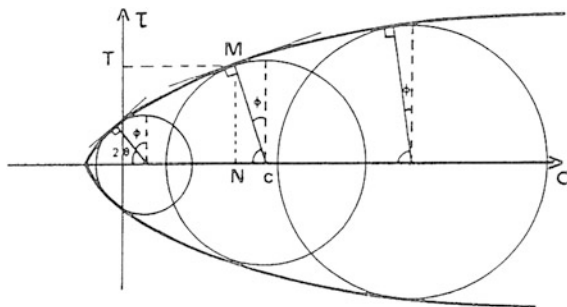


Fig. 2.27 Intrinsic curve of a limestone

- This angle increases, generally, when stress σ_1 increases. It will be, therefore, as much close to 90° as the greater will be the lithostatic pressure (i.e. at a greater depth) and it will be the lower when closer to the ground surface, where $\sigma_3 = 0$.
- (c) It provides the several values of φ ; φ is equal to the tilting of the envelope curve and $\tan \varphi$ corresponds to the internal friction coefficient. Therefore, if φ has a large value, the rock has a brittle behaviour; otherwise, it has a ductile behaviour. The brittle behaviour of a rock becomes ductile if the test is carried out by applying a value very large of σ_3 , i.e. if the deformation takes place at a great depth.
- (d) It shows, in general, that the tensile strength of a rock is considerably lower than the compressive strength and this is particularly true in the case of rocks with brittle behaviour. Angle θ reduces, actually, when φ grows up and, in tensile tests, it can be observed that θ achieves its minimum value; therefore, θ can assume very low values (10° – 20°), tending to zero at the depth where tensile stress goes to zero.

Failures, therefore, are considerably different if they are induced by compression or by traction, at the surface or at depth. The envelope curve, furthermore, assumes a different shape depending on the type of rock.

2.5 The Influence of Pore-Water Pressure

The rocks of the Earth's crust are very often saturated with water. This retained water influences abundantly their behaviour, in particular at failure.

Fluids, at great depth, are very often characterised by pressures greater than the hydrostatic. Sometimes, these pressures are as large as 95% of the lithostatic pressure.

Rocks, in general, are more deformable when they are saturated. They change their behaviour depending on the moisture content. From ductile for low fluids pressures, become brittle at high pore-water pressures. This can be easily understood with the aid of Mohr's circles.

Let us suppose that a rock, in the absence of fluids, therefore under drained conditions, is subjected to certain values σ_1 and σ_3 such as it is not subjected to failure (Fig. 2.28, curve A). If this rock is soaked with water, a pore-water pressure u develops and the stress applied to the rock is $\sigma_3 - u$ and $\sigma_1 - u$; the corresponding Mohr's circle on Fig. 2.28 is therefore curve B, shifting leftwards and intersecting the failure plane.

In these conditions is introduced the concept of *total stresses* σ and *effective stresses* σ'

$$\sigma' = \sigma - u \quad \tau' = \tau$$

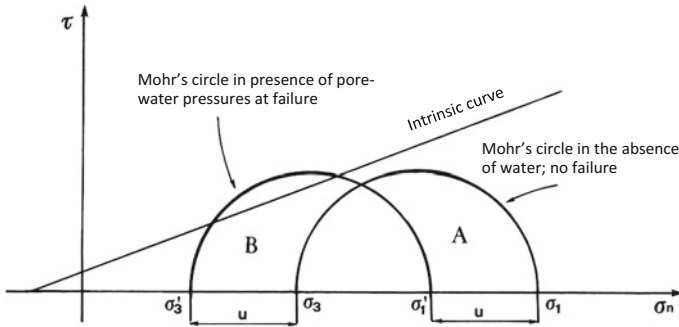


Fig. 2.28 Role of pore-water pressure on the failure of a cohesive rock

After the formulation of the principle of effective stresses (Terzaghi 1936) and of the related experimental confirmations, the Coulomb's equation $\tau = \tau_o + \sigma_n \cdot tg\varphi$ can be written, more properly, in terms of effective stresses

$$\tau = c' + (\sigma_n - u) tg \varphi' \quad (\text{corrected Coulomb's equation})$$

where

- σ_n stress normal to the shear plane
- u pore-water pressure
- c' drained cohesion (effective cohesion)
- φ' drained internal friction angle (under effective stresses).

Obviously, all the points in the circular segment *AB* external to the intrinsic curve have no physical meaning, as they represent a stress status that cannot exist in reality, as it is not compatible with the strength of the material.

In an analogous way, if the voids of an isotropic soil are filled only with air at the atmospheric pressure, the conditions $\alpha = 45^\circ + \frac{\varphi}{2}$ and $\tau = c + \sigma_n tg\varphi$ can be considered as verified (Coulomb's equation).

The analysis just completed on the *principle of effective stresses*, on the *conditions of equilibrium* and on the *failure process*, outlines the nature and characteristics of the soils within a reduced and homogeneous volume of themselves. This analysis assimilates the mechanical behaviour of the soil to a material with an elastic-perfectly plastic behaviour by supposing that under sliding conditions the stress field remains constant and independent from deformation and time. These general principles that rule the failure process remain valid and essential only if the strain at failure on natural slopes is considered as dependent, at the beginning of the sliding, on the initial stress field and varies from soil to soil within a rather recurrent range. In facts, a soil is never a homogeneous material. Also soils that seem to be homogeneous under visual inspection, when examined at a deeper level show almost always considerable heterogeneity in constitution and in physical characteristics. The definition of a model describing, from a global point of view, the

behaviour of different materials, intimately interacting, is a problem that admits only empirical and subjective solutions. Furthermore, in several cohesive soils macro-structures are present, constituted by discontinuity surfaces, organic inclusions, depositional joints and thin heterogeneous intercalations. The characteristics of deformability and resistance of a volume of soil large enough to contain a number of discontinuities with various orientations are substantially different from the ones of a small intact volume.

In other terms, both the heterogeneity and the natural discontinuities introduce in the behaviour of the soils the influence of a “*scale factor*”, intended generically as the ratio between the dimensions of the soil element considered and the spacing of the heterogeneity and of the discontinuities. A model of mechanical behaviour making reference to a continuous and heterogeneous medium has no possibility to describe a natural, heterogeneous and fissured soil. It is also true, however, that by introducing corrective empirical coefficients, the response of the general model of a continuous medium can be modified in order to make it more similar to the real behaviour of the natural soil, but the diversity of the mechanical phenomena that take place together with the deformations of a continuum medium and of a set of distinct solid elements, interacting along surfaces of discontinuity, substantially limits the validity of similar empirical solutions.

In the following it will be demonstrated how to solve these problems for the purpose of the *prediction* and of the *prevention* of landslides in cohesive soils.

References

- Alpan, I. (1967). *The empirical evaluation of the coefficients K_0 and K_{or}* . *Soils and Foundations*, 7, 31–40.
- Bishop, A. W. (1966). *The strength of soils as engineering materials*. *Geotechnique*, 16, 91–130.
- Blès J. L., & Feuga B. (1981). *La fracturation des roches*, Bureau de recherches géologiques et minières - Editions du B.R.G.M., BP 6009, 45060 Orleans cedex.
- Cancelli A., & Pellegrini M. (1987). Deep-seated gravitational deformations in the Apennines, Italy. In *Proceedings 5th International Conference and Field Workshop on Landslides*, (pp. 171–178), Christchurch.
- Cestelli Guidi C. (1987). *Geotecnica e tecnica delle fondazioni*, vol. 1, 8^a edizione, Hoepli U., Milano.
- Colomb P. (1978). *Elementi di Geotecnica*. Bologna: Zanichelli Editore S.p.A. (1).
- Coulomb C. A. (1773). *Essai sur une Application des Regles de Maximis et Minimis a Quelques Problemes de Statique Relatifs a l'Architecture*, Mem. Div. Sav. Acad., v. 7.
- Darcy H. (1856). *Le fontaines publiques de la ville de Dijon*. Paris.
- Eigenbrod, K. D., Graham, J., & Burak, J. P. (1992). Influence of cycling porewater pressures and principal stress ratios on drained deformations in clay. *Canadian Geotechnical Journal*, 29(2), 326–333.
- Guerricchio A., & Melidoro G. (1988). *Franosità nei Territori Comunali di Gorgoglione e Cirigliano (Basilicata)*. Conv. “Cartografia e Monitoraggio dei Movimenti Franosi” - C.N.R., Bologna, 10–11 novembre 1988, pp. 65–85.
- Henkel D. J. (1960). The shear strength of saturated remolded clays. In *Proceedings of ASCE Research Conference on Shear Strength of Cohesive Soil* (pp. 533–554). Boulder, colo.

- Jaky, J. (1944). The coefficient of earth pressure at Rest. *Journal of the Society of Hungarian Architects and Engineers*, 7, 355–358.
- Lancellotta, R. (1987). *Geotecnica*. Bologna: Zanichelli N. Editore S.p.A.
- Leroueil S., Vaunat J., Picarelli L., Locat J., Lee H. J., & Faure R. (1996). Geotechnical characterization of slope movements. In *Atti del 7° International Symposium on Landslides, Trondheim* (Vol. 1, pp. 53–74).
- Massarsch K. R. (1979). Lateral earth pressure in normally consolidated clay. In *Proceedings of the VII ECSMFE Brighton* (Vol. 2, pp. 245–249).
- Matheson D. S., & Thomson (1973) Geological implications of valley rebound. *Canadian Journal Earth Sciences*, X, 961–978.
- Mohr H. (1962). *Exploration of Soil Conditions and Sampling Operations*, Harvard Bull., No 208 revised.
- Pasek J. (1974). Gravitational block-type slope movements. In *Proceedings 2nd International Congress IAEG, Sao Paulo* (Vol. II, th. V-PC-1).
- Picarelli L. (1991). *Resistenza e meccanismi di rottura nei terreni naturali*. Atti del II Congr. Gruppo Naz. di Coord. per gli Studi di Ingegneria Geotecnica del CNR “Deformazioni in prossimità della rottura e resistenza dei terreni naturali e delle rocce”, TEMA II “Problemi al finito”, Ravello, Vol. II, pp. II-7-II-61.
- Rankine, W. J. M. (1857). On the stability of loose earth. *Philosophical Transactions of the Royal Society*, 147, 9–27.
- Schmidt, B. (1966). Discussion on earth pressure at rest related to stress history. *Canadian Geotechnical Journal*, 3, 239–242.
- Terzaghi K. (1936). The shearing resistance of saturated soils. In *Proceedings First ICSMFE* (vol. 1, pp. 54–56).
- Wroth C. P. (1975). In situ measurement of initial stress and deformation characteristics. In *Proceedings of the ASCE, Specialty Conference on In Situ Measurement of Soil Properties* (Vol. 2, pp. 181–230). Raleigh: North Carolina State University.

Chapter 3

The Dating of Landslides

3.1 Introduction

It is often necessary to date the landslides not only to trace the causes of the failure of a slope but essentially to define the environmental factors interacting in the process of changing the natural environment.

Archaeological evidences can provide some information on dating; Hutchinson and Gostelow (1976) used old maps, aerial photographs and historical evidences (including a nineteenth-century manuscript) to trace back the movement of a slope in the nearby of Hadleigh Castle in Essex, England. In other places, evidences of the regression of cliff lines have been obtained from old editions of OS maps. Aerial photographs can be enough supportive in type and number to replace topographic maps, although this is only possible in special situations, such as the Stag Hill landslide case (England), on which a part of the building of the University of Surrey was later built on.

3.2 General Overview of Quaternary Subdivisions in Marine Environment

To reconstruct the story of a landslide, especially if it is very ancient, it is necessary to determine the related spatial relations and the temporal succession from the moment of its genesis to the one of the quiescence. It must not be forgotten that a “*landslide is life and it does operate in a natural physical environment, harmonic and ordered as the Environment is*”. It is therefore considered correct to insert in this paragraph two tables (Tables 3.1 and 3.2), referring to Pleistocene and Holocene, of the lithostratigraphic objective units and of the sedimentary cycles

correlated via the scale of times to the conventional deductive units of glaciations, climatic oscillations, pollinic zones, and marine oscillations.

For our studies on the prediction, prevention and control of hydrogeological disruption in cohesive soils, dating has the placement of the time factor in the sequence of evolutionary processes of a slope and of its environmental conditions as the basic element. In order to obtain a proper understanding of the failure phenomena of natural slopes, the recognition and interpretation of climatic variations over time are decisive, since the hydrogeological disruption of a slope is closely connected to the amount of water seepage into the ground. It appears illusory, therefore, to elaborate a true study on the genesis of landslides in cohesive soils without knowing about their age. There are two methods of analysis:

- (a) *Method of absolute dating.* The technique of radioactive ^{14}C carbon is used to date, with good approximation, the organic material buried within landslides. This method was developed by the Nobel Prize winner Willard Frank Libby in 1947, who noted that the carbon isotope ^{14}C is produced by the isotope ^{14}N in the atmosphere due to the bombing of cosmic rays. When the organic material ceases absorption of atmospheric ^{14}C carbon, this begins to decay with a halving time of 5730 years; after further 5730 years it is reduced to a quarter, etc. Wood is the best material, but organic soils, shells and animal remains have also been used. With this method, it is possible to determine landslide origins up to a maximum of 70,000 years using sophisticated equipment. It is, therefore, to be considered that it can only be used for landslides happened at the latest during the Würm Glaciation of Upper Pleistocene, provided that the landslide mass contained mainly plant fragments.
- (b) *Method of relative dating.* This method is certainly the most used and establishes the age of a landslide in relation to eventual objects or materials embedded in the landslide or found within superimposed material.

If a river terrace has interbedments of silt-clay levels from a landslide (material with no fabric, with chaotic distribution including lithic fragments of angular shape and various dimensions), the age of the landslide is that of the river terrace or of the stratigraphic height where the soil is located. If chaotic horizons are multiple and at different stratigraphic heights within the terraced deposit, this means that the landslide body has undergone a number of movements over the time during the deposition of the terrace. Such movements are usually caused by earthquakes.

It must be noted that the mean values of the morphometric indexes of the pebbles on a terrace (flattening, angularity, asymmetry) can be related to the local climate taking place at the time of the deposition of the fluvial terrace. In this case, a limestone crust indicates the presence of a warm-arid climatic phase. If the river terrace has tensile meso-structures inside, due to the stress field acting during or after its deposition, it is indicative to observe if the meso-structures pass through or not the layers of failed material and what are the layers interested.

Proofs about the dating of landslides, more generally, come from the study of pollen or fauna groups. Some events in post-glacial history can be related to variations in flora or fauna (the second often consistent with the first one) and, therefore, with the preservation of an evidence that can provide the proof for dating. Pond sediments are particularly useful for the conservation of pollen: a pond originating from a landslide will provide data capable of post-dating the same landslide. The same happens with macro-fauna remains, such as bones, horns, etc., which are found in isolation, or small fragments of shells or chitinous coatings of cockroaches, which may appear in a large number and therefore statistically processed like for pollen.

Differently from relative dating of stratigraphic type, which compares the older or more recent age of a sequence of layers with another one, the relative dating applied to artifacts provides indications of the age in terms of years rather well-defined. However, dating a pre-existing landslide is not always a simple task, neither methodological rules exist that rely on easy-to-find elements.

Very often the landslide deposits incorporate various artifacts that may be of the Palaeolithic, if they are fragments of Natufian culture huts (13,000–10,000 BC—arid cold climate), or mud bricks of pre-ceramic Neolithic villages (10,000–8500 BC—humid hot climate), or fragments of decorated walls of the pre-ceramic Neolithic (8500–6100 BC—cold arid climate), or pillars from older temples (6100–4000 BC—warm temperate climate) or traces of domestication of plants and animals (4000–0 BC—cold arid climate with a temperate heat range between 2000 and 1000 BC) or medieval ruins (75 AD–1350 AD—medieval climatic optimum), etc.

It is understandable that the relative dating of a pre-existing landslide based on elements of human activity can be precise but certainly is also fortunate. In fact, to date a pre-existing landslide, methods and systems are multiple but all based upon to the observer's ability, who must be able to interpret the exceptional relativity among the elements of the specific subdivisions in the geological background.

Other data able to prove the dating of a landslide, in particular of a small landslide, come from the displacement of artificial linear configurations. These elements can be fences and walls, rows of trees, roads and railways, pipelines and electric transmission lines or tunnels. The latter obviously are only linked to deformations of relatively deep soils, while the others are sensitive to both superficial and deep movements. Obviously, the movement is subsequent to the construction of that particular structure, although it is not necessarily a proof that some movements did not take place before the start of construction.

Vegetation can be used as a guide to the dating of the last movement: trees, for example, often have some bending near the root, caused by shallow movements to the base of the slope; this is the initial phase of their life, followed by a period of quiescence, during which the vertical growth recommences. The coring of the tree with all its annual rings will provide an indication of the period within which the date of the last movement could clearly be identified. On steep slopes, bent trees may not indicate a quiescence period, but rather that their roots system stabilized

Table 3.1 General switchboard of quaternary subdivisions in marine environment—Pleistocene

| EPOCH | AGE (Ka BP) | SEDIMENTARY CYCLES (Ka BP) | MARINE ISOTOPE STAGE (MIS) | Ka BP (x 1,000) | GLACIATIONS | CLIMATIC OSCILLATIONS | POLLINIC ZONES (14c -1000 years) | MARINE OSCILLATIONS | | |
|-----------------------------------|-------------------------------------------------|------------------------------------------------|---------------------------------------|--------------------------------------------|-------------------|-----------------------------------------------------------|-----------------------------------------------------|-----------------------------------------------------------------------------------------------------------------------------------------------------------------|---------------------------------------|--------------------------------------------------------------------------------|
| HOLOCENE | PREBOREAL | 11.700 | 1 | 11,7 | LATE GLACIAL 11,7 | TEMPERATE | ALLEROD | INGRESSION | | |
| PLEISTOCENE | UPPER PLEISTOCENE - OR TARENTIAN 238.300 years | IV LEVEL A STROMBUS | 27,0 | 2 | 27,0 | WÜRM GLACIAL 62.300 years | II PLEINGLACIAL 27,0 | REGRESSION, MAX LOWERING OF SEA LEVEL 12.000 YEARS AGO; LEVEL WAS 90-100m, LOWER THAN THE CURRENT ONE. CONTINENTAL PLATES WERE EMERGED. | | |
| | | | | | | | | | TEMPERATE 32,0 | DRYAS II 12,3 |
| | | III LEVEL A STROMBUS | 74,0 | 5a | 74,0 | 74,0 | 74,0 | I PLEINGLACIAL 74,0 | AMERSFOORT 74,0 | 74,0 |
| | | | | | | | | | | |
| | | II LEVEL A STROMBUS | 130,0 | 6 | 130,0 | 130,0 | 130,0 | MAX DAMP WARM 130,0 | EEMIAN 130,0 | INGRESSION +2-3m ABOVE CURRENT LEVEL I 117,0 |
| | | | | | | | | | | |
| | | I LEVEL A STROMBUS | 220,0 | OSTIENSE EROSIVE PHASE | 220,0 | 120.000 years | RISS GLACIAL 120.000 years | DAMP WARM 220,0 | SAALE 220,0 | SMALL INGRESSION 220,0 |
| | | | | | | | | | | |
| | | MEDIUM PLEISTOCENE OR IONIAN 740.000 years | 3 rd SEDIMENT. CYCLE | 400,0 | 10 | 400,0 | MINDEL-RISS INTERGLACIAL 50.000 years 300,0 | DRY WARM 300,0 | TEMPERATE WARM 360,0 | INGRESSION 300,0 |
| | | | | | | | | | | |
| | 2 nd SEDIM. CYCLE | | 340.000 YEARS | CASSIA EROSIVE PHASE | 700,0 | 700,0 | GÜNZ-MINDEL INTERGLACIAL 50.000 years 700,0 | WARMEST PERIOD IN IONIAN 700,0 | ELSTER 250,0 | INGRESSION 700,0 |
| | | | | | | | | | | |
| | 1 st SEDIMENTARY CYCLE | | 990,0 | AULLA EROSIVE PHASE | 990,0 | 990,0 | GÜNZ GLACIAL 500.000 YEARS | GLACIAL COLD, MAX 800A 850,0 | GLACIAL COLD 250,0 | SMALL INGRESSION 850,0 |
| | | | | | | | | | | |
| | LOWER PLEISTOCENE OR CALAMBRIAN 1.591.000 YEARS | | 2 nd SEDIM. CYCLE | 1.125,0 | 28 | 1.200,0 | 1.200,0 | MODERATE COLD WITH FREQUENT CLIMATIC OSCILLATIONS BETWEEN WET COLD AND DAMP WARM (GLACIERS STATIONARY) 1.200,0 | 1.200,0 | MARINE INGRESSION BETWEEN 1.100 AND 1.200. 1.200,0 |
| | | | | | | | | | | |
| | 1 st SEDIMENTARY CYCLE | | 1.500,0 | URICA EROSIVE PHASE (UPPER LIMIT) | 1.500,0 | 1.400,0 | DONAU-RISS INTERGLACIAL 200.000 YEARS 1.400,0 | WARM TEMPERATE COLD 1.500,0 | 1.500,0 | NUMEROUS EROSIONAL PHASES DUE TO FREQUENT MARINE OSCILLATIONS 1.400,0 |
| | | | | | | | | | | |
| | 1 st SEDIMENTARY CYCLE | 1.806,0 | ACQIA TRAVERSA EROSIVE PHASE | 1.806,0 | 1.806,0 | 1.806,0 | GLACIAL COLD 1.806,0 | 1.806,0 | SMALL POSITIVE OSCILLATION 1.750,0 | |
| | | | | | | | | | | TEMPERATE WARM 360,0 |
| 1 st SEDIMENTARY CYCLE | 775.000 YEARS | BIBER - DONAU INTERGLACIAL 775.000 YEARS | 775.000 YEARS | 775.000 YEARS | 775.000 YEARS | GLACIAL COLD 1.900,0 | 1.900,0 | REGRESSION 1.806,0 | | |
| | | | | | | | | | TEMPERATE WARM 360,0 | ARCY 32,0 |
| 1 st SEDIMENTARY CYCLE | 2.581,0 | 104 | 2.581,0 | 2.581,0 | 2.581,0 | HIGHLY ARID WARM LOWERING TO THE UPWARDS 1.900,0 | 2.581,0 | REGRESSION 1.900,0 | | |
| | | | | | | | | | TEMPERATE WARM 360,0 | DENEKAMP 30,0 |
| PLIOCENE | PIACENTIAN | | | | BIBER GLACIAL | | | DURING PIOCENE SEA LEVEL WAS ABOUT 100m HIGHER THAN THE CURRENT ONE | | |

Table 3.2 General switchboard of quaternary subdivisions in marine environment—Holocene

| EPOCH | AGE (Ka BP) | SEDIMENTARY CYCLES (Ka BP) | MARINE ISOTOPE STAGE (MIS) | Ka BP (x 1,000) | GLACIATIONS | CLIMATIC OSCILLATIONS | POLLING ZONES (¹⁴ C · 1000 years) | MARINE OSCILLATIONS |
|--------------------------------|---------------------------------------------|---------------------------------------------|-------------------------------|----------------------------------------------------------------|-------------------------------------------------------------------------------------------------------------------------------------------------------|----------------------------------------------------------------------|---------------------------------------------------------------------------------------------------------------------------------------------------|---------------------|
| H O L O C E N E | UPPER HOLOCENE 3,000 YEARS | SUB-ATLANTIC STARTED 2.500BP; ONGOING | N O T C L A S S I F I A B L E | +2,000 AD | POST GLACIAL - CLIMATICALLY VERY VARIABLE | GLACIERS IN CONTINUOUS REDUCTION | WARM +0.5°C | ONGOING INGRESSION |
| | | | | +1,850 | | 1850 | GRADUAL RISE OF TEMPERATURE FROM -0.5°C TO +0.5°C | INGRESSION |
| | | | | +1,350 | | LITTLE ICE AGE | AVERAGE TEMPERATURE OSCILLATED BETWEEN -0.25°C AND -0.5°C, WITH MAX COLD IN 1670, 1790, 1810 AND 1850 | 1850 |
| | | +1,000 | | MEDIEVAL CLIMATIC OPTIMUM | | TEMPERATE MEDIEVAL PERIOD MAX +0.4°C IN 1300 +0.2°C IN 1200 | RISE OF MARINE LEVEL OF ABOUT 120M ABOVE THE LAST GLACIAL EXPANSION OF 4,000 YEARS BP | |
| | | +0.75 | | MINIMUM VARIABILITY OF THE THICKNESS OF GLACIERS | | TEMPERATURE GRADUALLY RISING TO -0.1°C BY 1000AD | 0.0 | |
| | | +0.0 | | ROMAN CLIMATIC OPTIMUM | | TEMPERATE WARM MAX AVG. TEMPERATURE +0.1°C | 2.0 | |
| | | 1.0 | | GLACIAL EXPANSION | | ARID COLD MIN TEMPERATURE -0.5°C BY YEARS 3,000 | 4.0 | |
| | | 2.0 | | GLACIAL STABILITY | | TEMPERATE WARM MAX TEMP. +1.2°C BY YEARS 5500 (HEAVY RAINFALL) | 6.1 | |
| | | 3.0 | | GLACIAL EXPANSION | | ARID COLD. MINIMUM TEMPERATURE -0.4°C BY YEARS 8000 | 8.4 | |
| | 4.0 | LATE GLACIAL | | MILD MAX TEMPERATURE +0.4°C BY YEARS 9000. HIGH RAINFALL | 10.0 | 10.0 | POST-BOLLING OSCILLATION | |
| | 5.0 | | | | | | | |
| | 6.0 | | | | | | | |
| | 7.0 | URM IV | | 16,500 YEARS | 8.4 | 8.4 | INGRESSION | |
| | 8.0 | | | | | | | |
| | 9.0 | | | | | | | |
| | 9.0 | PRE-BOREAL 2,700 YEARS | | BOREAL 1,000 YEARS | 9.0 | 9.0 | SEA LEVEL ROSE UP OF ABOUT 60M WITH REFERENCE TO THE POST-BOLLING OSCILLATION. DELTA OF PO RIVER REGRESSED ALMOST TO THE CURRENT POSITION. | |
| | 10.9 | | | | | | | |
| | 11.7 | | | | | | | |
| LOWER HOLOCENE 4,700 YEARS | ATLANTIC 3,000 YEARS | SUB-BOREAL 2,500 YEARS | 2.5 | 2.0 | REGRESSION: THE ADRIATIC SEA RETURNED TO THE SAME LEVEL OF PREVIOUS REGRESSION | | | |
| | | | | | | 5.0 | | |
| | | | | | | 8.0 | | |
| MEDIUM HOLOCENE 4,000 YEARS | ATLANTIC 3,000 YEARS | SUB-BOREAL 2,500 YEARS | 5.0 | 6.1 | FLEMISH INGRESSION SEA LEVEL ROSE UP OF ABOUT 3-6m. THE ADRIATIC SEA EACHED ITS CURRENT APPEARANCE | | | |
| | | | | | | 8.0 | | |
| | | | | | | 9.0 | | |
| UPPER HOLOCENE 3,000 YEARS | SUB-ATLANTIC STARTED 2.500BP; ONGOING | SUB-BOREAL 2,500 YEARS | 2.5 | 2.0 | REGRESSION: SEA LEVEL LOWERED OF ABOUT 11m. RE-EMERGED, IN PART, THE ANCIENT DELTAIC ENGRAVINGS OF THE RIVERS OF MARCHE REGION AND UPPER ADRIATIC. | | | |
| | | | | | | 5.0 | | |
| | | | | | | 8.0 | | |
| MEDIUM HOLOCENE 4,000 YEARS | ATLANTIC 3,000 YEARS | SUB-BOREAL 2,500 YEARS | 5.0 | 6.1 | INGRESSION | | | |
| | | | | | | 8.0 | | |
| | | | | | | 9.0 | | |
| LOWER HOLOCENE 4,700 YEARS | PRE-BOREAL 2,700 YEARS | BOREAL 1,000 YEARS | 9.0 | 9.0 | SEA LEVEL ROSE UP OF ABOUT 60M WITH REFERENCE TO THE POST-BOLLING OSCILLATION. DELTA OF PO RIVER REGRESSED ALMOST TO THE CURRENT POSITION. | | | |
| | | | | | | 10.9 | | |
| | | | | | | 11.7 | | |

IN THIS EPOCH THE LIMITS HAVE ONLY REGIONAL OR LOCAL MEANING. POLLING ZONES ARE REDUCED BY THE ANALYSIS OF MARIES

the soils in the nearby once the tree has reached a certain size. Most of the trees in mountainous areas have this effect at a greater or smaller degree and it could be said with certainty that the movement ceased only if all the trees younger than a certain age were straight, while all the older ones were bent.

Further evidence of possible movements, if not actually of the presence of landslides, come from the vegetation types present. Hydrophilic plants such as Equisetum or Thistle (*Dipsacea sylvestris*) are both commonly found in England on landslides within saturated clays. Other plants, especially those suitable for rapid

reforestation of the naked soil following landslides, are abundant. All varieties of river canes, bulrushes, brambles and some willows are useful indicators of high groundwater and of problems related to its presence in clay soils.

From this first approach to the importance of dating it is understood that the knowledge of natural environmental variations is a fundamental parameter that we must take into account if we want to evaluate in a scientifically realistic way the contribution that comes from hydrogeological disruption on changes in the environment. Without the knowledge of the history of climatic and environmental variations provided by Geological Sciences, it is certainly impossible to elaborate a predictive scenario for a landslide having the necessary reliability on its future development. The limits of the models that are often divulged about climate are confined to the contemporaneity of the phenomena taken into account, or to the lack of a natural basis taking account of environmental transformations. The in-depth analysis of the genetic development of a pre-existing landslide may indeed give a wider view of the environmental variations induced by climatic changes in the past and at the same time indicate the role that the landslide itself had in the evolutionary process of natural phenomena in every time scale.

3.3 Chronostratigraphic Evaluations of Landslide Units

For practical purposes, the two chronostratigraphic tables (Tables 3.1 and 3.2) serve different goals. The first one is definitely to have chronological units that can allow to merge, within defined timeframes, landslide units of the same period even though a number of sliding surfaces show that they are not synchronous. All in all, however, they have similar genetic connotations deriving from the same lithological nature of the soil, from tectonic fracturing with meso-structures belonging to the same stress field and permeability factor K almost similar at the same depth. Moreover, the sliding surface of a landslide has, to some extent, also a chronostratigraphic meaning as it is ever older than any morphological event occurring on the body of the landslide itself or at the toe (e.g., badlands, engravings, erosional or depositional surfaces, river terraces, secondary scarps, etc.). Hydrogeological hazard maps in this sense can and must be considered as a tool of synthesis at a regional scale. To this purpose also aims their use extended to the soils of continental Quaternary and to Vulcanites. In the former, the elements that border the potential or existing landslide unit should be identified, such as: (a) the recognition on the field of the elements that induced the triggering of the landslide (e.g. main and secondary landslide scarps, landslide terraces, front of accumulation, radial cracking, transverse ridges, cracks at the boundaries, landslide boundaries, etc.) or (b) approaching the failure condition (e.g. superficial ground cracking, lithological discontinuities, tension cracks, tilting of trees or of poles in the ground, etc.), often

determined with great chronological detail, even though it is generally marked out by monotonous lithologies.

For Vulcanites, the centres of origin and their eruptive periods will be highlighted by means of the choice of significant boundaries based on the identification of the soils resulting from the unitary succession of volcanic events. This will make it easier to find any correspondence with hydrogeological disruptions and morphogenetic units from environmental disasters associated with volcano-tectonic events of regional scale.

Another goal arising from the need of consulting a “*General Framework of the Quaternary Subdivisions of Marine Environment*” is devoted to the understanding of the spatial and temporal relationships of sedimentary cyclicality (e.g. transgressive-regressive cycles), that induces significant sea level oscillations and transforms into an increase or a decrease in coastal landslides and in changes in the base level of the hydrographic network. Even in this case, however, the dating of landslides can become, to a certain extent, subjective. For this reason, the use of Tables 3.1 and 3.2 should be carefully evaluated and put into practice only if detailed facies analyses minimise the risk of subjectivity. Actually, for cartographic purposes site surveys are drawn on a local scale, whereas the datings within the mentioned tables are defined on a basinal scale. An aid can be provided by the below informal scheme of nomenclature, based on the one used in sequential stratigraphy works and includes the following survey elements:

- *Informal Scheme of Nomenclature for identifying lands at risk of landslide*
- A. *Carry out a historical and cartographic retrospective of existing landslides on the slope:*
 1. Describe the type of existing landslide according to the classification by Varnes (1978), describing their lithology and morphology (main and secondary scarps, fronts, lengths, sides, radial cracks, boundary cracks, etc.);
 2. Find the depth of the shear surface of the existing landslide referring to the lithological succession;
 3. Establish the age and possible diachronicity of the sliding surface;
 4. Ascertain the possible seismic expression on the existing landslide unit.
- B. *Unconformities bordering the area considered at hydrogeological risk:*
 1. Define the elements the identification of the ground is based upon;
 2. Analysis of tectonic cracking and orientation of the groups of discontinuities;
 3. Superficial geomorphological aspects (slope steepness, sub-areal erosion, depositions—species of river terraces—hydrographic network, engravings and cracks, water features and drainages, existing structures and/or anthropic superstructures bearing onto the slope);

4. Grooves of the hydrographic network and possible regressive deformations of watercourses;
5. Existence of terraced deposits on the slope;
6. Water seepage phenomena in the ground;
7. Identification of the area under hydrogeological hazard.

Generally, the identification of a number of pre-existent landslides on a slope contributes to the definition of a vocational perspective of the slope itself, but does not provide a classification of the risk for landslides within potentially unstable areas or the prediction and prevention of landslides. The map of geographic distribution of the different types of landslides belonging to the same slope is actually based solely on the genetic process responsible of their development but does not take into account the spatial and temporal aspects of the disaster. A purely deterministic process, therefore, is unsuitable for dealing with the complexity of the vital actions taking place during the triggering of a landslide. “*Time is a physical reality, pre-existent to every action of Nature*” and therefore if we want to pursue the prediction and the prevention of landslides, we must consider the evolutionary capacity of the area at hydrogeological risk as an undivided totality of natural phenomena including, of course, the time factor. That is why it is believed that the dating of a landslide is one of the main factors of analysis to be investigated.

3.4 Analytical Procedure for the Chronological Evaluation of Pre-Existing Landslides by Means of Tables 3.1 and 3.2—Example Referring to Würm

The last ice age, named the Würm, had a duration of about 60,000 years and had frequent and varied climatic events. The coldest phase took place between 25,000 and 15,000 years BC. During this period, the northern icecap reached its maximum extension on all continents reaching the 40th parallel. Between 15,000 and 13,000 years BC circa, the glacial climate gradually became mild cold. In the Apennines as well as on the Andean slopes of the provinces of Salta and Jujuy, in northern Argentina (significant areas for our experiences), numerous have been the pre-existing landslides originated in this short, late glacial period of the Würm. The ascertained reason for this was found in two millennia of constant water percolation in clayey soils resulting from the slow melting of glaciers. Water infiltration within the ground, even at a great depth (40–80 m below ground level), was favoured by the modifications of the tectonic fractures subjected to periodic seismic events. Landslides that presented a very deep sliding surface, about a maximum of 80 m below the ground level, are those with a dense network of extension fractures.

During glacial periods rainfalls were uncommon due to the decrease in the water vapour produced from the oceans. Indeed, the genesis of pre-existent landslides is considered more frequent in warm-humid periods or, more generally, during an interglacial period characterized by a remarkable regression of the glacial systems and by a consequent rise in the sea level.

In the seventh millennium BC a particularly warm climate period started, with a thermal increase of 4–5 °C of annual average. This warm phase continued throughout the period, ranging from a mild climate (6250–5000 BC) to warm humid (4000–3200 BC), with a progressive increase in the number of landslides. Various tree species, from broadleaves to conifers, moved to the north and/or at greater altitude. In North Africa and the Middle East, along the current tropical zone, an arid stage developed and caused the disappearance, or at least the decline, of numerous plants and animal species. This climatic optimum had a positive influence on the development of Middle Eastern and North African civilizations. Indeed, the long-term warmth encouraged the populations to settle along the banks of the great rivers and there to develop the early techniques of transformation of the environment devoted mainly to agriculture and animal breeding purposes, giving rise to the development of Potamian civilizations.

Between 3200 and 2600 BC there has been a further cold phase in North Africa, Norway and the Alps, witnessed by the dating carried out using the radiocarbon method. Climatic conditions were associated with a cold and humid phase which led to the advancement, in the boreal mountains, of glacial and mountainous systems and an increase in rainfall in the Mediterranean countries and the Near East. The previous warm and temperate areas diminished as the cold climates expanded.

Around 2600 BC, during the age of copper and bronze, gradually took place a wet warm phase, lasted for about six centuries and then turned into dry warm between 2000 and 1600 BC. Initially, during a rather humid climate in northern Europe, forests and swamps developed, as witnessed by the numerous peat bogs found nowadays in Germany, Ireland and Scandinavia. Even Italy was covered with thick forests, particularly in mountainous areas. The mouths of the major rivers quickly enlarged due to the provision of solid material, as a consequence of the greater erosive capacity of the watercourses and the re-activation of rotational landslides often caused by the erosion due to the hydrographic network. Dated back to that period of heavy rainfalls the landscapes with diffused badlands on the hills made up of clays from the Pliocene and the Lower Quaternary and the characteristic stilt houses, built for defending from the frequent and abundant floods.

A period of gradually decreasing humidity followed this humid warm phase, until a warm dry climate (between 2000 and 1600 BC) took place. A lowering of the Caspian Sea, which around 1600 BC reached its lowest levels, seemed to witness such condition. According to some historians and archaeologists, there is evidence that in the inner Asian regions the progressive climate aridity heavily influenced the social and economic development of the populations. Even for the regions of North Africa, the same conditions seem to apply.

Between 1600 and 1000 BC, the dry warm climate was replaced by warm temperate climate, with a maximum annual temperature of $+0.1\text{ }^{\circ}\text{C}$ relative to the north-eastern lands of the Mediterranean. After 1000 BC and until 75 AD, there was a new lowering of the annual average temperature with glacial cold reaching $-0.5\text{ }^{\circ}\text{C}$ around the birth of Christ. In the last 1675 years, however, even with variable climatic conditions, the evolutionary and geomorphological process of European slopes was modest. The existing landslides predominantly tended towards a consolidation more than towards a reactivation, while the landslides originated at that time had modest dimensions and sliding surfaces very often located at the base of the alteration cover. These ones were predominantly caused by the erosion of watercourses and therefore developed on the slopes downslope of mountainsides. On high-energy mountainsides and alpine ones, however, the few rotational landslides of the same period showed deeper sliding surfaces and larger spatial dimensions. Forests were considerably developed there and certainly positively contributed to the protection of the slopes. The archaeological studies carried out on the period provide a completely new picture of the origin and development of complex societies. These ones, according to the latest theories, developed the need to assemble in order to participate to sacred rites, when they stopped to consider themselves as elements of nature and began to dominate it. Around year 75 AD, a “Medieval Temperate Period” gradually established, which lasted until 1350 AD, with a maximum annual temperature of $+0.4\text{ }^{\circ}\text{C}$ in 1200 AD. During that period, the rivers increased their flow because of the abundant rainfalls of a predominantly humid climate and, at the same time, deepened their channels with the relative incision of smaller watercourses. The slopes of the river terraces underwent further and deeper cuttings.

(From Castiglioni 1979): “A river valley is a complex system. It is the result of two groups of interacting processes: fluvial action within the riverbed and denudation processes on the mountainsides. Fluvial action in the riverbed is in fact conditioned by water inputs and debris coming from the slopes; the denudation processes on the slopes are conditioned by the efficiency of debris removal work or by erosional work, which the river acts at the toe of mountainsides.

In many river valleys, large sections, shaped like basins, suitable for human settlements, alternate to narrow, V-shaped channels, where sometimes there is just a small space for allowing the presence of a road next to the river bed; this is easily explained when the channels are engraved in stiff rocks, and the basins open in softer rocks. In Fig. 3.1a series of cross sections is presented, as a first start for studying the shape of valleys.

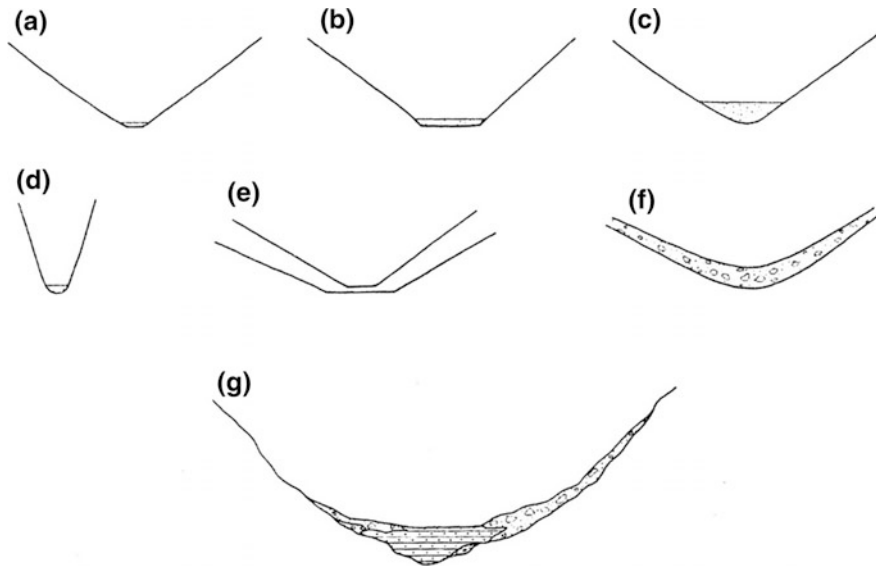


Fig. 3.1 Types of valleys, in cross section (from Castiglioni 1979). **a** V-shaped valley; **b** Flat bottom valley (in rock); **c** Alluvial flat bottom valley; **d** Canyon; **e** Evolution of the cross section of a valley where engraving was practically over; **f** Small valley with concave bottom with prevailing solifluction on the flanks and along the bottom (this is usually not a river valley, but a kind of periglacial modelling); **g** Valley with concave bottom resulting from the deposition of alluvium and slope debris

In general, the set of forms of river valleys depends on five groups of factors:

- (a) *Factors related to the behaviour of the watercourse, the type of riverbed, its history, when deepening stages, even if quick, may have alternated with stages of relative stability, of lateral erosion, of flooding, etc;*
- (b) *Factors linked to the dominant processes in the modelling of slopes which, in turn, depend on climate, vegetation, etc. (but also the factors mentioned within point a are affected by climate);*
- (c) *General and local tectonic factors: they are responsible for the initial differences in level in the slope and of eventual further deformations;*
- (d) *Factors linked to the rocks in the riverbed and on the flanks;*
- (e) *The time factor, influencing the evolutionary stage of the valley.*

The time factor (e) introduces to considerations of the evolutionary type. For example, it can be supposed that, during stable environmental conditions and after the achievement of a profile regularised by the water flow, the variations in level of the riverbed become negligible. As a consequence, the evolution of the valley will develop predominantly with modifications on the mountainsides, inducing the lowering and the thinning of interfluvial spaces (Case E, Fig. 3.1).

Observing Fig. 3.2, moreover, some problems of asymmetrical valleys can be pointed out. Cases A and B show two types of structural asymmetry: due to the

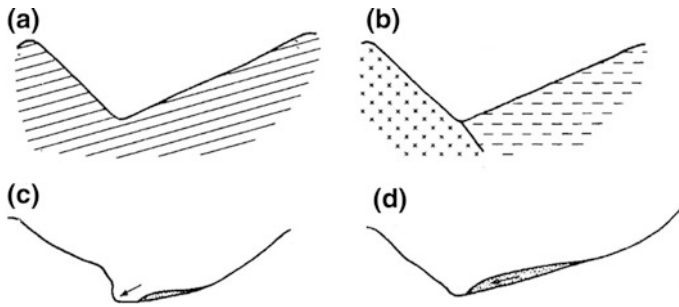


Fig. 3.2 Cross sections of dissymmetric valleys (from Castiglioni 1979). **a** and **b** Asymmetries due to structural reasons; **c** Asymmetry due to lateral erosion exerted by the river on a single bank; **d** Asymmetry due to different degradation of the two versants, influenced by the exposition factor

bedding of layers, for example a monoclinical valley (A); and for lithological reasons (B). Cases C and D, instead, focus the attention on the processes, i.e. on the morpho-dynamic causes.

Case C wants to show how the watercourse, due to its trend to move sideways, can be the cause for the dissymmetry. It is a frequent case within meandering valleys (alternated asymmetry, first left then right and viceversa), or where the watercourse undergoes the thrusting of tributaries located just on a single side. Movements of tectonic tilting can have this effect as well.

Case D wants to show that the dissymmetry can be found in processes of degradation of mountainsides. Usually is the difference in exposure making different the morpho-dynamic conditions on the two mountainsides. The exposure of slopes to the north or, respectively, to the south influences the frequency and intensity of the phenomena of freezing, thawing, desiccation, on the plant life, etc., depending from the solar insolation regime.

The exposure to dominant wind as well must be taken into account: wind can determine the mounding of snow, or of loess, preferably on downwind slopes, or can orientate the incidence of rain.

A phase of engraving followed a phase of predominant lateral erosion. Landslides induced by fluvial under-mining were more numerous than before, wider and with deeper sliding surfaces and steeper slopes. Subsequently, in the north-eastern Mediterranean areas, the “Little Ice Age” took place, with temperatures ranging between -0.25 and -0.5 °C with cold temperature peaks in 1670, 1790, 1810 and 1850 AD. The deposition work was prevalently carried out by the rivers, which started to build, very slowly, the current river terraces along the course of the riverbed. This was generally very large and characterized by a floodplain of alluvial cobblestone of modest size, cut by a network of canals just engraved in a wide bed with rambling branches, sometimes with small, well defined islands made up of predominantly sandy alluvium. In the latter period and until 2000 AD, hydrogeological disruption decreased, if compared to the previous period, and showed a primary dependence on the local climate, which is variable according to the seasons (Fig. 3.3).



Fig. 3.3 Nemoli (Province of Potenza, Italy)—Argillites of Black Clays (Crete Nere Formation)

3.5 The Importance of a Correct Site Analysis

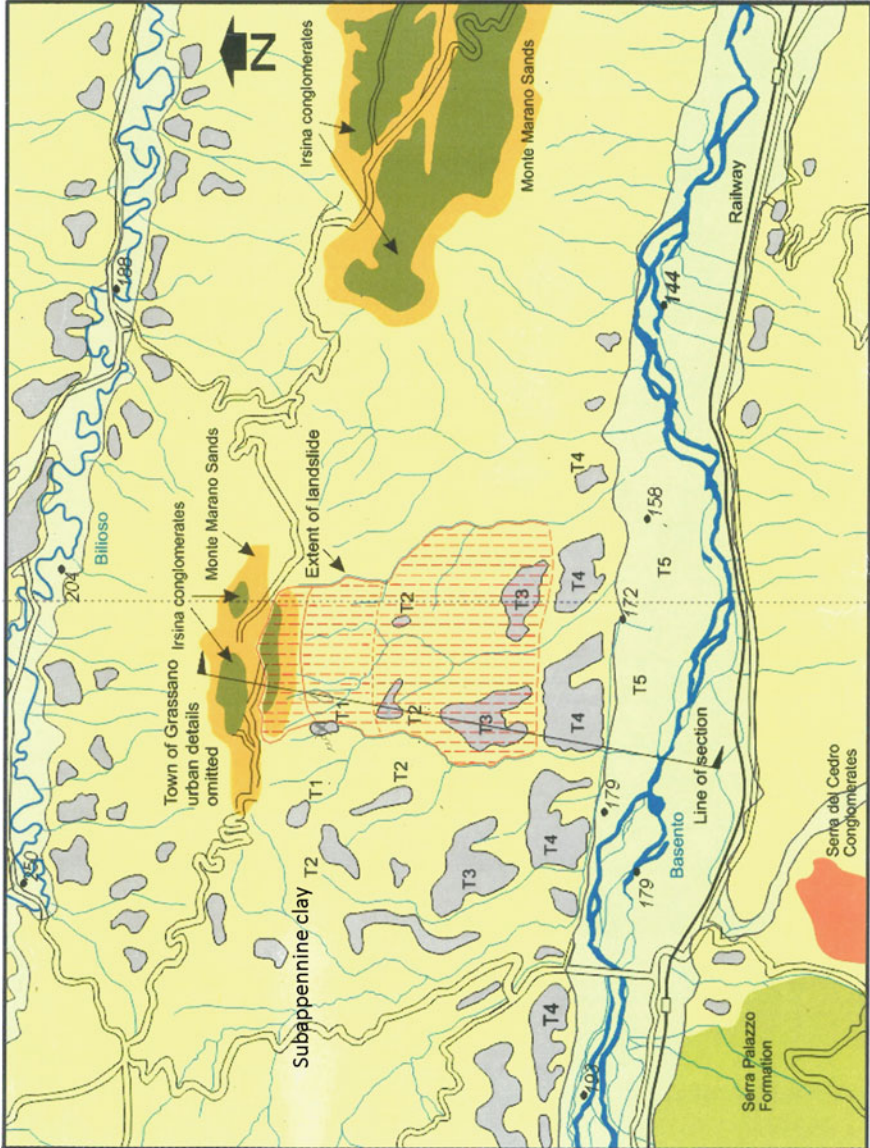
In order to emphasize the importance of proper site analysis on the structural and palaeographic structure of a slope subjected to hydrogeological hazard, a very significant experience is reported below, indicating how the configuration process of a landslide cannot be satisfactory for prediction purposes if the analysis does not take into account the general space-time relativity in which the phenomenon resides.

The perturbing element of the overall danger of a pre-existing landslide, in relation to the expansion of urban centres, is in fact constituted by the pre-existing sliding surface and by the need for knowing its initial triggering conditions and the correct determination of the geometry of the landslide. This is needed to evaluate the current equilibrium states in relation to the current mobilisation issues.

The example proposed is related to the landslide in Grassano, southern Apennines, in the province of Matera, Italy, erroneously considered as a single slope failure process and which represents an example of the complexity of this kind of landslides, providing an analytical method to be followed.

Example—Grassano—Light bluish marly-silty clay

The town of Grassano is located at 550 m above sea level, in a dominant location onto the middle of the valley of river Basento. The bottom of the valley was observed at about 173 m above sea level (Fig. 3.4) on southern Apennines in the Basilicata region, Italy.



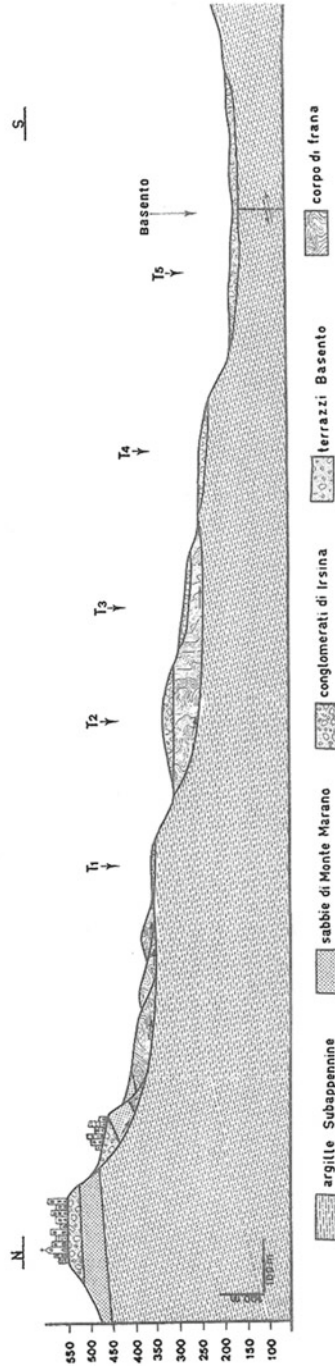


Fig. 3.4 Geologic map and cross section of the slope on the left bank of the middle course of River Basento; Southern Apennine, Basilicata Region, Italy

Geology of the slope

The stratigraphic succession of the slope on the left bank of the middle of the basin of river Basento (Fig. 3.5) is constituted of soils from the latest depositional cycle of the Bradano Foredeep, in predominantly pelitic facies (III Bradanic cycle—Selli 1962; Lentini 1971; Ricchetti and Scandone 1979; Lazzari and Lentini 1980; Casnedi 1988; Coppola 1993). They are greyish-light bluish clays and marly-silty clays with rare sandy interbedments 0.50–2.00 cm in thickness (Sub-Apennines Plio-Pleistocene Clays). The layering is often indistinct, however layers thicknesses range between 10 and 40 cm. The structure is of monoclinal type, dipping ENE (anti-dip slope structure) of between 5° and 15°. Locally, the lithological unit has a thickness of about 450 m (Fig. 3.5).

Upwardly, yellow quartz-calcareous sands outcrop (Monte Marano Sands, Calabrian Stage), locally cemented and presenting lenses and cobbles in the covering. The thickness of the deposit ranged between 25 and 80 m and the layers, undistinguished, dip towards ENE at about 5°.

The succession ends with heterometric and polygenetic conglomerates, made up of cobbles, with a maximum diameter of 40 cm, of calcareous, marly, arenaceous and siliceous origin (Irsina conglomerates, Calabrian Stage). The single elements show a high degree of flattening. The thickness at the outcrop in Grassano is just

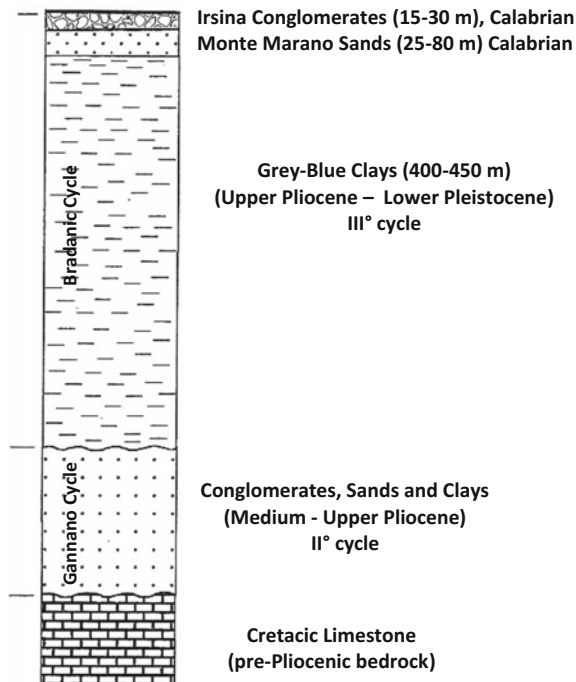


Fig. 3.5 Stratigraphic succession of the slope on the left bank of the middle basin of Basento river

slightly greater than circa 25 m and is in stratigraphic continuity on the Monte Marano Sands.

The tectonic cracking is characterised by two main groups of cracks: the first dipping in a N40 direction, the second in N20 direction. The dispositional orientations of these groups of discontinuities, however, do not represent potential instability phenomena for the slope because the intersection defining the dimensions of the Sub-Apennines Clays has an anti-dip slope configuration, orthogonal to the slope.

Morphologic analysis

Such analysis is circumscribed to just the southern versant of the town of Grassano, where the two pre-existing landslides from different periods are located: the first, to the upslope, was originated in the Mindel-Riss interglacial period; the second, to the downslope, was originated in the Olocene.

The historic centre of Grassano counted 6755 inhabitants and is set onto a hillside, at about 550 m above sea level, whose ridge, on a NE-SW direction, represents the watershed between the basins of river Basento and river Bradano. It is dominant on the middle valley of Basento, whose bottom is 173 m above sea level. The southern versant of the hill must be divided into two main morphologic sets, characterised by different distributions of the erosional forms (Fig. 3.6).



Fig. 3.6 Southern slope of the Grassano Hill, degrading towards the Basento river, whose riverbed is parallel to the succession of tall stem trees (to the bottom). The two landslide terraces, characterised by two large scarps, can be identified in the photo

- (a) *High energy slope*: ranging between 550 and 323 m above the current sea level, was mainly set in Sub-Apennines Clays overlain by the regressive sandy-conglomeratic plates of the Calabrian stage. The morphology of the hill presents a first large landslide terrace at 475 m above the current sea level, located to the front of the first landslide (T_1 in Fig. 3.4). Secondary scarps, with related small landslide terraces, were found at 468, 403 and 393 m above sea level. Finally, to the southern end of this type of slope, at a level of 345 m above the sea level, the first river terrace is observed, 45 m in height, indicating the separation between the high energy and the low energy zones. The average steepness is about 15° . The *1st order terrace* (T_1) has a thickness of 10 m and comprised well cemented cobbles in pseudo-layers dipping down towards SW, 10° (Fig. 3.7). It is located at 373 m above sea level and it is intersected by small sub-vertical steps on a SW-NE direction. Morphometric measurements carried out on the calcareous cobbles (Boenzi et al. 1978) indicated a deposition in predominantly cold climate (Mindel); moreover, among these alluvial elements, to the top of the deposit, some colluvium can be encountered resulting of great interest for the dating of the only landslide present on this type of slope. There, the hydrographic network is currently made up of 1st and 2nd order branches (according to Strahler 1958) and gives rise to a lightly engraved sub-dendritic pattern.
- (b) *Medium-low energy slope*: the slopes had the base at the river scarp between T_1 and T_2 (Fig. 3.4) and develops from 323 m above the sea level to the bottom of the valley (173 m above sea level). The surface profile shows greater regularity in comparison to the previous one, with an average steepness of 10° except in the last section of the slope, spacing from the 4th order terrace (T_4) to the current one (T_5), where a second river scarp is encountered, about 60 m in height and about 40° in steepness (Fig. 3.4).

The superficial drainage scheme is predominantly made up of 3rd and 4th order branches, organised into a *sub-parallel pattern*, in which the tributaries flow into the main collector according to sub-orthogonal angles. The pattern seems due to the structural control carried out by the N20 and N40 families of discontinuities

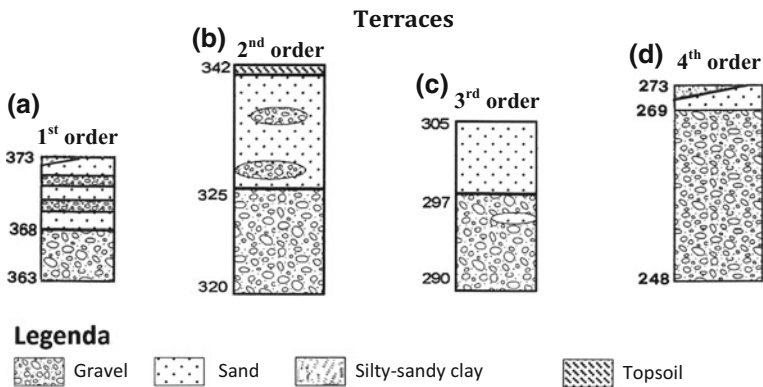


Fig. 3.7 a–d Stratigraphy of fluvial terraces

(extension cracks) and it explicates into an engraved landscape with very deep and articulated channels, un-vegetated micro-versants and very wide small valleys, especially to the bottom of the versant, where the engraved valley is almost at the same level of the riverbed of river Basento (Fig. 3.8).

This *pattern* is substantially due to a rejuvenation of the hydrographic network subsequent to a lowering in the basal level. Currently, however, the erosional work of the watercourses of 3rd and 4th hierarchical order seems to be as considerably slowed down as the sedimentation process prevails within the riverbed of river Basento already for some time.

The 2nd order fluvial terrace (T_2 in Fig. 3.7b) presents at the base well cemented deposits of conglomerates intercepted by vertical cracks with direction NE-SW; these are extensional cracks (*fentes*) with a length of tenths of a meter and parallel to the principal axis (σ_1) of compression of the Apennines. Terrace T2 therefore has been itself subjected to the uplifting Plio-Pleistocenic tectonic action of the blocks. It is located at a level of 348 m above the current sea level and has a maximum thickness of 22 m. To the upslope, the conglomerates become sand and clayey sand with conglomeratic lenses. The average values of morphometric indexes of the calcareous cobbles (flattening 2.60; smoothing 400; asymmetry 0.65) indicate a cold climate; furthermore, lithic artefacts were found within this soil which appear to refer to the Riss (Boenzi et al. 1978).

The 3rd order terrace (Fig. 3.7c) develops around a level of 300 m above the current sea level and has a maximum thickness of 15 m. A deposit of cobbles with a



Fig. 3.8 Small badlands valleys of the medium-low energy slope

sandy matrix ($\sim 30\%$), lightly cemented, lies at the lower boundary; to the upper boundary, a sandy bed of about 8 m in thickness is found, showing particle size distribution decreasing to the upwards. A calcareous crust of a thickness of 20–30 cm is observed to the upper part of the terrace and is referred to an arid-warm climatic phase, corresponding to the Riss–Würm inter-glacial stage.

The 4th order terrace is located at a level of 273 m above the current sea level and is well preserved. The thickness is of 25 m (Fig. 3.7d); polygenic cobbles of about 3–4 cm are present to the lower boundary, scarcely cemented, immersed into an abundant sandy matrix ($\sim 50\%$), imbricate and dipping 25° to SW. The values of flattening index (2.52), smoothing (420) and asymmetry (0.63) indicate a tendentially cold climate (Würm). To the upper boundary there are sands and clayey sands with silty-clayey interbedments belonging to a landslide front. The accumulation zone, in fact, shows the presence of a silty-clayey material with no fabric, chaotic and disordered arrangement incorporating angular fragments of variable size. The altimetric level of the terrace identifies, moreover, the front boundary for the development of a further pre-existing landslide on the slope. The accumulation deposits at the foot are still evident along the contour line at 258 m above sea level, even if the badlands erosion and agricultural works often obliterated the morphology of this phenotype. The sliding surface is about 55 m deep from ground level, whilst the main scarp of the detachment is identified at the current level of 323 m above sea level, with the fluvial scarp between terraces T_1 and T_2 . At the time of the triggering of this landslide river Basento was already developing terrace T_5 .

The *terrace of the 5th order* is the current one and extends widely along the middle valley of river Basento. The alluvial deposit is mainly made up of sub-rounded calcareous cobbles, sometimes flat and/or angular of a diameter of 8–13 cm at the lower boundary, with gradual reduction in size towards the top of the layer and with a progressive enrichment in the sandy and silty matrix. River Basento, therefore, at the end of the Würm had a water flow well greater than the current one and applied a considerable scouring action on the riverbed, with increase, on the low energy slope, of the number of hydrographic elements of 3rd and 4th order, arranged in a sub-parallel pattern, and with a production of sandy-silty-clayey rubbles, more and more abundant, mixing with calcareous cobbles coming from the upper course of the river.

Considerations on the dynamics of the slope

In order to carry out a valid analysis of the re-activation of a pre-existing landslide in cohesive soils it is always useful to understand the kinematics of the deformational processes acting on the slope under analysis. In particular, for what concerns the dynamics of pre-existing landslides it is necessary to define the structural and palaeographic setup of the site within a regional evolutionary context related to space-time relations among different tectonic regimes. Further information, able to assist in the identification of a slope subjected to a potential condition of hydrogeological instability, can be therefore obtained when related to the identification of the causes inducing the re-activation.

The current orogenetic setup of the southern versant of Grassano is the result of compressive deformational processes which acted through a series of tectonic

events since the Günz–Mindel inter-glacial period to the current day. The stress field taking place during this time interval is characterised by a sub-horizontal maximum stress axis (σ_1), permanently oriented in a NE-SW direction, and by intermediate (σ_2) and minimum (σ_3) components, also stationary and respectively oriented in a NW-SE direction, almost horizontal, and in a N-S direction, substantially vertical (Figs. 3.9 and 3.10) (Coppola 1993).

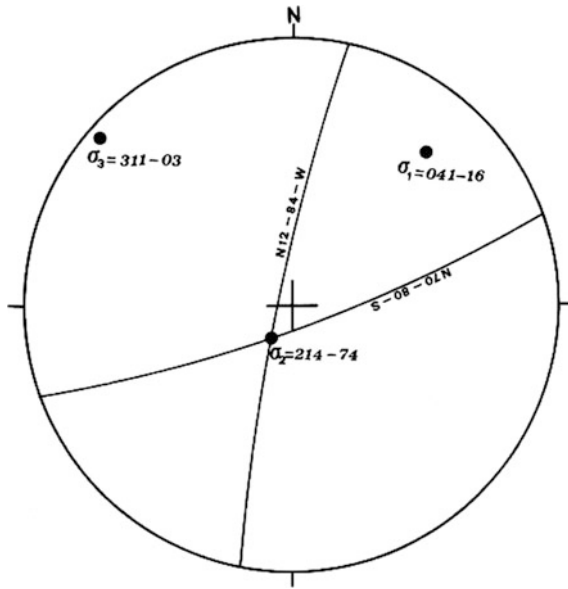


Fig. 3.9 Geometry of the stress field acting during the strike-slip regime

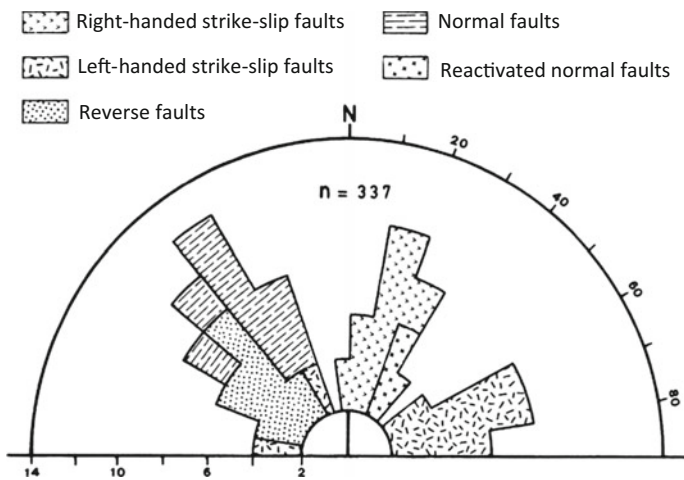


Fig. 3.10 Spatial distribution of the direction of minor fault planes subdivided into classes with angular frequency of 10°

The local deformational system, therefore, was compressive, with vergence towards the Garganic foreland (Gargano is a promontory to the south of the Italian peninsula, on the Adriatic coast—Fig. 3.11). In the medium valley of river Basento the deformation developed in a fairly simple way: tension cracks oriented $N40 \pm 20$, sub-vertical, stylolitic structures due to compression oriented $N130 \pm 20$, perpendicular to the stratification, right-lateral strike-slip faults $N20 \pm 20$ and left-lateral strike-slip faults $N70 \pm 20$, sub-vertical with pitch of the striations equal or almost equal to zero.

On the basis of these elements of structural analysis, taking into account the morphometric measurements carried out by Boenzi et al. (1978) on calcareous cobbles from fluvial deposits, the respective dating and considering that the sediments of these terraces include landslide material as well, it is believed that at least from the end of Calabrian (990,000 years BC) up to date, the slope underwent a process of continuous tectonic and morphologic evolution, the latter due mostly to two landslide events to be correlated to the post-glacial age of terraces T_1 and T_4 . Let us focus, therefore, on some of the moments of the evolutionary processes of the slope subjected to the space-time relations among tectonics, climate and sliding and use the chronological succession of cross sections on Fig. 3.12a–g. At the end of Calabrian ($\sim 990,000$ years BC), the basinal units of the Bradanic Foredeep (Fig. 3.5) emerged from water and, consequently, started the orogenic phase of the versants of the middle course of river Basento. During the Günz–Mindel inter-glacial period (700,000–650,000 years BC), the conglomeratic deposits of Irsina were already located at an elevation of ~ 50 m above river Basento (Fig. 3.12a).

During the Mindel glacial period (between 650,000 and 300,000 years BC—Table 3.1), the left versant of the middle valley of river Basento progressed, from an orogenic point of view, until it reached an elevation of 150 m above the current river course; furthermore, it moved about 270 m NNE with reference to the previous location (Fig. 3.12b). This was a very long period (350,000 years) during which the movements of the glacier induced, everywhere, the removal of pre-existing regoliths and the modelling of the Bradanic deposits influenced by their own structure. Furthermore, moraines deposited on the slope, quite irregular, at the final stage of the glaciation ($\sim 300,000$ years). River Basento applied a low erosion and a modest deepening of the riverbed because of the glaciation of the entire basin; the hydrographic network on the slope was more or less inexistent. Seismic activity was very low.

At the end of the Mindel period, the Mindel-Riss inter-glacial period progressively incomed, between 300,000 and 250,000 years BC, with a permanent dry warm climate. At the beginning of the new period, the slow melting of the Mindelian glacier induced in the ground a constant water seepage, keeping in a status of permanent saturation a horizon of sub-Apennines clay of about 60 cm in thickness. This layer corresponds to the sliding surface of the pre-existing landslide, whose accumulated soils are still today mixed to calcareous boulders to the highest part of terrace T_1 (Fig. 3.12c). It can be therefore deduced that at the time of the activation of the landslide river Basento was already deepening its own riverbed to the downslope of terrace T_1 , by carving the fluvial scarp between T_1 and T_2 , as shown in the following.

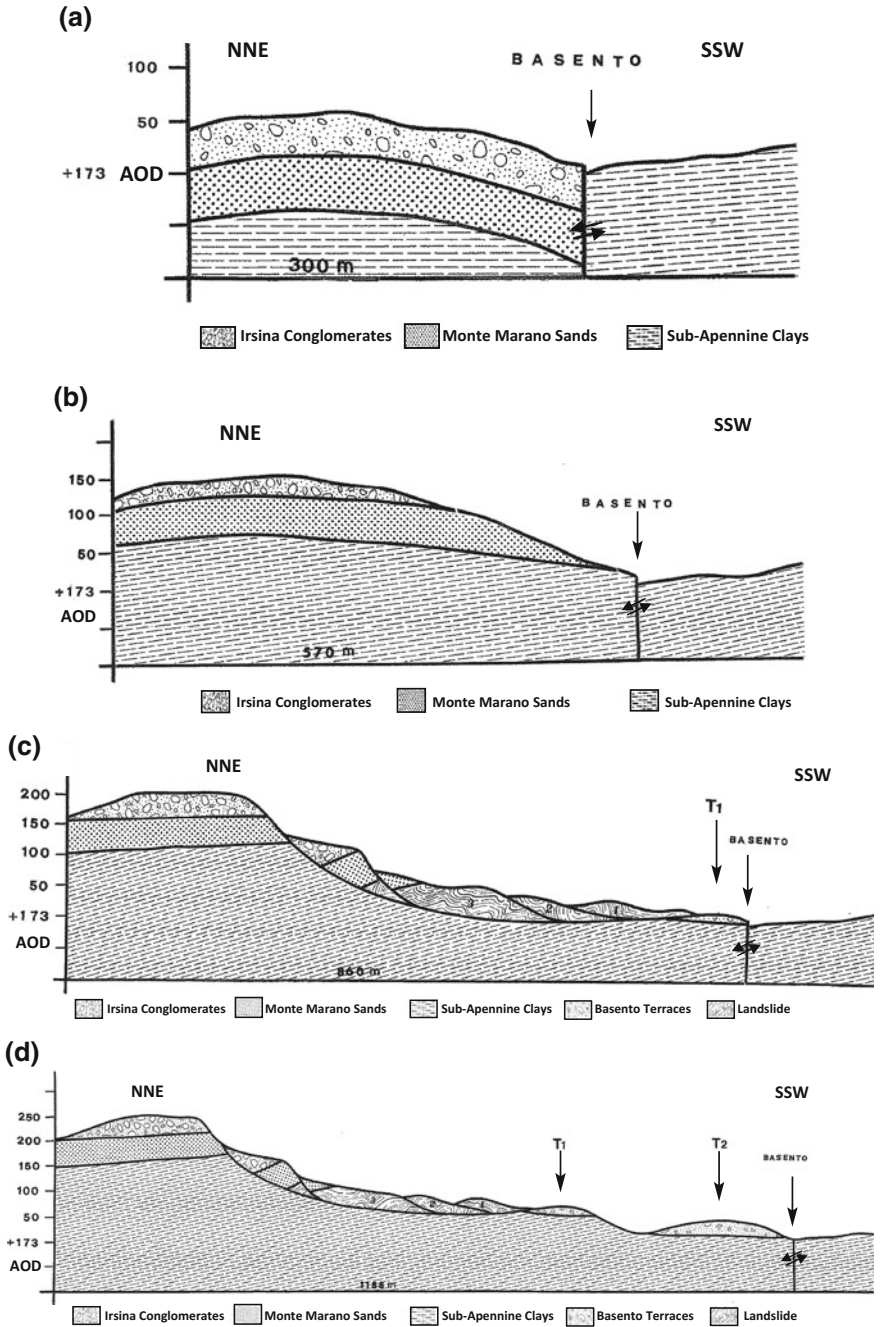


Fig. 3.12 (continued)

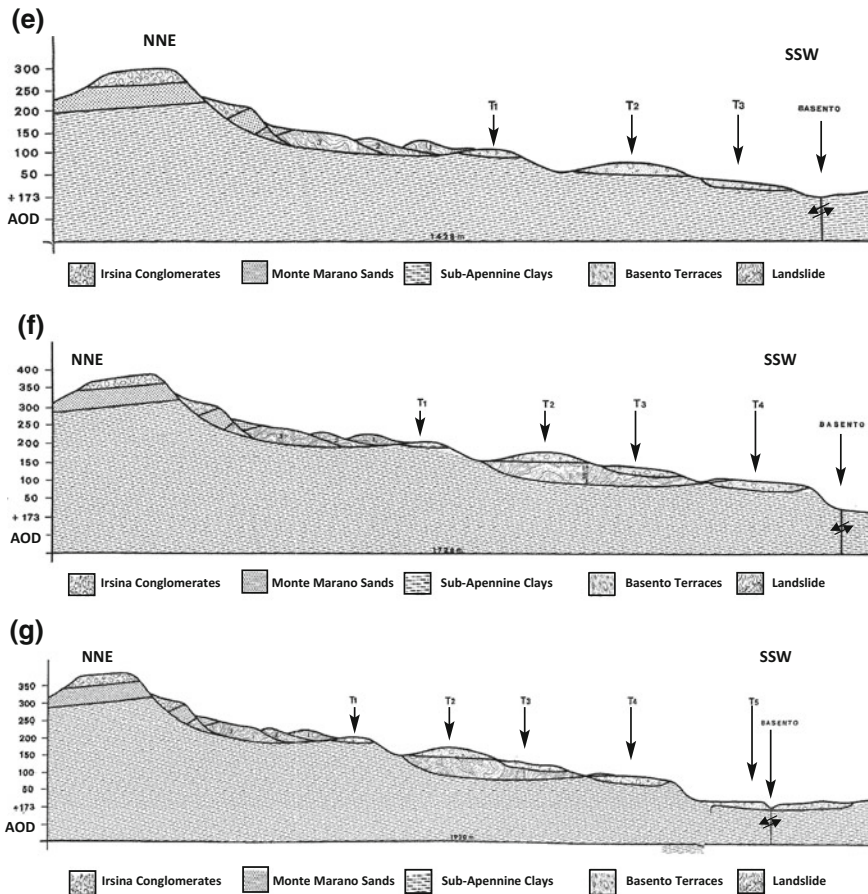


Fig. 3.12 **a** Sketch of the Grassano tectonic block and location of the Basento river (Southern Apennine), at the end of the Günz-Mindel interglacial period (650,000 years BC). Indicate the movement of the left-handed strike-slip fault along which the middle course of Basento flows. **b** Sketch of the Grassano tectonic block and location of Basento at the end of the Mindel glacial period (300,000 anni BC). Indicate the movement of the left-handed strike-slip fault along which the medium course of Basento flows. **c** Sketch of the Grassano tectonic block and location of Basento at the end of the Mindel-Riss interglacial period (250,000 anni BC). Indicate the movement of the left-handed strike-slip fault along which the medium course of Basento flows. **d** Sketch of the Grassano tectonic block and location of Basento at the end of the Riss glacial period (130,000 anni BC). Indicate the movement of the left-handed strike-slip fault along which the medium course of Basento flows. **e** Sketch of the Grassano tectonic block and location of Basento at the end of the Riss-Würm interglacial period (74,000 anni BC). Indicate the movement of the left-handed strike-slip fault along which the medium course of Basento flows. **f** Sketch of the Grassano tectonic block and location of Basento at the end of the Würm glacial period (8400 anni BC). Indicate the movement of the left-handed strike-slip fault along which the medium course of Basento flows. **g** Sketch of the Grassano tectonic block and location of Basento at the end of Würm. Indicate the movement of the left-handed strike-slip fault along which the medium course of Basento flows

The percolation of glacial water through the clayey layers in the ground was favoured by the presence of cracks originated by tectonic reasons and by repeated seismic events caused by the orogenetic activity until the melting of ice on the slope ended.

During the Mindel-Riss period, the tectonic block of Grassano underwent further series of uplifting events and movements towards NNE (Fig. 3.12c). The orogeny pushed the Irsina conglomerates to an elevation of about 200 m above Basento valley, while the translational movement of the block moved forward of further 290 m. There is therefore a relative acceleration of local tectonics if compared to previous periods, considering that in such a short period (50,000 years) the Grassano block moved of 290 m. In the early days of this period, river Basento flowed down with a large flow, rich in solid elements, due to the melting of the glacier. The river deepened rapidly, facilitated by the presence of a strike-slip fault with vertical ruptures where the watercourse was forced to flow.

By the end of the period, the river valley assumed an asymmetrical structure due not only to the influence of the strike-slip fault, but mainly to the layering of the Sub-Apennines clay strata. On the right versant, the latter had a monoclinical structure dipping 6° to NE (currently $i = 10^\circ$), while on the left side the slope dipped down 13° also to NE. In this area, the layers were configured as anti-dip slope due to the uplifting of the Grassano block. The cross section of the valley is therefore asymmetric because of structural reasons. This reconstruction shows that the scarp between T_1 and T_2 , about 50 m in height, is not a landslide scarp but a river scarp, originated by the incisiveness of river Basento and later modified by erosion (Fig. 3.12d). This scarp marks the separation between high energy and low energy slopes.

The 1st and 2nd order hydrographic network, which is currently characterised by a sub-dendritic pattern at the top of the slope, does not belong to that period. It belongs to a recent hydrographic system.

In the Riss glacial period, between 250,000 and 130,000 BC, the Basento built terrace T_2 . The Irsina conglomerates could be encountered at an elevation of 250 m above the valley while the block moved of further 328 m with respect to the displacement developed during the Mindel-Riss period (Fig. 3.12d). There were no significant changes in the morphological state of the slope. However, some general considerations can be drawn on the mechanisms of structuration of this part of the Sub-Apennines range given the long period during which this very important movement of the block has occurred; the orogenetic elevation, on the other hand, remained at average values if compared to other periods. This is due to the fact that the strike-slip faults affecting the Bradanic units, subjected to the maximum compression direction $\sigma_1 = N40$ sub-horizontal, have been reactivated by an impulsive invariant stress regime, typical of the structuration mechanisms of the Sub-Apennines range. As a result of that, a repercussion was triggered both on the structure of the versant, giving the low energy slope an average steepness of 10° , and on the erosive activity of river Basento, which after this period began a phase of predominant deposition with variation of the base level and subsequent modest development of the hydrographic network.

The presence of lithic artefacts between the deposits of terrace T_2 indicates that these areas of the slope were habitable and frequented by humans, even in a period of mostly perennial ice.

The beginning of the Riss-Würm interglacial period, between 130,000 and 74,000 years BC was characterized by maximum levels of heat for 13,000 years, later changed to temperate warm throughout the rest of the period. The slope of interest was interested by a small erosional scarp between T_2 and T_3 (Fig. 3.12e). The modest erosive effect and the depositional characteristics of terrace T_3 , presenting at the base modest sized limestone cobbles (2–5 cm) mixed with abundant sandy matrix and grain size distribution becoming more fine grained to the upwards, indicate the tendency of river Basento to wander across the area over the time with a predominant depositional action when passing from a humid climate to a relative dryness, as witnessed by the limestone crust of the thickness of 20–30 cm in the upper part of the terrace. As a consequence, from an initial phase in which the river was eroding the terrace it passed to the intermediate and final phase of the period, in which it progressively lost its energy and thus exerted a prevailing sedimentation function. These dynamics also affected the incipient hydrographic network that was forming through the 3rd and 4th order waterways especially in the initial phase of the interglacial period. The 4th order branches, in particular, by using the $N40 \pm N20$ extrusion fractures produced by the compressive tectonics under action as preferential routes of outflow, have lost erosive capacity because of the raising of the base level. The slope with medium-low energy, therefore, gained an adjustment of the superficial profile with a reduction in steepness and was characterised by a few modest landslide events, mostly superficial.

The orogenic activity was maintained in the norm; the uplifting of the Grassano block has actually recorded an increase of 50 m, reaching the elevation of 300 m above the valley of river Basento, while the slope moved forward longitudinally towards NE of further 240 m.

During the Würm glacial period, i.e. between 74,000 and 8400 BC, the orogenic block of Grassano gained about 70 m in height reaching the elevation of 370 m above the current Basento valley (Fig. 3.12f). The horizontal movement was about 300 m towards NE. The imbricated polygenic cobbles of terrace T_4 , dipping down 25° to SW, testify, in facts, of quite an active tectonic action taking place throughout the whole period as well as testified by the erosional scarp, highly steep and deep, ranging between terraces T_4 and T_5 . Furthermore, the 4th order terrace deposit shows a succession that is typical of the one generated by waterways initially poor in solid transport, presumably because of the presence of the vegetation mantle on the slope with low steepness, and then by the deposition of coarse grained debris with abundant sandy matrix due to glacial ablation.

By the end of the Würm glaciation, between 11,700 and 8400 BC (Würm IV), the local climate passed gradually from the dry and arid cold to a mild temperature (Table 3.2) with high rainfall, which reached, as a yearly average, the maximum value of $+4^\circ\text{C}$ around 9000 years BC.

The Würm IV period practically gave start to Holocene (starting 11,700 years BC), when the pre-Boreal sedimentary cycle began (11,700–9000 BC); during this period, Würmian glaciers were melting and interacted with the system of Apennines under evolution. On the low energy part of the southern slope of Grassano a large, pre-existent, rotational landslide developed, whose main scarp partially coincided with the river scarp between terraces T_1 and T_2 while the accumulation front dumped onto the top of terrace T_4 , by then under abandonment by river Basento (Fig. 3.12g). The landslide was 560 m long, while the sliding surface reached a maximum depth of 55 m below ground level. The origin of the landslide was certainly attributable to two main reasons: 1°) at the time of the triggering of the landslide, the ground was in a state of saturation, because of more than 2000 years of water infiltration due to the slow and progressive melting of the glaciers of Würm; 2°) the rather frequent and, presumably, high magnitude seismic activity induced the formation in the ground of more numerous and larger tension cracks, increasing in that way the permeability and the depth of percolation of glacial water.

At the end of Würm IV (late glaciation, 8400 BC), the interglacial or postglacial period took over into the Holocene, climatically very variable and tendentially warm and humid in the Mediterranean zone. However, already in the end of the Boreal sedimentary cycle (~8400 BC), a new glacial phase with a cold arid climate, lasting for 6400 years, took place interrupted by a temperate warm period with high rainfall between 6100 and 4000 years BC. In the latter period, river Basento was back into deep scouring and was developing the construction of the river scarp between terraces T_4 and T_5 (Fig. 3.12g). The erosion took place along a pre-existing failure zone due to the presence of the left-handed strike-slip fault along which the Basento has always been channelled during its processes of deepening of the riverbed. On the contrary, the fluvial dynamics have shown, in every age, rambling effects for the river when the deposition action prevailed, as it is currently happening within the alluvial plain of terrace T_5 .

Around 2000 years BC, the climate in European Mediterranean areas quickly changed after about 2000 years of intense cold and took over a period called “Optimum Climatico Romano” which lasted until 1000 BC, with mild warm and annual maximum temperature of +0.1 °C. Between 1000 BC and year 0 AD the intense cold went back, with an average temperature of –0.5 °C.

Although with alternative weather conditions, in the last 2000 years, the slope on the left hydrographic bank of river Basento has not undergone major evolutionary processes except those already started at the beginning of Upper Holocene, which, with modest variations, continued their action of morphological modification of the slopes in relation to the fluvial dynamics.

Between 450 and 150 BC on the same versant ancient Roman villas arose while the merchant ships of the Great Empire sailed river Basento back to the location of Serra del Cedro, currently in the municipality of Tricarico, where, at the top of the hill (858 m above sea level), today are still located the remnants of an ancient military post controlling the naval traffic along the river. This activity lasted until about year 1000 AD. Therefore, it should be assumed that, at least until that time, the riverbed of the medium Basento valley was much deeper than how it was later,

in the Middle Ages; it was thus still eroded, with water flows sufficient for navigation resulting from the abundant rains of a warm damp Mediterranean climate that lasted until 1350 AD, when the “Little Ice Age” (1350–1850 AD) took place in the same areas, with fluctuating temperatures of between -0.25 and -0.5 °C and with maximum levels of dry cold weather in years 1670, 1710, 1810 and 1850. In fact, already in the Middle Ages, the deposition action in the intermediate section of river Basento was predominant. In this period, the current terrace T_5 is formed as made up of calcareous cobbles coming from the upper river course, predominantly torrential, and from badlands tributaries, bringing in a mixture of mud and sand with high density.

In the meanwhile, the recent tectonics, invariably compressive, contribute to the rise of the tectonic block of Grassano, which reaches the peak of 550 m above sea level, or 377 m above the valley of Basento. At the same time, terrace T_4 reaches an elevation of about 100 m above the current valley base. This indicates that the combined action between uplifting tectonics and river erosion produced a 100 m elevation difference between the Basento and the low energy slope, which the pre-existing Würmian landslide is part of, from the end of the Atlantic sedimentary cycle (6100 AD) to date (2000 AD). In the same period, the erosive process exerted by river Basento depressed the basic level of the hydrographic network already developed during the Riss-Würm interglacial period. The 4th and 3rd order watercourses, respectively, entered a strong engraving phase. They deepened and extended to the upslope into the mountain, branching into a network of badlands separated by narrow ridges, with rapidly evolving plain micro-versants (Figs. 3.6 and 3.8). In particular, the 4th order water courses acted as the main axis of the badlands micro-basin and are those ones with an arrangement orthogonal to the direction of river Basento. On the low energy slope, the engraving phenomenon over time had the effect of consolidating the Würm landslide, preserving this from further mass movements. In fact, throughout the Holocene until today this landslide has never been affected by reactivation phenomena unlike the landslide from the Mindel-Riss interglacial period, which is still in slow impulsive motion. The consolidation of the former develops because of the depression of the neutral pressure regime, induced by the lowering of groundwater due to the deep engraved valleys.

In the current period, the river Basento has a rather modest flow due mainly to the climate that is variable according to the seasons. The riverbed is rising up for both solid deposition and for the rising of the eustatic level of the Mediterranean Sea. The sedimentation process is still prevalent but the solid input is mainly from the water courses of the 2nd and 1st order of the hydrographic network and from current modest landslides occurring on the engraved non-vegetated micro-versants during periods of intense and/or prolonged autumn or spring rainfalls.

On all the slopes on the left bank of the middle valley of the Basento, the existing active landslides are therefore those that belong to the high energy slope. These landslides however reactivate only after high-magnitude telluric events.

The interpretive error

Regarding to the Mindel-Riss Grassano landslide, resulted as paradoxical the intervention for consolidating the upslope, below the historic centre, where a few months after the earthquake of 23.11.1980 (Irpinia Earthquake) took place a mass movement of the pre-existing landslide mass, which caused some stability problems in the buildings on the 1st landslide terrace (see Fig. 3.13, Sections 1 and 2). It should be pointed out that the reactivation took place at a later time than the main seismic event, certainly as a result of the increase in interstitial water pressures. In most cases, reactivations of large landslides due to earthquakes are to be considered as indirect processes when movements are not simultaneous to seismic events, but are to be attributed to increases in interstitial water pressures, developing with time, in various ways, in relation to the main event. Referring to the previous temporal reconstruction of the landslide movements on the southern slope of the Grassano hill in relation to the fluvial dynamics of the river Basento, the error done was to correlate the sliding surface of post-Mindel age to that of post-Würmian age (Fig. 3.13, Section 1). The sliding surface, therefore, was considered at a depth of 185 m from the ground level of terrace T₁. In the Apennines there are no shearing surfaces to similar depths, in particular in Sub-Apennine clays, which are lightly fractured and, at this depth, dry and overconsolidated. During the excavation works for the consolidation of the slope, it was found that the original sliding surface had a depth of about 60 m from the ground level. The incorrect evaluation of the geometry of the pre-existing landslide and the depth of the sliding surface resulted in useless and over-expensive consolidation works on a slope that is today still in motion.

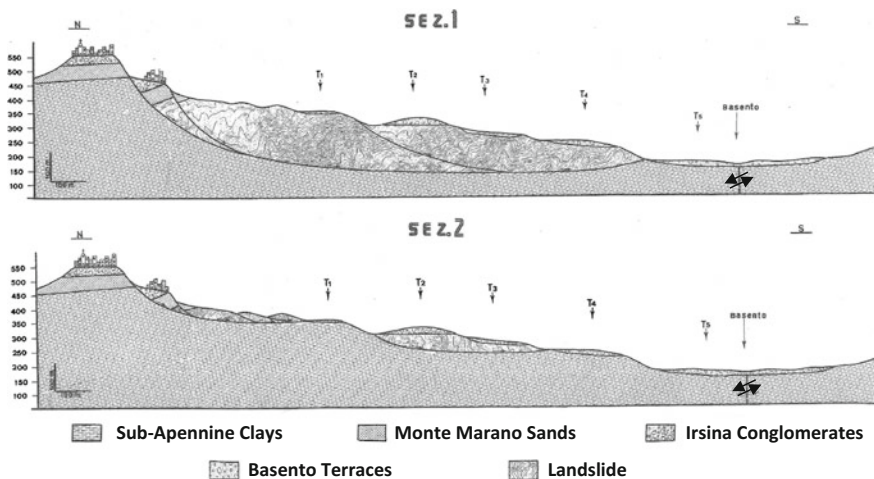


Fig. 3.13 Section 1 reports the interpretive error done during the survey for the slope consolidation works. It shows that the two landslides of different age were considered as two elements of the same landslide. Section 2, instead, shows the real configuration of the interactive process involving tectonics, fluvial deposition and hydrogeological instability of two landslides developed in different ages

References

- Bertini, T., Cugusi, F., D'Elia, B., & Rossi-Doria, M. (1986). *Lenti movimenti di versante nell'Abruzzo Adriatico: caratteri e criteri di stabilizzazione* (Vol. 1, pp. 91–100). Atti del 16° Convegno Italiano di Geotecnica, Bologna.
- Boenzi, F., Di Gennaro, M. A., & Pennetta, L. (1978). I terrazzi della valle del Basento (Basilicata). *Rivista Geografica Italiana*, LXXXV(4), 396–418.
- Casnedi, R., (1988). *La Fossa Bradanica: origine, sedimentazione e migrazione*. Atti del 74° Congresso Soc. Geol. It., 98–103.
- Castiglioni, G. B. (1979). *Geomorfologia*. Torino: UTET.
- Coppola, L., (1993). *Evoluzione tettonica e meccanismi deformativi della Media Valle del Basento*, Boll. Soc. Geol. It., 112, pp. 159–179, 20 ff., 1 tav. f.t.
- Hutchinson, J. N., & Gostelow, T. P. (1976). The development of an abandoned cliff in London clay at Hadleigh, Essex. *Philosophical Transactions of the Royal Society of London*, A283, 557–604.
- Hutchinson, J. N., Chandler, M. P., & Bromhead, E. N. (1981). Cliff recession on the Isle of Wight, SW coast. In *Proceedings 10th International Conference on Soil Mechanics and Foundation Engineering* (pp. 429–434).
- Lazzari, S., & Lentini, F. (1980). *Note illustrative del Foglio 507 Pisticci* (pp. 1–55). Regione Basilicata, Potenza: Potenza.
- Lentini, F. (1971). *La sedimentazione plio-pleistocenica di Pisticci sul bordo appenninico della Fossa Bradanica* (Vol. III, pp. 109–192). Atti acc. Gioenia di Sc. Nat. in Catania, VII.
- Ricchetti, G., & Scandone, P. (1979). Inquadramento geologico regionale della Fossa Bradanica. *Geologia Applicata e Idrogeologia*, vol. XIV, p. III, Bari.
- Selli, R. (1962). Il Paleogene nel quadro della geologia dell'Italia meridionale. *Memorie Società Geologica Italiana*, 3, 737–789.
- Strahler, A. N. (1958). Dimensional analysis applied to fluvially eroded landforms. *Bulletin of the Geological Society of America*, 69, 279–300.
- Varnes, D. J. (1978). Slope movement type and processes. In R. L. Schuster & R. S. Krizek (Eds.), *Landslides: Analysis and control* (Vol. 176, pp. 11–33). U.S. Natural Academy of Sciences, Special Report.

Chapter 4

The Pre-failure Deformation

4.1 Introduction

The analysis of phenomena of instability of slopes must be carried out based mainly upon the observation of the natural cracking of the soils and upon the interpretation of the mechanisms that induced them.

This analysis is far more important when the final purpose of the research is the *prediction* and *prevention* of disasters induced by the hydrogeological instability of the slopes. In this chapter, the subjects are the Apennines range and, in part, the Argentinian Pre-Andes of the Provinces of Salta and Jujui, that are the areas on which our experience is founded onto.

In a progressive-sequential deformation system of thrust tectonics, the Apennines chain was affected, from Upper Tortonian onwards, by subsequent over-sliding of large lithic masses advancing towards the Adriatic Foreland (Fig. 4.1). In an invariant compressive stress regime, in this context, exists the problem of the non-nativity of lithic masses, which, in a process of deconstruction, have become the place for numerous and wide areas of hydrogeological instability (Fig. 4.2).

Indeed, the current orogenetic arrangement of the Apennines lithological units is the result of compressive deformation mechanisms that have acted through a series of events from the Lower Miocene to the present making the soil structure chaotic, heterogeneous and anisotropic; layering is generally not identifiable, while the lithic mass is intimately fractured and folded. Therefore, the knowledge of the initial conditions and at the boundary of the soil, of the applied stresses, of the post-failure behaviour of the slope, which so much influence induces on the damage caused by landslide events, represents the necessary and preliminary condition for the development of tools of calculations capable of providing an adequate and credible response for the protection against hydrogeological risks. In general, the mechanical properties of the deposits with prevalent clayey component depend on both the mineral and granulometric characteristics and on the lithological discontinuities.

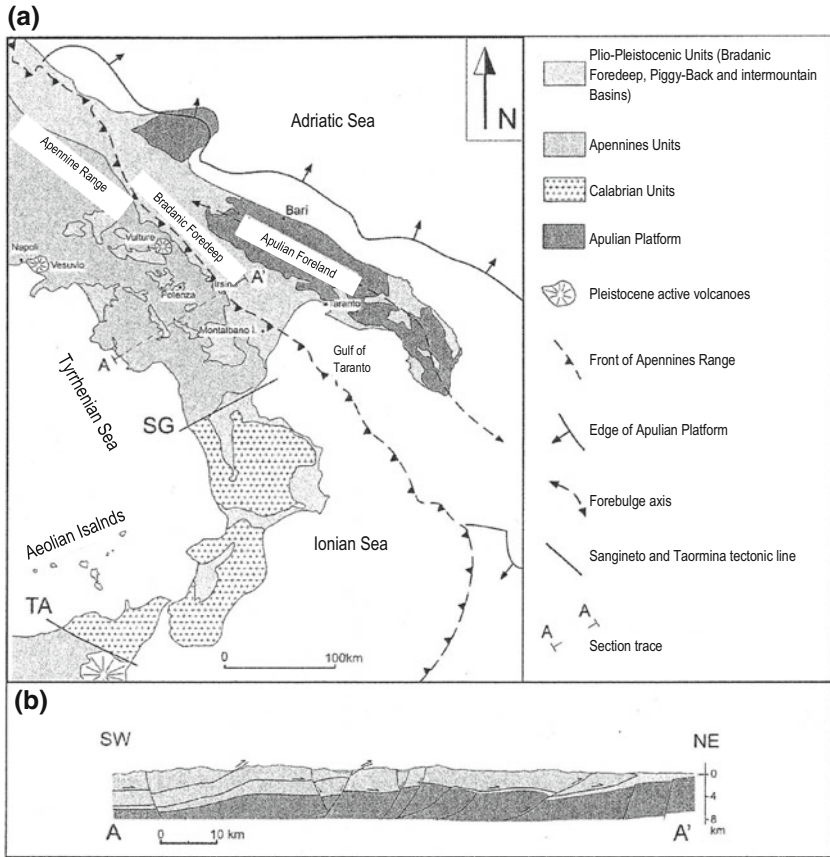


Fig. 4.1 Southern Apennine—lithologic scheme of the areas subjected to continuous monitoring because of the risk of landslides

The presence of a few discontinuities is sufficient to ensure that the overall mechanical behaviour of the soil becomes completely different from that of the soil matrix.

The evaluation of the mechanical characteristics of a rock mass (considered in the broad sense) can therefore only be derived from an accurate description of the discontinuities present and from a careful study of their properties. In addition, discontinuities indicate an oriented “structure” within the rock mass, even when this is intrinsically made up of isotropic rock; the discontinuities cause an obvious anisotropy of the mechanical characteristics and only in limit conditions of extreme fracturing it is possible to obtain again an isotropic structure, but only from a statistical point of view.

Particular attention must be paid to fissured overconsolidated clays. Actually, the presence of cracks and discontinuities affects both the in situ behaviour, both the response upon sampling and during laboratory testing.

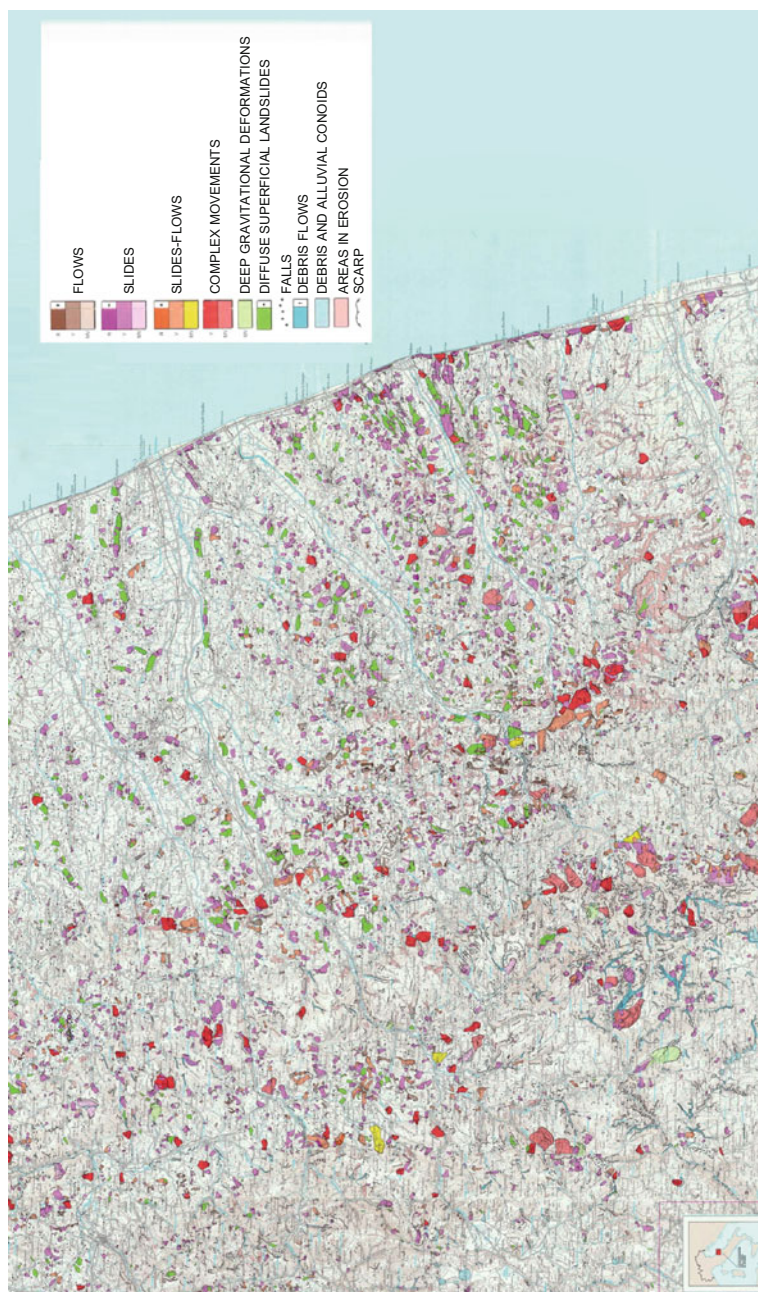


Fig. 4.2 Hydrogeological instability in Marche region (Italy) (CNR 1989)

Since it can be imagined that the resistance to shearing of a large sample of clay is mainly governed by the strength along the discontinuities, it can also be expected that this decreases as the sample size increases. In fact, the resistance obtained by means of large-plate loading tests (865 mm) clearly shows (Marsland 1974) that increasing the volume of soil tested, both the results dispersion and the resistance reduce considerably. From these considerations, the following indications can be made:

- when the soil has a macrostructure characterized by fissures, laboratory results are scarcely representative of the behaviour that a volume of soil may have on site; referring, instead, to in situ tests, representative values can be obtained, provided that the use of tests involve a significant portion of the ground;
- when comparisons are carried out on the results of various types of tests, the influence of several factors must be taken into account, among which the most important is the volume of soil tested and the phenomenon of progressive failure; furthermore, it still remains uncertain, according to the current state of knowledge, whether it is possible or not to speak properly of undrained behaviour in the case of fissured material (Simpson et al. 1979).

Given that at the origin of every technical investigation is needed a careful geological survey of the site, in order to establish the lithological application field, and a geomorphological survey, in order to classify and characterize the phenomena of slope transformation, for the choice of the methods of analysis, the study of rock fissuring should be directed essentially to the definition of a geomechanical model useful, for other professionalisms, for design analyses or specific assessments. For this purpose, the method of study and interpretation of fracturing must correspond to the following operations: (1) monitoring of deformations (in the wider sense) and measurements of the corresponding geometric elements; (2) geometric and kinematic interpretation of the observed deformations.

For the purpose of the geometric interpretation it is necessary to distinguish all the structures belonging to the same deformation phase, in order to obtain a model representative of the entire deformation system. For the kinematic interpretation, then, separate structures belonging to different systems must be separated to establish a relative time history of the corresponding deformation phases.

In this chapter, it is attempted, in a basic manner, to provide those useful notions that are in accordance with the laws of mechanics in order to arrive to this second phase of the study.

In geological practice, the analysis of rock fissuring embraces a vast field. It is essential for underground works, such as mining tunnels and tunnels for civil purposes or for water mains purposes, as well as for exploration and uptake of groundwater, for the underground storage of fluids and wastes and even for low-depth works, such as foundations, excavations, open-cast mines and, finally, surface works such as dams, coal or nuclear power plants, etc.

From the point of view of the stability of slopes or of mass movements the fissuring of rocks affects the characteristics of deformability and strength of the rock mass, which depends predominantly on geometry, spacing, orientation and mechanical-physical characteristics of the planes of discontinuity. Therefore, the first step towards

the analysis of the stability of a slope is to find a relationship between systems of discontinuities and possible kinematics of instability. Relationship to be obtained from the examination:

- (a) of discontinuities, unstable rock volume and possible failure surfaces;
- (b) of the slope and of the mechanical characterization of the discontinuities.

4.2 Development of Cracks Under Compression¹

It is very interesting to describe the development of cracks under monoaxial compression, i.e. without lateral stresses.

Considering an open, elliptical, very flattened crack, contained in a rock sample subjected to axial compression σ_1 , it is possible to distinguish several successive steps with the increase of σ_1 before achieving the failure (Fig. 4.3a).

1. Initially, a closure of the fissure is obtained (Fig. 4.3b).
2. A slight relative sliding of the two sides of the fissure is then induced (Fig. 4.3c).

This movement, initially elastic, is not entirely reversible because there is dissipation of energy, becoming movement.

3. By increasing σ_1 , crack tends to develop because of the formation, at its ends, of tensile cracks, which extend, initially, perpendicularly to the initial crack, but then tend to become parallel to the direction of σ_1 (Fig. 4.3d). This indicates that under monoaxial compression it is obtained the development of tensile stresses which produce secondary extensional cracks. These are always parallel to σ_1 .
4. If σ_1 increases beyond a certain threshold, the complete failure of the sample is obtained because of the unstable development of extensional cracks.
5. The new tension cracks do not propagate, if not at short distance from the main elliptic crack, until the value of σ_1 does not overtake a certain failure threshold. When, instead, σ_1 exceeds this threshold, a horizontal stress (σ_3), orthogonal to σ_1 , appears within the sample because of the confining stress of the lithic mass, that opposes to the trend of the increase in volume of extensional cracks. This is how the rupture of Fig. 4.3e is achieved. *The brittle deformation of a rock, therefore, always occurs under triaxial conditions ($\sigma_1 > \sigma_2 > \sigma_3$). The length of cracks is function of the ratio σ_3/σ_1 and of the length of the initial crack.*

Under triaxial conditions, starting from the development of the stable extensional crack of Fig. 4.4(1), there are small, almost capillary, extension cracks at the extreme ends of the initial crack. By increasing the triaxial stress state, the closure

¹The Content of Sects. 4.1–4.4 is Inspired by the Manual “La Fracturation des roches” by Jean-Louis Bles–Bernard Feuga (1981)

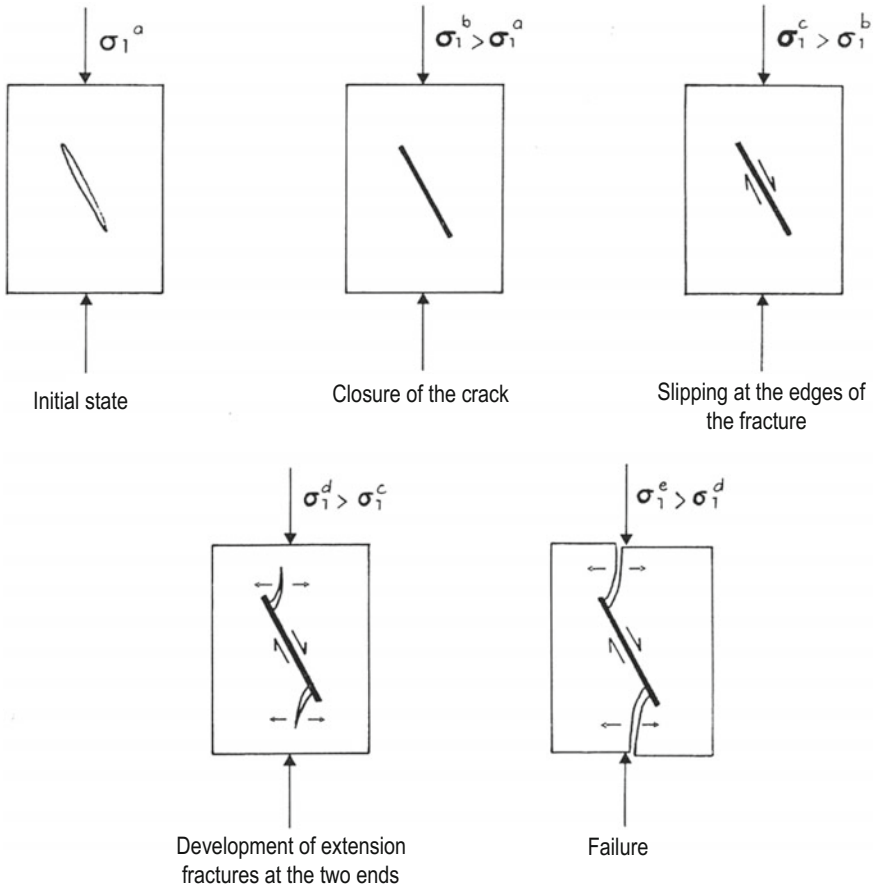


Fig. 4.3 Failure of a sample with a pre-existing internal crack under monoaxial compression (from Bles and Feuga 1981)

of the crack is initially obtained and then the sliding of the two parts of the rock along the initial penetration plane (Fig. 4.4(2)). The frictional resistance at failure between the two sides of the original crack is defined by Coulomb's law (1773).

$$\tau = \tau_0 + \sigma_n \tan \phi$$

where

$$\sigma_n = \left(\frac{\sigma_1 + \sigma_3}{2} \right) - \left(\frac{\sigma_1 - \sigma_3}{2} \right) \cos 2\vartheta$$

$$\tau = \left(\frac{\sigma_1 - \sigma_3}{2} \right) \sin 2\vartheta$$

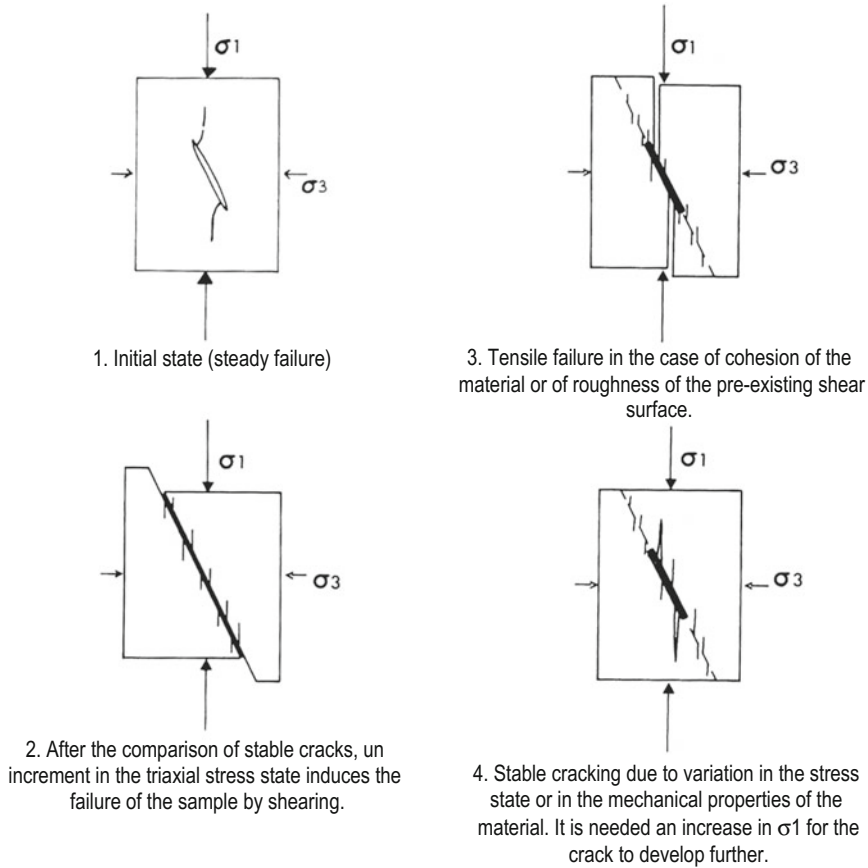


Fig. 4.4 Possible failure model under triaxial compression (from Bles and Feuga 1981)

The failure corresponds to a value $\tau = \left(\frac{\sigma_1 - \sigma_3}{2}\right)$ which is obtained when $\vartheta = 45^\circ$.

If after the formation of stable extension cracks (Fig. 4.3d) the shear resistance is exceeded, failure is achieved due to shear movement along the initial failure plane (Fig. 4.4(2)). However, the cohesion of the sample or the roughness of the shearing surfaces, can resist to failure and stop the development of extensions cracks parallel to σ_1 , located at the end of the original elliptical crack, and cause a tensile process with sliding and opening of the latter (Fig. 4.4(3)).

Alternatively, failure can be produced from the combination of the two previous processes according to a shear surface which is intermediate between the cracks parallel to σ_1 and the initial failure plane.

During the deformation, changes take place in both the stress field and the mechanical properties of the material. In this case the fissuring becomes stable (Fig. 4.4(4)). An increase in σ_1 is therefore necessary for the fissuring to develop further.

4.3 Analysis of Brittle Deformation

The rocks that are currently present on the surface of Earth have deformations that can be of two different types: bending, if the deformation is of plastic type, or cracking, if the deformation is rigid.

These deformations mainly develop under the effect of a tectonic thrust that influences the lithological nature and the mechanical characteristics of the rocks.

Geologists use the term “competent” for those rocks with a rigid or brittle behaviour; thus, they are those rocks that, under tectonic actions, develop failure without presenting a plastic-like behaviour, such as limestones, sandstones and granites.

Non-competent rocks, such as clays, are characterized by plastic behaviour and thus induce phenomena of bending. This useful distinction, however, does not take into account the conditions of pressure and temperature associated with the depth at the time when the rocks are stressed by tectonic forces. In effects, a rock which is competent when at surface can become non-competent at depth and vice versa. For example, limestones are competent on the surface as well as clays are non-competent, but from a certain depth the limestones become less competent than clays.

Under conditions of increasing pressure and temperature, i.e. when moving from surface to depth of an area of the Earth’s crust, a stratified and homogeneous rock may subsequently undergo the following types of global deformation:

1. cracking;
2. cracking and bending;
3. bending;
4. bending and flattening;
5. flattening;
6. flattening and melting;
7. melting.

This indicates that with depth the deformation of a rock always assumes a more plastic behaviour.

For the same tectonic domain, the mechanisms of deformation remain globally the same within large volumes, but these mechanisms vary vertically with depth; therefore, the notion of structural levels is created.

There are three major structural levels, that are identified, from top to bottom (Fig. 4.5a, b), as:

- higher structural level, characterized by the predominance of brittle behaviour of most of the rocks, thus showing an important fracturing by shearing or discontinuous deformation. However, very plastic rocks are subject to types of deformations by bending, that do not exclude that the same rocks can be equally fractured;
- intermediate structural level, corresponding, in general, to deformation by bending of stratified levels. Isopach folds are the result of this bending and are often accompanied by fractures and faults, especially in the most competent

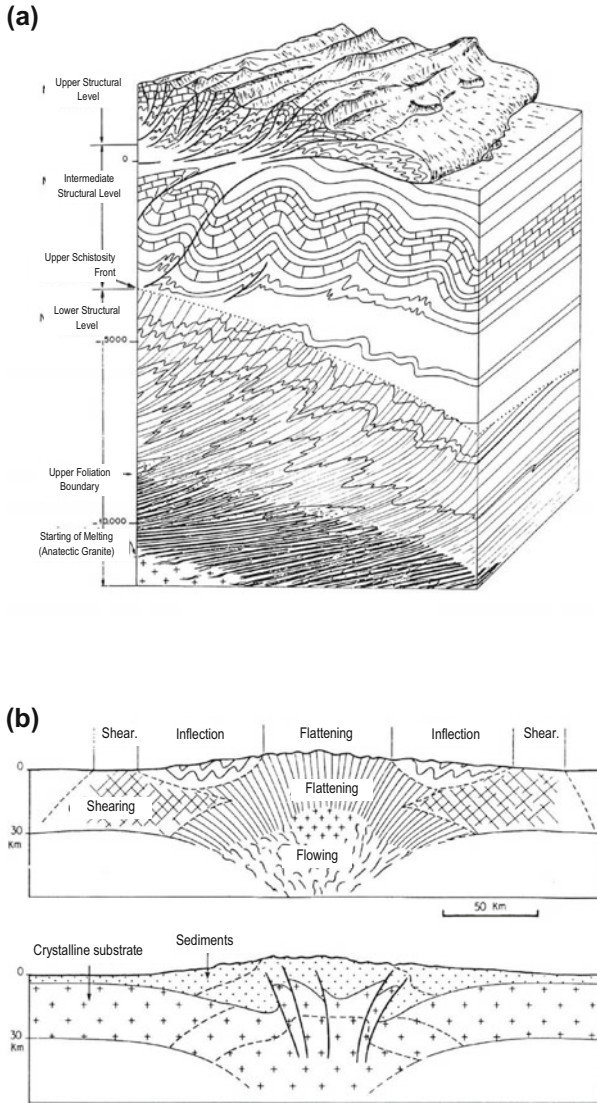


Fig. 4.5 **a** Block diagram of a portion of Earth's crust showing the superposition of several structural levels and the style of the corresponding structures (from Mattauer 1973). **b** Block diagram of a symmetric mountain range with small shortening and with distribution of the corresponding structural levels (b_1). It is evidenced that, following to lithologic contrast between the sediments and their crystalline substrate, shear can take place at the base of the zone subjected to bending (from Mattauer 1973)

rocks, that make up the skeleton of the rock volume. Incompetent rock levels bend in disordered or disharmonious modes in comparison to the isopach folds of competent rocks;

- lower structural level, characterized by the development of schistosity accompanied by metamorphism and subsequently by a flow because of the fusion of rocks.

The development of schistosity takes place generally on large thicknesses and can be then distinguished from top to bottom:

- (a) schistosity zones from cracks and cracks/folds (*cleavage, strain-slip cleavage or crenulation cleavage*);
- (b) schistosity zone by melting (*fluid-cleavage*);
- (c) flaking zone (*schistosity*)

This simplified scheme is applied to a tectonised zone affecting the thickness of sedimentary soils.

It is clear that this ideal breakdown of structural levels can be edited or varied according to whether sedimentary coverage or granitic mass or other type of soil is considered as well as deformation also depends on the intensity of tectonic stress.

An important factor in the deformation of rocks at great depth is fluid pressure or interstitial pressure.

The presence of important interstitial pressure can induce the development of extension fractures or produce a rigid behaviour in those rocks that are usually subjected to plastic deformations.

The deformation is thus produced during an epoch during which the rocks under discussion are at different depths and therefore subjected to different tectonic stresses according to the structural level the rock belongs to. In the same epoch, different deformations can be obtained according to the structural level the rock belongs to. The deformation however has the same orientation whatever is the structural level of belonging of the deformed rock. An epoch that has the same orientation of structures corresponds to a certain tectonic phase; more tectonic phases correspond to an orogeny or to an orogenic cycle such as the Hercynian cycle or the Alpine cycle.

More tectonic phases involve overlapping of deformation effects.

4.4 Definition and Description of the Various Types of Fractures

The term fracture is taken in the sense of tectonic discontinuity. It therefore incorporates diaclases, fentes or extension fractures, stylolitic joints and faults of various sizes.

Schistosity and foliations are not comprised in this term as, obviously, are not the different types of stratification.

The geometric description of the fractures can be made by defining, for each of them, type, morphology, extension, continuity, thickness and possibly the nature of the infill as well as the degree of opening.

It is not very easy to quantify these parameters, but their systematic description is often needed in applied geology or civil engineering works.

In this section it will be attempted to describe the morphology of fractures in order to interpret their genesis and thus to identify the generating stress field so as to obtain a reconstruction of the stress history of the rock mass and therefore to evaluate the difference in mechanical behaviour between a soil tested in the laboratory and investigated on site.

4.4.1 *Diaclases and Joints*

Diaclases and joints are lithological discontinuities that do not show any relative movement of the two detached parts. Typically, the terms diaclases or joints are used when discontinuities are perpendicular or oblique to the directions of stratification or schistosity (Fig. 4.6a, b).

Furthermore, stratification joints or schistosity joints are defined in the case of discontinuity planes parallel to these two types of structures.

Diaclases and joints are often arranged in groups of two, three or four directional families.

These discontinuities are generally planar or slightly wrinkled: their linear dimensions may vary from a few decimetres to a few metres or to a few decametres.

The original thickness of diaclases is null by definition, but following to later tectonic movements, subsequent to their formation, they can open of a few millimetres and then getting infilled with quartz or calcite.

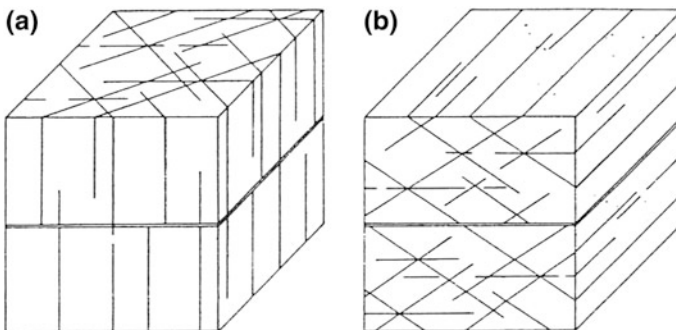


Fig. 4.6 Examples of diaclases (a) and of joints (b) (from Bles and Feuga 1981)

4.4.2 Extension Fractures (*Fentes*)

Fractures presenting lenticular-like cross sections are often observed in limestones or siliceous rocks. Their edges are open at the centre of the slit because of the tensile action perpendicular to the initial failure plane, the thickness of these extension fractures is generally centimetric and can reach a few decimetres (Fig. 4.7a–c).

The length, often of the order of the decimetre, can vary from a few centimetres to more than a meter and sometimes to a decametre. Longitudinal continuity must be significantly superior to cross-sectional continuity. Extension fractures are often infilled with crystallized calcite or quartz and show a structure made up of fibres perpendicular or slightly oblique to the failure plane. They are often arranged “*en echelon*” in the same way as shown in Fig. 4.7b. Figure 4.7c shows the different cross-sectional patterns of extension fractures that can be found on the ground.

4.4.3 Faults

A fault is a fracture where the two blocks show the sliding of one part over the other in a direction parallel to the failure plane. The sliding of one block over the other often produces the presence of striations on the failure plane that indicate the direction of movement. Faults often develop in two groups with different orientations called conjugated planes. The movement of a plane is opposite to that of the conjugated plane, but these two directions of motion show the same kind of deformation (Fig. 4.8a–c).

There are usually three types of faults, according to the orientation and direction of movement of the two blocks in relation to the horizontal plane:

- Normal faults, oblique to the horizontal plane, that present the lowering of one block with respect to the other (Fig. 4.8a);
- Reverse faults, equally oblique on the horizontal, that show the oversliding of one block on the other (Fig. 4.8b);
- Strike-slip faults, that present vertical planes and cause horizontal movements of one block with respect to the other; such movement may be dextral (right-lateral strike-slip fault) or sinistral (left-lateral strike-slip fault) with respect to the observation plane (Fig. 4.8c).

In ideal cases of Fig. 4.8, the striations are perpendicular to the intersections of conjugated faults. For normal faults and reverse faults, the striations are thus parallel to the maximum slope of the failure surface, while for strike-slip faults, the striations are horizontal.

Actually, in nature, if there is a plan of pre-existing discontinuity, it can be seen that the striations can have any position on the fault plane; so, there are intermediate positions of striations corresponding to the four major movements of the faults. They are spaced every 45° (Fig. 4.9):

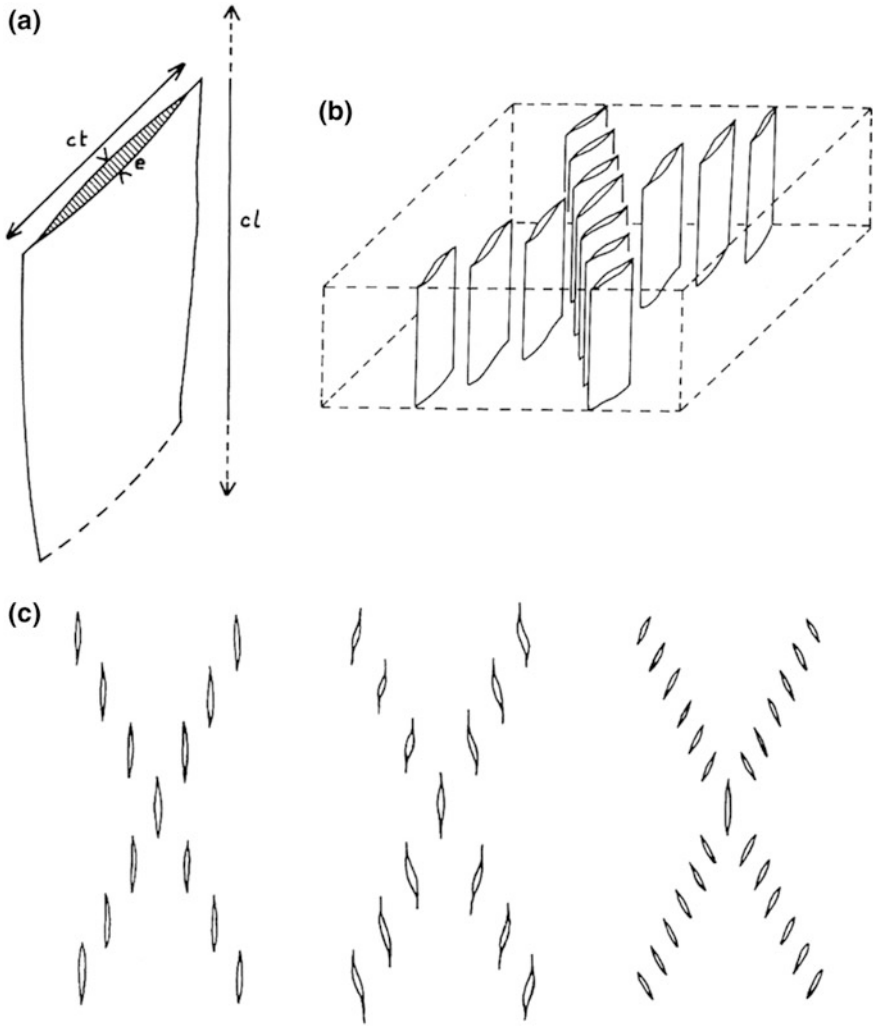


Fig. 4.7 Morphology (a) and *en échelon* arrangement (b and c) of tension cracks (Bles and Feuga 1981)

- sinistral-reverse faults;
- reverse-sinistral faults;
- reverse faults;
- reverse-dextral faults;
- dextral-reverse faults;
- dextral strike-slip faults;
- dextral-normal faults;
- normal-dextral faults;
- normal faults;

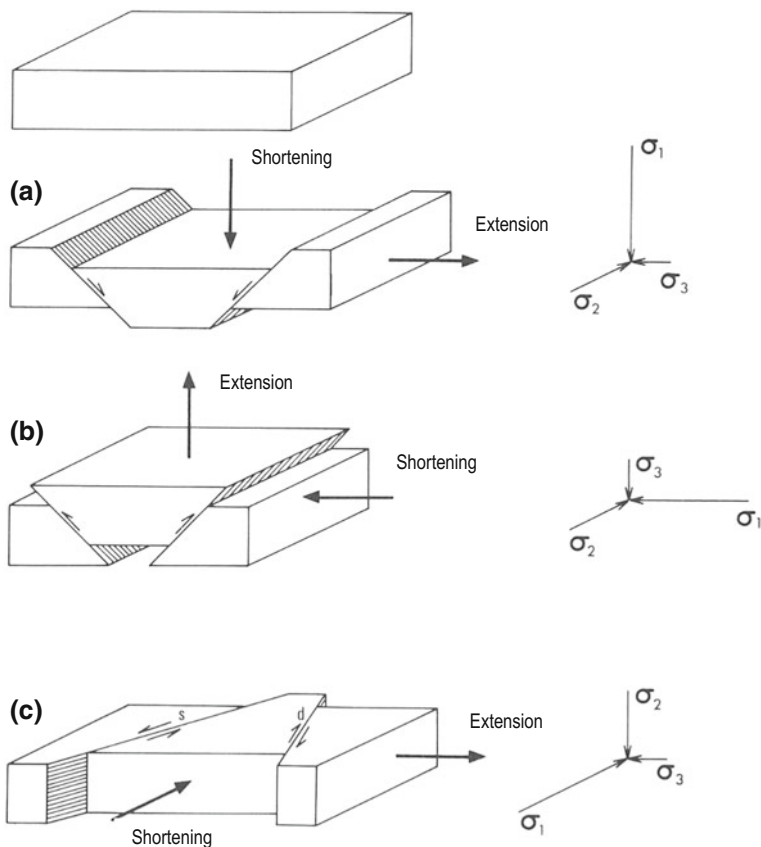


Fig. 4.8 a–c Different types of faults

- normal-sinistral faults;
- sinistral-normal faults;
- sinistral strike-slip faults.

The movement, measured in the direction of striations, corresponds to the real rejection of the fault.

The movement, measured according to random sections, corresponds to apparent rejections.

Normal faults cause a volume increase along the horizontal axis and a shortening in the vertical direction. They are related to distension phenomena that establish in tectonic regions.

Reverse faults and strike-slip faults correspond to a shortening along the horizontal axis, while the elongation for reverse faults takes place according to the vertical. These two major types of faults are related to horizontal compression actions during the period of the tectogenesis.

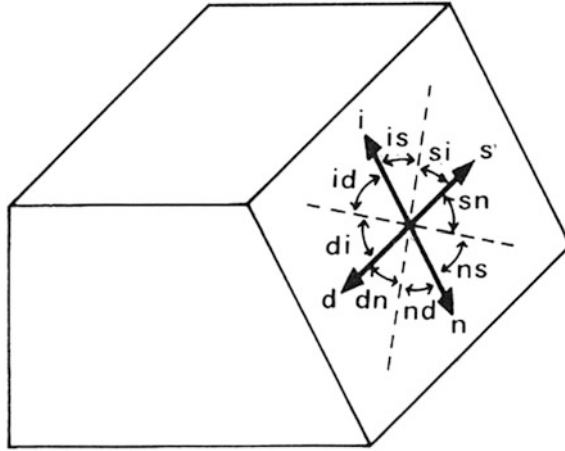


Fig. 4.9 Denomination of faults according to orientation and direction of motion (from Bles J.L. and Feuga B.). *i* reverse fault; *n* normal fault; *d* dextral strike-slip; *s* sinistral strike-slip; *is* reverse-sinistral fault; *si* sinistral-reverse fault; *ns* normal-sinistral fault; *sn* sinistral-normal fault; *nd* normal-dextral fault; *dn* dextral-normal fault; *id* reverse-dextral fault; *di* dextral-reverse fault

The size of faults is extremely variable, as they are produced on all scales; from small faults, of decimetric or decametric length, to large faults, of more than hundreds of kilometres. In particularly brittle materials, the faults can be found within areas of intense fracturing and the total rejection in the fault zone corresponds to the sum of all the rejections of the small faults that compose it.

4.5 Interpretation of the Mechanisms of Fractures Formation

4.5.1 Introduction

The study of fractures in terms of stresses is not theoretically possible, except in simple and ideal cases involving a continuous, homogeneous and isotropic medium, or considered as such, and in which faults appear according to planes where the shear stress is maximum.

However, rocks exhibit pre-existing fractures or discontinuities, in general, which result in planar anisotropies that disturb the distribution of the tensors of a stress field close to each of these discontinuities.

In these cases, theoretically, it is impossible to define a stress field tensor that is the same at all points of the rock mass. That is why Arthaud (1970) proposed to study fracture populations in terms of deformations. Usually, deformations (intended in the mechanical sense) are commonly distinguished between *continuous*

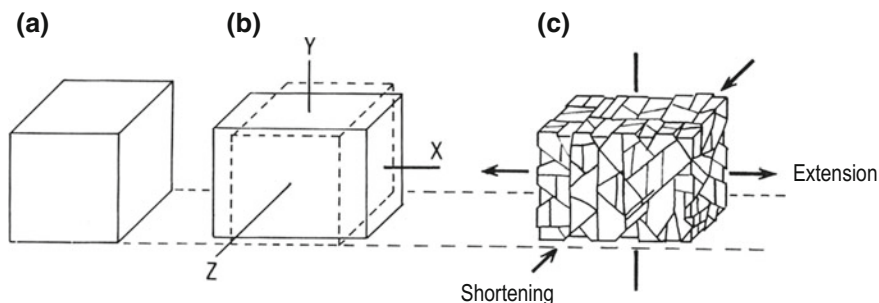


Fig. 4.10 The initially undeformed (a) soil element subjected to continuous (b) and discontinuous (c) deformation

and *discontinuous*. In the *continuous deformation*, two points initially close remain close (Goguel 1965). Continuous deformations, such as shrinkage, are penetrative and affect all the parts of the rock.

In *discontinuous deformation*, there is an important sliding of the parts that were initially close. Faults, as well as all other fractures (diaclasses, joints), are not penetrative elements of the rocks at the scale of the sample or of the outcrop.

Fracturing is therefore considered to be a discontinuous deformation that has three main deformation axes generating the ellipsoid of deformations of the stress field: σ_1 is the elongation axis, σ_2 is the direction of the intermediate axis, σ_3 is the direction of the shortening axis. These three directions are perpendicular to each other (Fig. 4.10a–c).

4.5.2 Formation of Diaclases and Joints

It is difficult to understand how diaclases and joints are formed because, by definition, these deformations do not show traces of movement. Moreover, diaclases and joints do not seem to be related to other types of deformations, such as large faults or folds.

However, the presence of diaclases or joints very often increases in the proximities of a fault and, moreover, it is understood that at least one family of them has the same orientation as the fault; in this case, it is logical to suppose that there is a relationship of continuity between minor discontinuities and fault resulting from the same stress field.

Sopena and Soulas (1973) highlighted the symmetry relationships between sub-vertical families of diaclases and the directions of global discontinuous deformation. Price (1959) showed that joints and diaclases are formed at the beginning of the deformation generated by tectonic stresses. These discontinuities can only be formed under the effect of the decompression the rocks are subjected to when these are brought from depth to surface, with a decrease in the lithostatic load, that tends to become null.

4.5.3 Formation of Extension Fractures and Fentes

The morphology of fentes or extension fractures indicates that they were formed under the effect of tension in the same way as fractures in direct or indirect tensile tests developed in the laboratory.

When fentes are filled with crystallised fibres, the orientation of fibres corresponds to the direction of the elongation (σ_1). When fentes do not involve crystallisation or when the infilled crystallization does not have a fibrous structure, the elongation direction σ_1 may be indicated for morphological irregularities of the fracture surfaces and these irregularities are sufficiently important to allow a reconstruction of the stress state before the opening. The alignment *en échelon* (Fig. 4.11(1–5)) of the extension fractures corresponds to deformed zones under the effect of shear stress. The development of these shear zones can be achieved in two different ways depending on whether the rock contains pre-existing fractures or not.

(a) *formation of extension fractures en échelon in rocks without pre-existing fractures*

In this case, three main stages can be distinguished starting from a primitive element subjected to shear stress:

1. Fentes are positioned in a medium subjected to shear and their orientation is 45° with respect to the direction of movement (Fig. 4.11(2)).
2. Fentes develop by extending their ends and are always oriented at 45° with respect to the sliding direction. However, in their intermediate part, which continues to open, they undergo a torsion or rotational deformation that can be considered as a simple plastic deformation movement (Fig. 4.11(3, 4)).
3. If the plastic deformation continues, a failure may occur on a plane parallel to the direction of movement and generally passing through the centre of the sliding area. Thus, a discontinuous deformation state is obtained with the formation of a micro-fault (Fig. 4.11(5)).

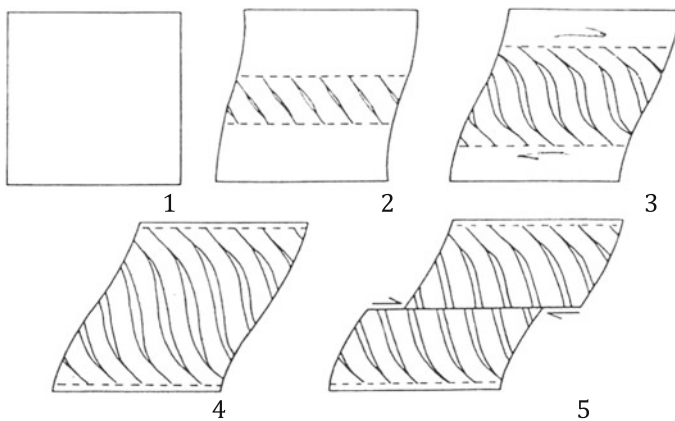


Fig. 4.11 1–5 Genesis and development of tension cracks *en échelon*

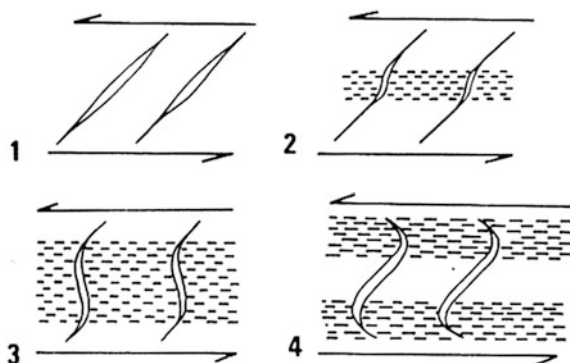


Fig. 4.12 Torsion of tension cracks *en échelon* (Roering 1968), 1 Initial tension cracks; 2 and 3 torsion of the middle part of the cracks; 4 torsion of the ends of the cracks

The plastic deformation due to simple sliding is not always located to the centre of the sliding movement as shown in Fig. 4.11. On the contrary, it may develop near the ends of the extension fentes and cause them to stretch (Fig. 4.12(4)). Torsion of the two ends of fentes is much less frequent than the torsion of their central part; this case was observed by Shainin (1950), Goguel (1965) and Roering (1968).

New rectilinear fentes overlapping the previously curved ones often appear on the rocks. In the case shown in Fig. 4.13(1–3), it is likely the formation of several generations of fentes in the same shearing zone; this is a phenomenon originated by the overlapping of several contiguous extension fractures and is schematized in Fig. 4.13(3); there is therefore no doubt that the oldest (F1 and F2) fentes underwent a rotation induced by the combined effect of tensile stresses that are different over time.

(b) *formation of extension fractures en échelon in rocks with discontinuous fractures*

During a tectonic phase, the maximum compression axis (σ_1) can lie obliquely on pre-existing fractures; it will create a shear stress along the plane of these. If the fractures have pre-existing discontinuity surfaces with very accentuated roughness, materialized by the angles of faces σ_1 and σ_2 with the median plane of the discontinuity, there are two possible directions of movement corresponding to the previously discussed laws, but which provide different results depending on the sliding that is produced on the edges with angles α_1 and α_2 . Figure 4.14a, b represent discontinuities where $\sigma_2 > \sigma_1$. If we assume that ϕ_P and ϕ_R are the same for the two shearing directions, it will be obtained:

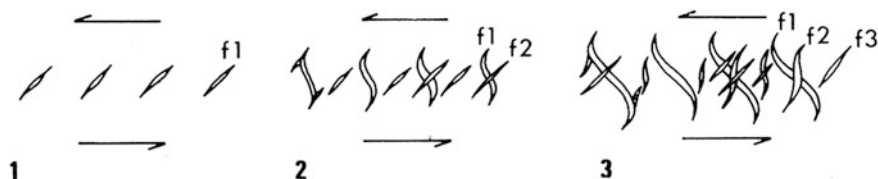


Fig. 4.13 Development of several generations of tension cracks within a shearing zone (Durney and Ramsay Durney and Ramsay 1973)

1. for sliding along the peaks,

$$\tau_1 = \sigma \operatorname{tg}(\phi_R + a_1) \quad \text{and} \quad \tau_2 = \sigma \operatorname{tg}(\phi_R + a_2)$$

2. at the failure of the peaks,

$$\tau_1 = Ca_1 + \sigma \operatorname{tg} \phi_P \quad \text{and} \quad \tau_2 = Ca_2 + \sigma \operatorname{tg} \phi_P$$

Existing discontinuities may have a cohesive behaviour when there are:

- a clay deposit in the stratification joints;
- clay infilled in the fault planes;
- mineralization or crystallisation of minerals (calcite, quartz or mica) between fracture or schistosity surfaces;
- existence of lenses of heterogeneous materials between diaclasses planes, shrinkage fractures or decompression joints.

Adherence to the walls of a diaclasis of cohesive material results in an upward movement of the τ and σ curves corresponding to the peak strength (Fig. 4.15a-c). In these figures is the behaviour of discontinuities containing lenses of cohesive material with heterogeneous roughness.

If a shear stress is applied to a pre-existing discontinuity consisting of a rock intercalation within a cohesive material, the movement due to shearing along the discontinuity plan is very fast, because a large amount of load induced stress is applied to it. This stress transmission is induced by the formation of tensile stresses

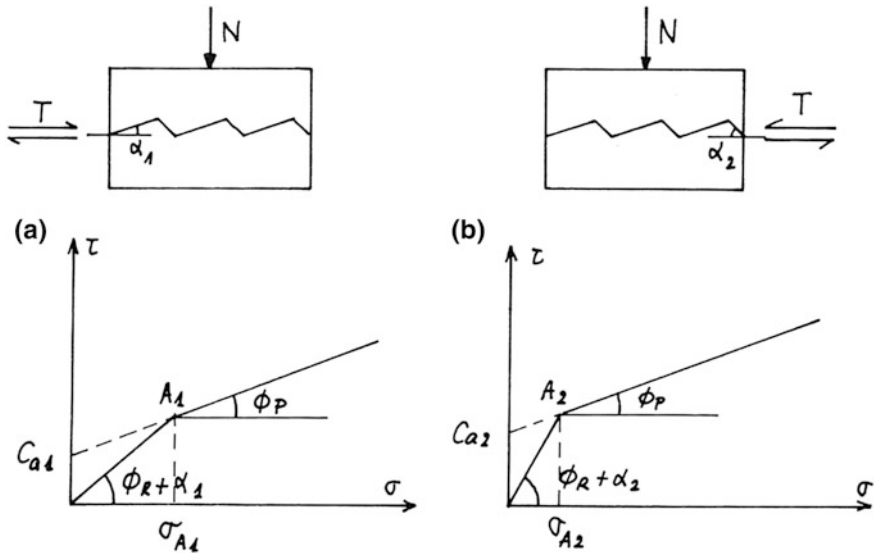


Fig. 4.14 Torsion of the tension cracks *en échelon*

at the ends of the existing discontinuities and by the emergence of secondary tension fractures which are oriented parallel to the direction of σ_1 induced by the shearing stress (Fig. 4.15b).

The shearing of a discontinuity with heterogeneous roughness is very similar to that of the case just described: areas with large roughness have a similar role to that of Fig. 4.15b (see Figs. 4.15c).

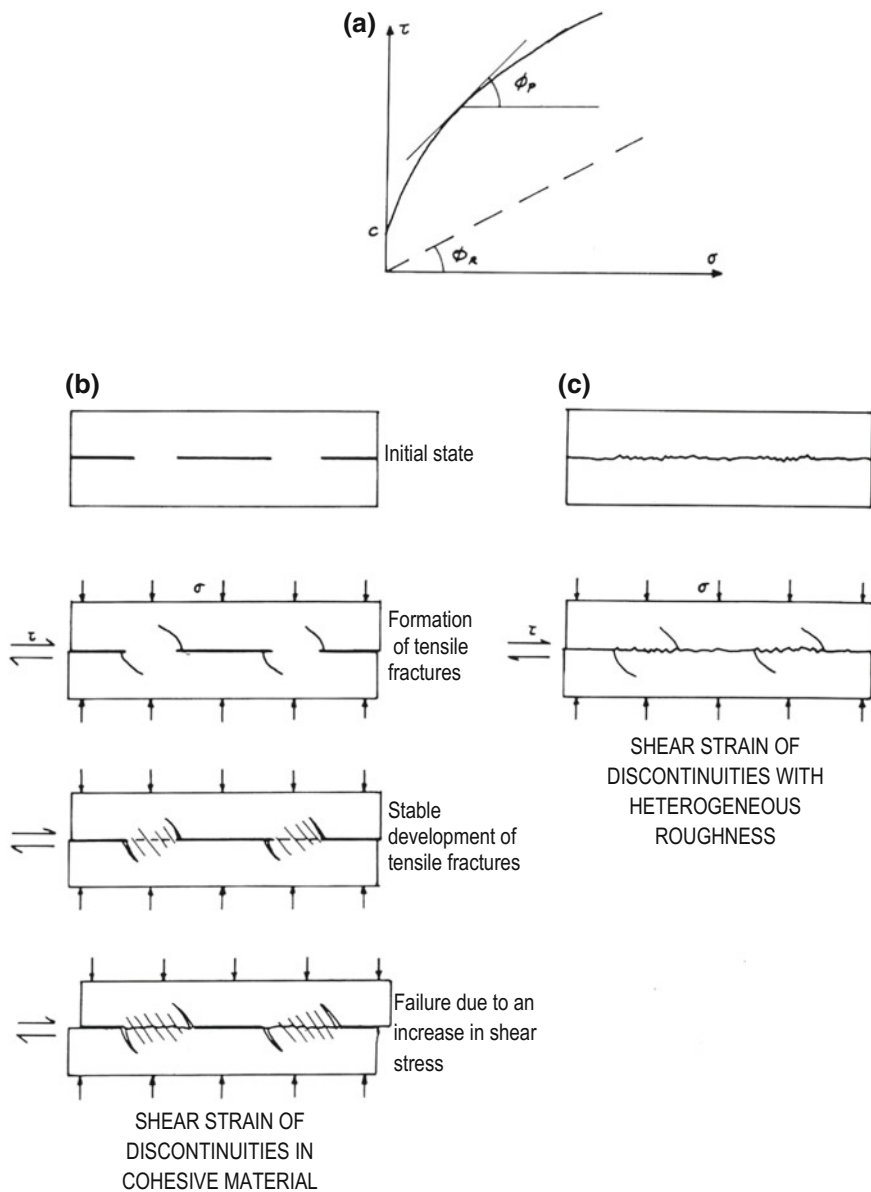


Fig. 4.15 Behaviour of discontinuities in presence of cohesive material

4.5.4 Formation of Faults

Distribution and morphology of faults may be different if the rock, though cohesive, has been affected by discontinuities before the tectonic phase.

The formation of faults will first be studied in rocks without pre-existing discontinuities and subsequently in those rocks that have pre-existing discontinuities.

(a) Formation of faults in rocks without pre-existing discontinuities

When rocks have no existing planar discontinuities, it is possible to use the results of laboratory experiments to interpret their deformation as a fault.

From mechanical laboratory experiments, the value of the angle θ between the failure plane and the main axis σ_1 is in direct relation with the internal friction angle of the rock φ : $\theta = 45^\circ - \varphi/2$. The angle φ varies with the value of minimum principal stress σ_3 . When σ_3 acts in compression, this can be tested using the triaxial apparatus. The value of θ varies from about twenty degrees to about forty degrees, and for elevated σ_3 values (from 100 to 300 bars) angles 2θ ranging from 60° to 80° can be obtained.

From experiences on triaxial tests, when the stress field can be represented by a revolution ellipsoid ($\sigma_2 = \sigma_3$), a series of fractures are obtained that are approximately tangent to 2 cones opposed to a failure point (Fig. 4.16); if this result is transmitted to faults formed in rocks considered isotropic, under the effect of a stress field in which the main stresses $\sigma_1 > \sigma_2 > \sigma_3$, the faults should appear at less than 45° from axis σ_1 . These can be subdivided according to one or two symmetrical systems in relation to σ_1 . Two faults are defined as conjugated if their intersection is parallel to σ_2 . The elongation, i.e. relaxation, takes place in the direction of σ_3 while σ_1 becomes the bisector of the dihedral angle between the two faults. In the ideal case of fault type fracturing, a relative movement of the blocks is produced. This movement often produces striations on the failure planes and when these are visible they are perpendicular to the intersection of the conjugated faults (Fig. 4.17).

There are two systems of intersection of conjugated faults (Fig. 4.18): in the first case the two faults may occur at the same time; at the point of intersection then numerous fractures are produced that tend to approach the central fracture point (Fig. 4.18(1)). In the second case, the two faults may occur during the same tectonic phase; the conjugate faults may therefore not be exactly contemporary: one lowers the other (Fig. 4.18(2)). When they occur, the first fault locally modifies the initial stress state and this modification may result in the formation of the second fault (Fig. 4.18(2b)).

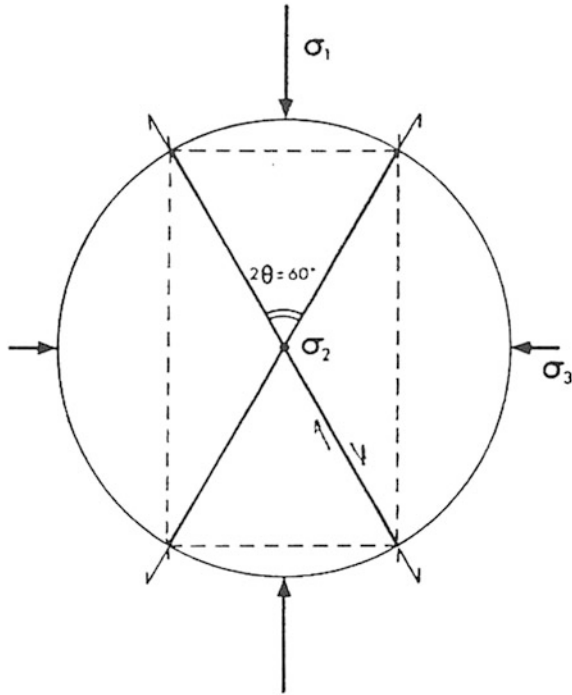


Fig. 4.16 Model of the formation of conjugated faults in rocks without pre-existing discontinuities

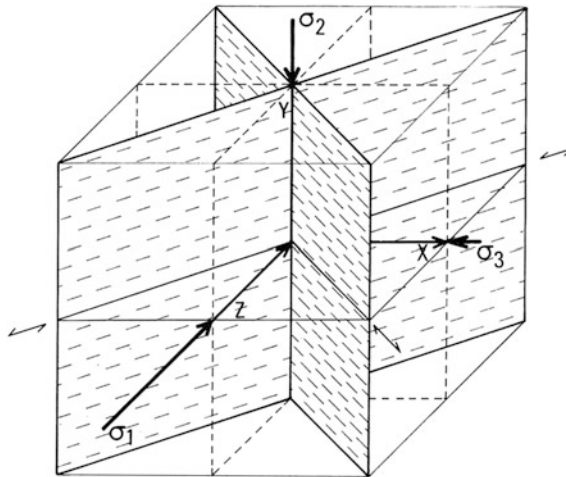


Fig. 4.17 Scheme of simple and ideal case of conjugated faults

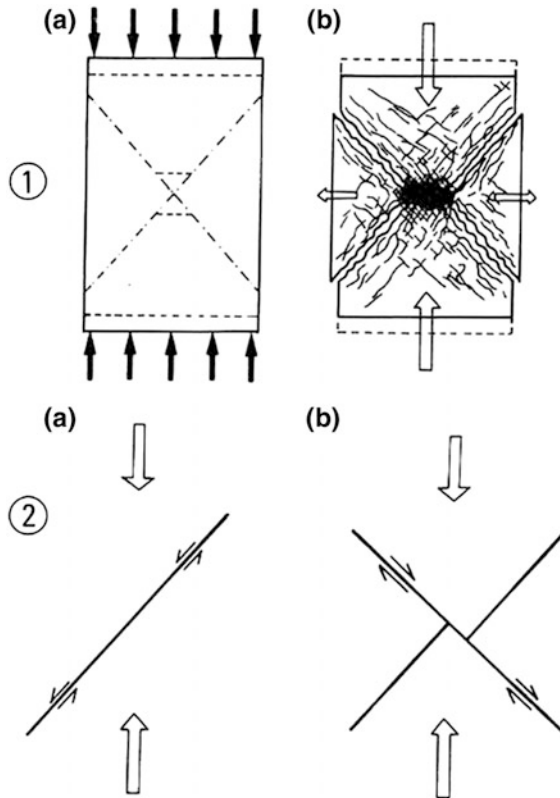


Fig. 4.18 Two modes of the intersection of conjugated faults. **1** Simultaneous faults with trend of closing the gaps (from Muller 1963). **2** Non-simultaneous faults with movement of the one (a) towards the other (b)

(b) *Formation of faults in rocks with pre-existing planar discontinuities*

In a rock subjected to tectonic stresses, existing planar discontinuities such as stratification, schistosity, or a set of diaclases may be the location of failures by sliding. Mechanical tests carried out in the laboratory show that the resulting faults can provide, depending on σ_1 , angles ϑ ranging from fifteen degrees to about sixty degrees.

These experiences also show that failure by sliding is more easily produced when the pre-existing planes form an angle θ with σ_1 of 30° or 35° . If the angle θ is less than 30° ($15^\circ < \theta < 30^\circ$), the sliding of the parts according to the existing discontinuities is often accompanied by extensional failure of the rock mass located between the failure axes and the main compression axis σ_1 . The faults thus created will not have planar surfaces but stepped surfaces where one face will undergo a sliding motion and the second an extensional movement (Fig. 4.19).

If the angle θ is greater than 30° or 35° ($35^\circ < \theta < 60^\circ$), axis σ_3 and axis σ_1 of the stress field are respectively stronger and less strong than those applied on the

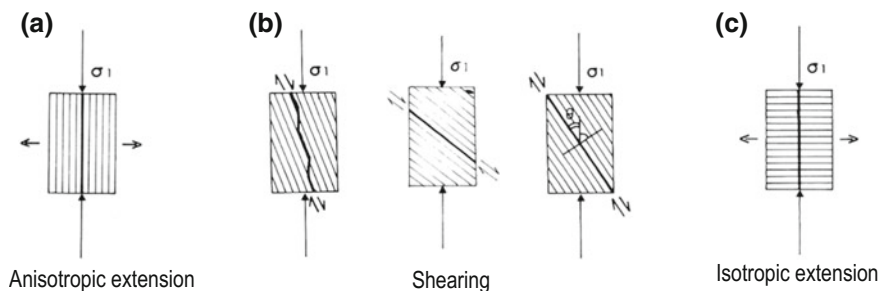


Fig. 4.19 Collapse of rocks containing a plane of discontinuity

planes rotated 30° or 35° from σ_1 . The compression stress required for the failure therefore must be necessarily greater.

In the rocks that involve two families of discontinuities of the same nature, the direction of axis σ_1 , applied to them by a new tectonic phase, will no longer be, in general, the bisector of the dihedral defined for the two families. It is therefore foreseeable that shearing failure will be more easily produced according to one of the two families of discontinuities for the sole reason of having a similar orientation. If the two families of discontinuities are of a different nature (e.g. stratification and schistosity), the ease of failure, always function of the orientation of the pre-existing planes, will be accentuated or opposed by the mechanical characteristics of the plane of each fault (internal friction angle φ' and cohesion c_u) (see Figs. 4.19 and 4.20).

(c) *Formation of faults with non-planar pre-existing discontinuities*

Natural discontinuities are not strictly flat, especially those along the shear surface. At the scale of the outcrop, for example, discontinuities considered as flat may have, instead, rather regular roughness due to an arrangement in succession. To interpret these deformation figures observed on the surface of natural faults, it is practical to use a model of discontinuities with regular and dissymmetric roughness used in the study of rock mechanics. For example, let us consider a fracture F with two opposite failure surfaces, F1 and F2, having respectively angles $i_1 = 15^\circ$ and $i_2 = 30^\circ$ with the median plane of fracture F (Fig. 4.21). In cross-section, F1 surfaces are about twice as long as F2.

This failure model is in common for the two directions of movement, which can be defined as “dextral” and “sinistral” movements in Fig. 4.21. For each of these movements, there may be two cases: sliding on surfaces F1 and sliding on surfaces F2 according to the orientation of the applied thrust in relation to the median plane of fracture F. In this figure, the planes corresponding to F1 have much greater areas than those of F2. However, these solutions are dependent on the direction of the maximum thrust tensor; therefore, according to the movement that is considered, extension or shortening will be obtained for surfaces F2. In fact, the dimensions of surfaces F2 are defined by the sliding of surfaces F1, that are produced for a sinistral movement in the fault model F of Fig. 4.21.

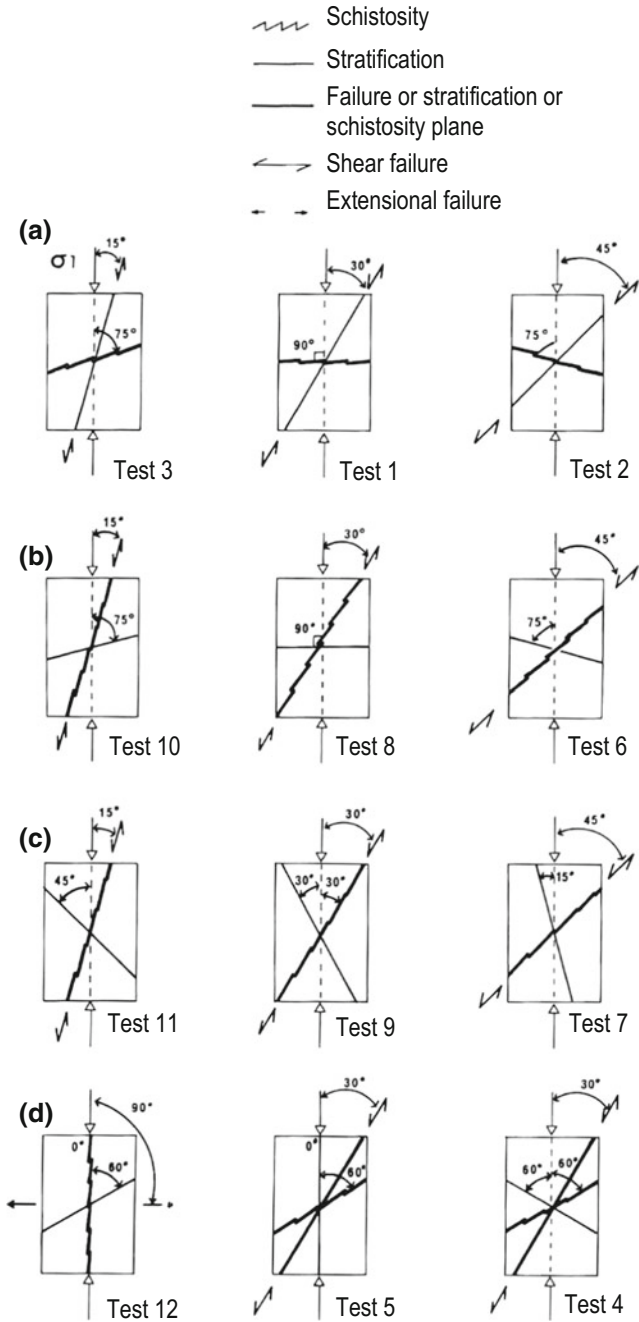


Fig. 4.20 Failure mode for simple compression of a rock containing two sets of pre-existing discontinuities (Masure 1970). **a** Shear along stratification planes; **b** and **c** shear along schistosity planes; **d** anisotropic extension and formation of new shear cracks

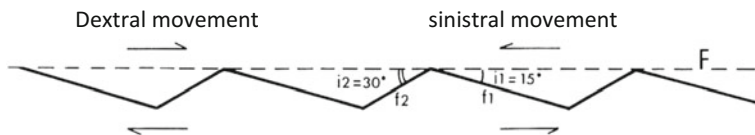


Fig. 4.21 Model of failure with regular and asymmetric roughness (profile perpendicular to the crack and to the roughness and parallel to the direction of movement) (from Bles and Feuga 1981)

This sinistral movement with sliding on F1 is only possible when the angle between σ_1 and F1 has a value around 15° , i.e. when the angle between σ_1 and the median plane of F is between 0° and 45° (Fig. 4.22a).

The movement can develop as shown in Fig. 4.22b, c; i.e. when:

1. at the beginning, shearing is applied to plane F1 and at the same time an extension according to planes F2 is produced (Fig. 4.22b). This is due to the fact that, during sliding, F1 surfaces can be striated, while the space generated from the opening on F2 can be infilled with calcite or quartz crystals, depending on the rock being calcareous or siliceous.

Calcite or quartz crystals often have a fibrous structure parallel to the direction of sliding and therefore parallel to the striations of F1 planes. In this case, it is likely that crystallization occurs during sliding. The arrangement of striations allows to define the direction of movement. This movement is accompanied by dilatancy perpendicular to the median plane of fracture F and therefore the fault is defined as stepped fault (Fig. 4.22b).

If the rock is made of soft cohesive soil, generally shallow-depth soil, this fracturing pattern is indistinguishable; however, by means of a careful analysis of the ground, it is possible to find dissymmetric gaps in succession along a section having an angle of about 45° with respect to σ_1 and a material often at the plastic state.

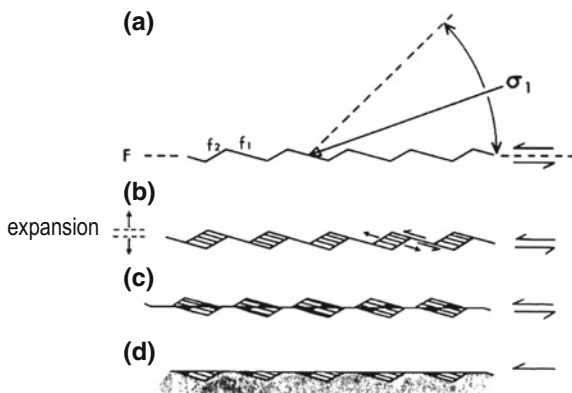


Fig. 4.22 Scheme of the evolution of a non-planar discontinuity with slipping faults, diverging faults and smoothing of roughness (from Bles and Feuga 1981)

2. During the sliding, the two contact surfaces become more distant and this results in an increase in the normal intermediate tensor. The breaking of the edges delimitating the F1 and F2 planes can therefore be achieved (Fig. 4.22c). Summarising, the surfaces of each block can undergo the sequences: striated rock → fibrous crystallization → crushed rock, indicating the direction of movement (Fig. 4.22d).

When the breaking of the edges occurs at the beginning of the movement, crystallization may be absent and replaced by rock fragments of the edges themselves of the block above.

Let us now analyse the case of faults in which the sliding of the blocks causes a shortening of surfaces F1 and F2 (Fig. 4.23a–d). Sliding on surfaces F1 is possible if tensor σ_1 forms with such surfaces an angle between 15° and 60° or if σ_1 is inclined of between 30° and 75° with reference to the average plane of fracture F (Fig. 4.23a).

Contraction of F2 and sliding on F1 can occur only when rock dissolution is possible, which implies a relatively high porosity value (Sellier 1976; Sellier and Morlier 1976). If this dissolution is possible, the sliding on F1 is accompanied by the formation of dissymmetrical stylolitic joints developed from surfaces F2 (Fig. 4.23b, c). This structure corresponds to a contraction of the two surfaces in the perpendicular direction to the median plane of fracture F and therefore the faults defined as “shortening faults” (Arthaud and Mattauer 1969).

When rock dissolution is no longer possible, a stop in the movement takes place at stage b or c (Fig. 4.23). In this case, a breaking of the most angular parts that exist in the median plane of the fracture is possible. If rock dissolution can go on indefinitely, the state of the deformation is likely to be similar to that of Fig. 4.23d.

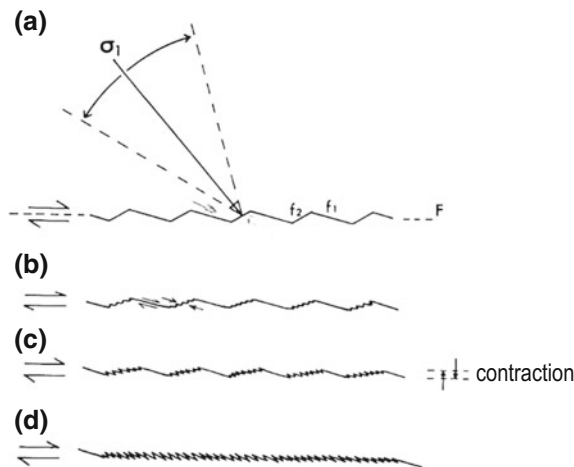


Fig. 4.23 Scheme of the evolution of a non-planar discontinuity with slipping and contraction (Bles and Feuga 1981)

Rocks having porosity compatible with the development of dissolution under tectonic stress are essentially limestones, sandstones, silts and clays.

In siliceous, non-porous, rocks, crushing of the rocks of F2 surfaces of the fault is produced, with shortening of the fault itself. Crushing can be accompanied by deep striations marked on surface F1 and, in the case of very high tectonic thrust, crushing can evolve and constitutes small “mylonitised“ areas (Petit 1976; Blès and Gros 1980).

4.6 The Stress Field

4.6.1 *Identification of the Stress Field*

Geologists often ask the question of where the stress field comes from. It can be said that this is originated as a “reaction” of bodies to external forces that are applied to them.

The rocks of the Earth’s crust are permanently subjected to forces. These may vary considerably according to the fact that they are subjected to compression, relaxation or at rest in an undeformed plate.

The in situ analysis, for the purpose of the prediction, the prevention and the control of hydrogeological instability, must take into account of the structural setup of the local orogeny and therefore of the processes of deformation and shearing. In fact, the pre-failure deformation is due to the combined effect of the stresses induced by the stress field and the regime of neutral pressures that develops in the ground. Nature and intensity of such deformations depend on the pre-existing stress field while the depth of the sliding surface is a function of the orientation of the maximum thrust tensor. From this it follows that if the fractures have a predominant orientation approximately parallel to the slope, the sliding surface is shallow; on the contrary, if the fractures are almost perpendicular to the slope, the shearing surface of the landslide is very deep; furthermore, in the first case the time occurring for the achievement of the deformation at failure is always lower than the other case. Obviously, the propagation mechanism in the shear area of a landslide in cohesive soils is much more complex than how it is generally described here for a number of variables such as those linked to consolidation and/or viscous ground deformations that may cause a redistribution of the stress field.

Let us consider a small element in the Earth’s crust with infinitesimal surface dS of random orientation, rotating around a point M (Fig. 4.24). The surface is subjected to a force dF . It is called tensor in M the limit of the ratio $\sigma = dF/dS$ when dS tends to zero (actually, a stress is a force divided by an area). Let us consider further elements of surface S, passing through the same point M but having different orientations: two cases can be produced:

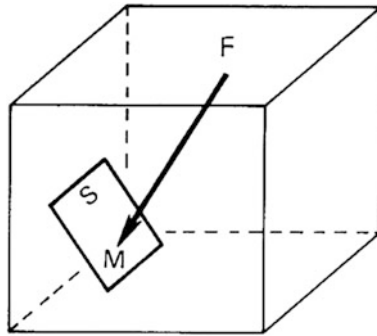


Fig. 4.24 Sketch taken from Mattauer (1973)

- (a) tensor (σ) remains constant whatever is the orientation of dS . In this case the tensor is termed as hydrostatic because it is the condition found within liquids. In fact, if using a manometric membrane at a given point of a liquid and allowing it to assume all the possible orientations it is found that the pressure is always the same. This tensor, which is called isotropic, can be represented by a sphere with radius σ_i (Fig. 4.25a).
- (b) the tensor varies in intensity and direction, while the orientation of dS varies. At point M there are therefore different possible values of σ .

When the rock is homogeneous and continuous, the locus of the end of the vector originated from M, having σ for length and dF as the direction is an ellipsoid, called ellipsoid of tensors or tension field where the axes are generally known as $\sigma_1, \sigma_2, \sigma_3$ and called the main axes of the stress field, respectively the main axis, the intermediate axis, the minimum axis; therefore, the stress field is triaxial (Fig. 4.25b) and defined by an ellipsoid of revolution.

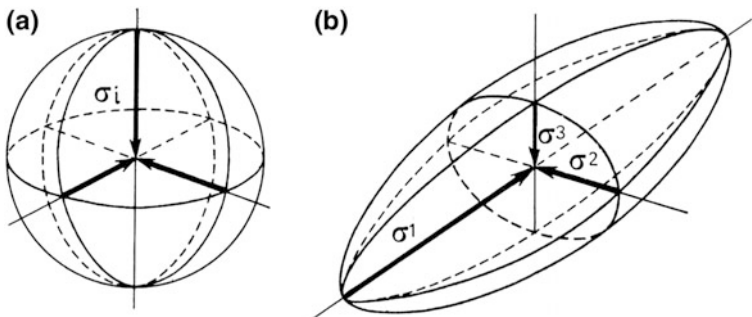


Fig. 4.25 a and b Representation of an isotropic (sphere) and anisotropic (ellipsoid) stress field (from Mattauer 1980)

The state of stress of rocks in the Earth's crust is given by:

(a) *Rocks at rest in a stable plate (very deep)*

In this case, a rock element located, for example, at depths of 5 km, is subject to the weight of the overlying rocks, which can be easily calculated if the natural density (γ) of the rock is known; if the density $\gamma = 25 \text{ kN/m}^3$, the pressure at 5 km depth is 125 MPa. Now it can be observed that this value does not change significantly if pressure measurements are made in the various directions. In short, it can be considered that in that portion of the Earth's crust a lithostatic stress field is observed, in which $\sigma_1 \approx \sigma_2 \approx \sigma_3$ and which increases in intensity with depth. This system is obviously extremely viscous and deformational effects only appear in the long-term (Fig. 4.25a).

(b) *Rocks subjected to stress fields*

The stress field is of triaxial type and is characterized by $\sigma_1 > \sigma_2 > \sigma_3$ (Fig. 4.25b). It can be considered as due to the overlapping of the lithostatic load σ_l and the tectonic thrust σ_t . Triaxial compression can occur in a continuous medium (intact rock) or in a discontinuous medium (fractured rock).

4.6.2 Stress Field in a Continuous Medium

Let us start from the case of intact rock (continuous medium) (Fig. 4.26(1–3)). Solutions that may occur are:

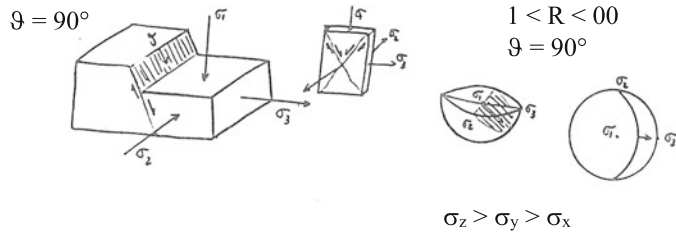
1. σ_1 is vertical: a relaxation regime takes place, whatever the position of σ_2 and σ_3 . The striations have the same direction of σ_1 and pitch $\vartheta = 90^\circ$.
2. σ_2 is vertical: strike-slip regime. Strike-slip can be both right-lateral and left-lateral. Striations have the same direction of σ_l and pitch $\vartheta = 0$.
3. σ_3 is vertical: reverse compression regime, whatever the arrangement of σ_l and σ_2 . Striations have the same direction as σ_l and pitch $\vartheta = 90^\circ$.

It should be noted that, in a continuous medium, striations always have the same direction of σ_l . The direction of movement of blocks is therefore always parallel to that of σ_l . The pitch is $\vartheta = 0$ or $\vartheta = 90^\circ$. The rejection (R) is always of pure type.

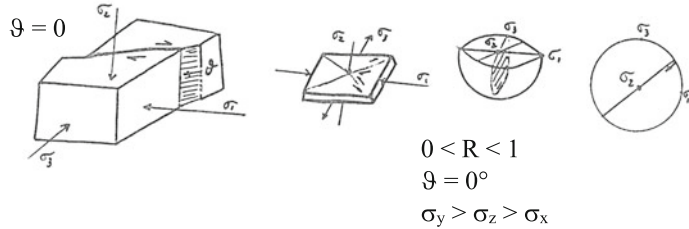
If rock P is intensely fractured (strongly discontinuous) it can behave as an isotropic material; especially if the rock mass contains several fracture planes. In this case, the determination of the stress regime can be reconducted to the type of the intact rock.

As it can be observed, the type of fault within a continuous material is a function of the orientation of the stress field, i.e. it is function of the direction of the tensors in the space. In addition, the direction of the movement is always the one of σ_1 and the blocks always move towards σ_3 .

1) σ_1 is vertical = *distension* regime (*normal dip-slip fault*)



2) σ_2 is vertical = *strike-slip* regime (*strike-slip fault*)



3) σ_3 is vertical = *reverse* regime (*reverse or thrust dip-slip fault*)

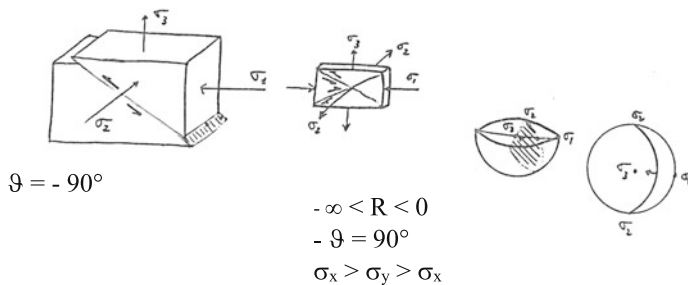


Fig. 4.26 1–3 Cases for intact rock (continuous medium)

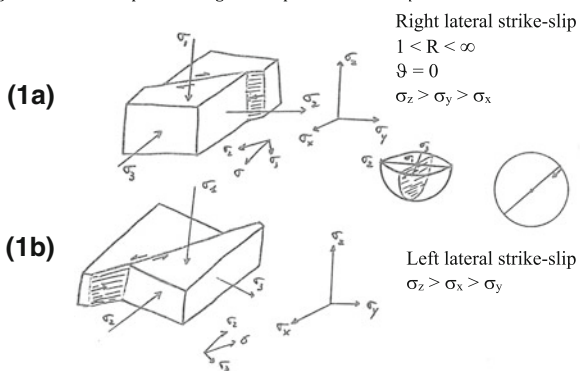
4.6.3 Stress Field in a Discontinuous Medium

If the rock is already fractured, i.e. it contains previous surfaces of discontinuity (discontinuous medium), then it is necessary to distinguish which of the three stress axes lie on the fracture plane and which are oblique to it (Fig. 4.27—cases A, B, C).

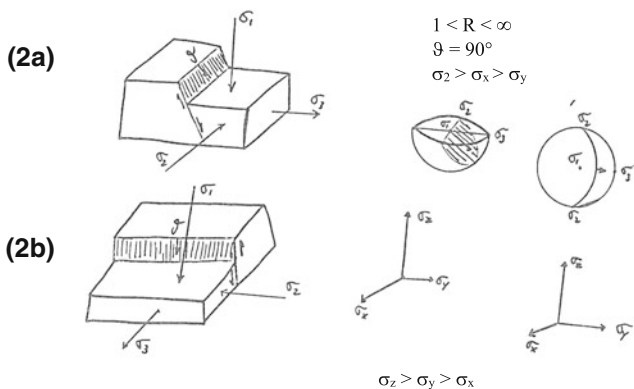
When a tensor lies on a pre-existing fault plane it becomes null; the movement of the blocks and then the direction of the striations will be given by the resultant of the two remaining stress components. The deformation is logically applied to a two-dimensional plane. In the case, instead, of pre-failure plane oblique to a pre-existing shear surface, then the stress field is three-dimensional and the motion will be the one deriving from all of the three components, σ_1 , σ_2 , σ_3 . Therefore, all of the cases that may occur are shown in Fig. 4.27A–C.

A) Case with σ_1 vertical = distension regime

1) If σ_1 lies on the pre-existing failure plane = strike-slip movement



2) If σ_2 lies on the pre-existing failure plane = pure normal movement



3) If σ_3 lies on the pre-existing failure plane = pure normal movement

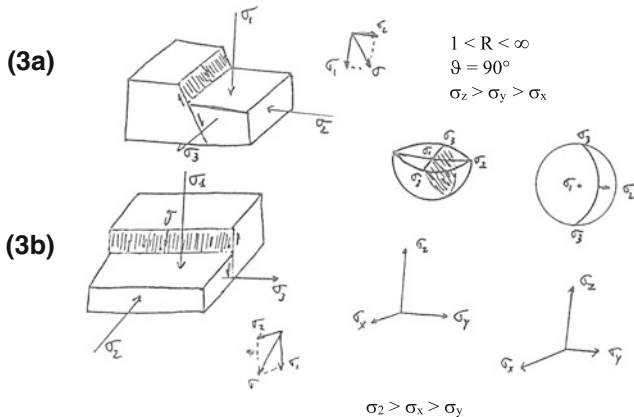
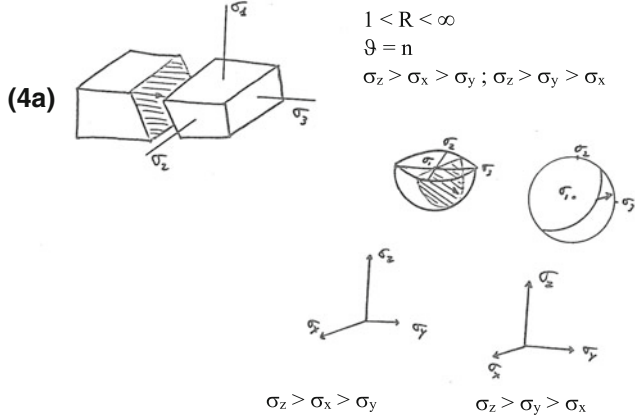


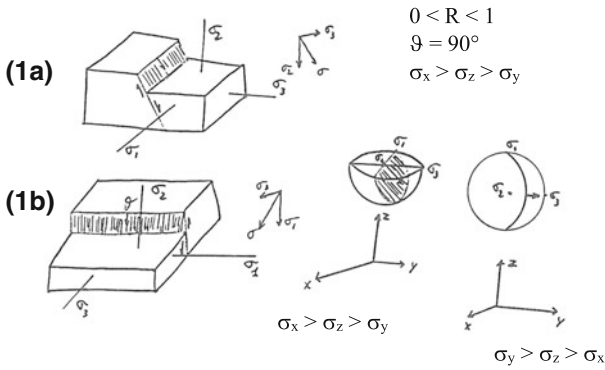
Fig. 4.27 A–C Cases for fractured rock (discontinuous medium)

4) if the failure plane is oblique to stress axes = *normal transitive*



B) Case with σ_z vertical = *Regime di trascorrenza*

1) If σ_1 lies on the pre-existing failure plane = *pure normal* movement



2) If σ_2 lies on the pre-existing failure plane = *pure strike-slip* movement

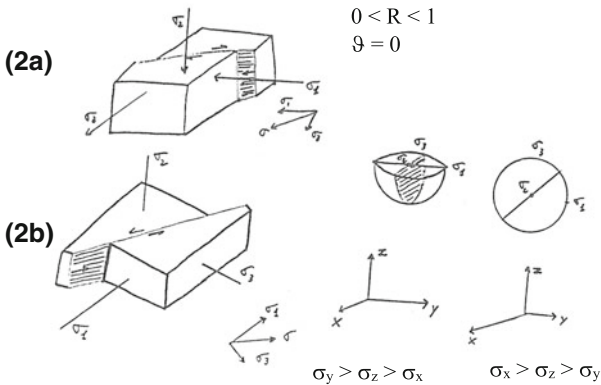
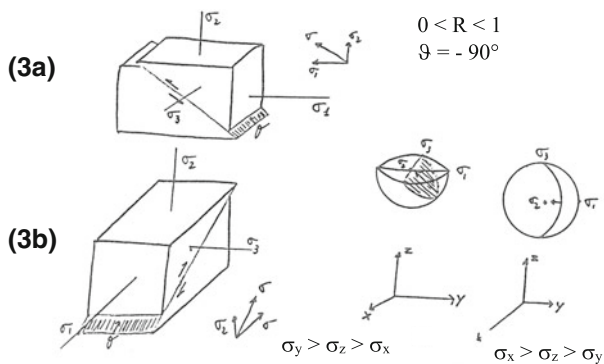
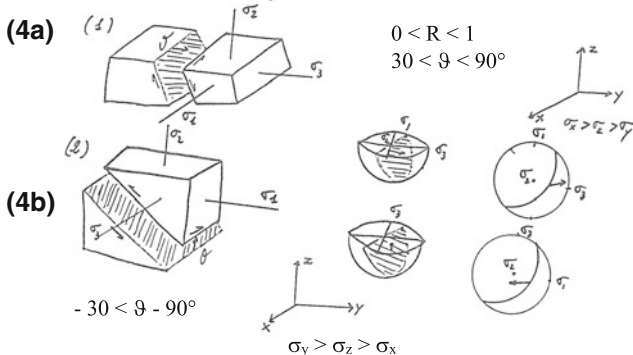


Fig. 4.27 (continued)

3) If σ_3 lies on the pre-existing failure plane = *pure reverse* movement



4) If the pre-existing failure plane is oblique to the stress axes = normal transtensive (4a) or reverse transpressive (4b) movement



C) Case with σ_3 vertical = *Reverse compression* regime

1) If σ_1 lies on the pre-existing failure plane = *pure reverse* movement

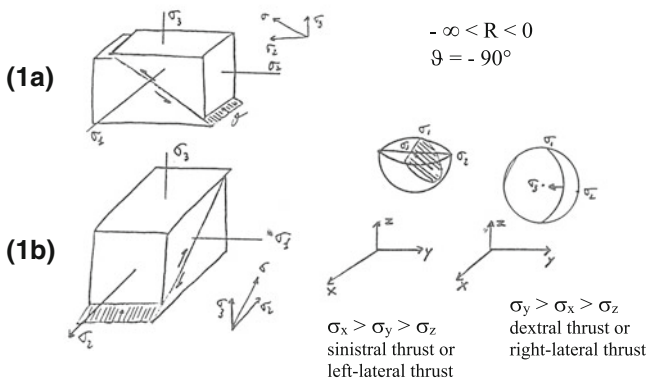
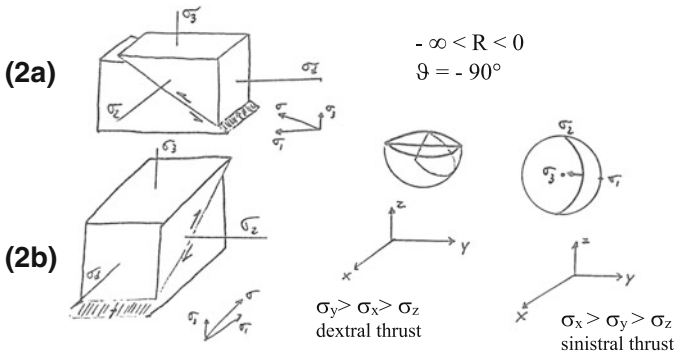
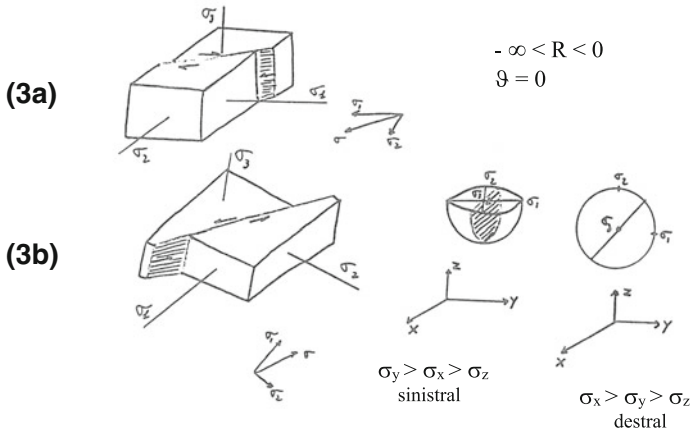


Fig. 4.27 (continued)

2) If σ_2 lies on the pre-existing failure plane = *pure reverse* movement



3) If σ_3 lies on the pre-existing failure plane = *pure strike-slip* movement



4) if the pre-existing failure plane is oblique to the stress axes – *reverse transpressive* movement

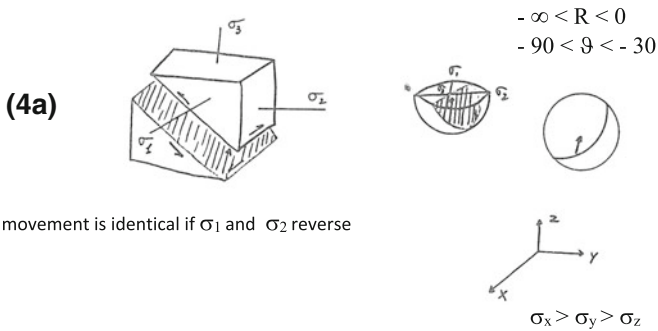


Fig. 4.27 (continued)

CASE A—The stress field consists of $\sigma_1 =$ vertical, σ_2 and $\sigma_3 =$ horizontal:

A1—Case where σ_1 , vertical, lies on an existing shear surface; $\sigma_1 = 0$ and the stress field becomes two-dimensional with σ_2 that assumes the role of the prevailing tension axis. The shear deformation will be, therefore, a strike-slip fault, dextral or sinistral according to the position of σ_2 on the horizontal plane. Sub-horizontal striations with pitch $\vartheta = 0$ can be observed (Fig. 4.27A, 1a, b).

A2—Case where σ_2 , horizontal, lies on the pre-existing failure plane. A normal pure fault is obtained, in the sense that the movement of the block free to move is vertical and therefore the striations have a pitch $\vartheta = 90^\circ$ whatever the position of σ_3 on the horizontal plane (Fig. 4.27A, 2a, b).

A3—The pre-existing rupture plane contains the stress axis σ_3 . Tensor σ_2 , in this case, becomes the one with lower intensity and therefore the movement follows an orientation in which a pure normal fault (pitch $\vartheta = 90^\circ$) is obtained whatever the position of σ_2 (Fig. 4.27A, 3a, b).

A4—The pre-existing failure surface is oblique to all of the three stress axes. In that case, a transtensive normal movement of the block free to move is obtained. The pitch ϑ will assume a value n , resulting from the intensity of σ_2 and σ_3 , and is between $30^\circ < n < 90^\circ$ (Fig. 4.27A, 4a).

CASE B—The stress field is composed of $\sigma_2 =$ vertical, σ_1 and σ_3 lie on the horizontal plane. The regime is of a strike-slip type. However:

B1—If σ_1 lies on the pre-existing failure plane, the vertical σ_2 component prevails as the axis of major tectonic thrust and therefore a pure normal motion is obtained in the sense that pitch $\vartheta = 90^\circ$ (Fig. 4.27B, 1a, b).

B2—The pre-existing failure plane contains σ_2 , vertical; a pure strike-slip movement with pitch $\vartheta = 0$ is obtained (Fig. 4.27B, 2a, b).

B3—If the pre-existing failure plane contains σ_3 , once again there is a two-dimensional stress field where σ_2 , vertical, is the axis with lower tectonic thrust. In this case, a pure reverse fault is obtained i.e. the pitch $\vartheta = -90^\circ$ (Fig. 4.27B, 3a, b).

B4—The pre-existing failure surface is oblique to all of the three stress axes. The movement may be of transtensive normal or transpressive reverse type according to the position of σ_1 lying on the horizontal plane (Fig. 4.27B, 4a, b).

CASE C—The stress field consists of σ_3 vertical, σ_1 and σ_2 lie on the horizontal plane. The regime is of reverse type. However:

C1—If the pre-existing failure surface contains σ_1 , horizontal, a pure reverse motion (pitch $\vartheta = -90^\circ$) is obtained. The striations direction is in line with that of axis σ_2 (Fig. 4.27C, 1a, b).

C2—In the similar case where σ_2 , horizontal, lies on the failure surface, the movement of the block is reverse with pitch $\vartheta = -90^\circ$ (Fig. 4.27C, 2a, b).

C3—If the pre-existing failure plane contains σ_3 a pure strike-slip movement is obtained, in the sense that the pitch $\vartheta = 0$ (Fig. 4.27C, 3a, b).

C4—The pre-existing failure surface is oblique to the three stress axes. In this case the movement is transpressive reverse and the pitch will be $-90 < \vartheta < -30$ (Fig. 4.27C, 4a).

In summary: Tables 4.1 and 4.2.

- (a) In a continuous medium the failure plane will always be determined by σ_1 and the direction of the striations will be parallel to that of the axis of maximum thrust, whether it is vertical or horizontal; the pitch can therefore always assume

Table 4.1 Type of faults and characteristics in function of the stress regime

| Stress regime | Types of shear deformations | Tensors on pre-existing planes | Pitch | Ellipsoid | Notes |
|----------------------------------------------------------------------------------------------------------------------|-----------------------------------------------------------------------------------------------------------|-------------------------------------------------------------------|----------------------------------------------------------------------------|----------------------------------------------------------------------------------------------------------------------------------------------------------------------------------------------------------------------|---------------------------------------------------------------------------------------|
| Triaxial distension $\sigma_1 = \text{vertical}$ $1 < R < \infty$ $30 < f_{(R)} < 90$ | Pure normal Pure normal Strike-slip Transtensive normal | Not existing σ_2 σ_1 Oblique | 90° 90° 0 $\vartheta = n$ | $\sigma_z > \sigma_x > \sigma_y$ $\sigma_z > \sigma_x > \sigma_y$ $\sigma_z > \sigma_x > \sigma_y$ $\sigma_z > \sigma_x > \sigma_y$ | Does not allow reverse faults Does not allow transpressive faults |
| Triaxial compression Strike-slip regime $\sigma_2 = \text{vertical}$ $0 < R < 1$ $-30 < f_{(R)} < 30$ | Strike-slip Strike-slip Pure normal Pure reverse Transtensive normal Transpressive reverse | – σ_2 σ_1 σ_3 Oblique Oblique | 0 0 90° -90° $\vartheta = n$ $\vartheta = -n$ | $\sigma_y > \sigma_z > \sigma_x$ $\sigma_y > \sigma_z > \sigma_x$ $\sigma_y > \sigma_z > \sigma_x$ $\sigma_y > \sigma_z > \sigma_x$ $\sigma_x > \sigma_z > \sigma_y$ $\sigma_y > \sigma_z > \sigma_x$ | Allows all the solutions |
| Triaxial compression Reverse regime $\sigma_3 = \text{vertical}$ $-\infty < R < 0$ $-90 < f_{(R)} < -30$ | Pure reverse Pure reverse Strike-slip Transpressive Reverse | – σ_1 σ_3 Oblique | -90° -90° 0 $\vartheta = -n$ | $\sigma_y > \sigma_x > \sigma_z$ $\sigma_y > \sigma_x > \sigma_z$ $\sigma_y > \sigma_x > \sigma_z$ $\sigma_y > \sigma_x > \sigma_z$ | Does not allow transtensive faults Does not allow normal faults |
| Radial distension $\sigma_1 = \text{vertical}$ $R = \infty$ | Pure normal Pure normal Pure normal | – σ_2 σ_3 | 90° 90° 90° | $\sigma_z > \sigma_y = \sigma_x$ $\sigma_z > \sigma_y = \sigma_x$ $\sigma_z > \sigma_y = \sigma_x$ | Normal faults arranged in radial direction – Does not allow strike-slipping |
| Uniaxial distension $\sigma_1 = \text{vertical}$ $R = 1$ | Pure normal Pure normal Trascorrente | – σ_2 σ_1 | 90° 90° 0 | $\sigma_z = \sigma_y > \sigma_x$ $\sigma_z = \sigma_y > \sigma_x$ $\sigma_z = \sigma_y > \sigma_x$ | Does not allow transpressive normal faults |
| Radial compression $\sigma_3 = \text{vertical}$ $R = -\infty$ | Pure reverse Pure reverse Pure reverse | – σ_2 σ_1 | -90° -90° -90° | $\sigma_y = \sigma_x > \sigma_z$ $\sigma_y = \sigma_x > \sigma_z$ $\sigma_y = \sigma_x > \sigma_z$ | Reverse faults arranged in circular pattern – Does not allow strike-slip faults |
| Uniaxial compression $\sigma_3 = \text{vertical}$ $R = 0$ | Pure reverse Pure reverse Strike-slip | – σ_2 σ_3 | -90° -90° 0 | $\sigma_y > \sigma_x = \sigma_z$ $\sigma_y > \sigma_x = \sigma_z$ $\sigma_y > \sigma_x = \sigma_z$ | Small reverse faults Does not allow normal faults |

Table 4.2 Characteristics of the deformation for continuous and discontinuous materials

| Discontinuous material | | Vertical axis | | | | Continuous material |
|-----------------------------------------|-----------------------------------------------------|---------------|--------------------------------------------|--------------------------|-------------------------------------------------------------------------------------------------------------------------------------|---------------------|
| | | σ_1 | σ_2 | σ_3 | | |
| Strike-slip $\vartheta = 0$ | Faults containing $\sigma_1, \sigma_2, \sigma_3$ | σ_1 | σ_2 | σ_3 | Rejection always of pure type. Striations with same orientations of σ_1 except when σ_1 is contained within the fault | σ_2 vertical |
| Pure normal $\vartheta = 90^\circ$ | | σ_2 | σ_1 | – | | σ_1 vertical |
| Pure reverse $\vartheta = -90^\circ$ | | σ_3 | – | – | | σ_3 vertical |
| | | – | – | σ_1 | | |
| Transtensive $\vartheta = n$ | Oblique faults $\sigma_1, \sigma_2, \sigma_3$ | σ_1 | $\sigma_{2\text{vert.}}$ $\sigma_{1=X}$ | – | Striations always oblique $-\vartheta = n$ | |
| | | – | – | – | | |
| Transpressive $\vartheta = -n$ | | – | $\sigma_{2\text{vert.}}$ $\sigma_{1=Y}$ | $\sigma_{3\text{vert.}}$ | | |
| | | – | – | – | | |

a pure value, which is $\vartheta = 90^\circ$ if σ_1 is vertical and $\vartheta = 0$ if it is horizontal while with horizontal σ_1 and σ_3 vertical $\vartheta = -90^\circ$, i.e. assumes a reverse regime.

- (b) In a discontinuous medium, the failure plane will always be determined by σ_1 as well as the direction of the striations, except when the maximum thrust axis lies on the pre-existing failure plane.
- A strike-slip movement is obtained when the vertical component is that contained in a pre-existing discontinuity plane. This means that all strike-slip structures in a discontinuous medium admit a pre-existing failure surface and thus can show a double striation system, of which the most recent one is superimposed to the older one. In the Apennines, generally, the striations showing a strike-slip movement are always overlaid by pre-existing normal faults (in Jurassic limestone).
 - In the case of pre-existent failure surfaces oblique to the three axes of the stress field, the strike-slip movement (σ_1 horizontal) is never pure ($\vartheta = 0$) but only transtensive or transpressive.
 - A transtensive normal regime is obtained when σ_1 is vertical whatever the orientation of σ_2 and σ_3 ; or when σ_2 is vertical and σ_1 is horizontal and corresponds to the axis of the X.
 - In no cases with σ_3 vertical is obtained a transtensive normal regime.
 - A transpressive reverse regime is obtained when σ_3 is vertical or when σ_2 is vertical and σ_1 corresponds to the Y axis.
 - In no cases with σ_1 vertical is obtained a transpressive reverse fault.

It is therefore very important to take into account the conclusions obtained using the model by Bott (1971). The direction of movement on a fault plane is function of the directions of the principal tensor but at the same time they depend on the relationship between the values of the tensors themselves. This relationship is called

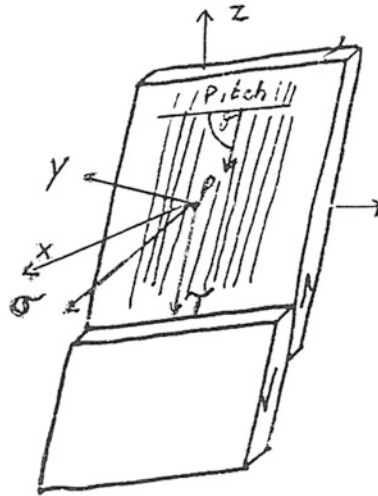


Fig. 4.28 p = line projection (a) perpendicular to plane. $\text{tg } \theta$ = direction of vector t producing striae l, m, n = direction cosines of P with reference to axes x, y, z

tensors ratio (R) and corresponds to the shape of the ellipsoid of the stress field which defined the regime of tectonic forces to which the rock is subjected. In fact, getting back to the study of the behaviour of already fractured anisotropic rock, it should be considered that the direction of the striations corresponds to that of the movement of the block, that is to that of the tangential component (τ) of a tensor (σ) applied to the plane of a failure surface (Fig. 4.28). The direction of motion is defined at failure by an average tensor, resulting from the three principal tensors of the field where the deviation due to the pre-existing plane can be calculated by measuring the striations of a set of fractures. In Fig. 4.28, therefore, σ is an average tensor of the stress field acting on a pre-existing surface.

Let us now consider the relationship existing between the values of the principal tensors and the direction of the striations on a pre-existing fracture plane.

By means of the principal directions of stress tensors, all the sliding directions can be obtained on the same shear plane by varying the values of the three principal tensors. The diagram is that of Fig. 4.9 for the definition of faults. In this diagram it can be observed that the direction of motion is independent from the arrangement in the space of the stress field, since it is function of the ratio (R) among the values of the three tensors.

Thus, since the striations give the direction of the tangential component (τ) of the average tensor (σ) on the fracture plane, the pitch of the striations, instead, is dependent solely on the ratio

$$R = \frac{\sigma^2 - \sigma_x}{\sigma_y - \sigma_z}$$

among the three principal tensors.

This relationship is valid only if the failure plane is oblique with respect to the three principal axes of the stress field, i.e. with respect to the σ_x , σ_y , σ_z tensors. In fact, by choosing a reference axis system x , y , z parallel to the principal axes of σ_x , σ_y , σ_z tensors for any sliding surface, oblique to the axes, where the pole is located, from direction cosines l , m , n , it can be determined the direction of the sliding through the formula

$$\operatorname{tg} \delta = \frac{n}{lm} \left\{ m^2 - (l - n^2) \frac{\sigma_2 - \sigma_x}{\sigma_y - \sigma_z} \right\}$$

(Bott's Formula, 1971).

Pole P is the projection of the straight-line perpendicular to the plane (in stereographic projection).

By means of this relationship it can be seen that, when the value of one of the direction cosines varies, so does the direction of $\operatorname{tg} \delta$, i.e. the movement of the blocks, as long as the failure plane is oblique to the axes of the stress field. The only surfaces that escape this rule are those on which lie the principal axes (σ_x , σ_y , σ_z). In fact, if a failure surface contains the z axis (Fig. 4.28), i.e. it is vertical and in agreement with the movement, axis σ will be perpendicular to it and will be perpendicular to z ; in this case, the angle formed by the straight line (σ) and the z axis will be 90° . The direction cosine "n" of this angle will therefore be $n = \cos \delta = \cos 90^\circ = 0$ and the whole expression will be equal to 0, or $\operatorname{tg} \delta = 0$ (Fig. 4.29).

The result is similar if the plane is parallel to axes x or y . This proves that if a pre-existing plane contains one of the tensors (σ_x , σ_y , σ_z), the direction $\operatorname{tg} \delta$ of the component τ is no longer dependent on the ratio of the tensors

$$R = \frac{\sigma_2 - \sigma_x}{\sigma_y - \sigma_z}$$

In this case τ and y are equal to 0.

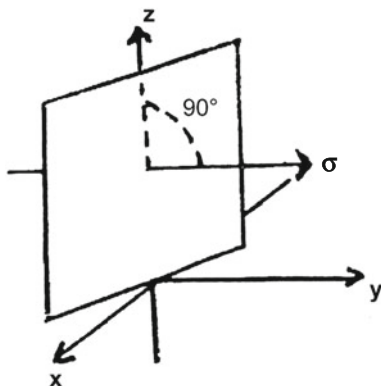


Fig. 4.29 Director cosine orthogonal to z

The pitch is independent from the regime of R ($n = \cos 90^\circ = 0$). Thus, it is equal to 0. Therefore, the striations will have an arrangement parallel to the direction of the pre-existing shear plane, condition that can occur only when the movement of the blocks becomes pure strike-slip.

If the plane contains σ_x or σ_y , i.e. it is perpendicular to σ_z , the pitch will be 90° , i.e. the striations will be perpendicular to the direction of the plane, condition that can only occur when the movement is purely reverse or purely normal.

Let us now observe the practical implications of this theoretical model.

First of all, it should be noted that all this analytical process is aimed at determining the relationship between the striations and the triaxial stress field. Actually, up to now we have dealt with this topic only for the relationship between movement (striations) and acting tensor. It is important to understand that all the operations so far expressed lead to a fact, irrefutable, that striations are the effect of a particular movement. Starting from this certainty, Bott sought a relationship between the striations produced and the acting stress field. The result is extremely reliable and therefore the structural interpretation is based on objective, incontrovertible evidence. There is therefore a correspondence among the values of the ratio of the tensors and the different tectonic regimes. The value of the ratio of the tensors of a stress field has a precise tectonic meaning, very useful for the study of a deformation and for the detection of the stress field established in the ground and sometimes still acting.

4.6.4 Method of the Minimum Dihedral (or Quick Method)

In the case of sub-vertical microfractures with strike-slip rejections, where the vertical component is negligible, an acute angle can be determined, the smallest possible between the two rupture planes.

The bisector of this angle gives the direction of σ_1 .

This is a method for determining the axes of shortening and of elongation, also known as “quick method”. It can only be used in the presence of small, strike-slip fractures, with sub-vertical planes. The method cannot be used if a normal or reverse rejection is associated to strike-slip surfaces, i.e. there is rejection with vertical component. The method consists in positioning the shortening axis along the bisector of the smallest angle between two strike-slip surfaces, dextral and sinistral. At 90° there will be the elongation axis.

The results obtained are comparable to those deriving from tension fractures and from the corresponding stylolitic peaks, respectively corresponding to the directions of the elongation and of the shortening.

The method has its validity as it is based on movements of planes close to the vertical and can be considered very often as neo-formed.

4.7 The Analysis Process

The combined effect of variations in the total stress state and of the neutral pressure regime due to fracturing, erosion, meteoric precipitation and seismic action results in the decrease of the intensity of the effective stresses field in predominantly clayey soils. At present, it is not yet very clear what are the major effects that result in a progressive reduction in the shear strength and in the size of the yield surface in pre-failure processes if not assigning to time an influence on the combined action of the factors mentioned in previous paragraphs. Picarelli (1999), quoting Eigenbrod et al. (1992), writes that they “*carried out specific laboratory investigations on the behaviour of slightly overconsolidated clays of medium plasticity subjected to cyclic oscillations of the **back pressure**, simulating in that way fluctuations in the neutral pressure regime. They observed that the effects produced are similar to those due to **creep** induced by monotonic increments of the deviatoric stress and consist in the accumulation of irreversible deformations of such an entity depending on the number of cycles, that means depending on time. In principle, also groundwater excursions could cause deformation and movements in the ground, especially when considering the additional effect of time on soil properties (mechanical decay)*” (Fig. 4.30a–c).

This problem presents some typical aspects. First of all, for a natural period, the stability analysis carried out using the Global Limit Equilibrium Method (Terzaghi 1943 and Taylor 1948) is always a verification of the existence of a limit condition of equilibrium. Only definitely unstable slopes are analysed, on which evident mass movements have already occurred, which later increase over time in relation to the evolution of some factors external to the slopes themselves. Consequently, the analysis of the limit equilibrium state of a slope cannot proceed by determining a coefficient of safety to which is attributed a supposed equilibrium condition of the whole unstable mass. In fact, if the analysis is correct, the safety coefficient is equal or very close to one. In addition, the variations in the stress state that can occur in a natural slope because of the evolution of external factors are always very limited, therefore variations in soil strength are modest and, considering also the relative value of mechanical parameters c and ϕ' , it can be obtained that ϕ' has slight influence on the variations in soil strength. The deduction of strength parameters of cohesive soils from stability analyses is a problem that is not easy to be sorted out because it often translates into the definition of implicit relations not correctly set and, above all, not considering the evaluation of the time factor. In addition, the evaluation in the laboratory of the “effective cohesion” c' , unlike of the angle of shearing ϕ' , varies considerably with the size of the samples tested as it is strongly influenced by the mesostructures existing in the lithic units present in the ground.

The analysis of unstable slopes can be carried out much more easily when failure occurs in terms of total stresses and, with reference to Figs. 2.21 and 2.25, where $\vartheta = 45^\circ$ for τ_{\max} , so that the cohesive material assumes a failure envelope with $\phi = 0$ and the failure resistance is solely supported by the undrained cohesion c_u

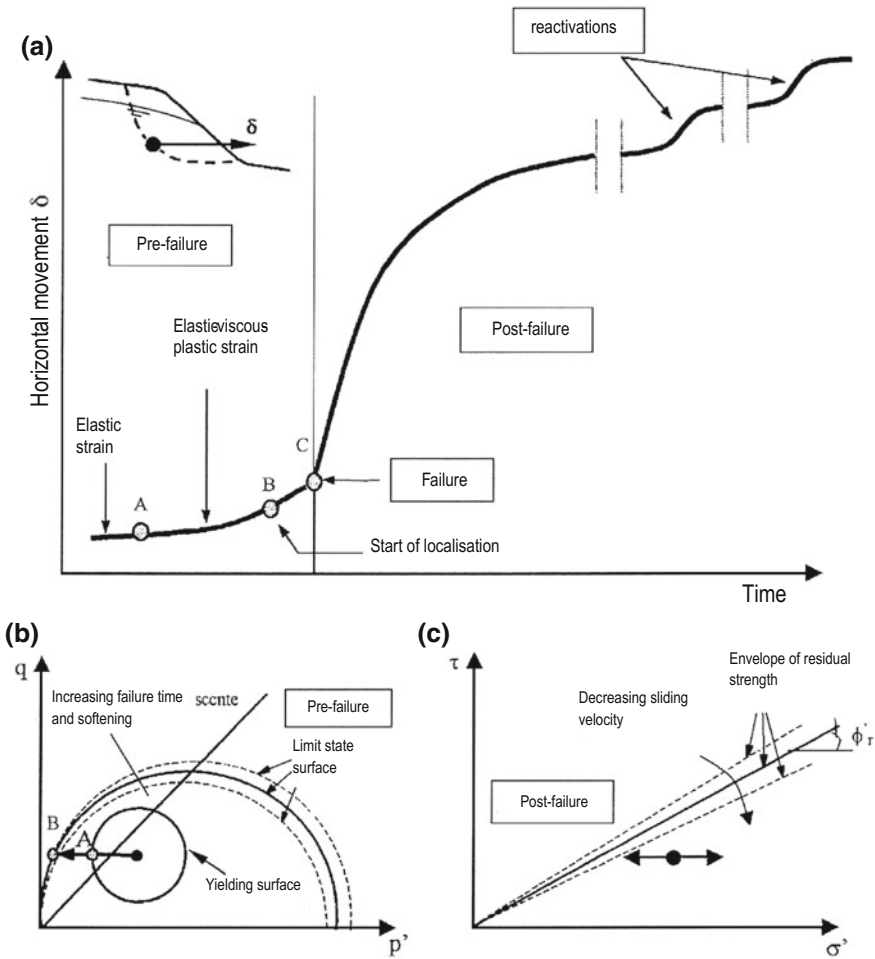


Fig. 4.30 a–c Hypothetic evolution of horizontal movement (a) of the pre-failure stress state (b) and of post-failure stress state (c) at a point of a natural slope subjected to fluctuations of the superficial groundwater table (from Picarelli 1999)

$$\tau_{max} = c_u;$$

condition that can only happen after tensile tests or under saturated conditions of cohesive soils.

Unfortunately, parameters $\phi = 0$ and $\tau_{max} = c_u$ are not the physical characteristics of the material but only mechanical parameters that describe a certain kind of behaviour. This is to say that the limited variation in the tension state, which characterizes the problem, is an artifice that allows to overcome the difficulty of describing the behaviour of the soil in terms of effective stresses and makes the

adopted model more similar to the real behaviour of the soil in order to solve more easily practical issues. However, on one hand increase the difficulties arising from the use of a strength parameter, c_u , heavily influenced by mesostructural, heterogeneous and anisotropic soil characteristics; on the other hand, the possibility to assess correctly the effect of the variations in the effective stresses on soil strength and slope stability conditions ceases to exist.

In conclusion, strength parameters expressed in terms of *effective stresses* are better defined than those in *total stresses*; but cohesion c' has a great influence on the stability of the slopes, it depends significantly on the mesostructures, in particular on discontinuities and swelling phenomena, while the advantage of the higher reliability of the values of friction angle ϕ' is often cancelled by the uncertainty in the values of interstitial pressure. On the contrary, solutions in terms of total stresses, which offer significant advantages in terms of analytical and experimental simplicity, always require the support of a wide and extended experience on the mechanical behaviour of the soils involved, which allows to establish reliable empirical correlations between undrained cohesion c_u and the actual in situ strength. However, they are really valid only in sufficiently homogeneous soils.

The difficulty in defining appropriate values of the strength parameters and of the factors related to slope stability analysis according to the current *Global Limit Equilibrium Method* is, therefore, one of the problems in geotechnical engineering presenting greater difficulty and uncertainty in the results, especially if the research is aimed to the determination of predictions and prevention conditions of the hydrogeological risk of a slope.

The problems of the instability of slopes in clayey lithotypes are therefore to be addressed through a detailed analysis of the geological and structural characteristics of the deposits as well as of their deformational behaviour by means of long-term monitoring, with particular reference to phenomena that accompany the development of progressive failure, as they are the ones that affect the mechanics of failure either along pre-existing shearing surfaces or along newly formed surfaces. Therefore, obtaining a preventive indication of the hydrogeological risk of a slope, the essential condition for starting the calculation stage, is at least to know beforehand the real depth of the sliding surface in the ground before it is activated, both in case of a pre-existing landslide and in the case of a recent landslide.

References

- Arthaud, F. (1970). *Etude tectonique et microtectonique comparée de deux domaines hercyniens: les nappes de la Montagne Noire (France) et l'anticlinorium de l'Iglesiente (sardaigne)*. Publ. Univ. Sci. Techn. Languedoc, Montpellier, série géol. struct. n° 1, 175 p.
- Arthaud, F., & Mattauer, M. (1969). Exemples de stylolithes d'origine tectonique dans le Languedoc, leurs relations avec la tectonique cassante. *Bulletin de la Société Géologique de France*, 7(11), 738–744.

- Arthaud, F., & Mattauer, M. (1972). Sur l'origine tectonique de certains joints stylolithiques parallèles à la stratification; leur relation avec une phase de distension (exemple du Languedoc). *Bulletin de la Société Géologique de France*, 7(14), 12–17.
- Blès, J. L., & Gros, Y. (1980). *La Fracturation du granite de Bassiès (Pyrénées ariégeoises - France): définition des phases tectoniques successives, évolution des diaclases et des failles*. *Bulletin de la Société Géologique de France*, 22(3), 377–390.
- Blès, J. L., & Feuga, B. (1981). *La fracturation des roches*. Bureau de recherché géologiques et minières, B.P. 6009, 45060 Orléans Ceax.
- Bott, M. H. P. (1971). *The interior of the Earth*. London: Edw. Arnold.
- Coulomb, C. A. (1773). Essai sur une application des règles de maximis et minimis a quelques problèmes de statique relatifs à l'Architecture. *Mem. Div. Sav. Acad.*, 7.
- Durney, D. W., & Ramsay, J. G. (1973). Incremental strains measured by syntectonic crystal growths. In K.A. de Jong & R. Scholten (Eds.), *Gravity and tectonics* (pp. 67–96). Wiley, New York.
- Eigenbrod, K. D., Graham, J., & Burak, J. P. (1992). Influence of cycling porewater pressures and principal stress ratios on drained deformations in clay. *Canadian Geotechnical Journal*, 326–333.
- Goguel, J. (1965). *Traité de tectonique*. Masson et Cie, 2^e édition, 457 p.
- Goguel, J. (1969). Le rôle de l'eau et de la chaleur dans les phénomènes tectoniques. *Rev. géogr. Phys. Et géol. Dynam.*, Fr., 2(2), 153–164.
- Goguel, J. (1975). La déformation des roches. *Ann. Mines. Fr.*, février-mars, 33–36.
- Marsland, A. (1974). Comparisons of results from static penetration test and large in situ plate tests in London clay. In: *Proceedings of ESOPT I, Stockholm*. Anche Building Research Establishment Current Paper 87–74.
- Masure, P. (1970). *Comportement des roches à anisotropie planaire discontinue, application à l'étude de la stabilité des excavations souterraines*. Thèse d'état. Sci. appl. Nancy, n° AO 4202, p. 272.
- Mattauer, M. (1973). *Les déformations des matériaux de l'écorce terrestre* (p. 493). Paris: Hermann éd.
- Mattauer, M. (1980). *Les déformations des matériaux de l'écorce terrestre* (493 p). Paris: Hermann éd.
- Muller, L. (1963). *Der Felsbau*. Stuttgart: F. Enko Verlag.
- Petit, J. P. (1976). *La zone de décrochement du Tizi N'Test (Maroc) et son fonctionnement depuis le Carbonifère*. Thèse de 3^e cycle, géologie appliquée (p. 99). Montpellier.
- Picarelli, L. (1999). *Meccanismi di Deformazione e rottura dei pendii*. Italy: Helvelius Edizioni.
- Price, N. J. (1959). Mechanics of jointing in rocks. *Geological Magazine*, 96(2), 149–167.
- Roering, C. (1968). The geometrical significance of natural en-echelon crack-arrays. *Tectonophysics*, 5(2), 107–123.
- Sellier, E. (1976). Approche expérimentale des mécanismes de la stylolithisation. *Reun. Ann. Sci. Terre*, 365.
- Sellier, E., & Morlier, P. (1976). Les stylolithes: approche expérimentale du processus de formation. *C.R. Acad. Sci., Fr.*, 282, 953–956.
- Shainin, V. E. (1950). Conjugate sets of en-echelon tension fractures in the Athens limestone at Riverton, Virginia. *Geological Society of America Bulletin*, 61, 509–517.
- Simpson, B., Calabresi, G., Sommer, H., & Wallays, M. (1979). Design parameters for stiff clays. In *Proceedings of VII ECSMF, Brighton* (Vol. 5, pp. 91–125), SOA Report.
- Sopena, J. P., & Soulas, J. P. (1973). *Etudes microtectoniques dans le Jura. Déformations des calcaires sous contrainte tectonique; essai d'interprétation et de corrélation des résultants pour l'ensemble de la chaîne*. Thèse Facul. Sci. Techn. Univ. Besançon n° 170. géol. appl. et Ann. Sci. Univ. Besançon, (3), n° 19 bis, 1973, (résumé) pp. 203–207.
- Taylor, D. W. (1948). *Fundamentals of soil mechanics*. New York: Wiley.
- Terzaghi, K. (1943). *Theoretical soil mechanics*. New York: Wiley.

Part II

Methodological and Analytical Aspects

From a dynamic point of view, it is evident that every landslide has an origin and an end in the time and that the time itself has a limited extension in the space, with a sliding surface having variable depth from soil to soil depending on their geological–structural conditions. Whatever is the genesis of landslides in cohesive soils, the soil matter they develop within is never isotropically distributed in the ground and, consequently, the direction of the movement is not only dependent on just the physical and mechanical properties of the soil. Furthermore, at failure a landslide starts moving along a pre-existing sliding or a neo-formed surface with a high potential in kinetic energy, which gradually dissipates along the path towards a new condition of equilibrium. The movement of a landslide, thus, is not uniform and diminishes moving progressively to the downslope. In this configurational process of a landslide unit, numerous mathematical models attempted, through a finite number of variables, to simulate the complex mechanical phenomena leading a slope to failure (Fellenius 1922; Skempton 1948; Bishop 1955; Morgenstern and Price 1965; Sarma 1979; Jambu 1973; Bromhead 1986; etc.). However, those methods essentially based on equations of the equilibrium of moments, even if appearing satisfactory from a deterministic point of view, cannot be considered as such if the analysis is addressed to the prediction and the prevention of landslides, because they do not take into account the *time factor*. In fact, by mediating the rationalistic positions of three-dimensional space of a physical body as the one of a landslide, the *Method of Limit Equilibrium*, which all the cited mathematical models refer to, results to be lacking in a four-dimensional space–time continuum that assumes dynamic valence in the deformation process of the pre-failure and triggering. The three-dimensional configuration of the failure mechanism of slopes coincides, in effects, with a statistical concept of the development of a landslide, while prediction and prevention require a dynamic cognitive process intended to the evaluation of the product of stresses times the measurable duration of a shearing deformational event.

A first evidence of the need of a connection between the local properties of a soil and the general relativity space–time of landslide events is identified in the paradigm between the energy of a lithic mass and the forces which induce the movement. Such a conjugation is based upon three principles that can be enunciated as: *individuality*, *objectivity*, *locality*.

Individuality allows to isolate the landslide system from the rest of the phenomena taking place at the boundaries; *objectivity* attributes the feature of physicality to the sliding mass as symbol of an autonomous and generalised subsistence; *locality* defines the space the phenomenon explicates within. These principles mean that the landslide is defined by intrinsic properties which are independent from the time. It seems, therefore, that a landslide mass is characterised by a set of distinct phenomena, concrete and independent and the application of which is enclosed in the so-called field theories, which describe the electrostatic phenomena of clays and reduce the movement to the gravitational attraction of mass.

The problem of deformational mechanic of slopes derives, at last, from the fact that it is constrained to describe the instability phenomena of cohesive masses by simplifying and reducing the analysis to a mathematical formalism which was developed during the course of the evolution of geotechnical engineering from the formulation of the first criterion of shearing resistance (Coulomb 1773). Given that it is impossible to achieve a complete deterministic knowledge from a quantum system because of the impossibility to insert in the mathematical calculations all the variables, often indefinite, such as the duration of a preliminary event to hydrogeological instability, the analysis cannot be devoted to the sole quantification of some parameters defined in the gravitational field, but must be addressed to the epistemological description deriving from the critical review of all the variables concurring to the definition of a landslide. In other words, the analysis for the *prediction* and the *prevention* of a landslide must be carried out not as the rationalisation of the hypothetical properties of a physical event, but as the result of experiments carried out on the field, obtained from the complementarity among measurement apparatuses.

References

- Bishop, W. A. (1955). The use of the slip circle in the stability analysis of slopes. *Geotechnique*, 5(1).
- Bromhead, E. N. (1986). *The stability of slopes*. New York: Surrey University Press.
- Coulomb, C. A. (1773). *Essai sur une Application de Regles de Maximis et Minimis a Quelques Problemes de Statique Relatifs a l'Architecture* (Vol. 7). Mem. Div. Sav. Acad.
- Fellenius, W. (1992). *Erdstatistische Berechnungen*. Berlin: W. Ernst.
- Janbu, N. (1973). *Slope stability computations* (pp. 79–93). The Embankment Dam Engineering Casagrande Volume. Wiley.
- Sarma, S. H. (1979). Stability analysis of embankments and slopes. *J. Geotechnique Engineering Div., An. Soc. Civ. Engrs.*, 105 (GT 12).
- Skempton, A. W. (1948). *The $F = 0$ Analysis of stability and its theoretical basis*, In 2nd ICSM, Rotterdam.

Chapter 5

The Dynamics of Disruptions

5.1 Introduction

The timely identification of ground deformation at failure in areas at high hydrogeological risk has as a key prerequisite the definition of the distinctive character of the type of disruption that may develop on the slope. For this purpose, prior to any instrumental survey, the area subjected to potential hydrogeological instability should be identified and circumscribed by using the traditional geological-structural and geomorphological surveys. This distinction is very important since the dynamics of instability assume different behaviour in relation to the causes of activation or reactivation of the landslide. The characteristics will therefore be sought for the identification of several types of landslides belonging to the large group of hydrogeological instabilities in predominantly cohesive soils in order to simplify and make immediate the identification of areas at risk.

A first fundamental distinction is the following:

- (a) the slope may be subjected to a landslide of recent origin; *recent landslides*, or:
- (b) the slope may be subjected to the reactivation of a landslide occurred in the past; *pre-existing landslides*.

5.2 Dynamics of Recent Landslides

An overview of the triggering mechanisms of recent landslides on predominantly cohesive slopes shows that such mechanisms depend on the changed soil technical characteristics and on pore-water pressures developing in the ground.

In general, hydrogeological instability develops according to a rotational-plastic deformation that takes place at the depth where pore-water pressure is maximum. In the Apennines this depth varies from a few meters below ground level (~ 3 to

~8 m) within altered clayey-marly soils overlying slightly fractured, overconsolidated, layered clay, such as the sub-Apennine clays of the Unit of the Bradanic Foredeep—Upper Pliocene—Calabrian (Richetti and Sandone 1979) or as the grey-blue clays of the Neogenic Basin of Siena (Costantini et al. 1992), up to a maximum of 45 m in tectonised, destructured and chaotic shaley-clay soil such as Varicoloured Clay (Ogniben 1969) or the Red Flysch (Scandone 1972).

Recent landslides belong to three different environments.

5.2.1 *First Environment*

The first environment is that of large moving masses that are bound to a neat and timely sliding sequence for which the deformational priority at failure is always provided to the downslope mass. On the slope takes place a type of hydrogeological disruption made up of several landslides, in regressive-sequential succession, that develop in different times. These landslides are always linked to long lasting periods of meteoric precipitation when, therefore, groundwater free surface is almost close to ground level. In cohesive soils, the sliding surface is rotational, either the main one and the ones of the other landslides that are often part of the sequential movement (Fig. 5.1).



Fig. 5.1 Recent composite landslide occurred in 1972 on the southern versant of the hill of Craco, Province of Matera, Southern Apennine, Italy. The town, of medieval origin, was located upon an arenaceous block overlying grey clays of Medium-Upper Pliocene



Fig. 5.2 Tilting towards the downslope of the slight slope of the temple of goddess Mephitis, developed by pre-failure deformation of the ground in Rossano di Vaglio, Province of Potenza, Italy

Slope failure is never instantaneous but passes from a pre-failure phase, typically very long lasting, to shearing. In the Argentinian Andes, where many of these instability phenomena have large and deep territorial extension, gestation periods take often more than 50 years and are heavily dependent on seismic activity. Sometimes the existence of the pre-failure deformation in the ground develops at the surface through a slight depression of the ground surface when the shearing zone is not particularly deep (Fig. 5.2). This suggests that the local slope is at hydrogeological risk.

One or more landslide scarps are always present along the contour of the slipped mass with transverse ridges and cracks as well as radial cracks at the foot. In this type of environment when the piezometric surface reaches the ground surface, a horizontal thrust value (σ_{ho}) is generated which is greater than the strength of the saturated soil; in these conditions, σ_{ho} has already exceeded the limit state equilibrium of a value greater than $2 c_u$, where c_u is the undrained cohesion.

Therefore, the cause of rotational plastic sliding in cohesive soils is due to a problem in pore-water pressure developed at the boundary of the sliding surface in conditions of saturation.

Campomaggiore Vecchio, in the province of Potenza—Southern Apennines, is a ghost town (Fig. 5.3) located on the left versant of river Basento. Between 8th and 10th February 1885, after three days of intense rainfall, the soils on which the area was built, belonging to the lithological formation of Red Flysch and precisely to its clayey-marly member (Figs. 5.4 and 5.5), were affected by a large and slow hydrogeological disruption caused by a landslide classified as rotational sliding.



Fig. 5.3 Landslide on which the town of Campomaggiore Vecchio lies in its urbanistic integrity. In the background, the depletion zone of the landslide where the town was originally located



Fig. 5.4 Red Flysch (Flysch Rosso)

The town, after being inhabited since 1300, had a period of abandonment, as it has often been recorded in areas of the Basilicata region, subjected to continuous migrations of population in search of new fertile lands to be cultivated. In 1622, the area of Campomaggiore, without feudal lords, was granted by Philip IV, King of Spain and of Naples, to Carlo Rendina, awarded of the title of Count, imposing on him to have the feud of ancient origins inhabited.

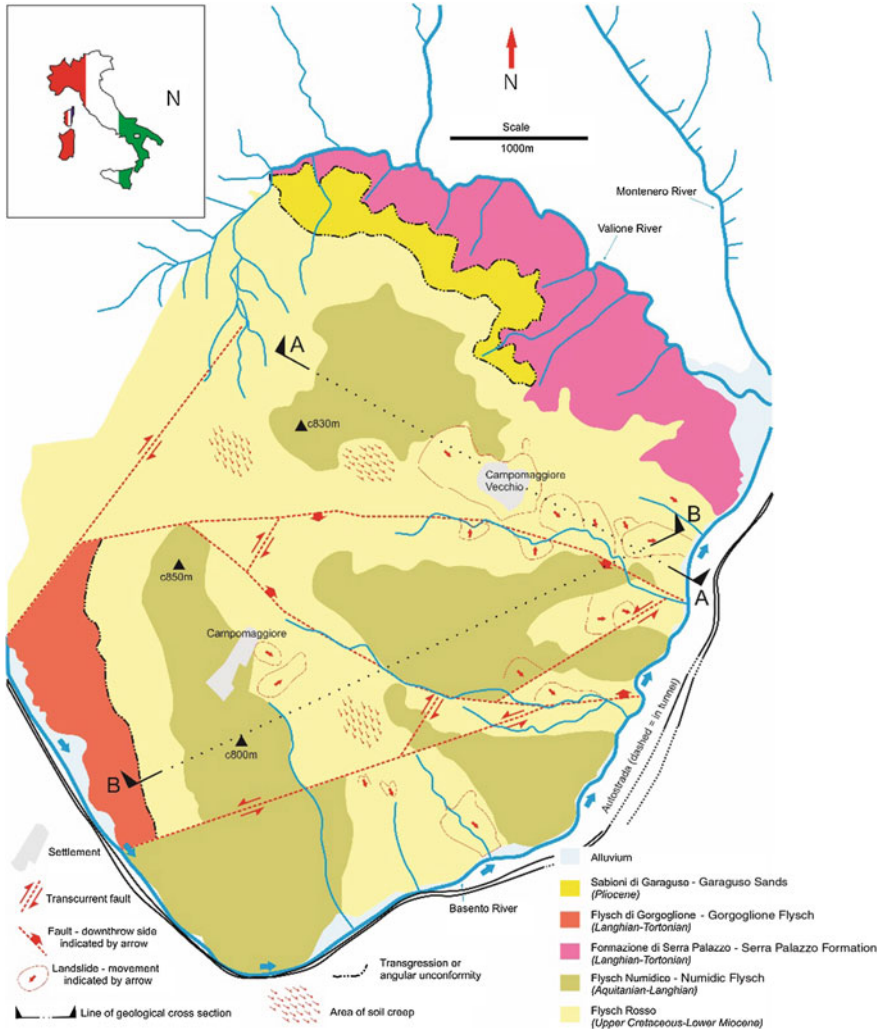


Fig. 5.5 Geological map of the area of Campomaggiore Vecchio

The sliding was slow and unitary so that the inhabited area underwent a gradual translation from the upslope to the downslope of about 200 m, partly preserving the integrity of the elevation of the buildings. The bell tower and the church itself (Fig. 5.6), Palazzo Rendina (Rendina Palace) (Fig. 5.7), the cemetery and the house buildings stayed up, but obviously underwent cracking and disarticulation of the structures so that the inhabitants were forced to abandon the site and to build a new one

about 2 km eastwards, on top of a hill. Campomaggiore Vecchio today has a significant importance both from the historical and from the architectural points of view as witness of the ancient lifestyle and of the types of buildings of that time as well as an example of an interactive relationship with the local environment and its evolution.



Fig. 5.6 Ecclesiastical nucleus



Fig. 5.7 Palazzo Cutinelli-Rendina (from Campomaggiore, archeologia dell'edilizia storica by Pierfrancesco Rescio, 1997)

In order to clarify this latter aspect related to the problem of the preservation of the architectural and cultural heritage of one of the many Basilicata towns with the same conditions of hydrogeological instability, it is necessary to step back in the analysis of the causes of this landslide and to ask first of all:

- (a) why a certain site which has been stable for more than two centuries (since 1622) slipped down exactly on February 1885?
- (b) why did the movement take place according to that specific type of sliding?
- (c) what are the real causes of the instability?

Referring to the causes of instability, the prolonged rainfall of February 1885 does not entirely satisfy these questions; a similar meteorological event, in fact, does not represent something exceptional within a certain historic period. Does there, therefore, exist a causal link?

- In 1673 Count Gerardo Antonio Rendina, son of Carlo, finally buys the whole area of Campomaggiore.
- In 1741, the town centralised in a single area, as wanted by Don Ferrante Rendina; those who wanted to live in the centre of Campomaggiore had to plant a vineyard for which, after 6 years, five *carlini*¹ had to be paid for each *tomolo*.² In addition, the residents were allowed to chop oak and Turkey oak woods for producing roof beams as long as three fruit trees, to be chose by the Baron, were planted to replace each oak cut. Between 1760 and 1780, Teodoro Rendina and its successors increased the agrarian economy; a small swamp was drained and the houses around the baronial palace were grouped together, thus creating a town with an ordered chessboard plant, with wide roads crossing at right angles. Everything was built in masonry. During this period many *Bitontini* (inhabitants of Bitonto in Apulia) settled in Campomaggiore, as per the will of Teodoro Rendina, and introduced the cultivation of olive trees in an area previously mainly relevant for forestry and pastoralism. In 1795 Campomaggiore counted 410 inhabitants; in 1820 they doubled to 820. In 1885, the landslide occurred.

By means of the analysis of slope stability (carried out using the Global Limit Equilibrium method) it was possible to determine the pore-water pressure in the slope or the rise of piezometric level at failure. In addition, it was possible to correlate the amount of rainfall with the variations in groundwater level by means of long-term piezometric monitoring, in order to derive the amount of precipitations corresponding to the pore-water pressure at failure.

The slope stability analysis provided values of the safety factor (F_s) always greater than 1 even under high interstitial water pressure conditions, i.e. with a piezometric level of 1 m below ground level (Fig. 5.8).

¹Carlino was an ancient currency from the Kingdom of the Two Sicilies in Southern Italy.

²Tomolo was an ancient unit of measure of surface locally adopted in Southern Italy. In the Basilicata Region it usually corresponded to 4088 m².

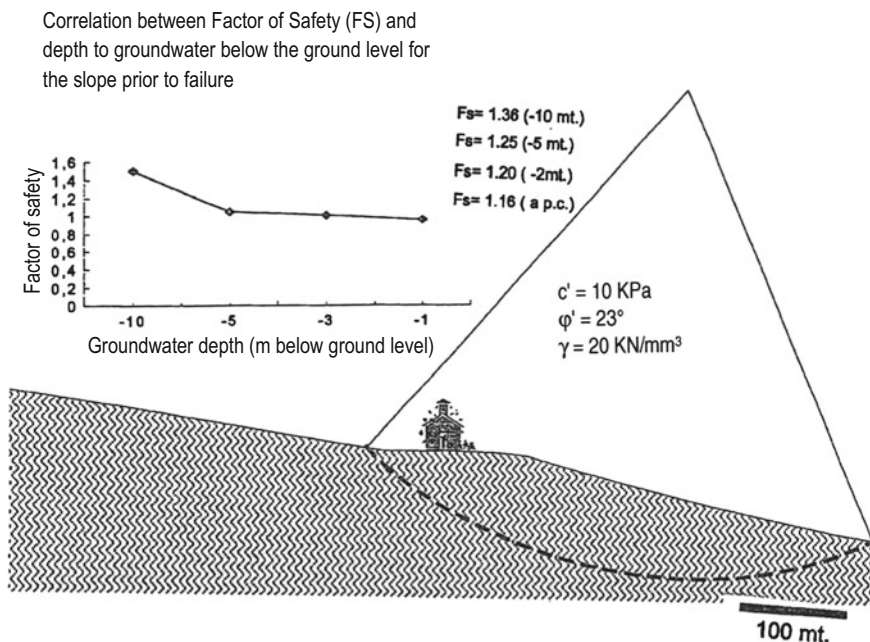


Fig. 5.8 Stability assessment of the landslide carried out on the original slope prior to the sliding happened in 1885. Slope gradient was $\alpha = 14^\circ$

This is probably due to low slope steepness ($\alpha = 14^\circ$) on which the village of Campomaggiore developed after 1662.

Re-developing the same analysis with a slope gradient of $\alpha = 25^\circ$, equal to the one of the slope at the time of activation of the landslide (1885), it was found that the landslide involving Campomaggiore Vecchio occurred in conditions of pore-water pressures corresponding to a piezometric level of 1 m below ground level (safety factor $F_s = 0.95$ —Fig. 5.9).

This indicates that the triggering of the landslide is due mainly to the variation in slope steepness, developed in a period between the settlement of the town in the area of *Scarrone del Salice* (1622) and that of the landslide of 1885. It seems therefore that the main cause of the reactivation of the existing landslide is to be attributed to the process of regressive erosion of the watercourses tributaries of river Basento, which in the present case acts as base level and, with the deepening of its riverbed over the centuries, has induced a morpho-evolutionary process on the slope with a gradual increase in the steepness of the surface. Using the diagram of Fig. 5.10 it can also be estimated the amount of rainfall that led to the mobilization of the landslide in 1855. This critical value of the piezometric level was reached roughly with 205 mm/month of rainfall. During the three days of bad weather, 8–10 February 1885, therefore, about 205 mm of rain fell down.

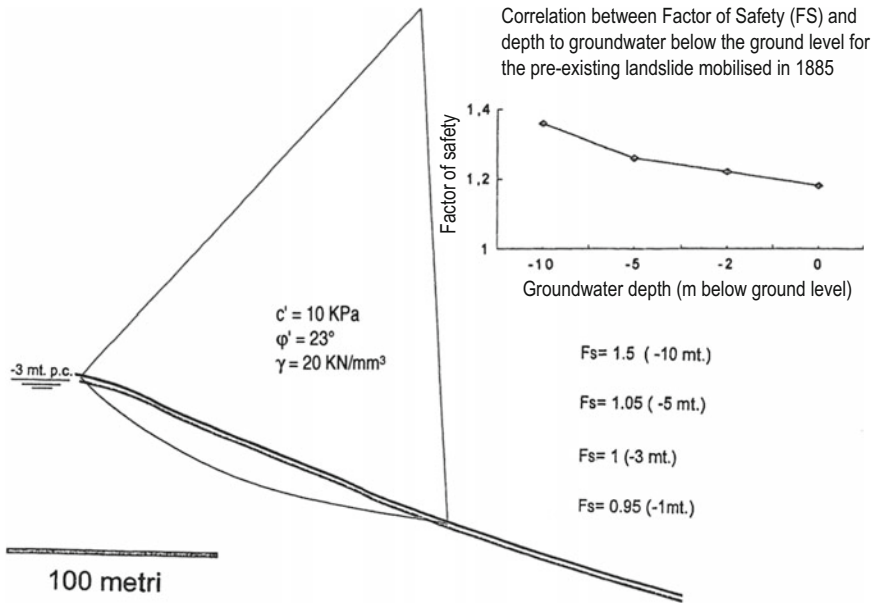


Fig. 5.9 Slope stability assessment at the time of the landslide in 1885. Slope gradient was $\alpha = 25^\circ$

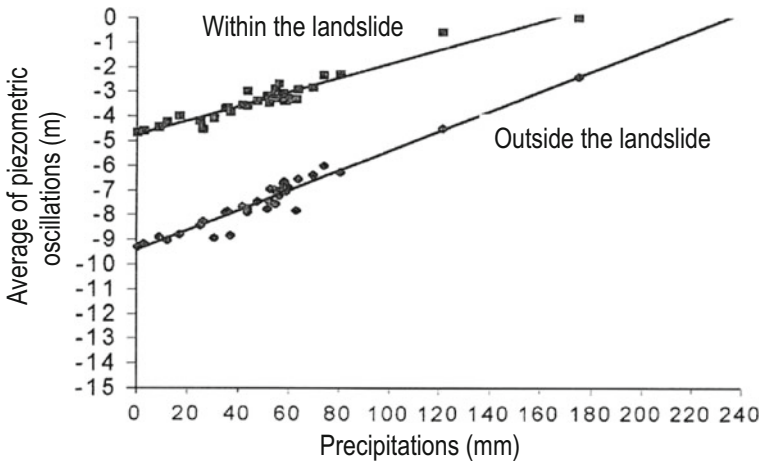


Fig. 5.10 Correlation between meteoric inflows and outflows and groundwater fluctuations inside and outside the landslide

From the current geomorphological observations carried out to the downslope of the landslide on which Campomaggiore Vecchio is located, it is evident that most of the landslides develop along torrential engravings that from river Basento climb back the slope. At the edges of these engravings, the Red Flysch clay undergoes an unloading with a decrease in consolidation pressure while the slope is subjected to a stationary seepage motion with a particularly high hydraulic gradient close to

ground level. *For this reason, the most frequent disruptions occur along the torrents and progressively evolve climbing back up the slope; It follows that the main cause of a further activation of the same landslide of 1855, currently lying halfway up the slope, is due to the regressive erosion carried out by the watercourses.*

In conclusion, it can be assessed that relations with the territory of archaic societies set up on the predominantly clayey hills of Basilicata region have undoubtedly transformed the specific ecosystem of these areas as a result of a productive process suited to social growth aggravated over the millennia from variations in the local climate. Recently, cultivation of new lands, reclamation, contractions of wooded areas, emigration from small centres and the crisis of agriculture at the foot of the hills have triggered phenomena of physical degradation of the territory. The change was sometimes immediate and violent, sometimes slow and gradual. However, the historical reconstruction of these environments, of their modifications as well as of locations, of changes, of reorganizations and of social crises of the centres of human aggregation can provide an assessment of the cause and effect factors in the historical process of transformation of the territory. *Following the path of modifications, it is possible to reconstruct the interactive path between the two systems over time and to evaluate the speed of the processes of modification. This will also enable the translation of this knowledge in terms of predictions and, presumably, allow to evaluate the future transformations of archaeological and architectural heritage as a function of environmental degradation (preservation of cultural heritage) and of time of use (history of the natural environment).*

5.2.2 Second Environment

It is referred to slopes strongly affected by the incisiveness of watercourses, including the slopes of badlands (Fig. 5.11a, b). Here mass movements manifest themselves by means of falls, solifluction and/or flows, due to water runoff on the slopes, along a single path as an essentially coherent unit (Fig. 5.12).

The sliding mass is always the one of the horizon of alteration, rather decompressed, resting on the same deposit which is competent and sometimes not fractured. Landslides along a layer characterised by acclivity lower than the one of the slope also belong to this environment.

These landslides are associated to abundant meteoric precipitation or to when the erosive effect of watercourses is strongly incisive in a short time. It is noted, in fact, that the swelling of clay caused by natural erosion processes modifies their structure and in more or less short times acts on the morphology and stability of vast areas of the territory. The formation of the side valleys is due to coupled phenomena of erosion and sliding. Generally, the process of the main riverbed develops along faults of tectonic origin, while the enlargement of side valleys is caused by landslides occurring on lateral slopes. Picarelli and Urciuoli (1993), following indications by Bromhead and Dixon (1984), have shown that there is a relationship between water content and swelling pressure, verified on a partially air-dried specimen and on a sample taken at great depth below the fault (Figs. 5.13 and 5.14).

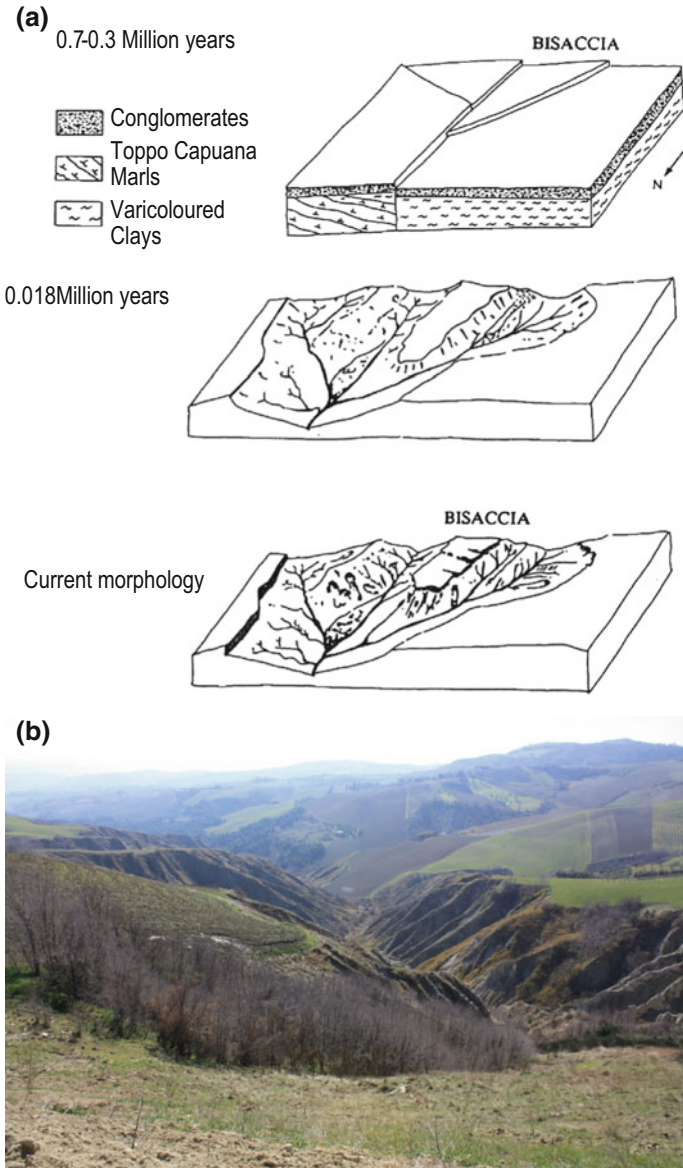


Fig. 5.11 a Geological evolution of the area of Bisaccia (from Fenelli and Picarelli 1990). The formation of side valleys has been attributed to coupled phenomena of erosion and sliding. The beginning of these phenomena was dated back to about 300,000 years ago. **b** Badlands in the middle sector of the basin of Chifente—Marche Apennines—Ascoli Piceno, Marche Region, Italy



Fig. 5.12 Northern Andes of the province of Jujuy—Argentina

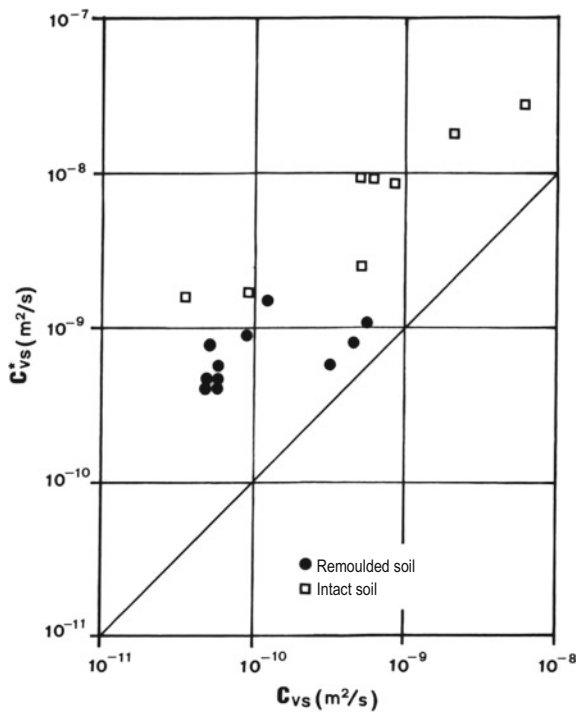


Fig. 5.13 Coefficient of hydraulic diffusion at swelling obtained from the analysis of movements (C_{vs}) and from neutral pressures (C^*_{vs}) (from Picarelli and Urciuoli 1993)

The strong swelling potential is certainly an important factor in controlling deformation processes induced by river erosion. It has been observed that the response to deviatoric stresses is strongly dependent on the mesostructure of the material and

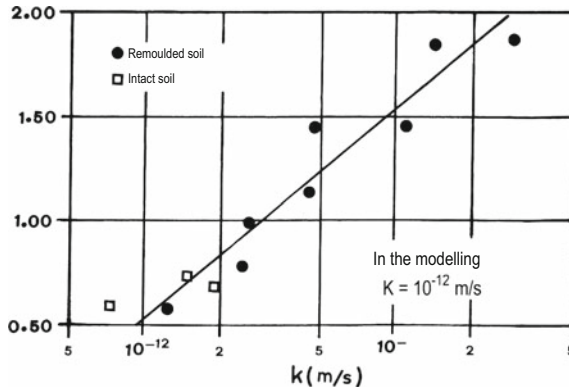


Fig. 5.14 Coefficient of hydraulic conductivity in argillites (from Picarelli and Urciuoli 1993)

especially on the presence of *principal shear* (Skempton and Petley 1967). In this type of environment, the free surface of groundwater table is often close to the ground level and the annual oscillations are limited to a few metres; the shallow lithic horizon therefore acts as a permanent water tank which in case of seismic stresses could be subjected to neutral overpressures able to lead the slope to failure.

However, the magnitude of the effects that reduce river valleys to degraded environments depends on a number of factors that are related to valley geometry, to the conditions of the deposits at the boundaries, to the physical and mechanical characteristics of these and to the stresses induced by groundwater in the ground.

It is evident that unfavourable combinations of these factors can induce particularly accentuated deformational phenomena and characterized by slower or quicker progression over time. The effects of erosion into relevant deposits of highly plastic and fractured clays are due to high potential for swelling and reduced permeability.

Surely, the availability of several hypotheses on the geological history of the territory, the use of larger volumes of soil than the ones locally taken out, or considering greater erosion rates and taking into account also the viscous deformation phenomena, which are particularly accentuated for low stress states, allow to obtain results that are even closer to the real situation as well as to understand the mechanisms that determine and/or affect the stability of the area and the geological evolution of the slopes.

An example can better clarify the evolutionary process of these slopes.

In the Pliocene basin of torrent Chifente, east of Ascoli Piceno, in the Marche Region (Italy), Central Apennine, it is observed the outcropping of marine deposits from the Pliocene constituted by basal pelitic units from the foredeep in predominantly silty-clayey facies (Fig. 5.15). On hills versants, in mainly Mediterranean semi-arid climate, are widespread forms of shallow disruption as morphological products of intense erosion of productive soils (Fig. 5.16). The affected areas are currently subject to desertification processes with heavy consequences on the socio-economic development of Marche region. From early investigations, carried out to assess the erosion phenomenon, the influence of expanding minerals was recognized as a peculiar effect in the process of disruption of the silty-clay material.

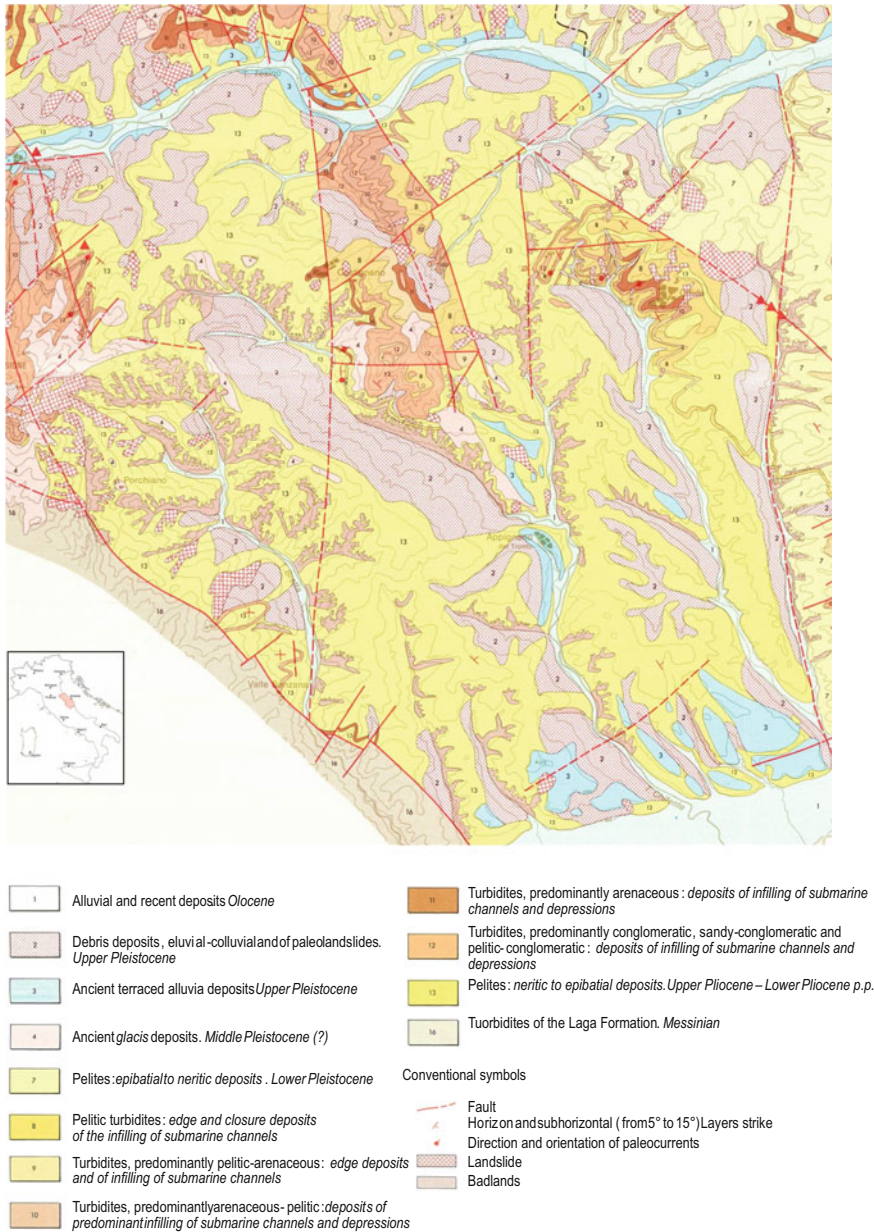


Fig. 5.15 Geology of the basin of Chifente (from Geological Map of Plio-Pleistocene Deposits between river Tenna and river Tronto by E. Centamore, Geological Studies Camerti, special number)



Fig. 5.16 Badlands in the middle sector of the basin of Chifente

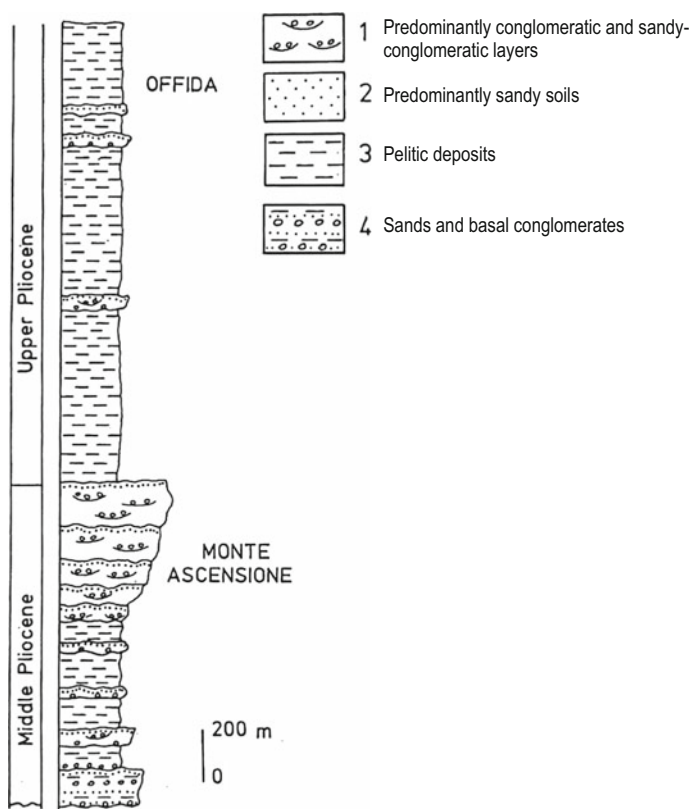


Fig. 5.17 Stratigraphy of the Pliocene succession of the basin of Chifente

The sediments analysed are those of the post-orogenic marine cycle that constitute the Medium to Upper Pliocene lithological succession deposited in a foredeep basin, in an external position with respect to the infra-Pliocene chain of Marche region (Fig. 5.17).

The stratigraphic succession begins with coarse, slightly cemented sand, containing small to medium sized pebbles, or with banks of discordant monogenic arenaceous conglomerates of the Laga Formation. To the top, sedimentation passes to gray-blue clayey-marly silts, rich in macro-fossils (Venus, Ostrea, Pseudamussium, etc.) attributed to platform deposits (Cantalamessa et al. 1986). In the surveyed area, the sequence has a thickness of about 2000 m and is in continuity of sedimentation on the underlying member. There are coarse clastic deposits at various stratigraphic levels, with lenticular shape, of limited thickness (10–35 m), which represent channel-like layers. These horizons are formed by polygenic conglomerates with low sandy content and/or sandy matrix. The depositional environment is initially infralittoral-circalittoral and finally bathyal (depth \approx 500 m).

The Pliocene pelitic sedimentation constitutes a very spectacular landscape, with badlands that form a drainage system deeply engraved in the silty-clayey substrate (Fig. 5.16), extremely hierarchical and characterized by narrow interfluvial areas, often made up of laminated jumps. There, the slope has an acclivity of more than 45° and anti-dip sloping layers. Inside the Badlands system the lateritic thickness is about 20 cm. Rotational sliding movements are frequent and often have large extensions. At the base of the valleys there are characteristic accumulations of mudflows, active during rainy periods.

The vegetation cover is made up of forest boundaries or remains of forest soils that somehow witness of a wider development of vegetation in earlier times. On the opposite side, where the monoclinical structure has dip-sloping layers inclined of 10°–15°, the acclivity of the slope is slightly greater than the one of the layers (15°–20°). There, Badlands are uncommon, whereas translational slip phenomena (Varnes 1978) or solifluction, generally very circumscribed, prevail. The alteration layer has a noticeably greater thickness, between 1.5 and 2 m. The vegetation is developed in woods of sufficient extension.

At the base of the hill, near the valley of river Tronto, the contour of the slope undergoes a sharp variation in gradient, with an average acclivity lower than 10°. Here, mass movements are limited to plastic-fluid flows, which usually interest only the alteration layer at surface (Fig. 5.18). This, on anti-dip sloping layers, has a thickness of 70–100 cm and has an intense cracking in dry periods. Vegetation is almost absent; on dip sloping versants ruled by stratification surfaces and with exposure to north-east there is abundant grass and frequent shrubs; here the alteration of silty-clayey layers has thickness greater than 1 m.

The 2nd and 3rd order ancient alluvial terraces, from Middle-Upper Pleistocene, located at various levels above the bottom of the valley (up to about 170 m), are all distributed on the right-hand side of the streams, with exposure to NE, while on the left-hand slope, where badlands erosion is predominantly developed, they are absent; this is indicative of the migration to NE of stream courses that must have started in postglacial epoch or in Middle Pleistocene. In addition, the first order



Fig. 5.18 Badlands produced by plastic-fluid flows within the shallow alteration horizon

terraces are inclined to NE of 10° – 15° , due to the tectonic arrangement acquired during the lifting phase subsequent to their deposition.

The results of the particle size distribution analyses are reported in Table 5.1 and it is easy to observe that the silt fraction is generally greater than that of clay. The material also contains low sand fraction. Sediments from the basin of Chifente are therefore identified as clayey slightly sandy silts and present a good uniformity in grain size distribution, being represented by obtaining a fairly narrow granulometric envelope (Fig. 5.19). However, a slight increase in clay fraction is obtained with depth and sometimes it becomes predominant at more than 12 m below ground level.

The Shepard triangular diagram (Fig. 5.20) shows, finally, a certain homogeneity of the grain size distribution of the samples and a variable clay content within a very limited range. This indicates that there are no significant differences between the samples from different areas and that the average tendencies are rather similar.

The results of the X-ray diffractometric analyses have shown the constant presence of clayey minerals (fraction $<2\ \mu\text{m}$) in average percentages of 60% of the total equally distributed across all the site. Smectite is the most abundant mineral (about 60%), prevalent on chlorite, illite and kaolinite (Table 5.2). It has a very mediocre crystallinity grade, of calcium-magnesiumiferous, dioctahedral and aluminiferous type. Chlorite accounts for 16% of total clay minerals; it is on average well crystallized and contains a small amount of iron in octahedral layers. Illite also is presented as dioctahedral aluminiferous, with a mediocre degree of crystallinity, sometimes in mixed layers of illite-smectite, with a percentage of 20–30% in expandable layers. The percentage, in weight, is 15% on average. Kaolinite has a modest presence, about 8%; is disordered and with low degree of crystallinity.

It should be noted that the sum of the amount of clay minerals is rather constant in the four areas investigated; however, chlorite and illite vary mutually with respect to smectite and sometimes record the prevalence of one or of the other.

Table 5.1 Particle size distribution of clayey silts of the basin of Chifente

| Location | Sample N. | Depth (m) | Fraction % | | |
|----------------|-----------|-----------|------------|----------------|-----------|
| | | | Clay | Silt | Sand |
| | | | <0.002 mm | 0.002–0.075 mm | >0.075 mm |
| Castel di Lama | 1 | 3.5 | 26.8 | 59.9 | 13.3 |
| | 2 | 11.7 | 45.5 | 47.8 | 6.7 |
| | 3 | 13.5 | 43.2 | 49.4 | 7.4 |
| | 4 | 9.5 | 39.7 | 52.0 | 8.3 |
| | 5 | 23.5 | 51.3 | 45.9 | 2.8 |
| | 6 | 10.0 | 41.0 | 53.2 | 5.8 |
| Appignano | 7 | 7.0 | 47.2 | 45.9 | 6.9 |
| | 8 | 25.0 | 53.4 | 43.4 | 3.2 |
| | 9 | 3.0 | 32.2 | 58.9 | 8.9 |
| | 10 | 2.5 | 29.5 | 58.8 | 11.7 |
| | 11 | 5.5 | 45.6 | 47.0 | 7.4 |
| | 12 | 8.0 | 49.7 | 47.7 | 2.6 |
| Castignano | 13 | 4.0 | 38.9 | 44.7 | 16.4 |
| | 14 | 17.0 | 43.0 | 47.6 | 9.4 |
| | 15 | 16.4 | 56.6 | 39.0 | 4.4 |
| | 16 | 13.0 | 45.7 | 49.2 | 5.1 |
| | 17 | 6.0 | 36.3 | 53.5 | 10.2 |
| | 18 | 4.3 | 41.2 | 53.3 | 5.5 |
| | 19 | 12.5 | 55.2 | 43.0 | 1.8 |
| Offida | 20 | 4.0 | 39.4 | 52.8 | 7.8 |
| | 21 | 3.0 | 28.8 | 53.7 | 17.5 |
| | 22 | 18.0 | 43.7 | 49.7 | 6.6 |
| Minimum | | | 26.8 | 39.0 | 1.8 |
| Maximum | | | 56.6 | 59.9 | 17.5 |
| Average | | | 42.45 | 49.8 | 7.71 |

The largest variations in weight are recorded in the percentage of smectite which, in the aggregate, appear to be independent from the location and the depth of the samples tested. With reference to the depth of the latter, the fraction of clayey minerals has the following distribution:

- from 0.00 to 5.00 m below ground level, smectite has values ranging between 39 and 60%, with a low relative average value (52%), chlorite (11–24%) and illite (11–34%) also have quite variable values but with relatively high percentage (\bar{x} = Cl 19–21%). Kaolinite (2–12%) has the same pattern as the latter.
- from 5 to 10 m below ground level, smectite increases in percentage (\bar{x} = 59%) and achieves a more uniform distribution (48–70%). At the same time chlorite and illite undergo a reduction in concentration by weight (\bar{x} = Cl 17–16%) and a slight increase in uniformity of values (Cl = 13–25%, I = 9–26%). Kaolinite has

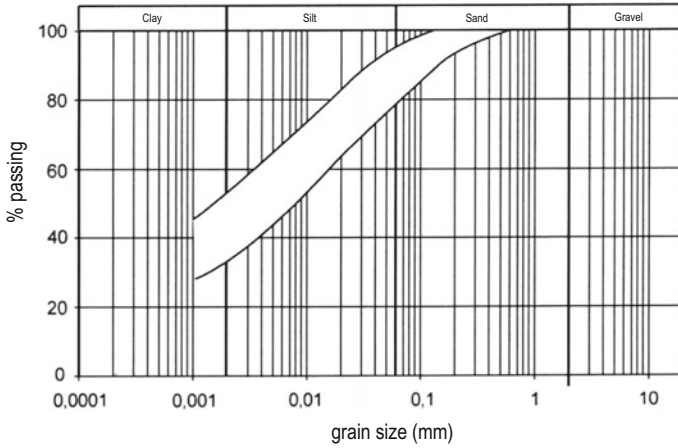


Fig. 5.19 Grain size distribution envelope of pelitic deposits in the Pliocene basin of Chifente

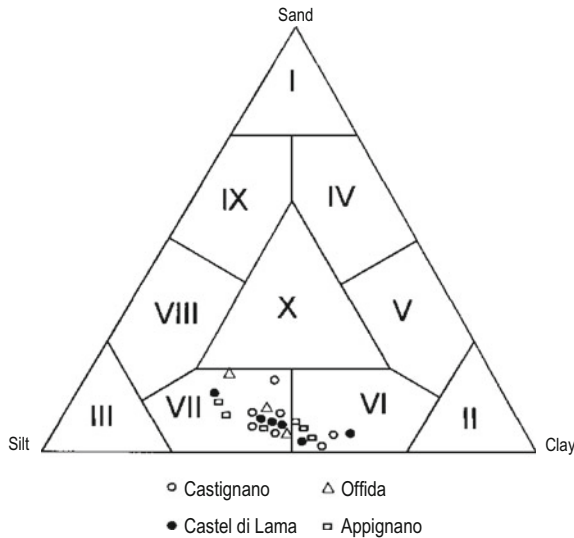


Fig. 5.20 Shepard's triangular diagram

more or less stationary average values ($\bar{x} = 8\%$) and is more uniform than the previous ones.

- from 10 to 23 m below ground level, smectite has much greater average values than the previous ($\bar{x} = 67\%$) while chlorite and illite decrease in percentage, respectively, to ($\bar{x} = 14\%$) and ($\bar{x} = 10\%$). For smectite and chlorite, distribution remains on the same uniformity values as before, while for illite a narrower uniformity range (I = 5–14%) is obtained. Kaolinite, on the other hand, does not undergo changes in the average percentage by weight ($\bar{x} = 8\%$); however, it presents a slight quantitative dispersion among the various samples of this bathymetric zone.

Table 5.2 Clay minerals from X-ray diffractometry

| Location | Sample N. | Depth (m) | Sm | Cl | I | K |
|----------------|-----------|-----------|----|------|------|------|
| Castel di Lama | 1 | 3.5 | 39 | 18 | 34 | 9 |
| | 2 | 11.7 | 65 | 17 | 10 | 8 |
| | 3 | 13.5 | – | – | – | – |
| | 4 | 9.5 | 69 | 15 | 10 | 6 |
| | 5 | 23.5 | 77 | 9 | 8 | 6 |
| | 6 | 10.0 | 70 | 13 | 12 | 5 |
| Appignano | 7 | 7.0 | 48 | 25 | 18 | 9 |
| | 8 | 25.0 | – | – | – | – |
| | 9 | 3.0 | 45 | 20 | 23 | 12 |
| | 10 | 2.5 | – | – | – | – |
| | 11 | 5.5 | 53 | 16 | 21 | 10 |
| | 12 | 8.0 | 51 | 15 | 26 | 8 |
| Castignano | 13 | 4.0 | 60 | 21 | 12 | 7 |
| | 14 | 17.0 | 62 | 16 | 14 | 8 |
| | 15 | 16.4 | 54 | 23 | 13 | 10 |
| | 16 | 13.0 | 71 | 11 | 5 | 13 |
| | 17 | 6.0 | 65 | 17 | 9 | 9 |
| | 18 | 4.3 | – | – | – | – |
| | 19 | 12.5 | – | – | – | – |
| Offida | 20 | 4.0 | 55 | 11 | 26 | 8 |
| | 21 | 3.0 | 63 | 24 | 11 | 2 |
| | 22 | 18.0 | 73 | 12 | 7 | 8 |
| Minimum | | | 39 | 9 | 5 | 2 |
| Maximum | | | 77 | 25 | 34 | 13 |
| Average | | | 60 | 16.6 | 15.2 | 8.12 |

Sm smectite; *Cl* chlorite; *I* illite; *K* kaolinite

X-ray diffractometric analyses have finally shown that passing from finer to coarser fractions the levels of carbonates, quartz and feldspar increase while the ones of smectite decrease sharply.

From these analyses, however, it seems that the chemical-mineralogical component of the soil is not sufficient to explain badlands morphogenesis. In fact, it seems that the badlands phenomenon evolves, ultimately, through a mechanical process depending on flow rate and velocity of the concentrated runoff, in the sense that rushing waters, in order to acquire sufficient energy to overcome the strength limit of the lithic material, must slide on slopes already presenting a certain degree of acclivity. As a consequence, if slope acclivity is a necessary prerequisite in the morphogenesis of badlands, there must be a limit value of slope angle α (α_{lim}) below which the erosive capacity of runoff factors is ineffective on soil resistance. Angle α_{lim} can therefore be defined as the angle of acclivity of a slope expressing the lower limit for the genesis of badlands.

In fact, the phenomenon of badlands ultimately develops through the balancing of numerous physical and anthropic factors such as soils grain size distribution, mineralogy, structural arrangement, fracturing of sediments, local climate, slope exposure, runoff water, heavy rainfall, deforestation, ploughing, etc. Physical components can also be subdivided into two sub-sets; the first, strictly bounded to the geometry of the slope, such as length (which affects the extension of the erosive process and the effects of surface runoff), predominant grain size and slope angle. The second group is somehow function of entities which are external to the slope itself, such as local climate, rainfall, isolation, etc. This elementary logic of the classification of the components that affect, in the first approximation, the dynamics of badlands, suggests the proposition of an interpretive model, capable of selecting states of the evolution of slope angle from equilibrium phases or erosive inactivity, compatibly with the average conditions of the causes of modification. The model can be summarised in a mathematical relation of the type

$$F_A - R_i = \alpha_{lim} \quad (5.1)$$

where the term F_A combines all the quantities governing the evolutionary process, i.e. those that cause erosion, while R_i integrates those quantities opposing to erosion; α_{lim} is the synthetic index that provides an assessment of the suitability to erosion of the system and identifies a condition of dynamic equilibrium of the slope with respect to erosive and modelling components.

In other words, the slope angle characterising badlands is the result of the balance between disruptive actions, generally external to the material, and the overall strength, intended as the ultimate effect, put in place by the whole slope.

Experimental observations highlighted some real cases where there is a lower bound of the angle of acclivity (α_{lim}) beyond which the slope is “strongly” active in relation to the badlands-like erosive trend; angles lower than α_{lim} , instead, generate stable slope configurations, which are not subject to hydrogeological instability. In the present case, numerous detailed measurements of slope angles have been carried out along a series of longitudinal sections on the hillside slopes of the Chifente basin representing incipient or immature badlands formations (Fig. 5.21a–c). In Fig. 5.22a–e are reported clinographic correlations from which a value of about 34° is shown as the angle below which there is no badlands activity on the observed slopes. The angle $\alpha = 34^\circ$, therefore, constitutes in the basin of Chifente the limit value for the genesis of badlands. This first result encourages the development of research on the analytical dependence among the measured slope angle and some of the quantities that represent both erosive “causes” and resistances. If, in fact, Eq. (5.1) is expressed in the form of a functional link between slope angle α and a set of parameters that intervene in the triggering and in the dynamics of the erosive process, it could be reformulated as:

$$\alpha_{lim} = \alpha(F_A; R) = \alpha(i; r_i; L; d; \varphi; M)$$

having considered, for the sake of simplicity,

$$F_A = i \quad \text{and} \quad R = (r_i; L; d; \varphi; M)$$

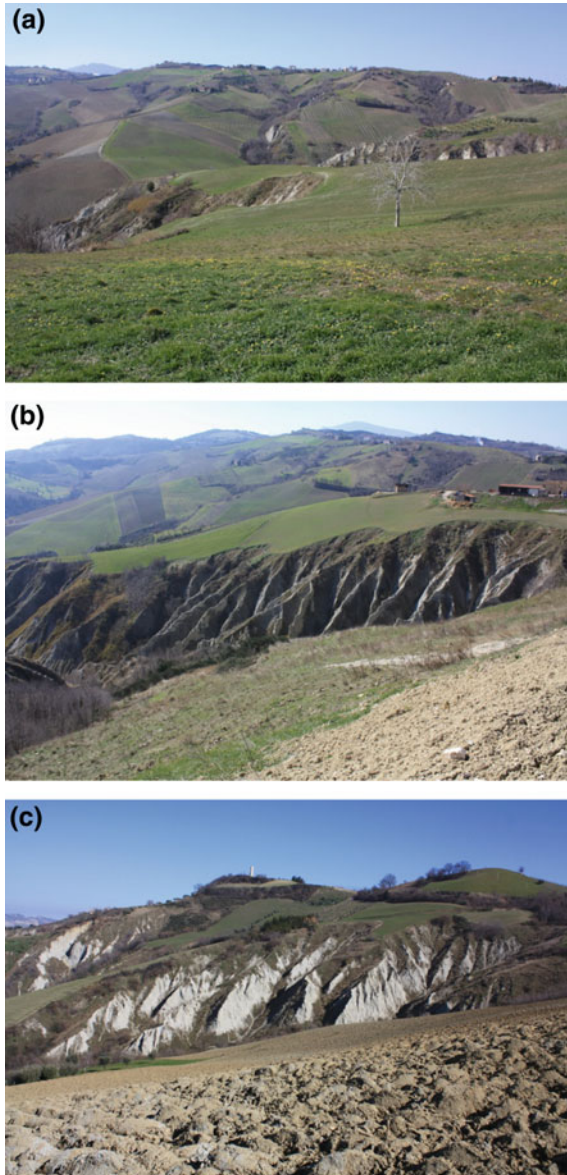


Fig. 5.21 Examples of incipient badlands configurations: **a** incipient badlands on slope with an angle of 34° ; **b** incipient badlands on slope with angle of 35° ; **c** incipient badlands on slope with angle of 37°

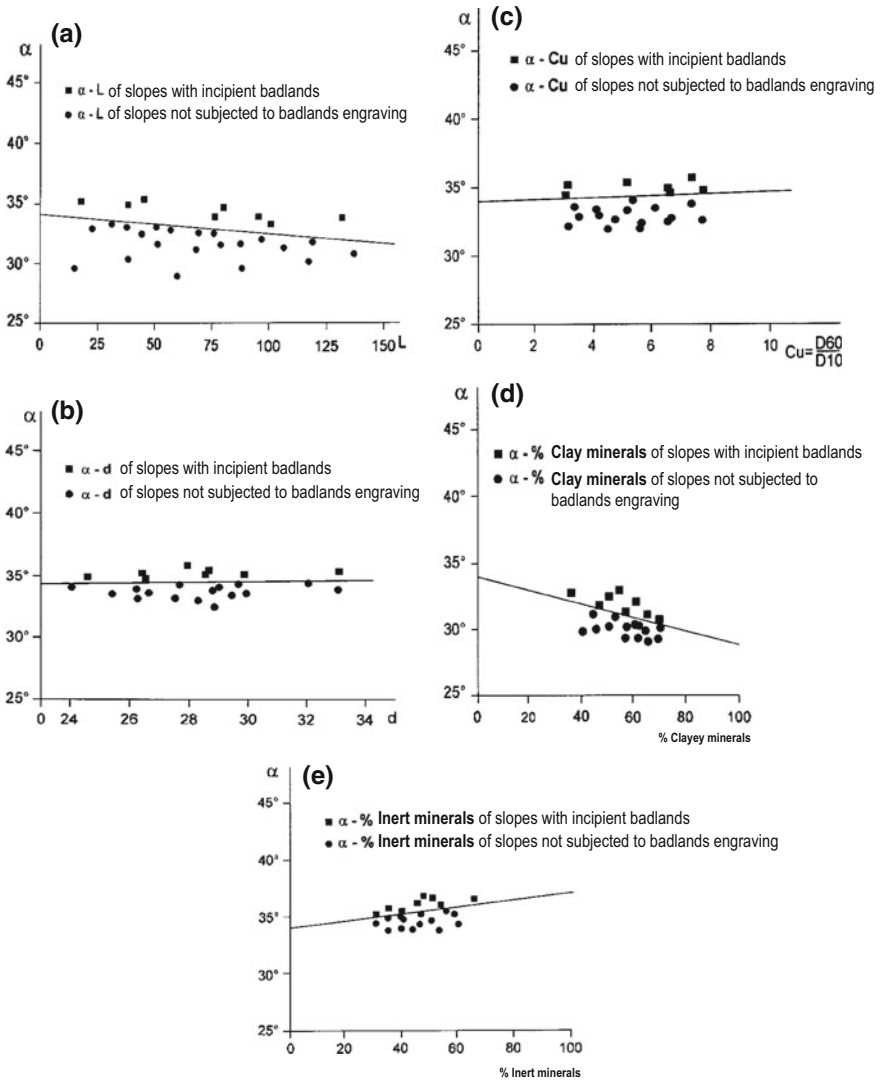


Fig. 5.22 Clinographic correlations between slope acclivity α and some of the main quantities ruling the evolutionary process of badlands: **a** α —slope length (L). **b** α —particle diameter (d) reported as % of sand respect to % of silt. **c** α —coefficient of uniformity of grain size distribution (C_u). **d** α —% of clay minerals. **e** α —% of inert minerals

where

i , is an index representative of average hydrology in the area under examination;
 r_i , hydraulic resistance to surface runoff, therefore function of the roughness of the surface upon which runoff takes place;

L, slope length;
 d, characteristic dimension of soil grains (or equivalent index);
 φ , potential seepage (or degree of saturation);
 M, mineralogy of the lithic mass.

Even in this formulation, it is necessary to introduce a simplification in the evaluation of the quantities involved in the dynamics of the process.

As a consequence, it is possible to report on a chart the value of slope angle observed with the quantities assumed as representative, all measurable or numerically quantifiable, so as to obtain abacuses or simple correlations, that express the dependence of α_{lim} from the magnitude of the quantities measured on site. In particular, this analysis was conducted by focusing on the dependence of the angle α_{lim} only on geometrical and compositional factors of the soil, considered as predominant in the formation and evolution of badlands.

Therefore, it is noted from Fig. 5.22a–e that an increase in slope length results in a slight reduction in the slope angle needed to develop badlands grooves on the slope (Fig. 5.22a).

Likewise, by correlating the slope angle with the uniformity coefficient of the silty-sandy component solely (fraction retained by sieves No. 16 to 200) found in the pelitic succession of the basin of Chifente, a direct function is obtained between the two variables (Fig. 5.22b). In general, by increasing the percentage in sand a slight increase in the α angle is obtained. Similarly, the $\alpha - C_u$ ratio (Fig. 5.22c) is shown, where C_u is the coefficient of granulometric uniformity of the silty-sandy component. From the point of view of the mineralogy of the lithic mass, the increase in clay minerals results in the decrease of the slope angle (Fig. 5.22d); this behaviour is more marked in presence of larger percentages of smectite and/or illite or of swelling minerals. On the contrary, in relation to inert minerals (Fig. 5.22e), angle α establishes a rather accentuated direct function for small increments especially in the presence of calcium or quartz.

In conclusion, marly deposits, made up of basal pelitic units of the foredeep in silty-clayey facies, outcrop in the neogenic basin of the Chifente. There, the mineralogical analysis of sediments revealed the presence of swelling minerals, such as smectite and illite, in percentages of about 60 and 16.6%, respectively, with reference to the fraction of clayey minerals. The potential for swelling of these minerals has a significant effect on the disruption of the lithic material, both under unloading and both when in contact with water. However, the linear process of degradation and erosion, carried out by runoff waters, is slightly effective on badlands morphogenesis if runoff energy does not reach such a value able to remove not only the swelling and inert elements of the clay fraction but, above all, the grains of silt and sand from their mutual interlocking. To obtain these conditions, it is necessary for the slope to reach a minimum of 34° , determined on the basis of numerous in-situ observations, defined as the slope angle expressing the limit value (α_{lim}) in the genesis of badlands in the soils under examination. As a result, physical and anthropogenic factors, such as sediments granulometric and fabric characteristics, slope structural position, local climatic conditions, slope

exposure, the tectonic process of uplift of blocks, sun exposure, heavy rainfall, anthropic activity, etc., are all factors that affect the modelling of the slopes and the angle of acclivity α is the result of the interaction among these factors.

5.2.3 *Third Environment*

This environment is characterized by a dense vegetation made up of high trees on mountain slopes. It therefore appears to be protective of the soil and in opposition to the hydrogeological disruption of the slopes themselves. On the contrary, current rotational landslide types are numerous, albeit of small dimensions and influence the landscape with unusual aspects of environmental degradation (Fig. 5.23).

The factors of the genesis of such hydrogeological processes are described below, by using as an example the Comarca de Aguas Negras Calilegua, province of Jujuy—Argentina.

Serrania Calilegua (Fig. 5.23) is a humid and fertile subtropical area occupied by a jungle-like forest of 70 km². Annual precipitations range between 1000 and 1800 mm, mainly concentrated during the summer (December–February), while winter (June–August) is a well-defined dry season. The Serrania encloses a variety of ecosystems. The Transition Jungle, extending from 350 to 500 m above sea level, is made up of tree species such as *cedui lapacho* and *palo amarillo*. Between 550 and 1600 m above sea level, the forest forms a dense dome of trees taller than 30 m, including ferns, epiphytes and vines, often surrounded by a shroud of mist. Above 1200 m it extends a mountain forest composed of coniferous, *alisio* and *quehoa*. Beyond 2600 m above sea level, the forest gradually gives place to wet meadows that become more arid as they proceed westward in the direction of *Quebrada de Humahuaca*. In this environment landslides develop only on the slopes covered by the thick forest of trees, i.e. between the river valley and the altitude of 2600 m above sea level, while they are missing or are very rare where the ecosystem is composed of grassland, even when it develops on slopes with the same lithology and acclivity of tree vegetated ones.

The soils outcropping at Comarca de Aguas Negras Calilegua (Fig. 5.24) are continental deposits belonging to the Calilegua Formation (Cellini 1973a, b) and comprises two members: (1) Valle Grande; (2) San Lorenzo.

The first is a succession of layers and banks of rose quartz sandstone rocks in a silty matrix alternating with large banks (5–7 m thick) of dark red silty clay containing thin levels of coarse sandstone (Fig. 5.25). They are ephemeral deposits, sedimented under arid climate in fluvial environment, very fractured.

The member of San Lorenzo is in stratimetric agreement on the previous one. It is made up of a dark red quartz silt with abundant clay matrix and with interbedments of thin mudflows, dark red and violaceous in colour; in the upper part it passes to dark grey pyroclastic deposits.

The two outcropping members have on the surface an altered layer about 3–6 m thick, consisting of a dark red, sometimes violaceous and greenish

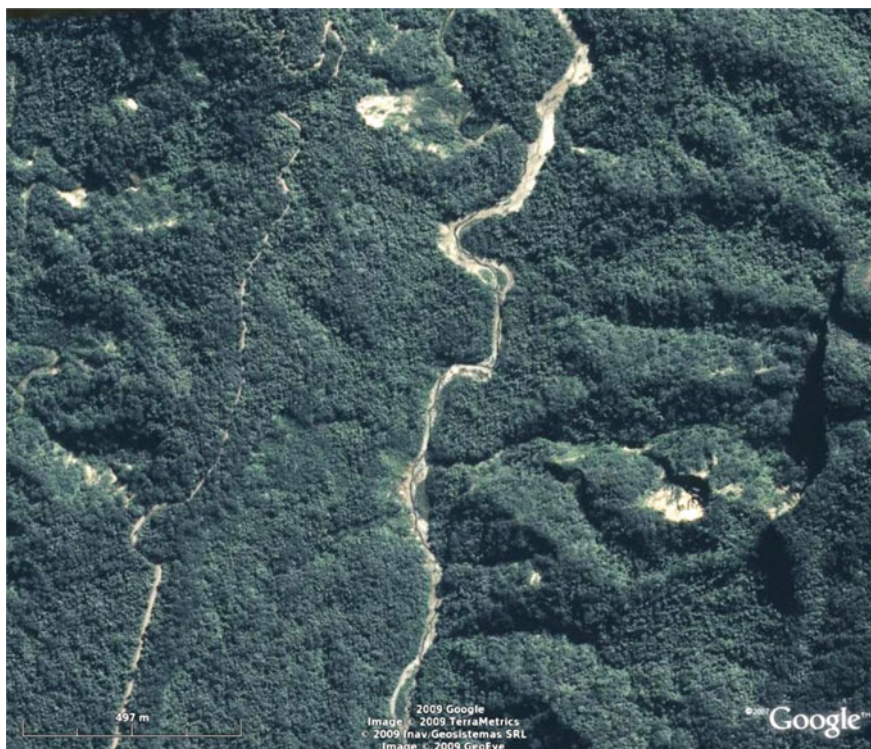


Fig. 5.23 Overview of the slope in the middle course of the Comarca de Aguas Negras Calilegua—province of Jujuy—Argentina

clayey-silty-sandy aggregate. The aggregative percentage of the lithic particles is extremely variable both horizontally and vertically: sand ranging between 3 and 18.6%; silt between 30.3 and 80.5%; clay between 0.9 and 67.7%.

From the attached geological map (Fig. 5.24) it can be observed that the current orogenic arrangement of the Comarca de Aguas Negras Calilegua is the result of compressive deformational mechanisms due to thrust tectonic which acted according to an invariant stress regime defined by the maximum thrust direction, NW-SE, with structures predominantly oriented NE-SW.

Here, the hydrographic network develops tendentially according to the direction orthogonal to the structures, with almost asymmetrical river valleys, where the regressive erosion carried out by watercourses accentuates the acclivity of the slopes. It is rather branched and in the clayey-silty soils of the Calilegua Formation it reaches the 5th order in the hierarchical river organization, with a dendritic pattern in which the tributaries flow themselves into the main collector according to angles very close to the right angle. It therefore appears that the local hydrographic network is not subject to the structural control of local orogeny, but mainly to the control of local erosion. Observing this pattern, it is evident that water found the shortest flow-path by flowing along parallel courses, engraved in clayey soils on

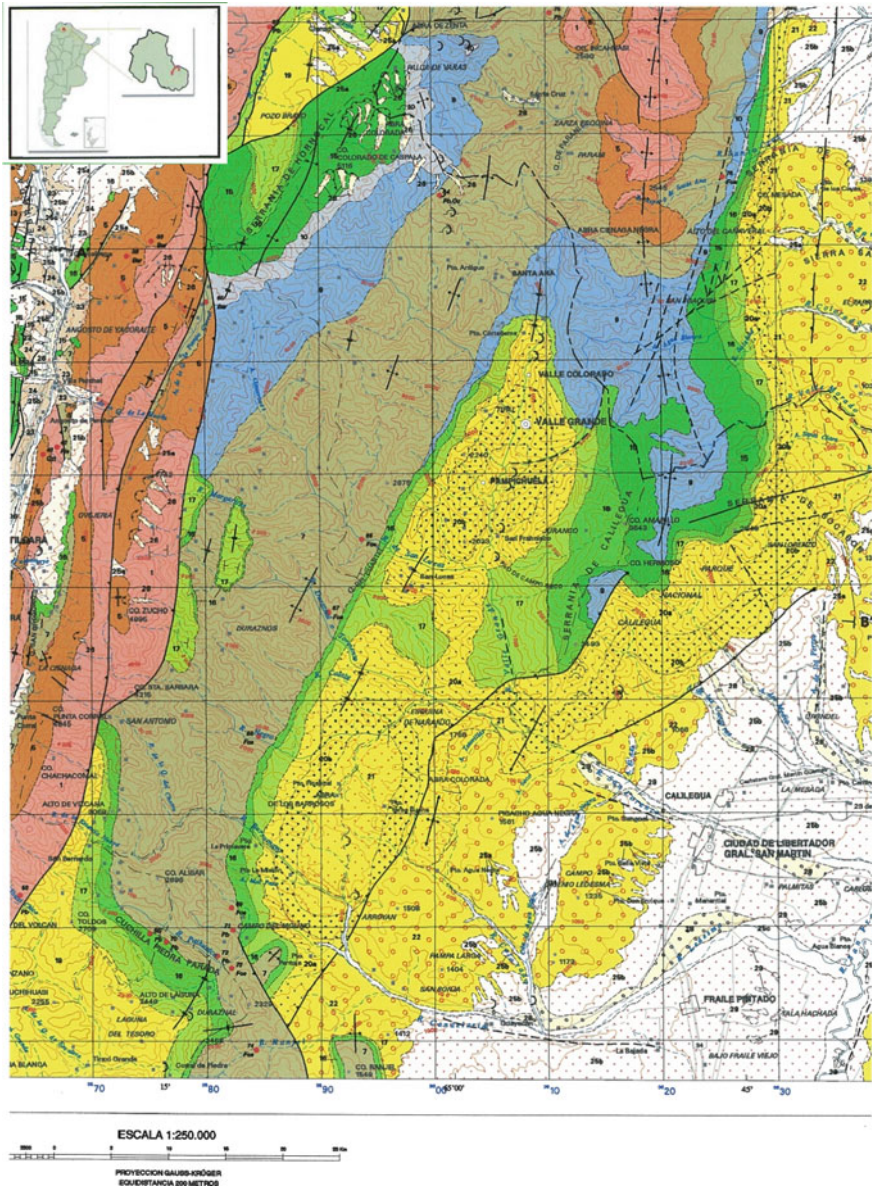


Fig. 5.24 Geological map of the Andes area comprising the Comarca de Aguas Negras Calilegua (from Cellini 1973a, b)

steep slopes or slopes with sensible acclivity. This involves a constant rejuvenation of Aguas Negras riverbed due to its progressive lowering; the deepening of the riverbed also affects the smaller branches to the upstream, which produce on the slopes a very intense state of erosion and hydrogeological instability.

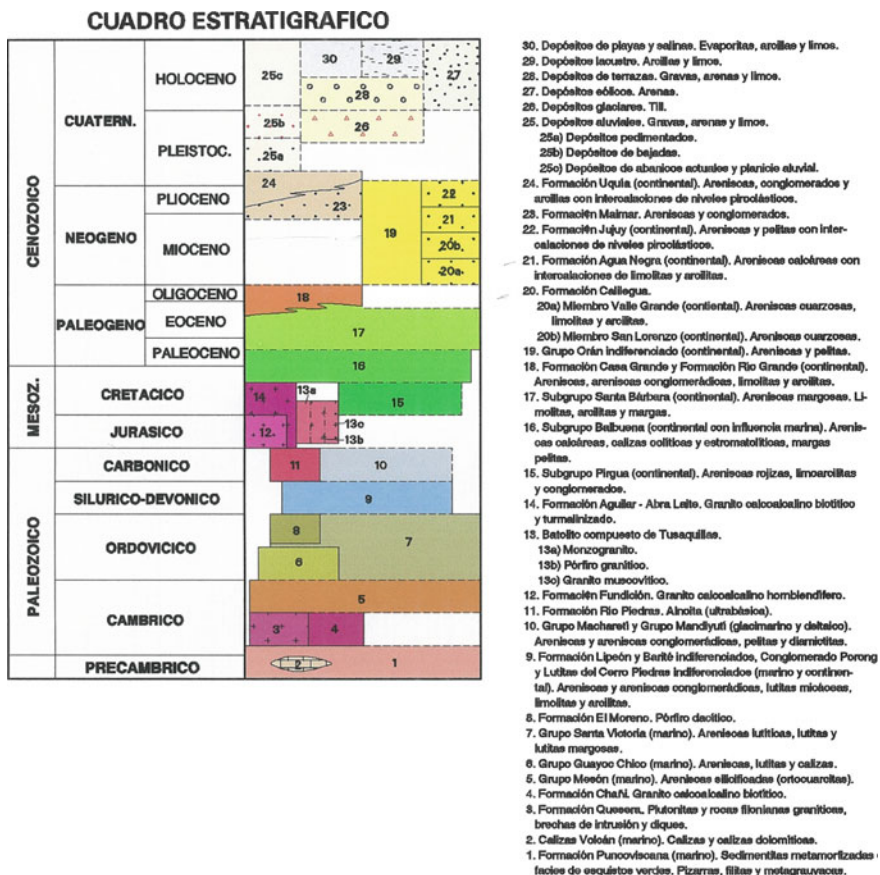


Fig. 5.24 (continued)



Fig. 5.25 Valle Grande member of the Calilegua Formation



Fig. 5.26 Slow shallow movements within the alteration horizon

In the Comarca de Aguas Negras, the phenomenon of landslides is widespread throughout the area of the outcropping of the Calilegua Formation and it usually manifests in periods of prolonged rainfall, when the piezometric surface reaches the ground level. These are shallow movements (Fig. 5.26), initially slow due to viscous-plastic deformations of the altered layer (Fig. 5.27), and evolve quickly to mud flows (Fig. 5.28) in fluid-plastic state, with high flow energy towards the valley. Initially, the saturated altered lithic mass undergoes corrugations or undulations, whose dimensions are directly proportional to the thickness of the horizon of alteration, while the velocity of the movement seems to be directly influenced by slope acclivity. This has angles (α) ranging between 22° and 35° , the value of



Fig. 5.27 Viscous-plastic deformation of the altered horizon



Fig. 5.28 Evolution of viscous-plastic movements in mudflows

which depends on the maturity of the micro-basin of surface water flow. In addition, the sliding surface, very articulated and discontinuous, develops only within the shallow horizon of alteration (1–4 m) where are located the roots of the tall trees that make up the jungle-like forest environment.

It has been noticed during the site survey that landslides in the alteritic layer occur where the clay fraction is greater than the one of silt and sand; this justifies the scattered arrangement of landslides on the slopes and, often, the relative low depth of the sliding surface.

The conditions of instability and the type of shallow mass movements depend on the global geomechanical characteristics of the horizon of alteration and on the direct seepage of meteoric water up to a critical value in the rise of piezometric level to ground level. The current sliding surface is located at a low depth below the ground level (1–4 m). The effective normal stress, given by the weight of the soil, is therefore low and shear strength is strongly dependent on the value of cohesion c' of the clay fraction present within the lithic mass.

Therefore, as already discussed in Chap. 2, Sect. 2.3, the ratio between the effective horizontal stress σ'_{ho} and the effective vertical stress σ'_{vo} is expressed by the coefficient of thrust at rest K_o .

$$K_o = \frac{\sigma'_{ho}}{\sigma'_{vo}} \quad \text{or also} \quad \sigma'_{ho} = K_o \geq \sigma'_{vo}$$

where σ'_{ho} is the geostatic horizontal stress in the absence of groundwater.

The evaluation of the current value of σ'_{vo} depends on the exact stress history of the clayey silt, which means on the magnitude and duration of the stresses to which the lithotype has been subjected from the formation phase to the current conditions.

However, this original stress state has been altered by other phenomena such as the variation of piezometric level and the vertical unloading due to erosion.

In presence of groundwater, the effective vertical stress σ'_{vo} assumes the value

$$\sigma'_{vo} = \sigma_{vo} - u_o$$

where u_o represents pore-water pressure.

When, instead, the horizon of alteration achieves the saturation state in undrained conditions, as it often happens within clayey silts in conjunction with abundant rainfalls, it results:

$$\Delta\sigma_{vo} = \Delta u \quad \text{and therefore} \quad \frac{\Delta\sigma_{ho}}{\Delta\sigma_{vo}} = 1 \quad K_o = 1$$

It is therefore clear that, for clayey silts, the horizontal stress σ_{ho} is dependent not only on soil type and history, but also on the magnitude of pore-water pressures. Near the ground surface, furthermore, σ_{vo} also has a very low value and the phenomenon can develop tensile stresses that occur with cracks in the ground according to principal failure surfaces. Therefore, as the material is cohesive and saturated, $\varphi_u = 0$, and the equilibrium, soil limit strength achieves:

$$\sigma_{ho} = \sigma_{vo} + 2c_u \quad \text{for} \quad K_o = 1$$

which physically corresponds to the plastic-fluid state.

Therefore, when the piezometric surface reaches the ground level, the horizontal stress (σ_{ho}) has already exceeded the limit equilibrium state of a value greater than $2c_u$.

The cause of the viscous-plastic movements of the horizon of alteration is therefore attributable to a problem with the pore-water pressure developed at the boundary of the sliding surface in the saturation state.

On-site permeability tests were necessary to identify the causes of the combined effect between the variation of the soil total stress state and the regime of interstitial water pressures or neutral pressures (Terzaghi 1936).

The determination of the permeability coefficient K in situ was carried out by means of the relationship (Torstensson 1978):

$$C_h = \frac{\tau}{t} \cdot R^2$$

τ = time factor corresponding to a certain degree of consolidation;

t = time related to the degree of consolidation considered (s);

R = equivalent radius of piezocone probe, CPTu (1.78 cm).

The coefficient of permeability K is:

$$K = m_v \cdot C_h \cdot \gamma_w$$

m_v = coefficient of volumetric compressibility;

γ_w = specific weight of water.

The values of m_v were determined by means of 5No. oedometric compressibility tests on undisturbed samples taken at progressive depths of about 1 m. In Table 5.3, the results of these tests have been reported from which it is possible to evaluate the local variation of permeability coefficient K (cm/s) with depth; this, in general, is inversely proportional to depth. However, in the upper 2 m of the horizon of alteration, coefficient K assumes approximately the same value of about $E \times 10^{-4}$ cm/s, while with the increase of the lithostatic load the horizon of alteration becomes more compact and, therefore, the value of K decreases with depth. At approximately 6 m below ground level, the clayey silt of Calilegua Formation seems to be very compact, slightly altered and slightly decompressed to present a coefficient of permeability K of less than $E \times 10^{-7}$. This value can be considered as the limit of water percolation in the soil and therefore as the base of the piezometric column. It can be therefore assumed that the maximum depth of the development of a shearing surface for viscous-plastic mass movements in the Comarca de Aguas Negras is 6 m below ground level; more often this value is approximately 4 m below ground level.

In conclusion, the current orogenetic arrangement of the Serrania Calilegua in the Province of Jujuy—Argentina is the result of compressive deformational mechanisms that acted through a series of events since the Tertiary to present. In this context, the hydrogeological instability of the slopes is predominantly shallow and affects only the lithological horizon of alteration, which in many micro-areas presents, both vertically and horizontally, a clay fraction greater than the fraction of silt and sand. Landslides of plastic-rotational type are of small size and develop on slopes of 22°–35° of acclivity.

The movement, initially of viscous-plastic type, evolves quickly in mudflow over very irregular and shallow sliding surfaces (1–4 m below ground level). During the triggering period, the piezometric level is at ground surface, indicating

Table 5.3 Evaluation of the coefficient of permeability K in situ

| Sample n. | Lithic horizon | Depth(m) | C_h (cm ² /s) | m_v (cm ² /kg) | K (cm/s) |
|-----------|-------------------------------|----------|----------------------------|-----------------------------|----------------------|
| S1 | Altered | 1.0 | 3.2×10^{-2} | 0.015 | 4.8×10^{-4} |
| S2 | Altered | 2.0 | 1.3×10^{-2} | 0.015 | 1.9×10^{-4} |
| S3 | Altered | 3.2 | 4.0×10^{-3} | 0.011 | 4.4×10^{-5} |
| S4 | Altered | 4.1 | 1.4×10^{-4} | 0.11 | 1.5×10^{-6} |
| S5 | Slightly altered or unaltered | 5.5 | 3.0×10^{-5} | 0.007 | 2.1×10^{-7} |

that the sliding lithic mass is in the saturated state. In-situ permeability tests show that the kinematics of a mudflow depend on the coefficient of permeability K of the affected soil and in particular on its inability to dissipate pore-water pressure or neutral pressure. Furthermore, in the potentially unstable alteration horizon, pre-failure deformative phenomena were detected, strongly influenced by the disruption of the lithic particles due to the penetration of tree roots in the ground. Wild vegetation, jungle-like, with tall trees and very intricate and dense undergrowth, prevents the quick elimination of rainwater on the slopes and favours a process of water seepage into the ground, already subjected to disruption and geoturbation of the soil carried out by the roots. Here, the altered lithic mass undergoes swelling due to the increase in volume of the clay fraction. Under these conditions, in the horizon of alteration, continuous stress changes take place due principally to the variations in the water content or to the slow rebalancing of neutral pressures.

The wild jungle vegetation therefore contributes as a hydrogeological risk factor for the instability of the slopes of the Comarca de Calilegua.

In addition, viscous-plastic deformations initially take place within the mass sliding on the slope, mobilising, in general, the residual strength of the soils and passing, subsequently, to the fluid-plastic state in the form of mudflow. These properties indicate that the stress phenomenon acts as a closed system within the altered horizon, where the adsorbed water does not flow out and, therefore, the viscous-plastic phenomena must be considered in undrained conditions. The deformation at failure is linked to the creep in the alteration horizon; it does not occur at the same depth as the pre-failure deformation, but occurs at a depth, where the permeability coefficient K assumes values in the order of $E \times 10^{-6}$ to $E \times 10^{-7}$ cm/s. This indicates that the mechanics of failure of the clayey silt in the plastic state is mainly influenced by the neutral pressure regime. Starting from the moment of failure, in fact, which occurs in various drainage conditions in relation to the ratio between the deformation velocity and the velocity of dissipation of neutral pressures, the behaviour of the soil, initially similar to that of a saturated continuous medium (piezometric surface at ground level) becomes permanently conditioned by neutral pressures, which change the lithic mass from the plastic state to that of a growing mudflow.

5.3 Pre-existing Landslides

In the Apennines, urban expansion at the periphery of historic centres of medieval origin has been subjected to instability problems over many decades, not only in terms of town planning, but also in terms of the real hydrogeological risk associated to the stability and durability of new buildings, which are often placed on pre-existing landslide terraces, now undergoing periodic reactivations with different waiting times.

These are landslides developing into lithological units with high clay fraction, which underwent a long process of tectonic fracturing. They are large chaotic masses, remained at rest for a long time, which have one or more predefined shearing

surfaces at variable depth, usually very high, directly proportional to the fracturing state of the ground. Large in size, they develop longitudinal sections of many hundreds of metres, sometimes of kilometres, with very large landslides. Their genesis is mainly to be found at the end of the last ice age (Würm), when the subsoil has been subjected to a slow and prolonged water infiltration for the melting of perennial ice, that has lasted for some millennia (Table 3.2). This time range varies according to the altitude and latitude of each local mountain range. The cyclic reactivation of these movements generally responds to the varied conditions in the acclivity of the slope over time and to the effect of the raising of neutral pressures within the cohesive mass after cycles of the fluctuations of groundwater that determine the continuous modification of the stress state and, consequently, the reduction of the shear resistance available along the existing failure surface. At present, on all the slopes in cohesive soils of planet Earth there is a generalized mobilisation of pre-existent landslides, as a result of mutated morphological arrangement of the slopes, due mainly to the renewed river network and to local seismic conditions.

The element of danger is therefore represented by the ancient failure surfaces. The recent sliding on these ones develops initially with relatively slow and short movements, opposed to those of recent landslides, that are usually smaller but quicker, then assumes higher speeds, but alternating with long periods of quiescence. In this kinematic framework of the conditions of activation of such landslides, the evaluation of current equilibrium states is prioritised in relation to the actuality of the causes of reactivation. Therefore, before asking about the causes of the reactivation of a pre-existing landslide, it is necessary to understand the relationships between stress and strain that interact in the ground using triaxial laboratory tests. Under the same lithology, the sliding of such landslides is deeper than the one of recent landslides. In the Apennines, the depths to the sliding surfaces of pre-existent landslides varies just slightly from cohesive soil to cohesive soil, ranging between ~ 40 and 70 m below ground level. All of them are set into non-native lithological units. On the Andean slopes of Cordillera Argentina, where compressive tectonics have always been dominant (tectonic structures generated by distension phases are missing), this depth reached 100–120 m.

The study of shear strain in the ground therefore requires the prior knowledge of the deformative behaviour of a cohesive soil which is subjected to different loading pressures.

5.3.1 Relation Between Stress and Strain

Let us consider a simplified type triaxial laboratory equipment where a cylindrical sample of marly clay is immersed in a hermetically sealed vessel filled with liquid under pressure. The sample is therefore subjected to a hydrostatic stress σ_1 (Fig. 5.29). In triaxial compression tests it is subjected to vertical stress from piston P with a pressure greater than σ_1 , until it breaks. In this case there is a stress state characterized by a revolution ellipsoid in which

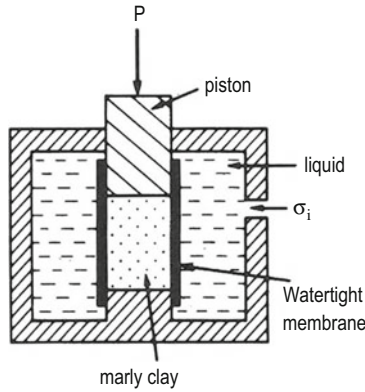


Fig. 5.29 Sketch of a triaxial test. σ_i : hydrostatic test (da Mattauer 1973)

$$\sigma_1 = P(P < \sigma_i)$$

$$\sigma_2 = \sigma_3 = \sigma_i$$

The sample deforms vertically subjected to compression; the deformation is initially continuous but, beyond a certain value, the sample itself undergoes failure along a plane oblique to the axis σ_1 (Fig. 5.30(1)).

In the tensile test, instead, the sample is subjected to an elongation; the axial pressure P is thus negative while the stress state is characterized by a revolution ellipsoid in which

$$\sigma_1 = \sigma_2 = \sigma_i$$

$$\sigma_3 = P(P < \sigma)$$

In this test, the sample initially extends and subsequently undergoes shear strain with reverse sliding plane (Fig. 5.30(2)).

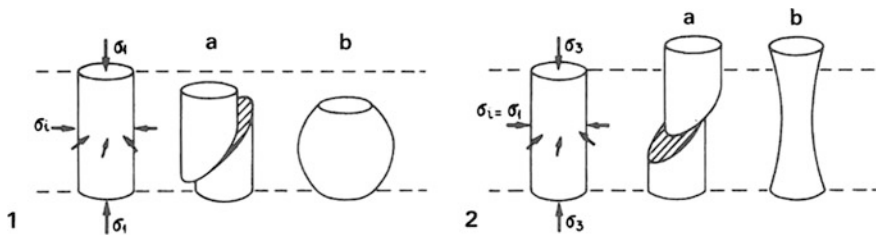


Fig. 5.30 Sketch of deformation in triaxial compression tests (1) and in tensile test (2). (a) Discontinuous deformation. (b) Continuous deformation (from Mattauer 1973)

These types of tests carried out in the laboratory are difficult to be reproduced in nature, at great depth and especially when there is no possibility of lateral expansion for a dry soil; the deformation, instead, appears at the surface, or on the ground immediately below the surface, where conditions of low lateral confinement take place (recent landslides).

(a) *Influence of confinement pressure on deformation*

When an increasing confinement pressure (σ_3) is applied to a given rock, it can be observed that the plastic deformation increases before failure (Fig. 5.31a, b); the rocks thus become so much more ductile as they are at a greater depth. This influence of confinement pressure, however, varies according to the type of rock; some rocks are more sensitive than others. In addition, the influence of σ_3 is different for compression or tensile tests. In fact, a rock with brittle behaviour at failure can be transformed into ductile rock if it is subjected to an increase in the value of σ_3 ; by increasing the temperature, these transformations need a lower value of σ_3 both under compression and under extension. This means that compression fractures at depth are less frequent than extensional ones (Fig. 5.32). However, the depth of the existing shearing surfaces of pre-existing landslides is never so deep in the ground to undergo a significant change in temperature. Therefore, the difference between the two types of fractures becomes evident depending on their inclination which is more marked as they approximate to the ground level. Knowing the influence of σ_3 on the behaviour of the rocks, in general, it is possible to have an idea of the variations of this depth-dependent behaviour in function of depth for a constant geothermal gradient.

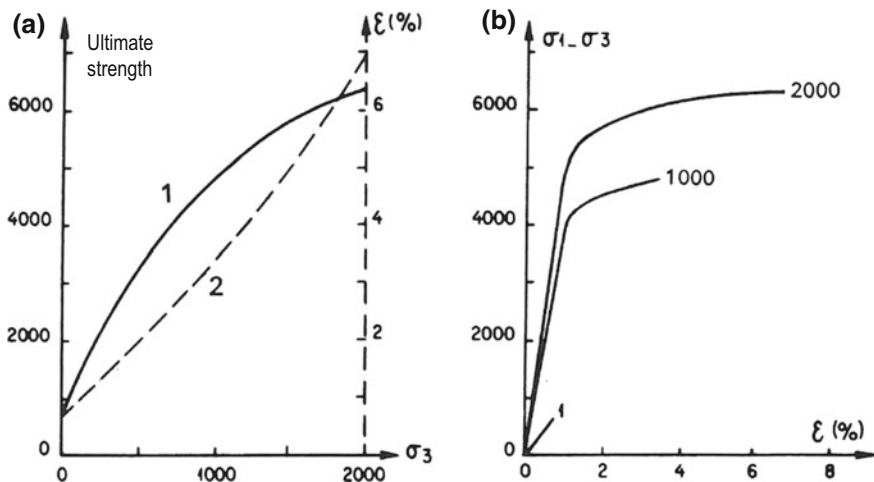


Fig. 5.31 Influence of σ_3 on the deformation of dolomite. a Variation in ultimate strength (1) and ductility (2). b stress-strain curves for various values of σ_3 (from Handing and Hager 1957)

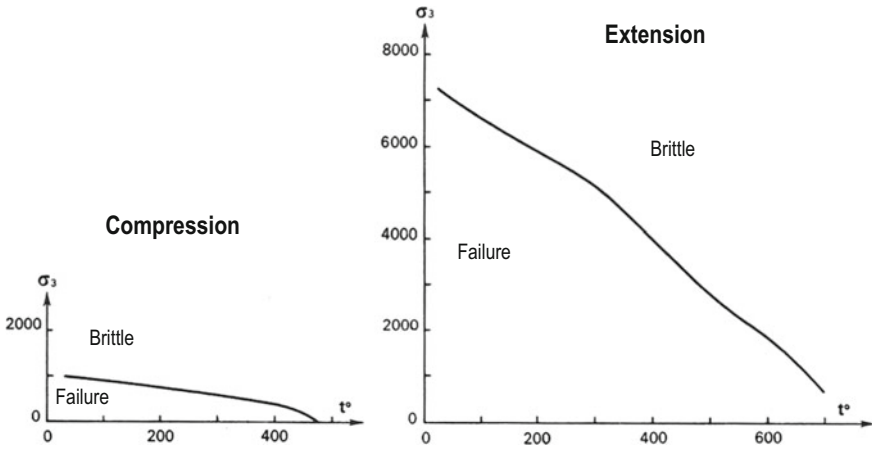


Fig. 5.32 distribution of ductile and failure domains in function of temperature for compression and tensile tests carried out on limestones (from Heard 1960)

Figure 5.33 shows the results of some experiences in conditions of increasing confinement pressure; it shows the behaviour of different types of rocks. It can be observed that the deformation increases with depth or that rocks become more ductile at a certain depth beyond which deformation becomes unstable. Each rock is ultimately characterized by a curve with typical slope, that separates a stable domain (or plastic deformation) from an unstable domain (failure). The curves of Fig. 5.33, however, correspond to laboratory experiences that may not always be applied to real cases. However, they are of utmost interest in understanding the behaviour of soils of different nature with depth, including the one of clayey soils.

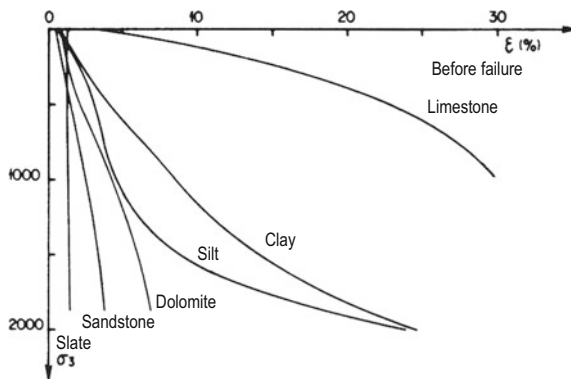


Fig. 5.33 Curves describing stable domains of a series of rocks in function of σ_3 , i.e. of depth (from Handin and Hager 1958)

(b) *Influence of fluids on deformation*

The majority of rocks has a structure susceptible to fluid retention. Such rocks often contain water even at great depths. It will be considered the case of water, as it is the one, among all the fluids, that has the greatest importance in the deformation of slopes in cohesive soils. Retained water is generally at pressures greater than the one of water stagnating at surface; this pressure often reaches 95% of the lithostatic pressure and, in particular cases, may be equal to or greater than the latter. Compression tests carried out in the presence of variable amounts of water in marl show that this value has a great influence on deformation. Figure 5.34 shows, as an example, that a marl is more easily deformable in presence of elevated retained moisture contents. By performing tests with various fluid pressures, it can be found that the marl also changes behaviour: from ductile with moderate fluid pressures it becomes brittle at high pressures.

This can be predicted with the aid of Mohr's diagram. Let us consider tests in the presence of σ_1 and σ_3 and without the presence of fluids; let us suppose that the sample does not break, meaning that σ_1 - σ_3 circles do not touch Mohr's envelope. Let us suppose now, performing the same test, that saturated rock is subjected to a strong pressure P. The fluid holds a portion of this pressure and consequently the stress that is exerted on the rock will be $\sigma_3 - P$ and $\sigma_1 - P$ (Fig. 5.35) which

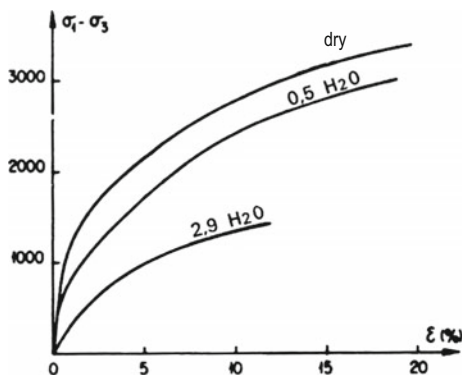


Fig. 5.34 Stress-strain curves for compression tests carried out on marls under variable water content ($\sigma_3 = 5000$ bar, $t = 300$ °C) (from Griggs 1936)

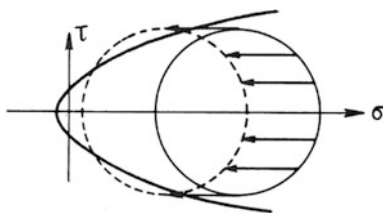


Fig. 5.35 Sketch showing the increase in fluid pressure in the soil before failure, with translation of Mohr's circle (from Hubber 1961)

corresponds to a circle of Mohr moving to the left of axes τ e σ and then intersected by the envelope line, which means undergoing failure simply because of the presence of an interstitial fluid.

(c) *Influence of rocks anisotropy on deformation*

All rocks are generally anisotropic; in particular the cohesive ones, because of stratification, even more shales and, in particular, the ones that underwent the effects of tectonic overthrusting. Experiences in-situ or in the laboratory easily allow to verify the influence of anisotropy on the behaviour of rocks. Stress-strain curves are in fact different according to the angle that σ_1 forms with the anisotropy plane. Figure 5.36 shows that for shales the value of $\sigma_1 - \sigma_3$ needed for achieving the failure varies considerably; it gets its maximum when σ_1 is perpendicular to the schistosity and its minimum for a 30° inclination. It is also seen that the angles between the fractures and the axis for σ_1 are strongly influenced by schistosity. They vary, for example, from 0 to 50°, with a maximum of about 45° as seen in Fig. 5.37.

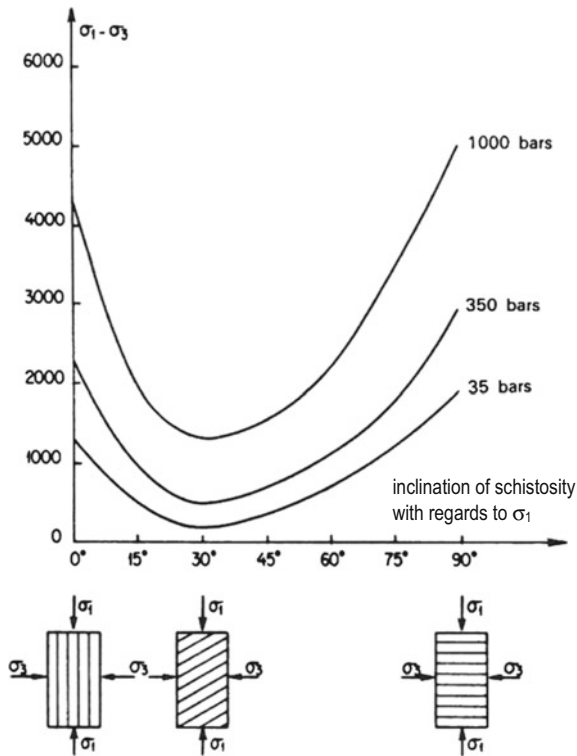


Fig. 5.36 Curves showing strength limits in function of the angle formed between schistosity and compression for a schist sample (from Donath 1963)

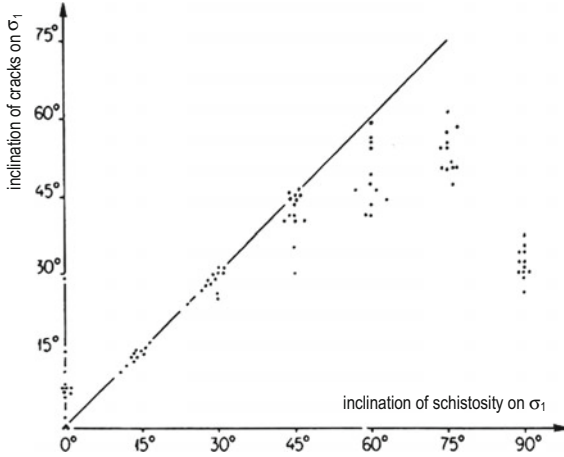


Fig. 5.37 diagram on the influence of schistosity on the orientation of fractures. Each point corresponds to a single triaxial compression tests carried out up to failure (σ_3 ranging between 35 and 2000 bar) (from Donath 1963)

(d) *Influence of stress, confinement stress and temperature on sliding*

Sliding varies considerably depending on $\sigma_1 - \sigma_3$. If this value is modest it is irrelevant; if, on the contrary, it is intense, the sliding increases rapidly (Fig. 5.38). This shows that testing on sliding is not easy to be performed for a given stress.

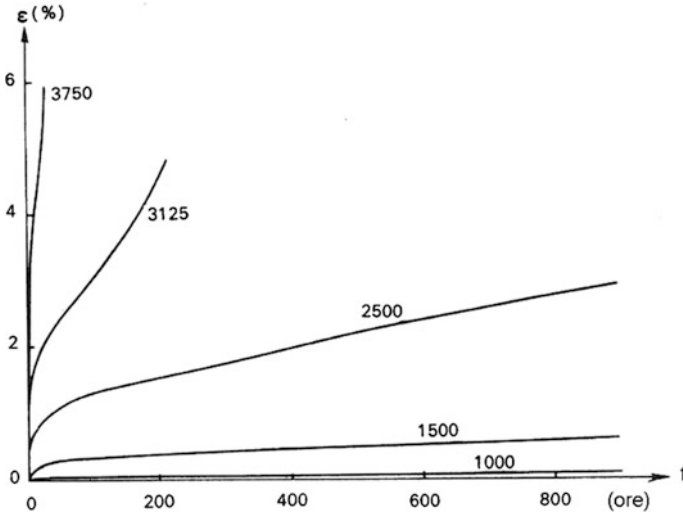


Fig. 5.38 Curves of shearing for extension tests carried out at different levels of confinement pressure (measured in lb/in^2). Failure is achieved only for the curves at confinement pressures of 3125 lb/in^2 and 3750 lb/in^2 ; below a certain value of $\sigma_1 - \sigma_3$ strain tends to zero (from Hendron 1969)

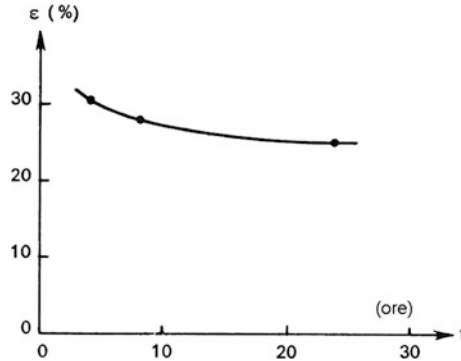


Fig. 5.39 Variation in plastic deformation before failure in tests with various durations carried out on calcareous marls ($\sigma_3 = 100$ KPas) (from Griggs 1936)

In fact, when the stress state is of low magnitude, this cannot cause major deformations, but only small ones develop in the ground, that can be detected by using very sensitive equipment inserted into the ground itself. In order to observe a real, visible sliding at surface, it is needed that the local loading stress exceeds a certain threshold which is a function of confinement pressure, temperature, pore-water pressure, tectonic fracturing state and rock anisotropy. In addition, sliding reduces intensity and duration of the plastic deformation that precedes the failure, as shown in Fig. 5.39. It is therefore understood that the sliding of a soil mass is as bigger as the deformation duration is applied for a longer time; that for pre-existing, large landslides, may be in the order of millennia. It does not seem, however, that a generalisation is possible on this point, since sliding is a function of the various factors mentioned that may be present in the ground entirely or only partially.

5.3.2 Causes of Deformation at Failure

It was already mentioned that the triggering mechanisms of pre-existent landslides in cohesive soils develops in extremely long times. In general, the sliding occurs at great depth and the movement occurs at very low speeds, interrupted by periods of more or less prolonged quiescence.

In addition, among the characteristics of pre-existent landslides, one is that they only develop within de-structured and chaotic cohesive soils, highly disturbed by tectonic compression. This explains their development at depth of the original sliding surface which, however, can hardly be attributed to the sole direct action of neutral pressure (u). In fact, Fig. 5.34 shows that *a marl is more easily deformable when the greater is the amount of retained water*, but also rocks change behaviour from ductile, with moderate fluid pressure, to brittle with high fluid pressures (Fig. 5.35). The influence of anisotropy on soil behaviour is also to be considered.

Figure 5.36 shows that the stress-strain curves are in fact different according to the angle that σ_1 forms with the plane of anisotropy. It must be reminded that in soils heavily disturbed by compressive tectonic the value $\sigma_1 - \sigma_3$ required for achieving the failure varies considerably; it reaches its maximum when σ_1 is perpendicular to schistosity and has its minimum for a 30° inclination. This explains the extreme variability of the depth of the sliding surface itself for a pre-existing landslide.

The causes of deformation and failure of a pre-existing landslide are therefore:

- (1) stratigraphic and tectonic discontinuities of cohesive rock, that play a decisive role in the seepage of water to high depth;
- (2) direct action of neutral pressure (u);
- (3) influence of fluid on deformation;
- (4) influence of soil anisotropy on deformation.

5.3.3 *Reactivation of Pre-existing Landslides*

Based on previous experimental analyses, it is possible to suggest some logic principles on the reactivation of a pre-existing landslide.

The example of Latronico landslide, Southern Apennines, is sufficient to define the methodological aspects for the identification of the dynamics of the reactivation of any hydrogeological disruption.

– The landslide area

The inhabited centre of Latronico extends to the top of a hill, on the south-eastern foothills of Monte Alpi, in the province of Potenza (Italy), between 820 and 875 m above sea level. The new urban settlement extends on a north to south direction on this hill, whose eastern slope degrades towards the Fiumitello stream, currently undergoing heavy erosion of the riverbed (Fig. 5.40). On this slope outcrops extensively the Formation of Crete Nere (Black Clays), originated during the Lower Cretaceous, consisting of argillites and marls, grey-black in colour, with intercalations of calcareous and calcareous-marly levels and with rare lenses of blackish calcarenites (Figs. 5.41 and 5.42). The lithological unit is characterized by very disturbed, chaotic stratification and significant de-structuration of the lithic material. The upper part of Latronico, between 850 and 875 m above sea level, is the oldest one and extends above conglomerate deposits (Units of the Conglomerates of Castelnuovo—Lower Pleistocene). These deposits rest on transgression and in angular discordance above the Crete Nere. They consist of well-rounded heterometric elements predominantly calcareous, calcarenitic, arenaceous and metamorphic. Sandy levels of modest thickness ($\sim 1/2$ m) are sporadically interbedded with the conglomerates (Latronico Geological Map, Fig. 5.43).

The morphological evolution of the eastern slope of Latronico is controlled by the surface water flow system, which flows into the Fiumitello stream (Fig. 5.44). This slope is currently undergoing the re-activation of a large pre-existing landslide (Fig. 5.45), whose sliding was already in act more than a century ago. In fact, with



Fig. 5.40 Overview of Latronico, south-eastern foothills of Monte Alpi—Southern Apennine. Eastern slope and trace of Fiumitello stream (to the right in the photo)



Fig. 5.41 Crete Nere Formation - Lower Cretaceous. Grey-blackish argillites and marls with intercalations of calcareous and marly limestones and rare lenses of blackish calcarenites. Very disturbed layering, chaotic and with noticeable destructuration of the lithic material

Regio Decreto (Royal Act) No. 299, dated March 2nd, 1916, all the residential area was transferred onto the more competent conglomerate deposits in the surroundings. In more recent times, the urban expansion, and in particular the development towards the north, parallel to Corso Vittorio Emanuele I (Vittorio Emanuele I Avenue), is now in a clear state of hydrogeological disruption (Fig. 5.46).



Fig. 5.42 Additional view of the deconstruction of the Crete Nere Formation

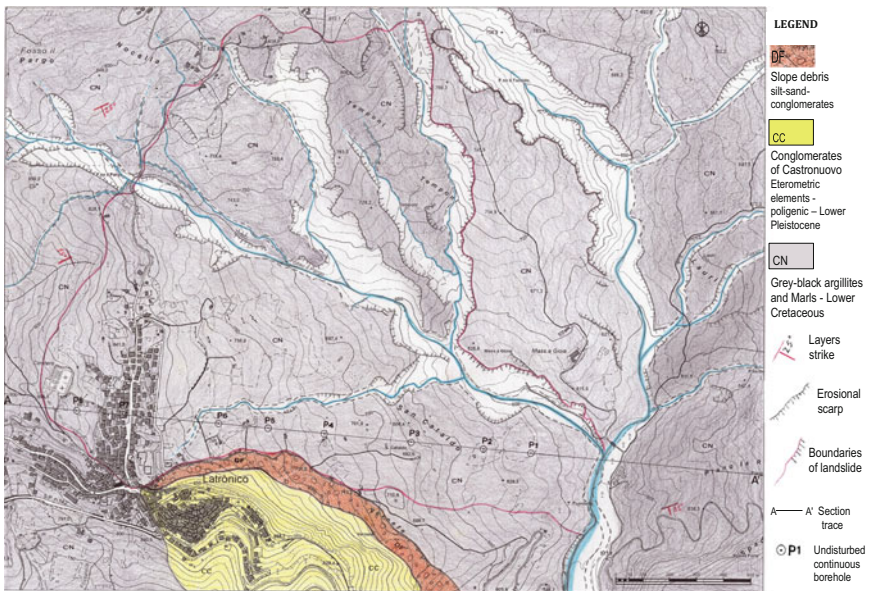


Fig. 5.43 Geomorphological map of the eastern versant of Latronico, Province of Potenza, Southern Apennine, Italy



Fig. 5.44 Riverbed of Fiumitello stream



Fig. 5.45 Overview of the landslide

As it will be seen later, the current mass movement is not always active but often manifests itself with slow surface movements on small slope portions, interpretable as a consequence of sporadic and discontinuous stress mechanisms in undrained conditions.

The landslide at Latronico, such as the majority of pre-existent landslides of planet Earth, was originated as a result of persistent water seepage in the ground due to the melting of Würm glaciers during the boreal cycle (between 10,000 and 8400 BC—see Table 3.2).



Fig. 5.46 Effects of the landslide to the upslope

Starting from this assumption, even before advancing any logical principles on the reactivation of this landslide, the need to promote a methodology of investigation able to ascertain the temporal existence of the landslide itself becomes a priority. In practice, the research must first be aimed to acquiring the distinctive features that characterize the presence of the pre-existing landslide on the slope. For this purpose, the best solution would be to find organic evidences embedded in landslide or within river terraces for a relative dating (see Chap. 3, Sect. 3.4 and example of Grassano). However, these opportunities are not always available. Alternatively, the old and well proven methods of geological analysis are always the most trusted ones. They are of two types: of geomorphological character the first, the second of geophysical character.

- (a) Geomorphological survey tends to map main and secondary landslide scarps, as well as the respective terraces belonging to the succession of the individual landslides found along a topographical section of the slope.
- (b) The second system is the most geological among geophysical methods. This is based upon the principles of the reflection of seismic waves, that is a survey methodology used for the underground exploration and to know the stratigraphic and structural arrangement of geological bodies as well as of faults, lithological discontinuities, shearing and/or sliding surfaces.

For the Latronico landslide it was used the methodology of the geomorphological survey carried out on topographic paper 1: 5.000, considering this more suitable to show the specificity of the remote hydrogeological instability on the slope. The first commitment was to map the traces of slopes of each landslide scarp

found on the slope as well as of the respective terraces. For each scarp, then, height and inclination were measured, while the length along the line of maximum slope was recorded for each terrace (see Table 5.4).

Section A–A', attached to the geomorphological chart, shows the morphometric aspects of these landslides in scale.

Moving from the bottom to the top of the section, landslide mass 1 has been identified, which was of small size with a sliding surface directly related to alluvial deposits of the watercourse. This tends to ramble when the deposition action prevails. Upslope of the landslide mass itself, the main scarp is 3 m high and its outcropping surface has an inclination of 26°, while the main terrace is almost non-existent. By prolonging the main scarp surface, so as to connect it to the current position of the watercourse, it is obtained the shape of the sliding surface of landslide n. 1. It follows that this is necessarily defined by current movements. In addition, the sliding surface intersects, to the upslope, landslide mass n. 2 in its foot, corresponding to the accumulation zone. Landslide mass n. 1 is therefore recent and the subsequent one is pre-existing to it.

Table 5.4 Dimensions of landslide scarps and of the sliding surfaces

| | | |
|---------------|------------------------------|-------------------------|
| Landslide N.1 | | Inclination = 26° |
| | Main scarp | Height = 3 m |
| | Landslide terrace | Length = inesistente |
| | | Height difference = - |
| | Max depth of sliding surface | 20 m |
| Landslide N.2 | | Inclination = 35° |
| | Main scarp | Height = 11 m |
| | Landslide terrace | Length = 74 m |
| | | Height difference = 5 m |
| | Max depth of sliding surface | 75 m |
| Landslide N.3 | | Inclination = 45° |
| | Main scarp | Height = 12 m |
| | Landslide terrace | Length = 45 m |
| | | Height difference = 5 m |
| | Max depth of sliding surface | 95 m |
| Landslide N.4 | | Inclination = 34° |
| | Main scarp | Height = 10 m |
| | Landslide terrace | Length = 60 m |
| | | Height difference = 0 |
| | Max depth of sliding surface | 65 m |
| Landslide N.5 | | Inclination = 29° |
| | Main scarp | Height = 4 m |
| | Landslide terrace | Length = 55 m |
| | | Height difference = 9 m |
| | Max depth of sliding surface | 55 m |

A significant element in the dynamics of reactivation of pre-existing landslides comes from the material constituting landslide N.1. This material is the chaotic and messy one belonging to the accumulation zone at the toe of landslide N. 2. At the height of landslide N.1, the riverbed of the stream is characterized by a mass of alluvial cobblestones grooved by a network of recently engraved channels. This morphological aspect, due to river dynamics, is typical of watercourses that produce the lateral erosional slopes, which move back continuously until they collapse, triggering the advancement of the soil mass towards the riverbed (Fig. 5.47). More specifically, this involves the mobilization of landslide mass N.2 along the pre-existing sliding surface as soon as a rise in neutral pressures develops within the slope, causing, following a linear function, a decrease in the available shear strength in the upslope due to the increase in thrust. When the action overcomes the strength available along the pre-existing shear surface due to the self-weight of the ground, the mass deforms by compression and starts sliding locally, producing secondary shear surfaces in the landslide mass necessarily mobilising it. In these cases, the slope may have deformations of viscous type concentrated exactly along the secondary shear surfaces. Of course, the evolution of the sliding of landslide mass N.2 occurs with the rising of the piezometric surface (section A–A').

The movement of landslide mass N.2 triggers also landslide mass N.3 with the same modes and deformational types already described. This explains their reactivation not only in recent times but also in the remote past within a continuous evolutionary process of the slope with intermittent states to which the same slope was repeatedly subjected in the long-term. In effects, whenever the neutral pressure regime reduces, due to the lowering of the piezometric surface, landslide masses N.2 and N.3 are subjected to a phenomenon of stress relaxation. During the following rainy seasons, however, not necessarily the increase in neutral pressures



Fig. 5.47 Fiumitello stream. Foot of landslide 1 covering cobbly alluvial soils of the riverbed

results in an increase of the stress state able to achieve the failure conditions. This is why the contribution of soil anisotropy is necessary as well as the influence of water retention (see points b and c of Sect. 5.3.1 respectively). It should also be noted that in the event of reactivation the mobilized strength is the residual one and the movements are generally slow.

The correlation of sliding surface N.1 to the riverbed of Fiumitello stream started with the measurement of the inclination of the main scarp of the landslide outcropping on the slope. This was reported in scale, with the resolution of one millimetre, along the slope contour of section A–A'. The same graphic process was therefore applied also to landslides N.2, N.3, N.4 and N.5. Here, the traces representing the sliding surface must be correlated respectively to those of the landslide mass downslope (see section A–A'). They also provide the depth at which the movement developed. The maximum depth of landslide mass N.2 is 75 m (Table 5.4). The graphic process is obviously inaccurate; however, it does not deviate too much from the actual values observed from measurements later undertaken by means of boreholes.

The validity of this graphical system is to have, at low cost, a first orientation on the number, typology, relative dating, and the behaviour of landslide masses on a slope subjected to hydrogeological instability. It also allows to schedule the subsequent investigation as well as the number of boreholes, their location on the slope and their depth. For the Latronico landslide, eight continuous coring boreholes were drilled, located according to the maximum gradient cross-section, in order to have a better understanding of the relation between sliding surfaces, their real depth, the competency of the material along the shear surfaces, the nature of argillites, the orientation of the schistosity, the fracturing state, etc. During this type of investigation, some secondary shear surfaces have been identified in landslides N.2 and N.3, with no corresponding mobilization of soil mass. They are proper physical discontinuities, not belonging to those of tectonic nature. During their development, the cohesive material was mainly present in the plastic state. This may seem anomalous within the process of deformation and failure of natural slopes, however, is very common in pre-existing landslides, in fact, it is a feature that has been found in all cohesive deposits whose lithology was subjected to tectonic fracturing.

In a regressive sequential process of shear deformation, landslide masses N.4 and N.5 are the most recent ones, subject to pre-failure phenomena and implicitly considered to be *at first-time failure*. In fact, unlike landslides N.2 and N.3, they have shallow sliding surfaces and, above all, are free from secondary shear strain, while the height of the main scarp is of a few meters, respectively 10 and 4 m. What are the distinctive features of a pre-existing landslide so that this can be distinguished from a recent one?

It can be concluded that features indicating pre-existing landslides in cohesive soils are:

- (1) intense fracturing and tectonic disturbance of the lithological succession due to the action of a compressive stress field;

- (2) very deep and complex sliding surfaces, which in terms of movements are conditioned by the structural characteristics of the deposit and the state of softening of the soil;
- (3) more or less widespread presence of secondary shear surfaces without distortional strain and acts of motion;
- (4) the main scarp of the landslide is generally very eroded when landslide mass is not active. On the contrary, if there is a reactivation in progress, the main scarp shows signs of a recent movement, like acts of motion at the base, greater acclivity in the downslope area than to the upslope, some minor scarps indicating the rupture;
- (5) if at the foot of the pre-existing landslide there are signs of swelling and/or ridges obliterating the main scarp of the landslide underneath, or this has been modified by the thrust of the immediately upslope body, it is sure that the whole slope corresponding to the pre-existing landslide is in motion. *This is the current condition of the eastern slope of the hill of Latronico.*

References

- Aguilera, N., Gallardo, F., & Chávez, Manrique A. (2002). *Geología del Parque Nacional Calilegua, Provincia de Juiuy. Acta XV Congreso Geológico Boliviano*. Bolivia: Santa Cruz.
- Boenzi, F., Di Gennaro, M. A., & Pennetta, L. (1978). I terrazzi della valle del Basento (Basilicata). *Rivista Geografica Italiana*, LXXXV(4), 396–418.
- Bromhead, E. N., & Dixon, N. (1984). Pore water pressure observations in the coastal clay cliffs of the Isle of Sheppey, England. In *Proceedings of the 4th International Symposium on Landslides*, Toronto, Vol. 1, pp. 385–390.
- Cantalamesa, G., Centamore, E., Colalongo, M. L., Micarelli, A., Nanni, T., Pasini, G., et al. (1986). *Il Plio-Pleistocene nelle Marche*. In *La Geologia delle Marche*, a cura di Centamore E. e Deiana G., Studi Geologici Camerti Numero speciale.
- Carter, N. L., & Ave Lallemand, H. G. (1970). High temperature flow of Dunite and Peridotite. *Geological Society of America Bulletin*, 81, 2181–2202.
- Casagrande, A. (1949). Soil mechanism in the design and construction of Logan Airport. *Journal Boston Society Civil Engineering*, 2, 36.
- Cellini, V. (1973a). Estudio geológico en la zona de Saladillo de la Brea, Sierra de Santa Bárbara Norte y El Oculito (Provincia de Jujuy). *Informe de YPF inédito, en Hoja Geológica 2366-IV Ciudad del Libertador General San Martín, Boletín SEGEMAR 274.1999*. Argentina.
- Cellini, V. (1973b). Estructura y estratigrafía del area El Naranjo – El Mirador (Provincia de Salta). *Informe de YPF inédito, en Hoja Geológica 2366-IV Ciudad del Libertador General San Martín, Boletín SEGEMAR 274, Argentina, 1999*.
- Costantini, A., Lazzarotto, A., Maccantelli, M., & Sandrelli, F. (1992). Ligurian units in the Monti della Gherardesca area (Southern Tuscany). *Bollettino della Società Geologica Italiana*, 110, 849–855.
- Donath, F. A. (1963). *Strength variation and deformational behavior in anisotropic rock. State of stress in the Earth's crust*. Amsterdam: Elsevier.
- Fenelli, G. B., & Picarelli, L. (1990). The pore pressure field built up in a rapidly eroded soil mass. *Canadian Geotechnical Journal*, XXVII(3), 387–392.

- Gebhard, J. A., Giudici, A. R., & Oliver Gascón, J. O. (1974). Geología de la Comarca entre el río Juramento y arroyo Las Tortugas, provincia de Salta y Jujuy. *República Argentina. Revista de la Asociación Geológica Argentina*, 19(5), 359–375.
- Griggs, D. T. (1936). Deformation of rocks under confining pressures. *The Journal of Geology*, 44, 541–577.
- Handin, J., & Hager, R. V. (1957). Experimental deformation of sedimentary rocks under confining pressure: tests at room temperature on dry samples. *Bulletin American Association Petroleum Geology*, 41(1), 1–50.
- Handin, J., & Hager, R. V. (1958). Experimental deformation of sedimentary rocks under confining pressure: tests at high temperature. *Bulletin American Association of Petroleum Geologists*, 42(12), 2892–2934.
- Heard, H. C. (1960). Transition from brittle to ductile flow in solenhofen limestones as a function of temperature confining pressure, and interstitial fluid. *Geological Society of America Memoirs*, 79, 193–226.
- Hendron, A. J. (1969). *Mechanical properties of rock*. *Rock mechanics* (pp. 21–53). New York: Wiley.
- Hubber, M. K. (1961). Mechanical basis for certain familiar geologic structures. *Bulletin Geological Society of America*, 62, 355–372.
- Mattauer, M. (1973). *Les déformations des matériaux de l'écorce terrestre* (p. 493). Paris: Hermann éd.
- Ogniben, L. (1969). Schema introduttivo alla geologia del confine calabro-lucano. *Memorie della Società Geologica Italiana*, 8, 2 tavv. a colori, Pisa.
- Picarelli, L., & Urciuoli, G. (1993). *Effetti dell'erosione in argilliti di alta plasticità*, *Rivista Italiana di Geotecnica*, Anno XXVII, no. 1, gennaio-marzo 1993, Napoli: Edizioni Scientifiche Italiane.
- Ricchetti, G., & Scandone, P. (1979). Inquadramento geologico regionale della Fossa Bradanica. *Geologia Applicata e Idrogeologia*, XIV, III (Bari).
- Scandone, P. (1972). Studi di geologia lucana: Carta dei terreni della serie calcareo-silico-marnosa e note illustrative. *Bollettino della Società dei naturalisti in Napoli*, 81, 225–300.
- Skempton, A. W., & Petley, D. L. (1967). The strength alone discontinuities in stiff clays. *Atti della Geotechnical Conference*, Oslo, Vol. 2, pp. 29–46.
- Terzaghi, K. (1936). Stability of slopes of natural clay. In *Proceedings of the International Conference on Soil Mechanics and Foundation*, Cambridge, Mass., Vol. I, pp. 161–165.
- Torstensson, A. B. (1978). The pore pressure probe. *Nordiske Geotekniske Mote*, Oslo. Paper 3.
- Trevisan L. (1968). *I diversi tipi di alvei fluviali e la loro evoluzione*. Accad. Naz. Lucca, Quaterno n° 112, Roma, pp. 531–561.
- Varnes, D. J. (1977). *Types of slope movements*. Transportation Research Board Committee, A2T58, USA.
- Varnes, D. J. (1978). *Slopes movement type and processes*. In R. L. Schuster & R. S. Krizek (Eds.), *Landslides: Analysis and control*. U.S. Natural Academy of Sciences, Special Report, 176, pp. 11–33.

Chapter 6

The Role of the Coefficient of Permeability K

6.1 Introduction

The seepage of water in cohesive soil is governed by two principles of different origin: the head determining the flow of water downwards under the action of gravity; the capillary force that is generated by the variation of the capillary potential from point to point. The water content of a certain area of the slope may decrease due to evaporation or to a network of tree roots, which results in increased suction force (pF) or to the migration of excess water in the wettest lithic horizons in the nearby. These conditions mean that the lower the hydraulic head in the ground, the more difficult the development of shearing processes due to landslides on a slope.

In this chapter it will be therefore analysed the downward movement of water due to gravity, favoured by a permeability (K) more or less large, whereas the ascending, generally superficial, movement will be treated in the end for particular cases where even on jungle-like, intensely forested slopes (see Fig. 5.23 in Chap. 5) it is possible that there are plastic-rotational landslides that evolve in flows.

6.2 The Effect of Ground Anisotropy on Permeability

The coefficient of permeability K indicates the capacity of seepage of water by gravity into the ground, which is much higher as the greater is the porosity of the soil (Baver 1948). Researches on this subject (Combeau and Monnier 1961; Vigneron and Desaunettes 1960) have shown for long time that permeability is subjected to the predominant influence of soil structure in relation to its fabric.

The value of the coefficient of permeability therefore depends on the characteristics of both the fluid and the soil.

Structurally chaotic and mineralogically heterogeneous clayey soils are much more permeable than those with a compact and homogeneous structure. It is also to

be taken into account that the permeability of unaltered cohesive soil is influenced by the electrostatic forces present on the surface of clay platelets (see Chap. 1).

Taylor (1948), developed an equation that links the permeability coefficient K to both fluid and soil characteristics:

$$K = D_s^2 \frac{\gamma}{\mu} \cdot \frac{e^3}{1+e} \cdot c$$

where

K Darcy's coefficient of permeability

D_s diameter of soil particles

γ specific weight of the fluid

μ viscosity of the fluid

e porosity index of the soil

c shape factor of soil grains.

This equation is very useful for examining the factors affecting the permeability coefficient of which are first considered the ones dependent on the permanent fluid and subsequently those dependent on the soil (Table 6.1).

On natural slopes, the lithic horizon of alteration, rather shallow, is generally poor in organic matter and the percentage of silt and sand is very small compared to that of the upper agricultural ground. In it, permeability decreases progressively in inverse proportion with depth. The clay layers of the underlying lithic unit, if they do not present generic discontinuities, behave as impermeable horizons that can lead the overlying ones to total saturation during wet periods. These ones, in lack of air become asphyxiating and reducing, iron partially passes to the ferrous state (marbling phenomenon), while the other chemical components take on particular properties defined as "hydromorphic". There are two cases of temporary hydromorphism due to impermeability.

- (1) *Surface hydromorphism*, which occurs without a real impermeable substrate, resulting from the jamming of impermeable substances released by capillary water in very small interplatelet voids. This usually occurs at a depth of a few meters from ground level, not because of the gravity of infiltration water but

Table 6.1 Classification of soils based upon permeability

| Permeability | Values of K (cm/s) |
|--------------|------------------------|
| High | $>10^{-1}$ |
| Medium | 10^{-1} to 10^{-3} |
| Low | 10^{-3} to 10^{-5} |
| Very low | 10^{-5} to 10^{-7} |
| Impermeable | $<10^{-7}$ |

From Terzaghi and Peck (1967)

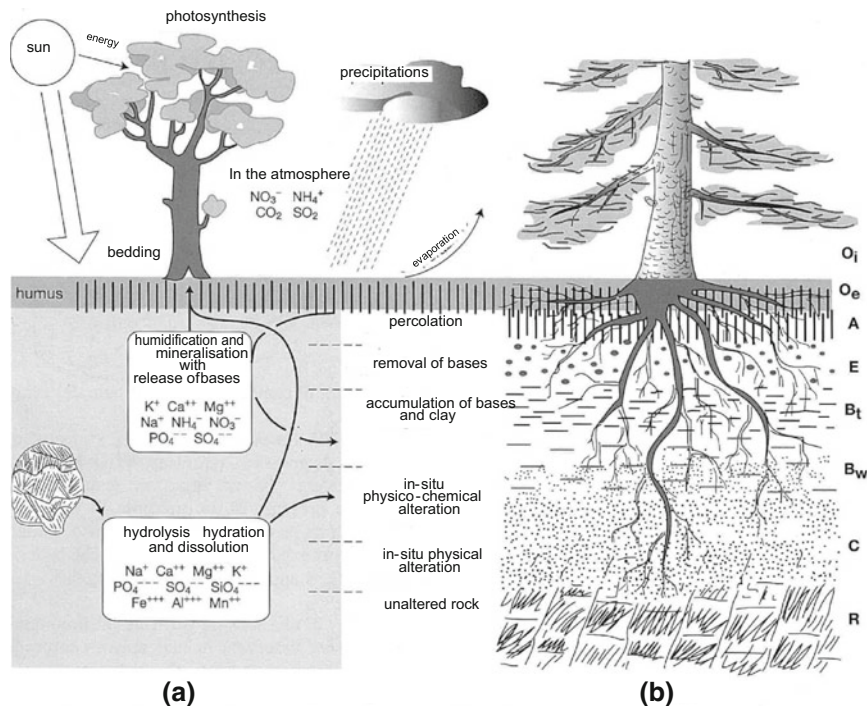
because of the slow progression of capillary water with depth. When these conditions occur on a slope, the failure due to landslide of the lithic mass happens always at the base of the hydromorphic horizon and the maximum shear component is represented by gravity and not by pore-water pressure (u), which always has a very low value. In this case, a very shallow, flow type landslide is developed on the slope, but not less dangerous because of this (Fig. 6.1). The flow is due to the saturation of this horizon, with the piezometric surface at ground level, and occurs under very viscous fluid conditions. The landslide tends to be canalised into pre-existing erosional grooves that act as real riverbeds, downslope of which material accumulates in the fluid state and in the form of a conoid. This phenomenon of hydrogeological instability occurs only in very degraded soil, with a high index of voids when the platelets of clay component are detached from each other, i.e. when the frictional strength is equal to zero. Water infiltration is not the same at all the points of the shallow horizon and reaches different depths on the same slope, thus resulting in a discontinuous and wavy sliding surface.

- (2) *Deep hydromorphism*, it is always characterized by the presence of three overlapping lithic horizons (Fig. 6.2). The first is the horizon of agricultural soil, with very rough fabric and relatively good structure, due to the presence of organic material and characterised by very high non-capillary porosity (Fig. 6.2 —Horizon O_e , A, E); the second horizon, underneath, is the lithic horizon of



Fig. 6.1 Flow instability due to the saturation of the shallow alteration horizon. The flowing material, widely heterogeneous, tends to canalise within pre-existing erosional grooves and deposits downslope in the form a viscous conoid (superficial hydromorphism)

alteration (Fig. 6.2—Horizon B_t, B_w, C), composed of clayey-silty soil with a chaotic structure, in which the non-capillary porosity is virtually absent. The permeability of this horizon gradually decreases with depth; it retains free gravity water from the upper horizon which in wet periods becomes stagnant and forms a perched groundwater table if the underlying clayey soil, generally layered and light blue in colour, is impermeable (Fig. 6.2-R). This table disappears by evaporation during dry periods. The marbling process starts from the base of the permeable layers and develops progressively towards the



- O_i Horizon formed exclusively of organic matter in which the original vegetal nature can be still identified
- O_e Horizon formed exclusively of organic matter in which the original vegetal nature cannot be identified any longer
- A Horizon rich in organic matter but with presence, more or less relevant, of mineral part mixed to organic part
- E Mineral horizon with concentration of organic matter lower than the one present in A. The most characteristic element of horizon E is downward leaching of bases, of clay and sometimes also of organic matter
- B_t Almost exclusively mineral horizon, with accumulation of clay deposited on the faces of structural aggregates present within the horizon
- B_w Almost exclusively mineral horizon with relative enrichment of clay deriving from in-situ alteration of rock. In this case clay presents discontinuous and does not coat the structural aggregates
- C Mineral horizon (organic component not excluded but this is to be put in relation with the eventual presence of roots) deriving from the predominantly physical alteration of rocks. The identification of horizon C presents some difficulties within alluvial soils
- R Unaltered rock

Fig. 6.2 Lithic horizons (according to Fitz Patrick 1988, modified)

surface. There, hydromorphism is often temporary, so tree roots are forced to penetrate deeply until they reach layers of low permeability and competent clay. The roots are then alternately subjected to asphyxiated conditions in periods of saturation and to desiccated conditions in dry periods. Slope stability factors depend essentially on the inclination of the contact surface between the horizon of alteration and the underlying unaltered lithic unit. This surface is very often wavy and discontinuous, with an average inclination similar to that of the slope, according to which, occasionally, oblique drainage can occur when the parent rock has an impermeable layer. In this case, the surface can facilitate the evacuation of gravity water and therefore local conditions of instability can hardly develop. When the ground is made up of predominantly clayey but tectonically fractured units, as almost all the units of the Earth's mountain ranges basins are, perched groundwater tables in the horizon of alteration find a percolation pathway among the fractures tectonically originated. Under these conditions, the hydraulic head assumes a very important function in the mechanism of slopes deformation at failure.

Notably, the cause of plastic-rotational landslides (Varnes 1978) is to be attributed to a condition of pore-water pressure developed at the boundary of a saturated sliding surface. Moreover, in predominantly clayey soils, different hydraulic gradients between contiguous areas are easily developed, while the slope above acquires more potential energy than the one downslope in accordance with the assumptions introduced by Tison (1953), for the motion of a flow on an inclined impermeable plane (Fig. 6.3a-c).

Assuming that the groundwater table has an impermeable substrate inclined in the same direction of flow, Tison (1953), starting from Darcy's Law, derives (Fig. 6.3c):

$$dy = dz \cos i + dx \sin i$$

where

$$Q = Kz = \left(\frac{dz}{dx} \cos i + \sin i \right)$$

therefore

$$x = \frac{1}{\operatorname{tg} i} \left[z_o - z + \frac{Q}{K \sin i} \ln \frac{K z_o \sin i - Q}{K z \sin i - Q} \right]$$

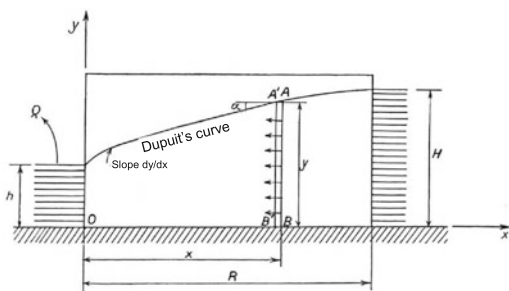
x is the distance between the piezometer and the axis of the pumped well;

i is the hydraulic gradient at point x ;

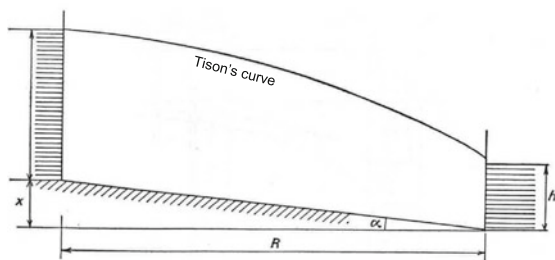
K the coefficient of permeability;

Q flow capacity in m^3/s ;

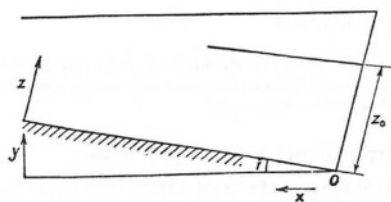
\ln Neperian logarithm.



a) Cylindrical groundwater table on impermeable horizontal substrate – downslope flow condition (from Castany G., 1967).



b) Cylindrical groundwater table on impermeable inclined substrate – upslope flow condition (from Castany G., 1967).



c) Calculation scheme for inclined substrate (from Tison L.J., 1953).

Fig. 6.3 a–c Cylindrical groundwater flow (two-dimensional)

The application of this formula shows that the curve of Dupuit is less accentuated for the inclined substrate than for the horizontal one. On the contrary, for a reverse inclination, the curve is more pronounced.

However, the depression curve of the piezometric surface of groundwater does not always reach a profile of equilibrium linked to a constant radius of action, as if it

was characterized by a permanent regime, since anisotropy of the ground prevents that the equipotential flow lines become perfectly parallel to each other. This could only happen where the subsoil presents an isotropic and homogeneous distribution of permeability, that soils actually do not have. The heterogeneity of these occurs for a number of reasons; for example: a different nature of the lithic components of the soil; a variation in the particle size distribution during the sedimentation process; different interaction of the electrostatic bonds between the platelets; chemical effects of the precipitation of substances in soil pores; the consolidation pressure, variable both horizontally and vertically; fissuring of rocks; stratification; cementation; etc. Such heterogeneity causes a variation in the physical characteristics of the soils and a curved and asymmetric pattern of flow lines that are predisposing for the variability of the permeability coefficient K from one area to another. Bromhead (1986), pointed out that the effect of the anisotropy of the soil lowers or raises neutral pressure (u); “*Which one of these two cases actually occurs depends on the length of the drainage path*”. There is a sudden spacing of flow lines if the soil has distinct areas with variable permeability. Furthermore, if the slope is subjected to load increase, such as for the overlapping of glacial masses, of earth dams, of artificial water basins, etc. or is subjected to tectonic compression forces, the volume of fractures or generic discontinuities decreases and thereby also decreases the permeability of the ground along the infiltration pathways, especially of those of the lesser depths. In these cases, inevitably increases the neutral pressure, which is directly proportional to the extension of the fractures. Moreover, during the triggering of a new landslide, extension fractures are initially discontinuous and occur at different depths below the ground level, within a zone where the tensile stress, due to gravity water, is greater. Therefore, for predictive purposes, it is needed to be cautious in identifying the depth of the sliding surface of a first-generation landslide, since this surface will manifest at failure as corrugated even if obtaining surface continuity.

In highly permeable soils ($K \geq 10^{-4}$ cm/s), instead, the excess of neutral pressure hardly establishes due to the absence of a response in terms of pore-water over-pressure due to the flow of fluid among soil pores. In that case, the soil tends to consolidation.

6.3 Consequence of Slopes Erosion on the Variations of the Coefficient of Permeability K

Geological and geotechnical literature have often highlighted the consequences of the erosion of a slope on soil structure and fabric variations as well as on the regime of neutral pressures and on the stability of natural slopes.

Matheson and Thomson (1973) analysed swelling phenomena developing in some valleys in Alberta, Canada, due to the effect of river erosion (Fig. 2.1). In the example considered, the stratigraphic sequence is composed of overconsolidated grey clays underlying sandstone layers from the Pleistocene. The erosion of the arenaceous horizon produced a kind of unloading of the clays, so that the latter underwent a continuous modification of the consolidation state and a reduction in the effective strength over time. In the outcropping clay, cyclic oscillations of the neutral pressure regime gradually took place, with the development of softening and swelling phenomena on the scarps as well as of sliding and collapsing of the latter. In fact, the total swelling of the clay in the eroded valleys was estimated at approximately 12% of the depth of the excavation carried out by the watercourses.

Similar situations have also been observed by Pasek (1974), which presented a deformational model of some valleys subject to fluvial erosion, whose slopes are composed of fractured competent layers (e.g. sandstone, conglomerates, limestones, etc.) laying on a substrate of deformable cohesive soils such as consolidated clays, marly-silty clays, pelitic flyschs, etc. From Fig. 6.4a, b it can be noted that the deepening of the river initially results in the swelling of the clay soil (phase 4) and then in the instability of the competent rock masses (phases 5–6–7). The dynamics of the disaster is characterized by an initial and progressive opening of the vertical fractures producing to the overturning (toppling) of the blocks on the slope due to the movement of the clays at plastic state (phases 6 and 7). This mechanism of slope deformation and failure, already influenced by the incisiveness of water, occurs only when the outcropping cohesive soils undergo a decay in strength due to softening (Fig. 6.5). It should be noted that the moving blocks are just the front ones, projecting towards the valley under erosion. Indeed, it is precisely towards this front that the clay may undergo a state variation for softening. Subsequent studies (Di Maio 1996a) showed that the phenomenon of state variation is particularly important in the case of overconsolidated clays and very competent and fractured argillites of high plasticity. The phenomenon is attributed to the alteration of the physical-chemical characteristics of zeolitic water due to the infiltration of rainwater, characterised by lower salt content. However, the shear strength of these types of cohesive soil also depends on empirical parameters that are function of time, such as oscillations of the piezometric level (Yoshida 1990).

Cerere and Lembo Fazio (1986), by means of a finite element numerical model, examined the stress states induced for two different hydraulic conditions of the slope corresponding to the presence or absence of a deep permeable layer and assuming elastic-plastic behaviour of the clay material. The results have shown the emergence of traction efforts in the rock mass, if the clay formation extends to a considerable depth from the bottom of the valley. The increase in tensile stress near the vertical wall of the rock mass becomes greater, if it is assumed the presence of a band of softened material at the base of the mass and along the slope.

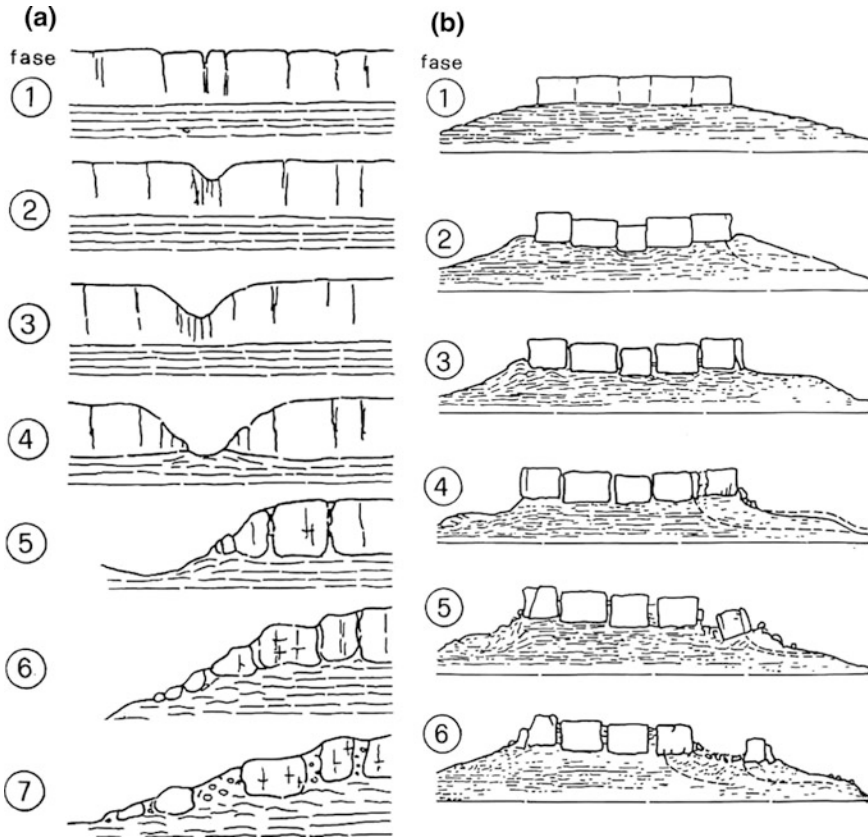


Fig. 6.4 Mechanisms of deformation and failure for rock slopes on clayey substrate: **a** model by Pasek (1974); **b** model by Cancelli and Pellegrini (1987)

Cancelli and Pellegrini (1987) pointed out that among the joints of an arenaceous plate laying on argillites, a very common lithologic condition on the hills of the central and northern Apennines (Fig. 6.4b), differential slides take place among the arenaceous blocks due to the variation in state of the underlying argillites, which induce the central blocks to settle more than the lateral ones. The blocks projecting toward the valley under river erosion, however, are involved in sliding and/or flow phenomena that mainly affect cohesive soils.

Last but not least, Lefebvre (1987) described a typical stratified structure found in some valleys of Canada, generated by the erosive action of the watercourses. This is a sequence of layers, with different permeability, which strongly influence the pressure regime in the ground. In fact, when such layers outcrop in the valley

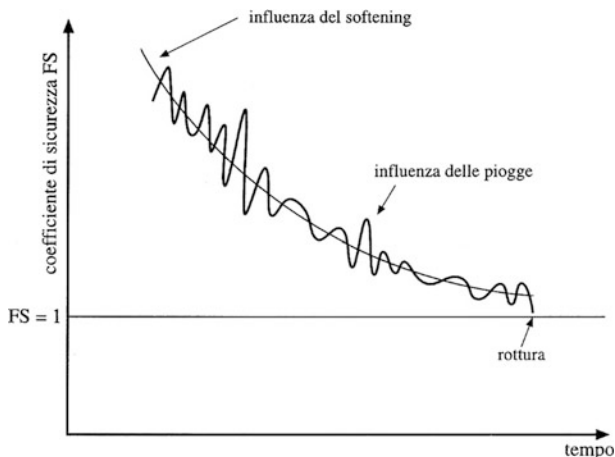


Fig. 6.5 Hypothetic evolution over time of the factor of safety of a natural slope subjected to oscillations of the groundwater table (from Picarelli 1999)

for the incisiveness of the watercourse, they act as drainage pipes for the surrounding layers, thus altering the regime of neutral pressures in favour of slope stability.

Picarelli (1993) studied the theme of excavations in cohesive soils with particular reference to the distribution of short and long-term pore-water pressures and the stability of the slopes. A neutral pressure regime which is depressed due to drainage may also be induced by natural excavations, such as those due to erosion. This situation was observed in the area of the municipality of Bisaccia, southern Apennines, where for several years surveys and monitoring have been carried out by Fenelli et al. (1992) (Fig. 6.6). Starting from such observations, a numerical analysis was carried out that fully confirmed the relationship between erosion and the neutral pressure regime and revealed that the geomorphological situation in the area itself depends on the erosive phenomena in progress.

Despite of the considerable interest in these studies, it should be noted that none of the Authors has ever been concerned by variations in the permeability coefficient K as a consequence of the stability of slopes, unless implicitly. In this sense, Bromhead (1986) in his book “*The stability of slopes*” performed, in specific terms, an analysis on the effects of variations in the permeability coefficient K on the stability of slopes.

From the 1950s, wrote Bromhead (1986), “*techniques based on flow-nets for solving problems of steady seepage were introduced in Soil Mechanics books. However, the flow net technique requires an isotropic and homogeneous distribution of permeability, which is not observable in natural soils. Intrinsically, soils are variably heterogeneous and anisotropic in all the natural slopes of the Earth’s globe. Consequently, also the permeability varies from place to place in the ground as well as pore-water stresses that develop into it. Therefore, flow nets based*

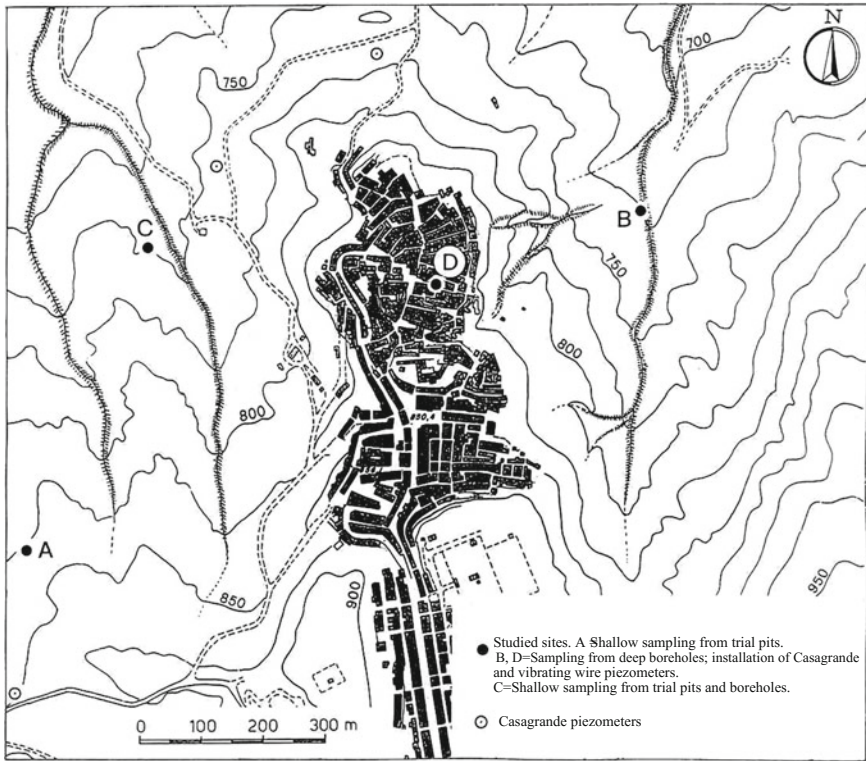


Fig. 6.6 Map of Colle di Bisaccia hill and investigation locations (from Fenelli et al. 1992)

techniques can be used only to solve seepage problems for small areas characterised by low thickness, where the soil is homogeneous and isotropic. In effects, even in this case, the flow net technique is lacking in concreteness and it is very difficult to be applied'.

The effect of anisotropy on permeability is to prevent that equipotential and flow lines could cross at right angles (except in the particular case of water flow parallel to one of the anisotropy axes) while this is the condition for the development of square mesh flow nets (Fig. 6.7). This distraction can be sudden if the ground is made up of a succession of layers or beds with different permeability. Both of these effects can be defined using simple numerical models. Finite element techniques are particularly suitable for such demonstrations.

Soil layering can therefore be the source of a significant anisotropy of permeability. Morphological and structural variations of a slope may also cause anisotropy of permeability. Soil compaction can induce a reduction in porosity and therefore of permeability. The effect of the permeability variation is therefore to increase or decrease the value of pore-water pressure or neutral pressure.

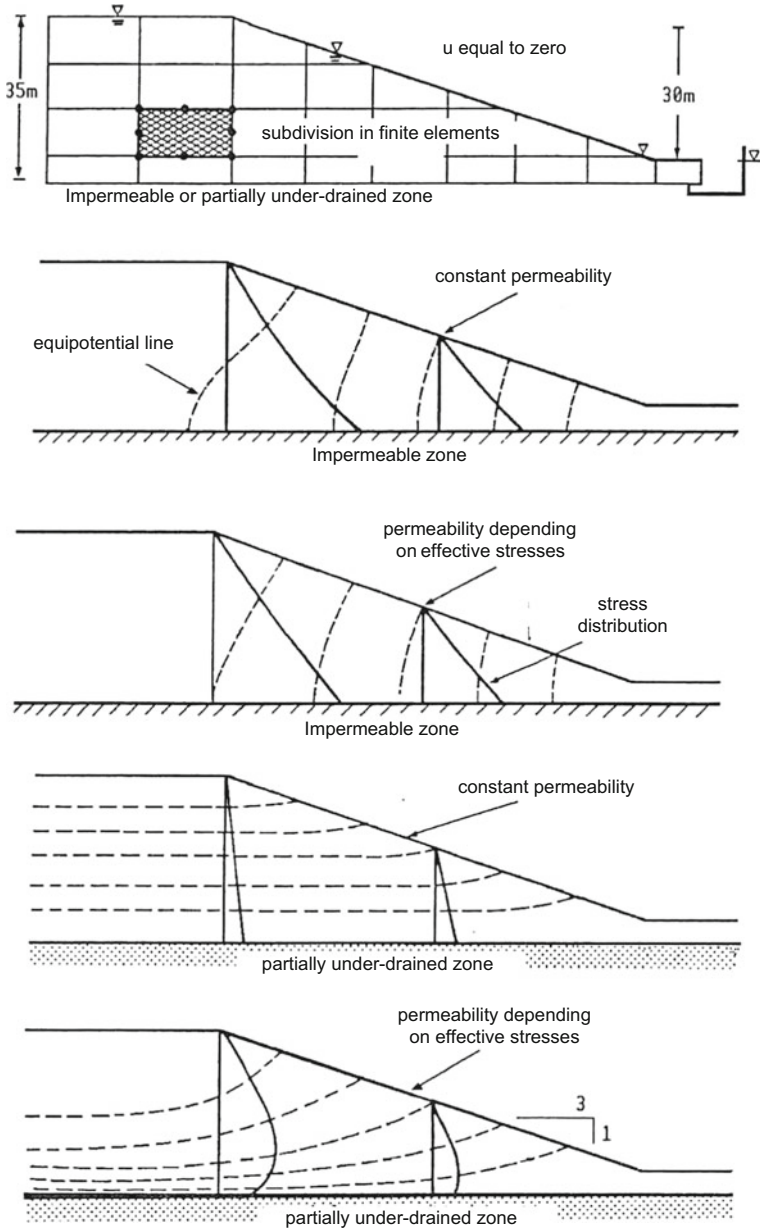


Fig. 6.7 Effect of variations in permeability. Even in a steady seepage analysis, slight alterations in the parameters ruling infiltration have a disproportionate effect. As an example, subterranean drainage is important and where it is present, the influence of reduction in permeability with depth is remarkable (Bromhead 1986)

The heterogeneity in particle size distribution of a soil as well as chemical processes in the ground are also reasons for variations in permeability.

An important case in the change in permeability is the presence in the ground of tectonic fractures caused by compression and/or distension, especially for what regards the activation of pre-existing landslides. If the ground is subjected to an increase in effective stresses, for natural or artificial causes, the volume of fractures or joints decreases and therefore permeability reduces. Whatever is the cause for the reduction in soil permeability, a consequent increase in neutral pressures and in shear stresses takes place, which can destabilize a cohesive slope.

There are soil permeability conditions for which the stress variation is null or negligible. This occurs when the water flow in the ground is intermediate between the maximum flow and the minimum during the yearly season cycle.

In slightly compressible and, therefore, low permeability soils (e.g. overconsolidated clay) the effect of cyclical variations in stress is negligible; these are generally deep soils, still subjected to important lithostatic loading. This also occurs in heavily fractured soils for tectonic reasons, such as Varicoloured Clay, Red Flysch, Flysch of Crete Nere, etc., so that each slope has always a limit depth where the seepage regime is stationary and in balance with the average conditions of the groundwater table in the above ground; this global pathway of the seepage of surface water is the one that controls the overall stability of a slope in cohesive soils. It is possible, however, that on a slope a more superficial shearing surface develops with respect to the value of its limit depth; this in fact depends on short-term variations in the infiltration path, that are induced by hydraulic conditions at the boundaries of the surface. For example, as it happens in the hydrogeological basin of the Comarca de Aguas Negras Calilegua, in the province of Jujuy in northern Argentina (Fig. 5.23). In this context the hydrogeological instability of the slopes is predominantly superficial and affects only the lithological horizon of alteration, that abrupt and abundant tropical rains lead to saturation in a short time (a few hours). The inability to rapidly dissipate interstitial water pressure causes an immediate mass swelling and constant stress changes due to variations in water content. Starting from the moment of failure, the behaviour of the cohesive soil, initially assimilated to that of a saturated continuous body, becomes definitively conditioned by neutral pressure, which transforms the lithic mass from the plastic state to that of a growing mud flow (Figs. 5.28 and 6.1—Surface hydromorphism).

A very different situation is the one where the underground drainage of a slope is influenced by a single permeable layer or by a succession of permeable layers at depth. By changing the flow conditions in the latter, varies also the total head of groundwater and, therefore, also the infiltration paths as well as the neutral pressure conditions. If, for example, by pumping water out of wells is obtained a reduction in the piezometric level within the slope and a reduction in neutral pressures, with consequent consolidation of the soils.

This function certainly improves the stability of the slope itself. Very dangerous, instead, is a rise in the piezometric level within the wells themselves, as it can change the underground drainage path from the previous one, potentially to the opposite direction. The effects may be those of a destabilization of the slope. Therefore, any variation in the hydraulic conditions of a slope occurring faster than

the correspondent variation in neutral pressures, will produce unbalanced stresses in the ground.

Summarising, it can be said that neutral pressures in a slope may not be in equilibrium with the hydraulic conditions at the boundary and this for two main reasons. The former considers that there may be excessive pore-water pressure in the slope due to phases of loading or unloading under undrained conditions; the latter considers that there may be a recent variation of the hydraulic conditions themselves at the boundary, which, however, has not yet reached its maximum potential.

An example showing the application of both of these conditions is on the north-eastern slope of the hill of Tricarico, southern Apennines, province of Matera, Italy.

6.4 The North-Eastern Slope of Tricarico

6.4.1 Location

The small town of Tricarico is located to the south of the Apennines range in the territory of the Basilicata region (Fig. 6.8). It is an ancient medieval town (Fig. 6.9a, b) whose residential area extends across an organogenic calcarenitic plate oriented along the Apennine direction (NW-SE), at between 620 and 680 m above the average sea level (Fig. 6.10).

6.4.2 Lithology of the Slope

At the north-eastern boundary of the town, calcarenite forms a 30 m thick steep slope, while it gradually reduces in thickness towards SE, where it gets 10 m thickness at its outer boundary. The calcarenitic mass is clinostratified, dipping of about 30° to SW, not clearly distinguishable due to amalgamation phenomena of the sediments. It rests locally in stratimetric continuity on grey-light blue marly clays of the Lower Clayey Member and belongs to a short, superficial, supralittoral sedimentation episode of the basin before it collapsed during Upper Pliocene (Calabrian), giving place to the deposition of the Upper Clayey Member of the Unit of the Bradanic Foredeep (Fig. 6.11 by Coppola 1993).

The clayey-marly layers have a thickness of 30–50 cm and are highlighted by millimetric interbedments of grey silty sand.

On the north-eastern side of the hill there is an extensive colluvial layer that rests directly on the marly clays of the Lower Clayey Member (Figs. 6.11 and 6.12); these are grey and grey-light blue silty-clayey deposits, with, to the upslope, fragments and stone blocks coming from the calcarenitic mass at the top of the



Fig. 6.8 Schematic map of Southern Apennine (Italy) with location of the town of Tricarico

slope. The silty-clayey material is heterogeneous, chaotic, sometimes altered. Lithological and granulometric variability develops both horizontally and vertically within the deposit. The thickness of this varies between 35 and 20 m respectively from the upslope to the downslope. The two lithologies, overlying and underlying, are separated by a discontinuity surface that acts as a sliding surface only under certain physical-mechanical conditions of the colluvial mass.

6.4.3 Morphological Processes in Place

At the northern edge of the colluvial mass flows the torrent Milo (Figs. 6.11 and 6.13), whose riverbed, heavily engraved within the Lower Clayey Member, follows

(a)



(b)



Fig. 6.9 a Medieval Tricarico of 17th century. b Current Tricarico

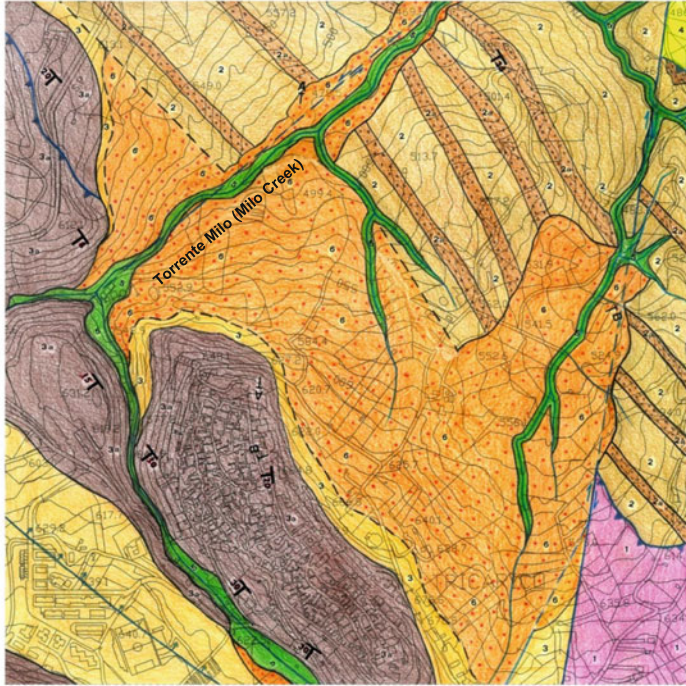


Fig. 6.10 Areal distribution of the town of Tricarico

a pre-existing sinistral strike-slip fault surface that acts as the main collector for the flows and runoff coming from the surrounding slopes. It exerts a decisive action on the mechanisms of deformation and failure of colluvial deposits.

The north-eastern slope of Tricarico hill can be represented by two sections corresponding to sections A-A, B-B (Figs. 6.14 and 6.15).

- *Depletion zone* (1) upslope, home of landslides in stratified marly clays and of falls of calcarenite blocks whose debris feed the accumulation zone downslope. The average acclivity is about 30°;



Legend

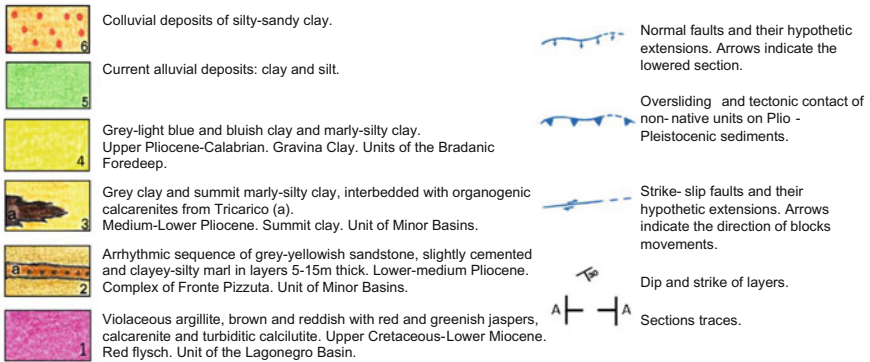


Fig. 6.11 Geological scheme of the north-east slope of Tricarico

- Accumulation zone, intermediate zone and valley areas, where the colluvial mass extends to; is home to the most important rotational type mass movements. The upslope ground surface (2a) has an average inclination of $= 20^\circ$ while the average of the downslope Section (2b) is $= 22^\circ$. Furthermore, the accumulation zone (2) is typically bilinear due to the different nature of the deposited lithic components. In 2a the colluvial mass has a ground surface conditioned by the presence of a sandy-arenaceous fraction mixed within the clay component, in

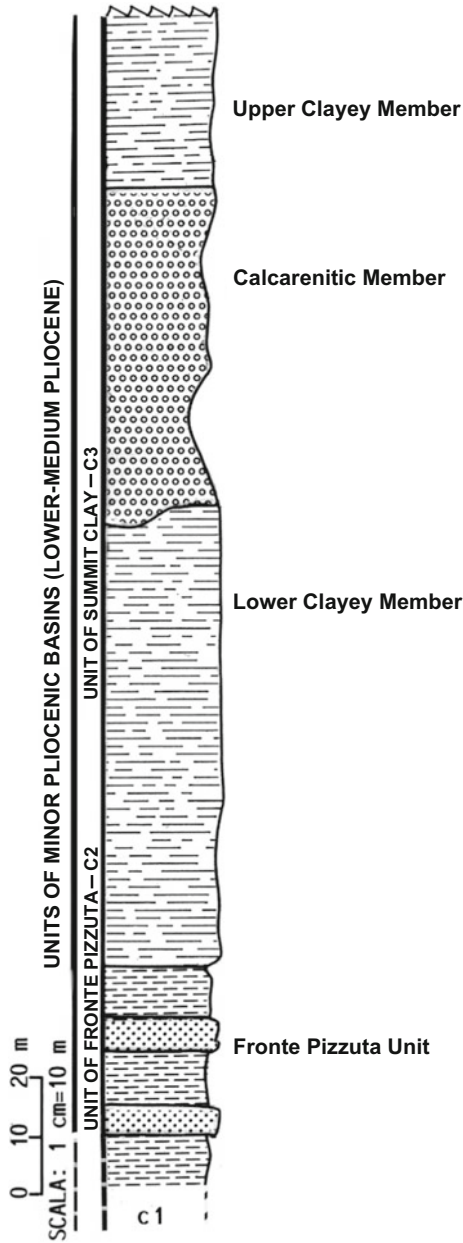


Fig. 6.12 Stratigraphic sketch of the area of Tricarico. The Upper Clay Member outcrops to the west of Tricarico (partially reported on the geological map)



Fig. 6.13 North-east slope of Tricarico. Colluvial deposits in hydrogeological instability laying on marly clays from the Lower Member

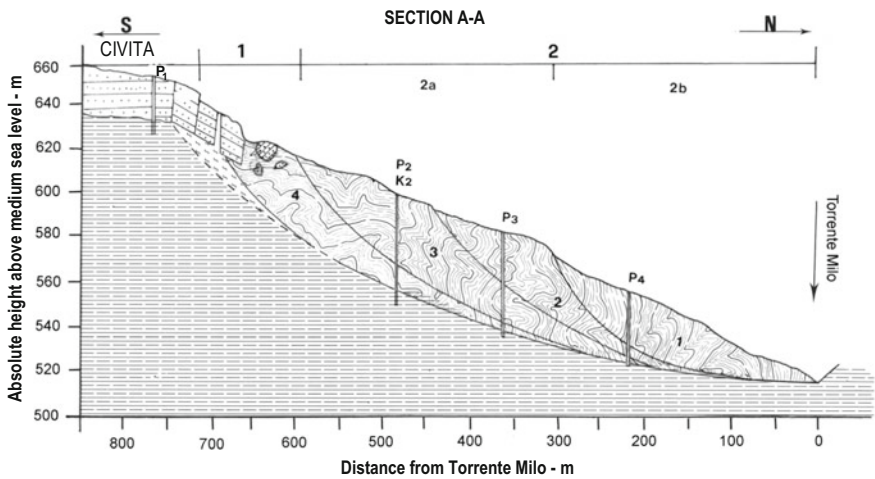


Fig. 6.14 Zone 1 corresponds to the zone of depletion; zones 2a and 2b instead are zones of accumulation. Boreholes P₁, P₃, P₄ were provided with piezometers; P₂, K₂ with piezometers and inclinometers

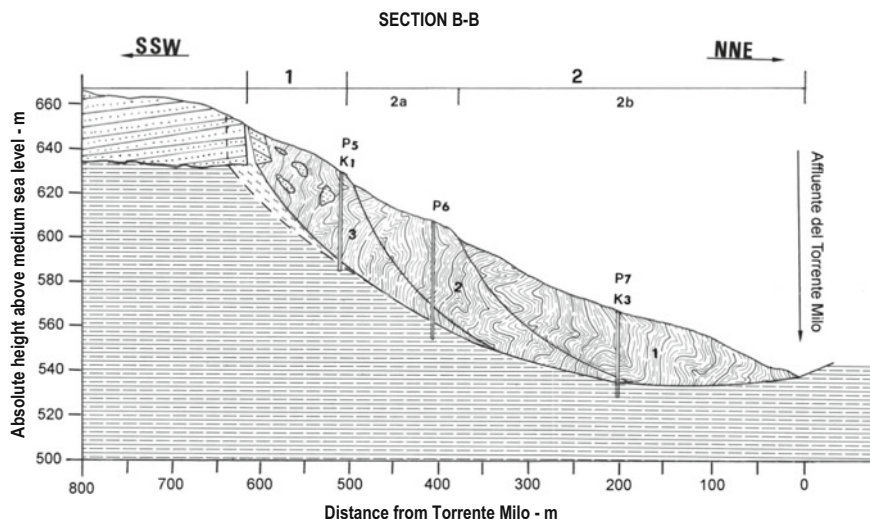


Fig. 6.15 Zone 1 corresponds to the zone of depletion; zones 2a and 2b instead are zones of accumulation. Boreholes P₅, K₁ e P₇, K₃ were equipped with piezometers and inclinometers; P₆ with piezometer

greater percentage than that of zone 2b below. In fact, from the particle size distribution of some colluvial soil samples, it resulted that the silty-sandy fraction increases from 10 to 30% of the total within deposit 2a, especially at ground level. The difference in slope between 2a and 2b is minimal and irrelevant to the slope failure mechanisms; however, a different deformation process develops between the two zones. In 2a, during rainfall, an excess in the seepage of rain-water is obtained in the ground that corresponds to a load increment in undrained conditions. There, the deposit deforms by compressing at the foot, being confined from the downslope (zone 2b), not necessarily moving. In 2a, therefore, undulations develop tending to expand upwards, well visible at ground surface. The upslope part (zone 1) undergoes tensile stresses and hence the plastic-rotational failure process of the clay beneath the foot of the calcarenitic mass, which has already undergone softening. These are neutralised by applying to the base of the calcarenitic mass itself a tensile reaction with the protruding blocks upwards opening according to an inverted V (\wedge) shape. The blocks are involved in the stress process of the clays under conditions of passive resistance of the wall (Fig. 6.16). In practice, the calcarenitic front undergoes initially vertical deformations parallel to the front itself, with a maximum opening at the base that tends to close upward (Figs. 6.14 and 6.15; Sect. 6.2). The blocks, therefore, settle and sink into the ground at the plastic state, toppling to the upslope.

Mass movements, with a plastic-rotational behaviour in 2a, occur only when the roto-traslational kinematic process in zone 2b, of impulsive type, frees up the

landslide front; the accumulation at the foot develops only for the downslope landslide mass (N. 1 in the cross section) where the debris from the sliding zone is pushed into the riverbed of torrent Milo.

6.4.4 Instrumental Monitoring

Instrumental monitoring was performed through n° 7 boreholes (p), aligned along sections A-A and B-B (Figs. 6.14 and 6.15), some equipped with multi-parametric columns (K) for 2D inclinometric and piezometric monitoring.

Boreholes drilling started on Monday 8th September 2008, while continuous monitoring began on Tuesday 1st October 2008, and ended on Monday 30th May 2011. It has been determined via mechanical borehole drilling that colluvium thickness decreases to the downslope (Table 6.2); it is 34.3 m in the upper part of the slope (P5) and 45.7 m in the middle (P6), while downstream it is about 31.5 m (P4).

The same measurements, of course, concern the depth of the discontinuity surface between the colluvium and the underlying stratified marly clays. However, this surface does not uniformly act as a sliding surface along the path of the moving mass. This, in fact, depends on the position the sloping mass assumes on the slope. This means that the shearing surface of colluvium in the medium and upper part of the slope is not conditioned by the pre-existing lithological discontinuity surface, but that activation can develop by means of a progressive deformation mechanism induced by pore-water pressure at a certain depth of the colluvial deposit. On the other hand, to the downslope such deposit has a reduced thickness, often insufficient for the hydraulic head to be equivalent to that of collapse and therefore the landslide moves along the pre-existing surface of lithological discontinuity where the resistance to be mobilized is certainly the residual strength, subjected to the hydraulic head of the torrent riverbed. Therefore, while to the upslope the failure occurs due to the rise of neutral pressures (Figs. 1.2 and 6.17), to the downslope the colluvial mass moves for the strong hydraulic head of the torrent and for the active thrust of the upstream soils.

Table 6.2 Referring to Figs. 6.16 and 6.17

| Geological sections | Boreholes depth (m) | Parametric columns depth (m) | Colluvium depth (m) | Rupture depth (m) |
|---------------------|---------------------|------------------------------|---------------------|-------------------|
| A-A | P ₁ = 27 | – | – | – |
| | P ₂ = 50 | K ₂ = 50 | 42.5 | 28.2 |
| | P ₃ = 48 | – | 44.3 | – |
| | P ₄ = 36 | – | 31.5 | – |
| B-B | P ₅ = 43 | K ₁ = 43 | 34.3 | 34.3 |
| | P ₆ = 54 | – | 45.7 | – |
| | P ₇ = 38 | K ₃ = 38 | 31.5 | – |

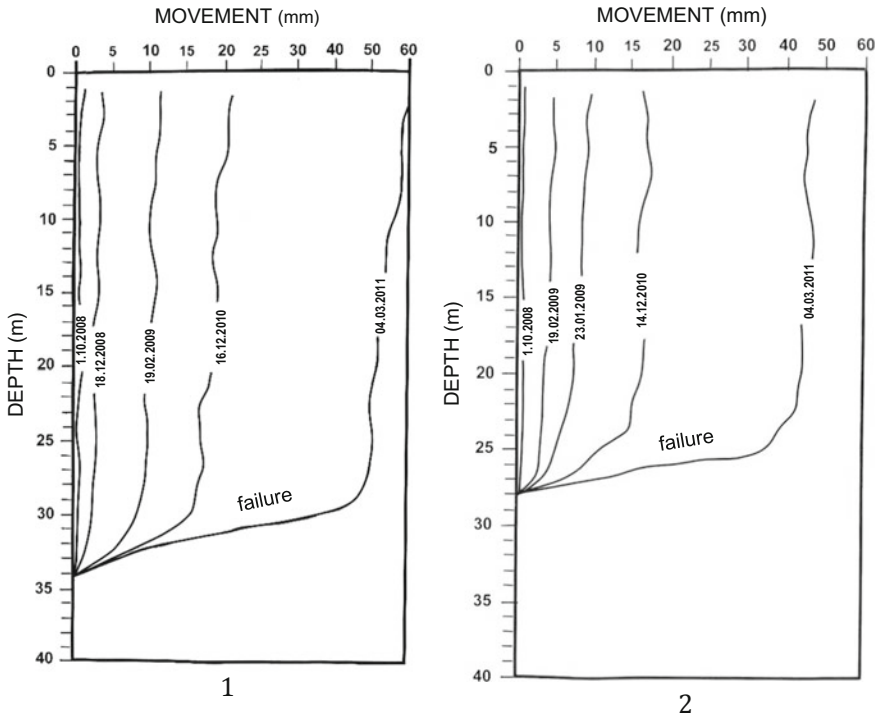


Fig. 6.17 1 and 2 Elastic-viscous-plastic deformation measured within landslide units n. 3 Sez. B-B and Sez. A-A, respectively in K_1 and K_2 up to failure

In structured cohesive soils, the pre-failure phenomena are identified by means of tension cracks of centimetre and/or decimetre length that appear at a certain depth under the effect of the neutral pressures induced by the cyclic variations of the piezometric level. They are irreversible deformations that define the initial state of the sliding surface. Tension cracks therefore represent one of the most important predictors of landslides, as they contribute to the definition of the incipient shearing area in propagation prior to collapse.

In colluvial soils, instead, although cohesive, the pre-failure deformation occurs through an elastic-visco-plastic deformation process along a very irregular continuous surface, as shown on Figs. 1.2 and 6.17. The colluvial mass of the medium to upper slope towards the east of Tricarico therefore deforms without sliding. However, as landslide masses 2 and 3 on sections AA and BB undergo the release of the lithostatic counterthrust of the immediately downslope colluvium, progressive failure propagates exactly along the pre-existing surface of visco-plastic deformation and not along the underlying surface of lithologic discontinuity. The piezometric level at failure is at 2.3 m below ground level (mean of the piezometric values obtained in the different landslide masses mentioned).

6.4.5 Discussion

In cohesive, chaotic, heterogeneous and sometimes altered soils of colluvial accumulation, widely spread on the Plio-Pleistocenic hills of the Apennines range, the cause of landslides is to be attributed to an interstitial water pressure condition developed at the boundary of the potential sliding surface at saturation state. Consequently, the determination of the conditions for the activation of landslides on the slopes formed by these soils requires adequate knowledge of groundwater regime, as there is often quick mobilization as a result of substantial variations in pore-water pressures in conjunction with intense and/or prolonged rainfall events.

The deformation related to the distinctive features of landslides in colluvial soils has been reconstructed in this explorative context by checking the progress of field experiments obtained from the complementarity between measurement apparatuses.

The morphological analysis immediately pointed out a peculiarity of colluvial soils, due to the fact that the landslide masses are well marked on the slope even before the triggering of their movement along the sliding surface. This is due to the fact that following to meteoric precipitation the colluvial mass is subjected in the short-term to a load increase in undrained conditions and deforms slowly by differentiating itself into several units of landslide, in succession on the slope, without triggering their sliding.

The drilling of boreholes showed a further characteristic feature of colluvial deposits; not all landslides use the pre-existing surface of lithological discontinuity, obtained by overlapping the colluvial mass on the underlying stratified marly clays (surface of separation between colluvial deposits and marly clay of the Lower Member), which has a low frictional resistance. Upslope landslide masses 2 and 3 in the sections reveal a pre-rupture surface at depths of 28–34 m below ground level, while the lithological discontinuity is at around 36 m. Furthermore, it has been found by means of the boreholes themselves that the thickness of the colluvial mass decreases to the downslope as well as the depth of the surface of lithological discontinuity, which passes from 36 m below ground level from the upslope to 16 m below ground level to the downslope.

Instrumental monitoring, in particular by means of the multi-parametric columns for inclinometric and piezometric monitoring, carried out to the upslope, revealed that the pre-failure deformation in colluvial soils is of elastic-viscous-plastic type.

There, at a minimum depth of 28 m from ground level, the colluvial deposit behaves like a closed system without seepage motions; the effect of the variations in the stress state therefore largely depend on the oscillations of the piezometric level, which results in a substantial change in the effective stress field able to cause the elastic-viscous-plastic deformation without sliding of the lithic mass. The sliding occurs, instead, only when ceases the lithostatic counterthrust of the landslide mass immediately downslope. Therefore, the deformational dynamics of landslides in colluvial soils explicate via a deformative process of regressive-sequential type.

The downslope landslide mass (n. 1), close to torrent Milo, does not undergo pre-failure deformations. It moves along the pre-existing discontinuity surface only

when the debris at the foot of the landslide have been removed from the water-course and in conjunction with an appropriate hydraulic head existing within the torrent riverbed itself, under the thrust of the upslope soils.

In summary, what characterizes the activation of landslide movements in silty-clayey soils of colluvial accumulation is:

- (1) the destabilizing action of colluvial soils is due to the oscillation of the piezometric level, which at failure reaches the value of 2 m below ground level;
- (2) in colluvial soils landslide masses are identified on the slope in terms of shape, size and sequence even before their movement by collapse;
- (3) the pre-failure deformation in colluvial soils is elastic-viscous-plastic;
- (4) the pre-existing discontinuity surface between the colluvial mass and the underlying structured soils does not always work as a sliding surface, especially where the colluvial thickness exceeds 30 m;
- (5) the mechanics of the collapse of landslide masses in colluvial soil are influenced by the passive resistance applied by the landslide mass immediately to the downslope;
- (6) the deformational action of a slope in colluvial soils is of regressive-sequential type for subsequent collapse of the landslide masses.

6.5 Hydraulic Conductivity and Hydraulic Potential at Failure

Based upon field experiences by means of monitoring equipment it has been observed that in saturated soils under undrained conditions ($\varphi' = 0$) the depth of the sliding surface depends solely on the permeability coefficient K, whatever the structural and mineralogical conditions of the lithotype. In fact, K decreases progressively with depth until it reaches the value of $K = E \times 10^{-7}$ cm/s where the substrate becomes almost impermeable. There, the excesses of interstitial water over-pressures, that do not dissipate in a short time and have a significant influence on soil behaviour at failure, tend to stabilise. Flow lines, fed by the infiltration of meteoric waters, are initially directed vertically downwards because of the high permeability value ($K = E \times 10^{-3}$ to $E \times 10^{-4}$ cm/s) within the colluvium and/or the alteration layer, then change gradually direction at greater depth, describing a typical arched shape, becoming parallel to the slope (Fig. 6.18) and finally coming out to surface at the bottom of the slope. This experimental observation is explained as follows: starting from a dry soil, the infiltration velocity (V_i) is directly proportional to the permeability coefficient (K) and reduces approximately according to the inverse of the square root of time (t) during which the process takes place.

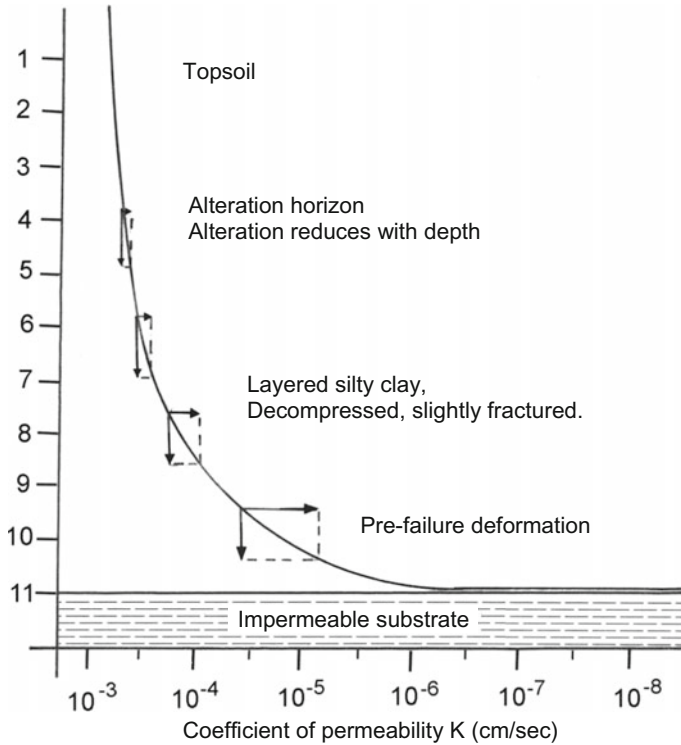


Fig. 6.18 Schematic representation of the path of water flowlines in cohesive soils

$$V_i = K/t$$

Given that K reduces with depth, in parallel reduces also the infiltration velocity V_i .

The amount of water (I) seeping through the ground during time (t) instead is proportional to the square root of time

$$I = K \cdot \sqrt{t}$$

When the soil is partially saturated, the infiltration velocity V_i tends to remain constant and the previous formulas, in practice, become

$$V_i = K \quad I = K \cdot t$$

As it can be observed, the infiltration (I) is strongly influenced by the hydraulic conductivity (K) of the soil and by the hydraulic potential already existing in the soil, which reduces enormously the infiltration velocity (V_i).

The depth at which flow lines become horizontal is the maximum depth of infiltration of water into the ground, where the water potential reaches its maximum (Fig. 6.19). In a cohesive soil, therefore, *this potential is maximum at the depth where $K = E \times 10^{-7}$ cm/s*. At this depth develops the shear strain which takes place, initially, through tension cracks (Fig. 6.20). However, even before the shear strain of the slope there are some cases that affect the processes of decay of the mechanical properties of the soils.

Picarelli (1999) highlights the destabilising action of the oscillations of the free surface of groundwater table on a slope in cohesive soils. The ground is in fact subjected to cyclic stresses due to the continuous variations of the “*mean normal effective stress and to minor changes in deviatoric stresses*”.

The seasonal oscillations of the piezometric line in the ground induces, over time, a yielding in soil resistance conditions. The stress field within which do move the corresponding paths of the maximum oscillations is delimited by that soil band where the permeability coefficient K assumes values ranging between $E \times 10^{-6}$ and $E \times 10^{-7}$, i.e. where the neutral stress remains the maximum during its variations.

A second effect induced by the fluctuations in neutral pressure regime is that observed by Eigenbrod et al. (1992), who carried out specific laboratory investigations on the behaviour of slightly overconsolidated clays of medium plasticity

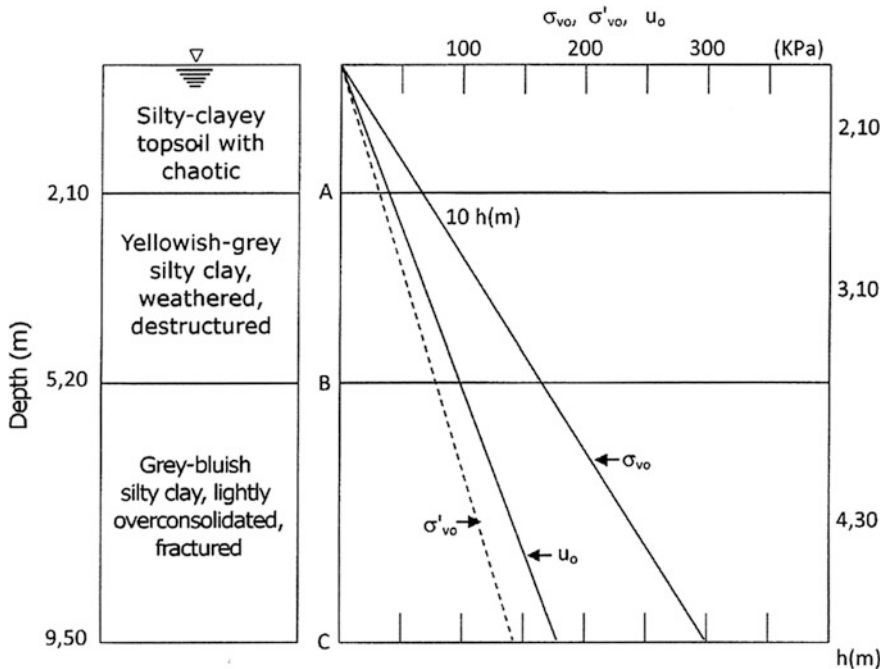


Fig. 6.19 Diagram of total vertical (σ_{vo}), of effective (σ'_{vo}) and of pore-water stress (u_o) with groundwater at ground level with reference to the stratigraphy of 2nd member (A2) of the Formation of Serra Palazzo. In C the soils has a value of $k = E \times 10^{-7}$ cm/s. Along the same line, u_o has its maximum value

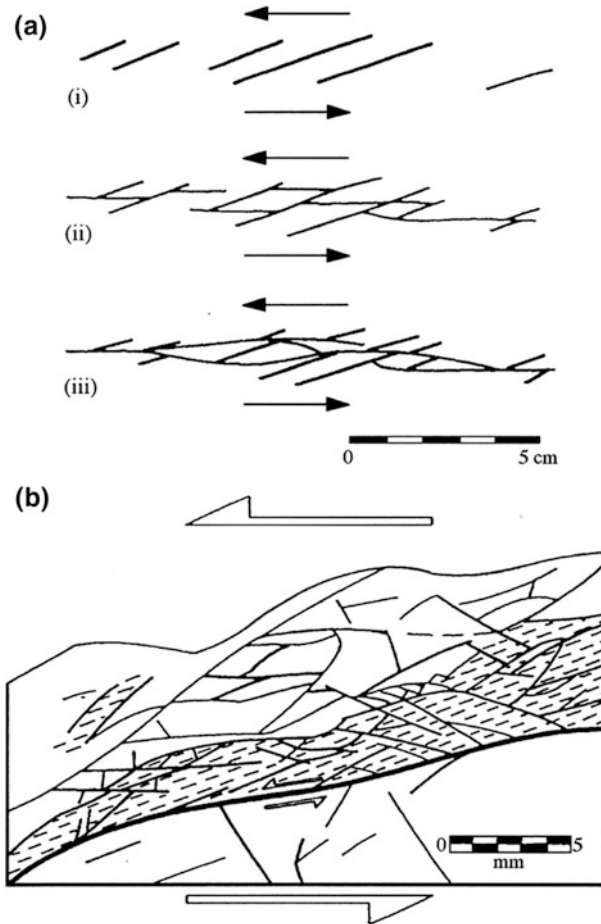


Fig. 6.20 Mesostructural detail of the shearing zone of Guildford landslide (from Skempton and Petley 1967—modified)

and, by means of these, they noted that the excursions of groundwater table produce, in the long-term, viscous and softening effects, with the triggering of gradually increasing deformations, favoured by the reduction of soil stiffness characteristics. Even this second aspect of the reduction of soil strength has been detected on site, by means of the monitoring equipment, at the depth where the value of K ranged between $E \times 10^{-6}$ and $E \times 10^{-7}$, whatever is the nature of the clay deposit.

The importance of undertaking detailed experimental investigations to identify any shearing areas present in the subsoil is therefore of utmost importance in order to achieve the prediction and prevention of hydrogeological instability, since the

shearing phenomena present in the ground are all dependent on the time factor, usually not defined through numerical analysis.

It was observed (Fig. 6.19) that at the depth where $K = 10^{-7}$ cm/s the hydraulic head is maximum, if the overlying cohesive soil is saturated. By determining the coefficient K in situ along the vertical then the shearing zone can be identified, described by Skempton and Petley (1967) (Fig. 6.20), which manifested precisely where the coefficient of permeability reaches the value of $K = E \times 10^{-7}$ cm/s.

These are cracks that indicate the state of incipient shear deformation of the ground. It should be noted that at this depth the cohesive rock is subjected to a triaxial compression state σ_1 , due to the hydraulic head, and the confinement pressure σ_3 . The behaviour at failure depends on the values of σ_1 and σ_3 of the local stress field; σ_3 plays a very important role on the formation of pre-failure cracks (Fig. 6.20). Indeed, since the laboratory data indicate that the intermediate principal stress σ_2 has less influence on the peak strength than the minimum stress σ_3 , the criteria of more general use reduce to the form:

$$\sigma_1 = f(\sigma_3)$$

Mohr's circles can easily represent this stress situation. Their construction comes from the failure experience (Chap. 2, Figs. 2.16 and 2.17). Putting τ and σ on the Cartesian axes, the values of σ_1 and σ_3 from the test are reported on the abscissa and the circle of Mohr (Fig. 6.21a) is traced. The angle θ subsequently defines the inclination of the failure plane with respect to σ_1 (Fig. 6.21b). Expressing this relationship in terms of shear stress τ and of normal stress σ_n is obtained

$$\tau = f(\sigma_n).$$

See—*Theoretical failure in presence of σ_3* —Chap. 2.

It is worth specifying that tension cracks are not the ones considered as of pre-failure. The latter are neoformation cracks generated by interstitial water pressure and lithostatic load. The failure process takes place as follows: the interstitial water pressure is maximum at the depth where $K = E \times 10^{-7}$ cm/s. At that depth, the cohesive material absorbs water up to saturation; it becomes therefore

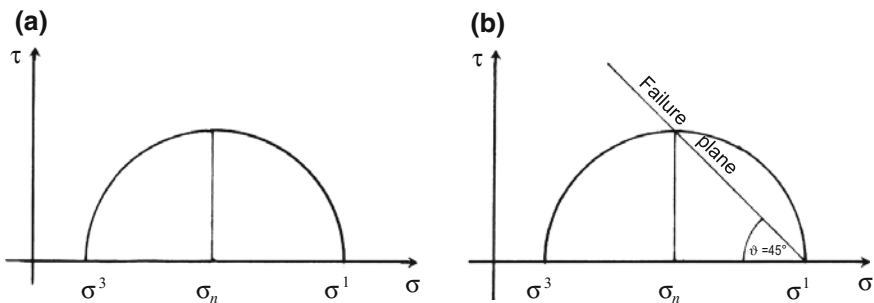


Fig. 6.21 Representation in terms of Mohr's circles

completely impermeable in the absence of shear strain, since its expansion is prevented by the confinement in all directions. There, the percolation water stagnates or flows out slowly along a surface path characterized by $K = E \times 10^{-7}$ cm/s. In the overlying lithic horizons, in the meanwhile, the clayey soil undergoes a process of hydromorphism resulting from the jamming of impermeable substances released by capillary water within very small interplatelet voids (see Sect. 6.2). It thus forms an alteration horizon that contains groundwater within itself. At the base of this horizon, the electrostatic effect of clay platelets tends to create a local stress field which is not perfectly isotropic at all points but reveals a privileged direction along which the resistance to loading is lower. The direction of the deformational axis at failure depends not only on the orientation of τ but also on the brittleness of the reaction of the soil which is greater along the surface of discontinuity between the horizon of alteration and the intact formation, i.e. at the depth where $K = 10^{-7}$ cm/s. From Figs. 6.2 and 6.5, it can be observed that the factor of safety of a natural slope subject to oscillations of the groundwater table decreases over time. Furthermore, the failure is influenced by the factor of vertical oscillation of groundwater table (σ_1), even getting that the orientation of the stress axes remains constant: $\sigma_1 =$ vertical, $\sigma_3 =$ perpendicular to the slope and τ_{\max} oriented at 45° from the vertical, parallel to the surface of the impermeable layer.

In the very common case, where the intact cohesive soil formation is made up of tectonically fractured units, the groundwater suspended in the horizon of alteration finds a percolation pathway among tectonic fractures and penetrates to a depth where the permeability of the ground is characterised by a value of the permeability coefficient $K = E \times 10^{-7}$ cm/s. In this situation, the hydraulic head can reach a very high value and in the long-term, with a piezometric surface often at the ground level, the deformation mechanism at failure occurs by explosion of the cohesive rock, in the close proximity of very steep slopes, similar to vertical walls, projecting towards the river valley. There, indeed, the confinement pressure is very low (Fig. 6.22a–c).

Otherwise, if the slope has medium or low acclivity, the confining pressure can exert a value greater than the hydraulic head. In this case, for composite landslides, the masses to the upslope are blocked by the lithostatic counterthrust of the downslope ones. They can develop pre-failure deformations only when they are subjected to movements induced by the stress-path (Fig. 6.16).

Referring to Fig. 4.3a–d in Chap. 4, the appearance of unstable fractures subjected to triaxial compression can develop in several ways.

- If at the depth where $K = 10^{-7}$ cm/s there is a pre-existing stable crack (Fig. 4.3 a) this is subjected initially to a closure if the vertical load σ_1^b is greater than the initial σ_1^a . If the load value increases, such that $\sigma_1^c > \sigma_1^b$, the faces of the crack undergo sliding (Fig. 4.3c). When the fracture plane is subjected to a further vertical load, where $\sigma_1^d > \sigma_1^c$, extensional cracks develop at the two ends of the fissure due to traction parallel to σ_1 (Fig. 4.3d). The failure occurs if the value of σ_1 is furtherly increased becoming greater than σ_1^d (Fig. 4.3e).



Fig. 6.22 a–c Explosion of marly rock, very fractured, happened live on 9.5.2010 after three days of persistent rainfall on the southern slope near Quebrata del Toro—ancient road—Yuyui Province, Argentinian Pre-Andes

- Changes can take place both in the stress field (because of the dissipation of σ_1) and in the properties of the material ($\varphi \gg 0$) during the development of cracking; this can produce a stabilization of the crack. In this case, an increase of σ_1 is required for inducing the growth of the crack.

These stress conditions concerning the mechanics of failure of natural slopes heavily influenced by pre-failure deformation phenomena occurred in December 1982 on the northern slope of Montagnolo hill in Ancona, Central Apennines, giving place to the Great Ancona Landslide, which will be discussed in Chap. 7. Not only the progressive failure but creep and softening as well there played an important role, resulting in a continuous modification of the stress states and a on the reduction in the available shear strength.

References

- Baligh, M. M. & Levadoux, J. N. (1980). *Pore pressure dissipation after cone penetration*. Research Report R. 80-11, Mit, Cambridge, MA.
- Baver, L. D. (1948). *Soil Physics* (p. 398). Chapman and Hall Ltd.: Londres.
- Bishop, W. A. (1955). The use of the slip circle in the stability analysis of slopes. *Geotechnique*, 5(1).
- Bromhead, E. N. (1986). *The stability of slopes*. Blackie & Son Ltd.
- Bromhead, E. N., Coppola, L., & Rendell, H. M. (1994). Geotechnical background to problems of conservation of the medieval centre of Tricarico, southern Italy. *Quarterly Journal of Engineering Geology*, 27, 293–307.
- Cancelli, A., Pellegrini, M. (1987). Deep-seated gravitational deformations in the Northern Apennines, Italy. In *Proceedings of the 5a International Conference and Field Workshop on Landslides* (pp. 171–178). Christchurch.
- Castany, G. (1967). *Traité pratique des eaux souterraines* (deuxième ed.). Paris: Dunod.
- Cello, G. & Coppola, L. (1984). Assetto Geologico-Strutturale dell'Area Anconetana e sua Evoluzione Plio-Quaternaria. *Bollettino della Società Geologica Italiana*, 103, 97–109, 6 ff., 2 tavv.
- Cerere, V., Lembo Fazio, A. (1986). Condizioni di sollecitazione indotte dalla presenza di una placca lapidea su un substrato deformabile. In *Atti del XVI Convegno Italiano di Geotecnica* (Vol. I, pp. 191–202). Bologna.
- Combeau, A. & Monnier, G. (1961). *Sols africains*, 6(1), 4–32.
- Coppola, L. (1993). Evoluzione tettonica e meccanismi deformativi della media Valle del Basento, *Bollettino della Società Geologica Italiana*, 112, 159–179, 20 ff., 1 tav. f.t.
- Coulomb, C. A. (1773). Essai sur une Application de Regles de Maximis et Minimis a Quelques Problemes de Statique Relatifs a l'Architecture. In *Mémoires de Mathématique & de Physique, présentés à l'Académie Royale des Sciences par divers Savans, & lus* dans ses Assemblées* (Vol. 7).
- Delpont, G., Deramont, J., Guchereau, J. Y., Joseph, J., Majeste-Menjoulas, C. L., Soula, J. C., et al. (1973). Ruptures extensives et cisailantes dans des series rythmiques sédimentaires (Montagne Noire et Pyrénées). *Revue de Géographie Physique et de Géologie Dynamique, France*, 15(5), 567–574.
- Di Maio, C. (1996a). Exposure of bentonite to salt solution: Osmotic and mechanical effects. *Geotechnique*, 695–707.
- Di Maio, C. (1996b). The influence of pore fluid composition on the residual shear strength of some natural clayey soils. In *Atti del VII International Symposium on Landslides* (Vol. 2, pp. 1189–1194). Trondheim.

- Dupuit, J. (1863) *Etudes théoriques et pratiques sur le mouvement des eaux dans le canaux découverts et à travers les terrains perméables*, 2e édit. Paris: Dunod.
- Eigenbrod, K. D., Graham, J., Burak, J. P. (1992). Influence of cycling porewater pressures and principal stress ratios on drained deformations in clay. *Canadian Geotechnical Journal*, 326–333.
- Fellenius, W. (1992). *Erdstatistische Berechnungen*. Berlin: W. Ernst.
- Fenelli, G. B., Picarelli, L., Silvestri, F. (1992). Deformation process of a hill shaken by the Irpinia earthquake in 1980. In *Atti del Conv. Italo-Francese "Stabilità dei Pendii in Zona Sismica"*. Bordighera.
- Fitz Patrick, E. A. (1988). *Soil horizon designation and classification*. Technical Paper 17 Isric, Wageningen.
- Janbu, N. (1973). Slope stability computations. *The Embankment dam engineering: Casagrande Volume* (pp. 47–86). Wiley.
- Lambe, T. W. & Marr, W. A. (1979). *Stress path method* (2nd ed., 724–738) JGED, ASCE, June 1979.
- Lefebvre, G. (1987). Slope instability and valley formation in Canadian soft clay deposits. *Canadian Geotechnical Journal*, XXIV(3), 261–270.
- Matheson, D. S., & Thomson, S. (1973). Geological implications of valley rebound. *Canadian Journal Earth Sciences*, X, 961–978.
- Morgenstern, N. R., & Price, V. E. (1965). The analysis of the stability of general slip surfaces. *Geotechnique*, 15, 79–93.
- Pasek, J. (1974). Gravitational block-type slope movements. In *Proceedings of the 2th International Congress* (Vol. II, th. V-PC 1). Sao Paulo: IAEG.
- Picarelli, L. (1993). Structure and properties of clay shales involved in earthflows. In *Atti dell'International Symposium "The Geotechnical Engineering of Hard Soils-Soft Rocks"* (Vol. 3, pp. 2009–2019). Atene.
- Picarelli, L. (1999). Meccanismi di Deformazione e rottura dei pendii. In *Argomenti di Ingegneria Geotecnica* (Vol. 14). Hevelius Edizioni.
- Sarma, S. H. (1979). Stability analysis of embankments and slopes. *Journal of the Geotechnical Engineering Division, American Society of Civil Engineers*, 105(GT 12).
- Skempton, A. W. (1948). The $\phi = 0$ analysis of stability and its theoretical basis. In *2nd ICSM*. Rotterdam.
- Skempton, A. W., & Petley, D. J. (1967). The strength along discontinuities in stiff clays. In *Atti della Geotechnical Conference* (Vol. 2, pp. 29–46). Oslo.
- Taylor, D. W. (1948). *Fundamentals of soil mechanics*. New York: Wiley.
- Terzaghi, K., & Peck, R. B. (1967). *Soil mechanics in engineering practice* (2nd ed.). New York: Wiley. The first edition was published in 1948.
- Tison, L. J. (1953). *Cours d'hydraulique*, 2e parties (pp. 265–430).
- Torstensson, B. A. (1975). Pore pressure sounding instrument. In *Proceedings of the ASCE Specialty Conference, Measurement of Soil Properties*. Raleigh: North Carolina State University.
- Torstensson, B. A., & Peterson, A. (1985). Bat water monitoring system. In *ASTM Symposium of Field Methods for Ground Water Contamination Studies and their Standardisation*. Cocoa Beach, FL, USA, February 2–7, 1985.
- Varnes, D. J. (1978). Slope movement types and processes. In R. L. Schuster & R. J. Krizek (Eds.), *Landslides: Analysis and control*. Washington, DC.
- Vigneron, J., & Desautettes, J. R. (1960). *VII congrès international de science du sol* (Vols. 1, I, 5, pp. 114–121). Hadison.
- Yoshida, N. (1990). *Time-dependent instability in fissured overconsolidated clays and mudstones* (Ph.D. thesis). University of Alberta, Edmonton.

Chapter 7

Landslides Types and Their Failure Mechanisms

7.1 Introduction

In the evolutionary framework of mountain ranges of planet Earth, where compressive tectonics takes place with uplifting and/or overthrusting of blocks, slopes assume a greater and particular propensity to deformation by shearing.

In an invariant stress regime, cohesive soils, and not just these, undergo a process of de-structuring which is currently home to numerous and vast areas of hydrogeological instability. The peculiar aspects of the behaviour of these soils subjected to landslide can be summarised as:

1. deformation at failure develops according to a rotational landslide when the piezometric surface rises up to a certain depth below ground level;
2. the critical surface at failure for landslides is preceded by small size shearing deformations that develop along pre-existing discontinuities with a minimum coefficient of resistance. This indicates that the mechanics of collapse is strongly influenced by pre-failure phenomena;
3. the sliding surface always manifests itself at the depth of the previous pre-failure deformations whatever is the time between the two deformational phenomena. There is, therefore, a relationship between pre-failure factors and triggering factors, usually related to oscillations of pore-water pressures;
4. a certain rate of resistance is released during the progressive failure process when the lithostatic contribution of a good portion of the sliding mass immediately downslope becomes missing;
5. when the piezometric surface comes to the ground level, the horizontal stress (σ_{h0}) has already exceeded the limit state of a value greater than $2 c_u$, where c_u is the undrained cohesion of the soil. The cause of rotational plastic movements is therefore mainly attributed to a problem in pore-water pressure developing at the boundary of the sliding surface in a saturated state;
6. the depth to the sliding surface results from a significant reduction in the permeability coefficient K with depth. The failure occurs within a lithic horizon

with the permeability coefficient K ranging between $E \times 10^{-6}$ cm/s and $E \times 10^{-7}$ cm/s. This minimum value of permeability ($E \times 10^{-7}$ cm/s) is the limit of percolation of groundwater and is due to the fact that the lithostatic load (σ_v) tends to compact the material at depth and to tighten the tectonic microfractures by reducing the voids index (e) of the cohesive soil. The ratio K -depth, however, *is not a linear function*. The behaviour at failure points out that the stress factor acts as a closed system, where adsorbed water does not escape and therefore it must be assumed that the sliding surface is originated under undrained conditions;

7. the typical arched form of rotational movements is given by the decrease in permeability K inversely proportional to the depth. The flow lines are initially oriented downward vertically ($K = E \times 10^{-2}$ to $E \times 10^{-3}$ cm/s) and then gradually change direction ($K = E \times 10^{-4}$ to $E \times 10^{-5}$ cm/s) following a concave curvilinear path towards the lower part of the slope to then align horizontally and outcrop at the bottom of this (Fig. 6.18);
8. On very steep slopes ($\sim 60^\circ$ slope) in highly clayey soils, the relatively widespread vegetation, like for jungle trees of equatorial and tropical areas, represents a further hydrogeological risk factor to the instability of natural slopes. The disruptive and geodisturbing action of the soil, already chaotic and destructured, favours the process of water seepage because of the presence of roots. Stress changes continuously take place on the slopes, mainly because of variations in water content or of the slow re-balancing of pore-water pressures.

Landslides with rotational plastic movement are genetically subdivided into two groups: *monotype landslides* and *composite landslides*.

7.2 Monotype Landslides

Monotype landslides consist of a single landslide body, typically small or medium sized. The depth of the sliding surface is dependent on the thickness of the horizon of alteration. It reaches the limit state of shearing resistance between 6 and 13 m from ground level; this depth is dependent on the state of fracturing and on the attitude of cohesive layers, often interbedded with sandy and silty beds of variable thickness.

From the graph of Fig. 7.1 it is noted that the pre-failure deformation, that is generated at the depth where 10^{-6} to 10^{-7} cm/s, is confined within section B'-C' of the hypothetical sliding surface. In that area, in fact, the hydraulic head is maximum (see Figs. 6.18 and 6.19). Cracking is the one appearing in the initial state of the genesis of a landslide as a basal deformation. The cause is to be given to a particular hydraulic head condition that develops at the boundary of the potential sliding surface in saturated state. Cracks have an angle ranging between 30° and 50° with respect to σ_1 along the vertical.

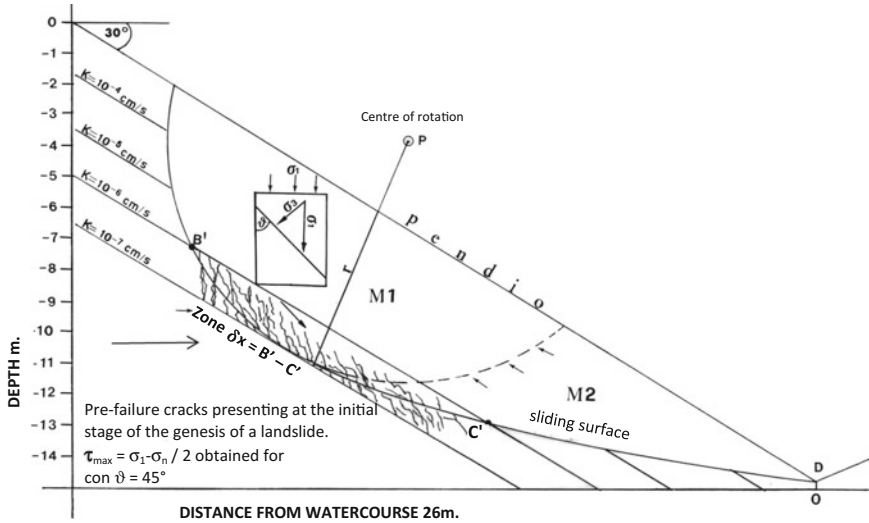


Fig. 7.1 Hologenic sketch of the evolution of a mono-typical landslide describing, through 2D representation, the events of a sliding cohesive mass

During the shearing deformation, an increase in the volume of mass M1 is obtained that occurs because of the growth and propagation of microdiscontinuities already existing in the soil and subjected to oscillations in the mean effective stress following to seasonal cycles of the piezometric level and to time. In other words, the variations in groundwater levels induce cyclic stresses in the soil of which the maximum ones are obtained at the depth where K ranges between 10^{-6} and 10^{-7} cm/s, meaning at the base of mass M1. There deformation develops by traction, with cracks oblique to the direction of the slope and arranged along a line inclined of about 30° – 50° with regards to stress axis σ_1 (Fig. 7.1). The minimum strength corresponds to an angle $\vartheta = 45^{\circ}$. The maximum failure stress is concentrated in point C' of Fig. 7.1. This condition about the attitude of cracks has been verified through multiple instrumental monitoring experiences that confirm the deformation at the base in tract B'-C as the initial state of failure in the slope. The stress state remains in equilibrium until mass M2 at the toe, which applies a lithostatic counter-thrust on the mass to the upslope, triggers the motion because of its activation, at several times, due to oscillation in the mean effective stress within mass M1. In mass M2 the deformation takes on, with time, a predominant viscous-plastic state especially in cohesive soils already altered and decompressed or within colluvial soils comprising clay and silt. In this case, the contour of the slope in M1 is wavy and more frequently swelling near the slope surface in M2 (Fig. 6.16).

At the base of mass M2, the initial deformation is not the shearing one, since the neutral stresses regime undergoes a variation of the hydraulic conditions at the boundary of C'-D curve, due to the progressive reduction in total stresses when going downslope. In situ instrumental observations allowed to note that the

cohesive soils along the potential sliding surface undergo a deformation process of viscous-plastic nature, with evident effects on the alteration of mineralogy and softening. “Experience has shown that softening is particularly important in the case of stiff fissured clays of high plasticity, especially in shaley argillites (Picarelli 1999).” Also from the studies of Di Maio (1996a, b) and of Picarelli et al. 1998, it can be noted that in clays of marine origin softening may be induced by modifications in the physical-chemical characteristics of the porosity water due to the seepage of rainwater, characterised by a lower content in salt. Hoek and Brown (1980) and Yoshida (1990) demonstrated that the effects of softening depend on some empirical parameters that are function of time. In particular, the softening process essentially takes place along the path of water seepage in the ground (Fig. 7.1) which tends to come to air downslope because of the water head in D, now facilitated by values in the permeability coefficient K that are progressively greater downstream than in the area of B'-C'. At the toe of the downslope mass, therefore, the strength at failure to be mobilized is certainly the residual strength given that this block is subjected to the active thrust of the upslope soil, that tends to rotate along path B'-C because of the trend in increasing the volume of fissures and their propagation. In its classical definition, the active thrust of upslope mass M1 can be compared to the centripetal acceleration of a body constrained to its centre of rotation P (Fig. 7.1) where V_f is the escape velocity of the moving mass and r the radius of the circle.

Centripetal acceleration a is given from the expression

$$a = \frac{V_f^2}{r} \quad (1)$$

Starting from this formula, velocity V_f corresponds to the stress of the thrust applied to the base of mass M2 from the rotating mass M1. As a consequence, velocity V_f is:

$$V_f = \sqrt{a \cdot r} \quad (2)$$

In this case, a is the gravitational acceleration of Earth

$$a = \frac{G \cdot M}{r^2} \quad (3)$$

where M is the mass of the object subjected to the gravitational attraction of Earth (6×10^{24} kg); G is the gravitational constant (6.67×10^{-11} m³/Kg S²); r is the radius of the circle describing the movement of mass M1.

If putting such value in formula (2), velocity V_f can be obtained, i.e. the stress applied by M1 on M2 along the potential sliding surface.

$$V_f = \sqrt{G \cdot M/r} \quad (4)$$

However, it must be considered that mass M1 is not free to rotate around its centre of gravity, likewise a celestial body, because it slides along a shearing surface presenting a value, albeit residual, of the angle of internal friction. Velocity of rotation V_f , therefore, is not constant; it is influenced from the value of friction angle ϕ'_r which must be inserted into formula (4).

Fluctuations in the pore-water pressure regime in mass M2 are, however, the main cause of deformation as they induce in the ground changes in the conditions of clayey soils that in the long-term cause a progressive reduction in soil strength (viscous effect). At the same time, the active thrust of mass M1 on M2 is also significant but secondary in determining the displacement of mass M2. The behaviour of the sliding surface at failure is, however, conditioned by deformational pre-failure phenomena which result in a continuous modification of the stress state in the ground, especially if the pathway of water flow is almost horizontal. In the hologenic diagram of Fig. 7.1, the acclivity of this path was of just 8°.

In the long-term, progressive failure processes are triggered, starting from point D, that induce significant movements through a sequential regression movement that takes place within a very short time until the upslope mass (M1) is affected. This, already defined in its identity, has the possibility to slide along the pre-constituted sliding surface by releasing the potential energy already accumulated and producing some terraces, due to tensile actions, the most upslope of which is generally larger and constitutes than the main scarp.

In this reconstruction of the deformational state of a failed slope, time plays the most important role in decreasing the shear strength of the soil. A landslide, in fact, is not triggered overnight; the time needed for the genesis, development and activation of a landslide is always very long. Sometimes it takes decades for small-sized landslides, like the monotype ones, while for large moving masses the activation time is almost secular. The more compact and less fractured the outcropping lithological unit, the less deep is the zone with a value of $K = 10^{-7}$ cm/s and consequently the sliding surface of a monotype landslide; in this case the process of landslide formation on predominantly clayey slope is short.

7.3 Composite Landslides

Composite landslides are formed by several landslides in succession on the same slope line (Fig. 7.2). They, unlike monotypes, engage a rather large thickness of altered soil within which viscous, plastic deformations and softening processes develop due to fluctuations of groundwater, with consequent changes in the neutral pressures regime. Time is one of the most important factors for this type of landslides, which determines the progressive reduction of soil resistance. It turns out to be the most important physical entity in the development of the dynamics of

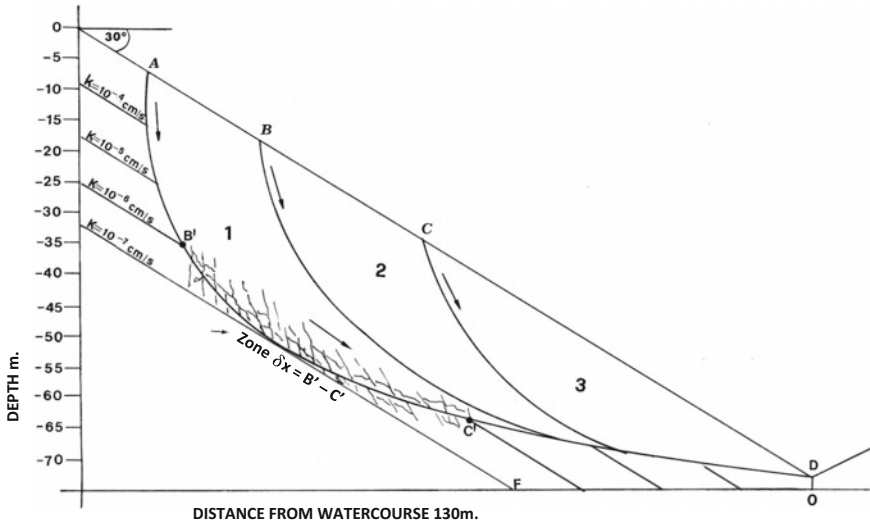


Fig. 7.2 Hologenic sketch of the evolution of a landslide with 3 bodies part of the same event of hydrogeological instability

landslides and justifies the long period between an event of hydrogeological failure and the subsequent one. In addition, the larger and the deeper the composite landslide, the longer the time for failure. As for monotype landslides, the horizon of alteration rests on an impermeable substrate at a depth where the coefficient of permeability assumes the value of $K = 10^{-7}$ cm/s. This substrate is actually the surface of the limit state of shear resistance of the altered ground and divides the latter from the intact zone.

By means of Fig. 7.2 can be better clarified the genesis and development of a composite landslide.

Considering a slope with a scarp of 30° in a schematic condition of parallelism between the lithic horizons with different permeability, made up of topsoil, altered soil and unaltered unit, the latter impermeable ($K < 10^{-7}$ cm/s). For geometric uniformity, the impermeable surface is considered flat and dipping 30° to the downslope. Groundwater, contained within the horizon of alteration, applies onto it the maximum value of neutral pressure (u_0) in the B'-C section where develop the deformational phenomena of pre-failure.

Seeped meteoric waters flow within the ground from the upslope to the downslope along the impermeable surface due to gravity down to point C', as shown in Fig. 6.18. The underground flowpath, however, extends from C' to D, subjected predominantly to the water head in the valley and facilitated by the permeability values that become progressively higher. As with monotype landslides, the C-D zone is not affected by pre-failure phenomena, as the hydraulic head to the downslope is progressively lower than the one upslope (B'-C').

“The morphological analysis of the slope has immediately highlighted a peculiarity of composite landslides, due to the fact that the individual landslides are well visible on the slope even before their triggering along the sliding surface they share. This is due to the fact that, because of meteoric precipitations, the layer of altered soil is subjected in the short-term to an increase in loading under undrained conditions and deforms slowly by differentiating into several potential landslide units, in succession on the slope, without mobilizing them” (Chap. 6, Sect. 6.4.3, Fig. 6.16). Actually, the mass deforms by compressing to the foot, being confined to the downslope, and swelling at ground surface. The swelling contributes to the formation of a wavy surface profile with low steepness. To the upslope of landslide unit 1, instead, a relaxation takes place within the lithic mass, the effect of which is to create a depression due to tensile effects (main scarp).

Thus, by means of a good survey of the site, the number of incipient landslides can be easily identified and mapped before the failure.

Mechanical drilling (see in next paragraph “The Great Ancona Landslide”) has also shown that the sliding surfaces of landslide units 2 and 3 of Fig. 7.2 developed in the horizon of alteration and originated in discrete, very irregular levels, highly dependent on variations in the state of the soil where creep and softening phenomena determine the reduction of local stresses within the altered mass. The sliding surface, therefore, is not well defined by pre-failure effects as it happens for the shearing surface upslope. This one is developed because of the high hydraulic head, while the sliding surfaces of masses 2 and 3 are characterised by a low value of $\tau = \frac{\sigma_1 - \sigma_3}{2}$, unable to induce ground failure subjected to triaxial compression, being $\vartheta \ll 20^\circ$. It is also possible that these sliding surfaces develop at the exact moment of activation.

The deformational process of a composite landslide can therefore be summarized in the following timeline: in a slope, the first deformation phenomenon at failure is of brittle nature, called by Bjerrum (1967) *progressive failure*, and occurs to the upslope, at depth, where the value of the coefficient of permeability K ranges between 10^{-6} and 10^{-7} cm/s. There, initially, the effect of variations in the stress state depends largely on oscillations of the piezometric head, which results in a substantial change in the effective stresses field able to cause the pre-failure deformation without triggering the sliding of soil mass. The sliding takes place only when it occurs a lack in the lithostatic counterthrust provided by the landslide units immediately to the downslope.

Downslope landslide units (Fig. 7.2, units n. 3 and 2) are not influenced by the effects of pre-failure deformation at the toe. They are triggered by the passive limit state developing in the altered ground (see Fig. 6.18—stress-path). The shear strain in the ground is due to the progressive reduction in limit state induced by viscous and softening processes as well as alteration. In particular, landslide unit n. 3, downslope, even if subjected to deformations due to stress-path, slides only when the debris from previous landslides, or other, are removed from the downslope watercourse and concurrently with an adequate groundwater head. The same process applies to coastal landslides. The dynamic of the movement of landslide mass No. 2 is subjected to the same principles of instability just described and even if it is

identifiable at embryonic state for shape, size and sequence, remains waiting for the concomitant failure of landslide mass n. 3.

The sliding surface of unit 2 is usually detected at the moment of the sliding of unit 3 and has an irregular shape, often with portions of soil sliding in the form of flow.

Landslide unit 1, previously constrained by the passive resistance induced by landslide mass 2, is now free to move along its sliding surface, already identified at the boundary of the pre-failure lines, and is correlated in point C' to the sliding surface defined by landslide masses 2 and 3. However, the surface is not always very long as its path is obstructed by the mass of the two units previously collapsed. The morphological aspect of the failing slope points out the evidence of this with very undulated slopes that, over the time, will be smoothed when the downslope watercourse has disposed the debris progressively accumulated in the riverbed.

7.4 The Great Ancona Landslide

7.4.1 *Chronicle Notes (from Carciofi 1983)*

“Ancona, night of 13th December 1982, at 22.40: the large strip of land that from Fornetto declines to the sea began to slip, dragging in its slow motion the houses that were on it. This vast and ancient slope has therefore restarted moving, following the intense and prolonged rainfall occurred after a long period of dryness. The first signal comes from Borghetto, then, immediately after, from via delle Grotte a Posatora; then a generalized alarm puts into action all the emergency services of the town.

In the middle of general panic, it could not be clearly understood what was happening; then the light of the new day highlighted the size of the disaster: a huge landslide hit all the neighbourhood to the north of Ancona, ripped off the railway line and via Flaminia, cut water and gas networks.

The most dramatic situation is due to the conditions of the two hospitals invested by the landslide: the Geriatric and Oncologic. These are now cleared; the hospitalised are transferred to other hospitals in the town with ambulances and private means.

It is in this circumstance that it has to be registered the only indirect victim of the landslide: a hospitalised has died of heart attack while being loaded into an ambulance.

While on Posatora hill three thousand people suddenly found themselves homeless, downslope the event manifested itself in all its power: the railway and the via Flaminia, running parallel to the coast, literally do not exist anymore. For a length of at least 2500 m the tracks are crumpled up, the track sleepers ripped out, the poles of power supply ruined to the ground. The road is like burst, swollen up, raised by 4–5 m above its original level.

Halfway of the slope, also water and gas networks (which run parallel to the coastline, the railway and the via Flaminia) are disrupted and the city will remain for a few days without these essential services. Many of the homeless said that even before they heard the crunches of the houses they felt a very strong smell of methane.”

The landslide manifested itself mainly in terms of plastic-rotation following to prolonged rains (170 mm in one week). Its front was 1730 m in length, while the main scarp, upslope, occurred at 170 m above sea level. In total, the affected area was just less than 350 hectares (Fig. 7.3).

On Posatora hill, such hydrogeological disruption turns out to be cyclical, with periods of 60–70 years; in particular from 1770 to 1858 (data from M. Carciofi’s 1983 thesis—Polytechnic University of Ancona—Italy), there is only indirect information on the sliding of the northern slope of the hill, which concerns the viability of “Palombella Consular Road”, several times affected by the landslides there originated.

The first description of a massive mass movement manifesting on the same hillside was carried out by Engineer De Bosis in 1859. For the first time, a detailed description of the phenomenon was obtained on 16th November 1858, through topographical, lithological, stratigraphic, agricultural and morphological analyses.

A further landslide occurred in 1919. Engineer Segré carried out a very accurate and methodologically modern study of the causes of the Barducci landslide on Posatora hillside. This study was published in Boll. Soc. Geol. It., Vol. 38, No. 3



Fig. 7.3 Area of development of the Large Ancona Landslide: to the bottom is Località Barducci; to the top is Località Montagnolo

(Bulletin of the Italian Geological Society, Vol. 38, No. 3). On the same slope, the author distinguished a lower landslide mass (Barducci) and an upper landslide mass (Montagnolo) for which a single sliding surface was observed.

7.4.2 Summary of Damages (from Carciofi 1983)

1. *The landslide has affected a total extension of 341.5 ha, equal to 11.14% of the urban area and 3% of the municipal area.*
2. *The affected population was 3661 citizens (1070 households) of whom 2,346 received clearance orders, while 1315 live in areas subjected to marginal danger.*
3. *Citizens accommodated at the expense of the municipality in hotels or pensions have reached the peak of 1562 units.*
4. *280 buildings were damaged or destroyed for a total of 865 inhabitants. 80% of this asset is classified as irrecoverable.*
5. *The dwellings on the edge of the landslipped area are over 300.*
6. *Irreparably injured: the Faculty of Medicine, the Oncology Hospital, the Geriatric Hospital, the “Tambroni” retirement home for elderly people.*
7. *Severely injured: the Adriatic railway line, via Flaminia, Posatora postal road, some minor urban roads, water and gas distribution networks.*

7.4.3 Geological-Structural Framework of the Landslide

The area of the Barducci–Montagnolo landslide (Fig. 7.4), situated on the northern slope of Posatora hill, is partially part of succession I, consisting of marls and sands of Monte dei Corvi (n. 12 on the geological map) and partially to succession II, composed solely by Pleistocene soils (9 and 8 on the map) that stand in angular discordance (transgression) on the previous ones (Cello and Coppola 1979). It is bordered to the west by the great normal fault No. 18. The outcropping soils are marly clays and bluish silty marls in layers 30–60 cm thick, with thin silty sandy layers (3–5 mm) interbedded. Proceeding downwards with the succession, meaning towards the oldest soils, layers of sand increase in frequency and, sometimes, in thickness; upwards, instead, the sedimentation of clayey-marly soils appears predominant. In the end, the unit becomes completely clayey-marly, with layers of 20–30 cm originated in the Lower-Medium Pliocene. The succession rests in a stratimetric concordance on the Marl “a Colombacci” from the Upper Messinian.

By means of mechanically drilled boreholes (see attached stratigraphy at the end of the paragraph), a superficial lithic horizon was identified, sometimes of great thickness, influencing the evolution of the slope (horizon of alteration). Grey and greyish-yellowish clay to marly clay, altered, highly fractured, wet, decompressed,

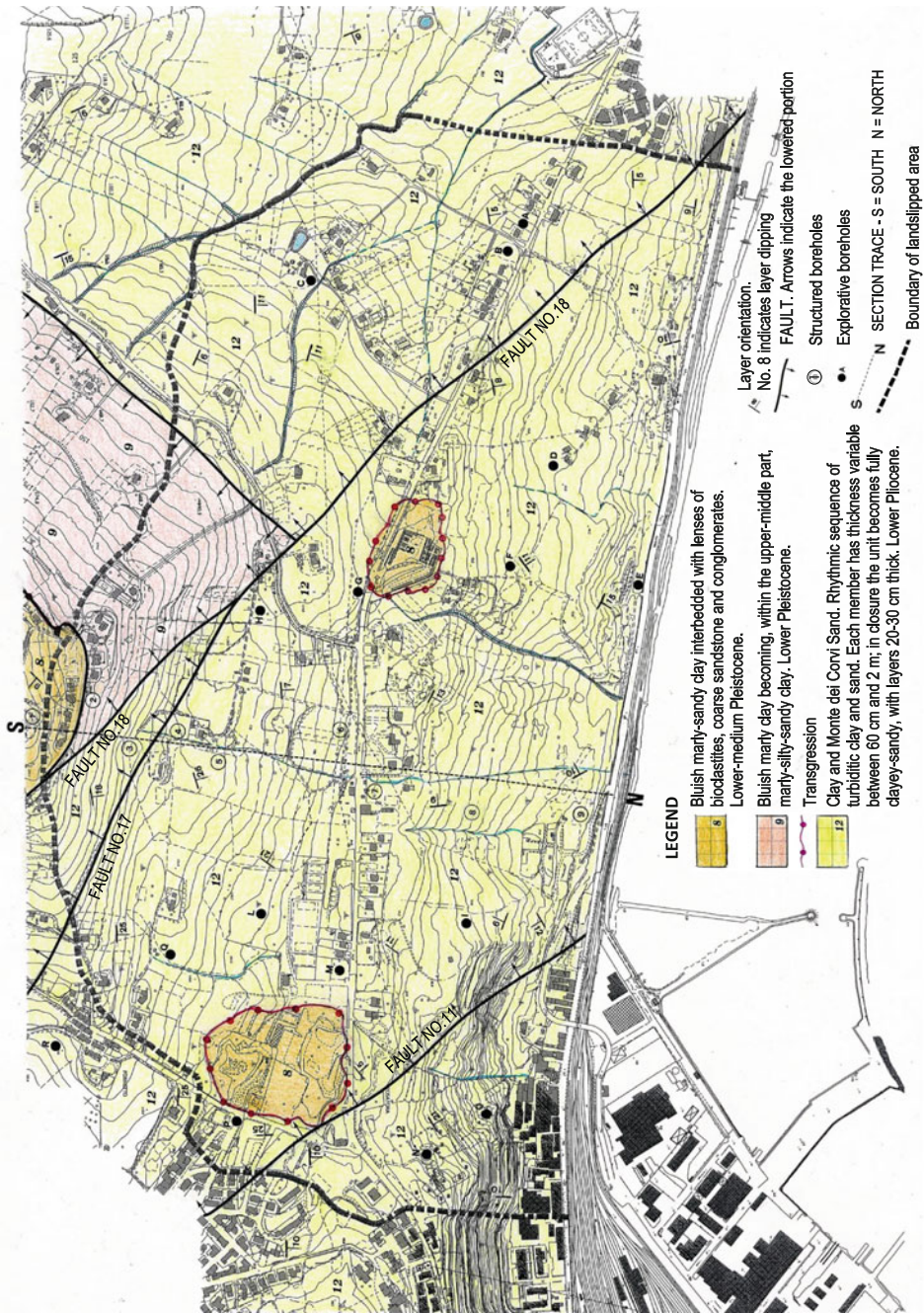


Fig. 7.4 Geological-structural map of the landslide area

destructured at the top, with thin intercalations of fine sand. With depth, the alteration decreases, the characteristics of compactness and aggregation of clay laminations improve, sometimes the stratification surfaces can be distinguished. However, in the lower part of this horizon there are always thin water levels that often directly affect the stability of the mass. The percolation of waters, predominantly meteoric, is arrested at the base of this horizon, which in average reaches 23 m in depth. However, the tectonic fracturing of the Monte dei Corvi unit allows the percolation of seepage water at greater depths, as shown in S7 borehole log, where percolated water reaches 35 m from the ground level. Here the water is deposited on an impermeable substrate made of bluish marly clay.

Fault n° 18 acts as a separation limit between two structurally different areas which, starting from the basal Pleistocene, have undergone a different tectonic evolution. The coastal zone to the east of fault n. 18 will be called “Zone A” and “Zone B” the one to the West (Cello and Coppola 1979).

The results of the analysis of fractures and faults affecting the soil of succession I, outcropping along the coastal zone, are illustrated on the diagram of Fig. 7.5 where are cumulatively reported the data for n. 471 single structures. As it can be observed, the iso-frequency curves, plotted at 1% intervals, define an absolute maximum in the NW quadrant and a relative one in the SE. The first (with a polar density > 10%), identified from pole P 290-75, corresponding to a system of structural discontinuities oriented preferably in the N 20° direction with prevailing ESE dips. The second (with polar density > 9%), identified from pole P 165-80, corresponds instead to a preferential system N 75° dipping to NNW.

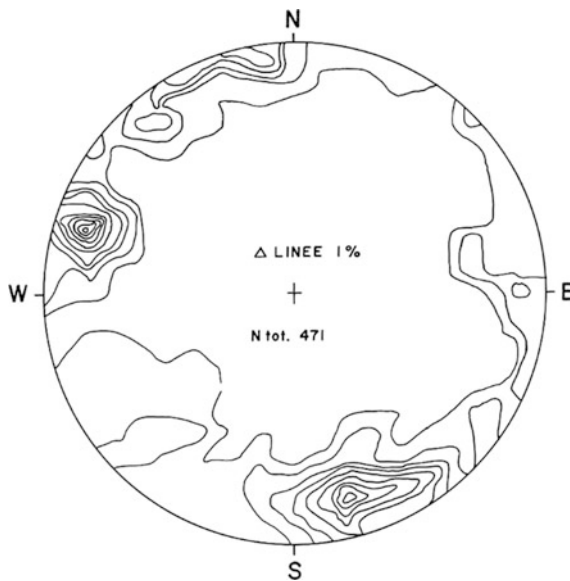


Fig. 7.5 Diagram of polar density related to meso-structural elements of Zone A

Based on these data and referring to the failure criteria of Mohr-Coulomb type (Handin 1969; Mogi 1974) it was possible to reconstruct the geometry of the stress field acting in this area. The type of solution obtained, shown in Fig. 7.6, indicates that Zone A was subjected to compression in a SW-NE direction being the geometry of the tension field $\sigma_1 = 228/24^\circ$; $\sigma_2 = 065/64^\circ$; $\sigma_3 = 310/6^\circ$. The coastline therefore and, with it, the northern slope of Posatora Hill has been subjected, in recent times, to compression along the same SW-NE direction. These data, however, are very well framed with the solutions of six focal mechanisms for low energy crustal earthquakes ($M < 5$) recorded between February 1971 and February 1972 near Ancona coast (Console et al. 1973; Gasparini et al. 1980). These events show that the release of seismic energy has occurred through strike-slip mechanisms compatible with the above-mentioned geometry.

In the more general picture of a quaternary tectonic of an essentially extensional feature, which affects the whole central Apennine range (Ambrosetti et al. 1981; Selli 1967), in the Ancona area there still seems to be an active compressive tectonic. This is explained by admitting that the area under examination is a segment of the overlapping zone between the outer margin of the range and the Adriatic micro-plate (Gasparini and Praturlon 1981). The structural and seismological features, as well as the thickening of the crust in this sector, as evidenced by the Elba-Ancona seismic profile (Giese et al. 1979), confirm this hypothesis.

Ultimately, it can be well understood what state of fracturing can be found today in the lithic horizons of the supra-Pliocene deposition on the northern slope of Posatora hill.

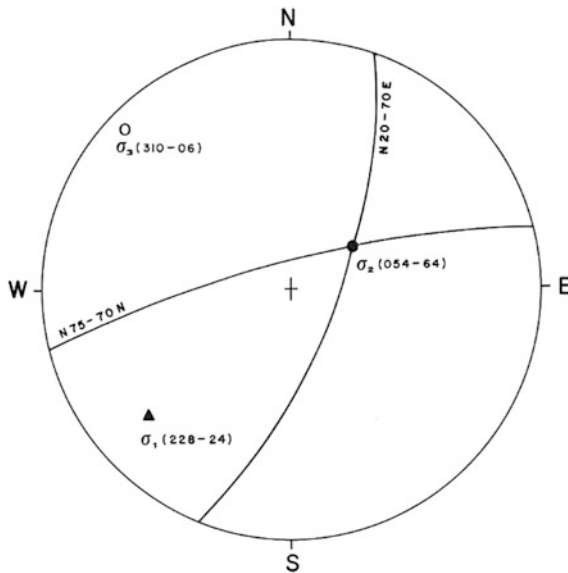


Fig. 7.6 Geometry of the stress field acting along the coastal zone

7.4.4 Morphological Aspects of the Slope

The main factor in the survey of the Ancona area was the tectonic uplifting complicated by dislocations due to minor faults and fractures according to systems with different orientations; these have given rise to a typical morpho-structural block structure which later exerted a significant influence on the modelling of the whole area of the northern slope of Posatora hill. A major and generalized selective erosion has been produced at Palombella failure front, which has progressively increased the physiographic differences between the areas characterized by substrates with different erodibility. The slope, furthermore, has also suffered over the centuries of a continuous process of retreat of the coast line between Ancona and Falconara. Not least, the layout of the hydrographic network has been clearly controlled by structural factors; the channels are essentially characterized by linear engravings consistent with the main fracture systems that have forced the discharge of water into a mandatory direction. The morphogenetic control of the Ancona area also appears conditioned by local tectonic as well as by the structural system.

It is important to understand the nature of the outcropping soils and their compactness and/or cementation. For example, the stratification of sandy and/or silty deposits increases the degree of steepness of the slope. In contrast, the lithic horizons mainly composed of clay and/or marly clay have less steep slopes and the forms of hydrogeological disruption are considerably larger.

The photogrammetric analysis has highlighted how the geometry of the slope is strongly conditioned by the lithological nature of the outcropping horizons. It resulted evident the abundance of steeper slopes in soils of sandy-arenaceous nature, where the steepness ranged between 30° and 60°. A progressive reduction in steepness occurred, instead, where there was an increase in clay content in the outcropping horizons. Clayey-marly lithotypes presented slopes with inclination ranging from 20° to 30°.

The process of alteration of the outcropping lithological units, therefore, took place in different ways depending on the lithological characteristics of the various horizons. In predominantly clayey and marly ones, mostly forming the slope itself, this process was determined by the elastic reaction of the air contained in soil pores and there compressed by the effect of the molecular actions of water (surface tension between soil and water and interface tension between air and water).

The temperature influenced magnitude and speed of degradation of the clay slope, as it acted on the air and the water contained in the soil mass in direct linear function. In fact, being the presence of air in the soil an essential condition for alteration and disintegration, the clayey rock was the more susceptible to the variation of state as the more it was humid.

Overall, therefore, the variations in temperature and humidity induced an intensification of rock alteration in situ, with the formation of different thicknesses of mobilizable materials.

On the slope, a horizon of alteration developed over time, favouring and accelerating, in wet conditions, the swelling and degradation of clay material, with a reduction in global resistance due to the electrostatic interaction between water and clay laminations. The thickness of this lithic horizon is due to site topography and to the penetration depth of seepage water as well as to rainfall regime. It varies between 21 m and 35 m where the slopes dip by 20°–30°, while in those with steepness angles greater than 30° the thickness of altered soil gradually increases between 12 and 7.6 m. In these conditions of relaxation of the superficial lithic material, the Great Landslide of Ancona manifested itself through four landslide masses of limited volume, initially with reduced displacements occurring in a temporal succession, which was regressive towards the upslope along sliding surfaces developed at the base of the horizon of alteration (Fig. 7.7—sections SN).

7.4.5 *The Landslide*

With regards to the geomorphological aspect, this type of landslide is classified as a composite landslide. It has four landslide masses in succession on the same slope line (see section S–N).

It has been mentioned that the conditions of hydrogeological disruption of Posatora slope and the type of mass movements that occurred depended on the global geomechanical characteristics of the soil mass, on the tectonic fracturing and the quantity of unregulated water freely circulating within the ground.

In particular, it has been seen that structural characteristics assumed decisive importance in the soils where the disruption occurred with plastic-rotational modes.

Laboratory tests allowed to characterize the technical behaviour of the material; the values of soil plastic characteristics are reported in the Casagrande's plasticity chart (Fig. 7.8). It is noted that these values are fairly uniform within the same lithic horizons and that between the altered and the intact one there is a slight difference that places the marly clay, respectively, between medium and high plasticity materials. The plasticity index (I_p), in fact, is within the range 21–32% and 26–41%, while the liquid limit (W_L) fluctuates between 43–65% and 55–70%. This indicates that the material constituting the slope has a plastic behaviour and consequently the consistency state is closely related to the amount of adsorbed water.

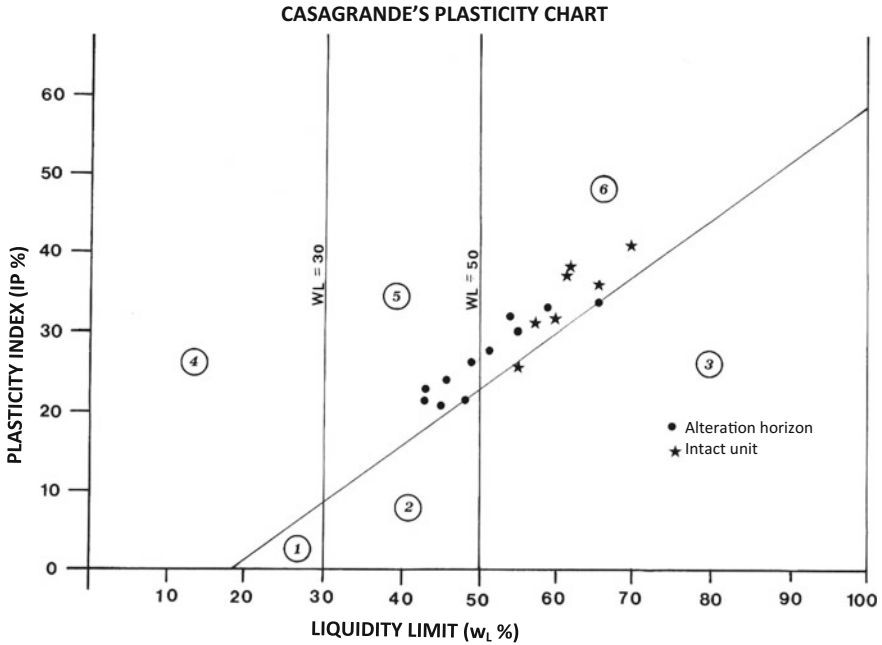


Fig. 7.8 Casagrande's plasticity chart

The way to depend on the various parameters that affect the stability of the slope is certainly different between levels of different nature, especially because the stratigraphic succession of the various units is heterogeneous and therefore anisotropic is the value of the physical quantities (hardness, strength, plasticity index, friction, etc.) in all directions. In addition, the partial movements of the individual equivalent volumes of soil are related to the relations between the direction of the slope, the spatial position of the geological structures, the presence and orientation of natural surfaces that determine the geometric configuration of the same lithological units. All the influences associated with water effects are related to the structural setup of Plio-Pleistocene units and to the properties and characteristics of the fractures, hence it results that the slope instability process is extremely variable from zone to zone; this involves the splitting into four landslides of the hydrogeological disruption itself on the slope of Posatora.

For the analysis of the equilibrium conditions of the slope, then, must be taken separately into account the peculiarities of the stability of the horizon of alteration and, in this context, of the portions of the slope with different steepness, which are the ones that differentiate the different units of a single landslide.

The monitoring of piezometers showed a condition of rather high hydraulic head, especially in the central area of the slope in question, in correspondence of boreholes S6 and S7, while in those piezometers located at the top of the slope, boreholes S3–S4–S5, the hydraulic head was found to be lower (see the related borehole logs descriptions).

The analysis of the logs sampled at the time of drilling the boreholes essentially evidenced that the sliding surface of landslide mass 3 is located at the base of the horizon of alteration, where this reaches the depth of 27 m from ground level in correspondence of borehole S5.

The maximum depth of the sliding surface, however, belongs to mass 2, the intermediate one, where in borehole S7 it reaches 35.1 meters below ground level. There was encountered the presence of greyish-yellowish marly clay containing lenses of bluish silty sand with chaotic attitude and presence of water whose piezometric surface rises to 24.5 m below ground level (measurement carried out 5 months after the landslide event). In all the boreholes (S4–S9) the sliding surface was always found at the base of the alteration horizon, usually in a plastic state.

This condition is of great interest for the localization of the sliding surface in the ground. The systematic monitoring of piezometric heads along the S–N cross section did therefore represent an essential prerequisite for defining the hydraulic head at failure of Posatora slope. In fact, the direct supply of water due to the seepage of rainwater, further to inducing the saturation of the horizon of alteration has also influenced its mechanical behaviour.

Of great importance is the “in situ *permeability*” factor as from this depends the potential of the soil to be seeped through or to retain groundwater. The motion of water in a filtering medium is regulated by the Darcy’s Law, $V = K i$: the velocity of seepage V is directly proportional to the piezometric gradient (or drop or hydraulic gradient) i , by means of a coefficient of permeability K , whose value essentially depends on the amount and size of intergranular or interlaminations voids through which water passes. In order to provide permeability with defined numerical dimensions, such to allow a comparison of the different lithotypes, the “*permeability coefficient K*”, which is defined as the volume of water subject to the force of gravity passing through the unit surface of a cross section of an aquifer in the unit of time, under a unit gradient (100%) at 20 °C; K is usually expressed in cm/sec, i.e. it has the dimensions of a velocity.

Borehole n° 1
 Level 238 m a.s.l. – Depth = 50 m

| Depth m. b.g.l. | Lithology | Stratigraphic description | Lithic horizon | Vertical permeability K=cm/s | Ground water | Depth to sliding surface |
|--------------------|-----------|----------------------------------------------------------------------------------------------------|----------------------------------------------------------------------------------------------------------|------------------------------------|-----------------|--------------------------------|
| 1 | | Sandstone and yellowish sand, locally layered | Unit S' 3 Low-medium Pleistocene | | | |
| 2 | | | | | | |
| 3 | | | | | | |
| 4 | | Bluish marly clay becoming marly-silty-sandy clay to the medium-upper part. Intact material | Unit A 3 Lower Pleistocene transgression | Tests not undertaken | Dry Material | Non-Sliding Material |
| 5 | | | | | | |
| 6 | | | | | | |
| 7 | | | | | | |
| 8 | | | | | | |
| 9 | | | | | | |
| 10 | | | | | | |
| 11 | | | | | | |
| 12 | | | | | | |
| 13 | | | | | | |
| 14 | | Marly clay, grey-bluish, layered, interbedded with thin sandy layers | Monte dei Corvi Unit, Pliocene inf. – Succession of intact layers with tectonically originated fractures | | | |
| 15 | | | | | | |
| 16 | | | | | | |
| 17 | | | | | | |
| 18 | | | | | | |
| 19 | | | | | | |
| 20 | | | | | | |
| 21 | | | | | | |
| 22 | | | | | | |
| 23 | | | | | | |
| 24 | | | | | | |
| 25 | | | | | | |
| ↓ | | | | | | |

50 m.

Borehole n° 2
 Level 200 m a.s.l. - Depth = 40 m

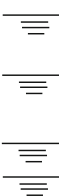
| Depth m. b.g.l. | Lithology | Stratigraphic description | Lithic horizon | Vertical permeability K=cm/s | Ground water | Depth to sliding surface |
|--------------------|-----------|---------------------------------------------------------------------------------------------------------------------|------------------------------------------------------------------|------------------------------------|-----------------|--------------------------------|
| 1 | | Terreno vegetale | Aggregato | | | |
| 2 | | Marly silty-sandy clay, poorly layered, becoming marly clay to sandstone, well layered towards the base | Unit A3 Lower Pleistocene. Undisturbed Normal fault | Tests not undertaken | Dry Material | Non-Sliding Material |
| 3 | | | | | | |
| 4 | | | | | | |
| 5 | | | | | | |
| 6 | | | | | | |
| 7 | | | | | | |
| 8 | | | | | | |
| 9 | | | | | | |
| 10 | | | | | | |
| 11 | | | | | | |
| 12 | | | | | | |
| 13 | | | | | | |
| 14 | | | | | | |
| 15 | | | | | | |
| 16 | | | | | | |
| 17 | | | | | | |
| 18 | | | | | | |
| 19 | | | | | | |
| 20 | | | | | | |
| 21 | | | | | | |
| 22 | | | | | | |
| 23 | | | | | | |
| 24 | | | | | | |
| 25 | | | | | | |
| ↓ | | | | | | |

40 m.

Borehole n° 3
Level 160 m a.s.l. – Depth = 25 m

| Depth m. b.g.l. | Lithology | Stratigraphic description | Lithic horizon | Vertical permeability K=cm/s | Ground water | Depth to sliding surface |
|--------------------|-----------|------------------------------------------------------------------------------------------------|------------------------------------------------------------------------------------------------------------------|------------------------------------|-----------------|--------------------------------------------------------------|
| 1 | | Grey-yellowish altered silty clay, with disordered lenses of sandy silt | Alteration horizon - Soils of Monte dei Corvi Unit- Lower Pliocene Upper part – Lower Pliocene - | Tests not undertaken | Dry Material | Non-Sliding Material Lightly Disturbed between 8m and 10m |
| 2 | | | | | | |
| 3 | | | | | | |
| 4 | | | | | | |
| 5 | | | | | | |
| 6 | | | | | | |
| 7 | | | | | | |
| 8 | | | | | | |
| 9 | | | | | | |
| 10 | | | | | | |
| 11 | | Sequence of grey-bluish clayey-marly layers. Interbedments of thin sandy layers (2-3 cm thick) | Monte dei Corvi Unit – Lower Pliocene - Upper part of the sequence. Intact material with tectonic fissures | Tests not undertaken | Dry Material | Non-Sliding Material Lightly Disturbed between 8m and 10m |
| 12 | | | | | | |
| 13 | | | | | | |
| 14 | | | | | | |
| 15 | | | | | | |
| 16 | | | | | | |
| 17 | | | | | | |
| 18 | | | | | | |
| 19 | | | | | | |
| 20 | | | | | | |
| 21 | | | | | | |
| 22 | | | | | | |
| 23 | | | | | | |
| 24 | | | | | | |
| 25 | | | | | | |

Borehole n° 4
Level 142 m a.s.l. – Depth = 25 m

| Depth m. b.g.l. | Lithology | Stratigraphic description | Lithic horizon | Vertical permeability K=cm/s | Ground water | Depth to sliding surface |
|--------------------|-----------|-----------------------------------------------------------------------------------------------------------------------------------------------------------------------------------------------------------------------------------------------------------------------------|-------------------------------------------------------------------------|------------------------------------|-----------------------------------------------------------------------------------|--------------------------------|
| 1 | | Disturbed Topsoil | Aggregate | | | |
| 2 | | Ochre silty-clayey sand, with marine organogenic shell fragments Altered and chaotic silty clay with silty-sandy interbedments. Very disturbed material Layer of greyish-yellowish silty sand about 1 m thick Greyish-yellowish destructured silty clay | Alteration horizon Chaotic soils from M. dei Corvi Unit Landslide | 6,8 · 10 ⁻⁶ |  | 12 m |
| 3 | | | | | | |
| 4 | | | | | | |
| 5 | | | | | | |
| 6 | | | | | | |
| 7 | | | | | | |
| 8 | | | | | | |
| 9 | | | | | | |
| 10 | | | | | | |
| 11 | | | | | | |
| 12 | | | | | | |
| 13 | | | | | | |
| 14 | | | | | | |
| 15 | | | | | | |
| 16 | | | | | | |
| 17 | | | | | | |
| 18 | | | | | | |
| 19 | | | | | | |
| 20 | | | | | | |
| 21 | | | | | | |
| 22 | | | | | | |
| 23 | | | | | | |
| 24 | | | | | | |
| 25 | | | | | | |



Borehole n° 5
Level 135,6 m a.s.l. – Depth = 40 m

| Depth m. b.g.l. | Lithology | Stratigraphic description | Lithic horizon | Vertical permeability K=cm/s | Ground water | Depth to sliding surface |
|--------------------|-----------|--------------------------------------------------------------------------------|----------------------------------------------------------------------------------------------|------------------------------------|-----------------|--------------------------------|
| 1 | | Disturbed topsoil | Aggregato | | | |
| 2 | | Ochre silty sand with fragments of organogenic limestone | Chaotic soils from M. dei Corvi Unit Alteration horizon Landslide | | | 27 m |
| 3 | | | | | | |
| 4 | | | | | | |
| 5 | | Altered and chaotic silty clay with silty-sandy interbedments. | | | | |
| 6 | | Very disturbed material | | | | |
| 7 | | | | | | |
| 8 | | | | | | |
| 9 | | | | | | |
| 10 | | Silty sand, greyish-yellowish at the base | | | | |
| 11 | | | | | | |
| 12 | | Altered and chaotic silty clay with interbedments of yellowish sand lenses. | | | | |
| 13 | | | | | | |
| 14 | | Very disturbed material | | | | |
| 15 | | | | | | |
| 16 | | | | | | |
| 17 | | | | | | |
| 18 | | Layer of greyish-yellowish silty sand, about 1.30m thick | | | | |
| 19 | | | | | | |
| 20 | | Greyish-yellowish silty clay with rare silty- sandy interbedments | | | | |
| 21 | | | | | | |
| 22 | | | | | | |
| 23 | | | | | | |
| 24 | | Greyish-yellowish marly clay, altered and destructured | | | | |
| 25 | | | | | | |
| 26 | | | | | | |
| 27 | | Greyish-yellowish marly-silty-sandy clay | | $5,2 \cdot 10^{-7}$ | | |
| 28 | | | Monte dei Corvi Unit – Lower Pliocene Sequence of intact layers with tectonic fissures | | | |
| 29 | | | | | | |
| 30 | | | | | | |
| 31 | | | | | | |
| 32 | | Grey-bluish marly clay, well layered, | | | | |
| 33 | | interbedded with thin sandy layers | | | | |
| 34 | | (2-3 cm thick) | | | | |
| 35 | | | | | | |
| 36 | | | | | | |
| 37 | | | | | | |
| 38 | | | | | | |
| 39 | | | | | | |
| 40 | | | | | | |


Borehole n° 6
 Level 88,5 m a.s.l. –Depth = 39 m

| Depth m. b.g.l. | Lithology | Stratigraphic description | Lithic horizon | Vertical permeability K=cm/s | Ground water | Depth to sliding surface | |
|--------------------|-----------|---------------------------------------------------------------------------------------------------------------------------|-------------------------------------------------------------------------------------------------------------|------------------------------------|-----------------|--------------------------------|---------------------|
| 1 | | Remoulded topsoil | Aggregate | | | | |
| 2 | | Grey-yellowish sandy silt with scarce % of clay. | Chaotic material from the Unit of Monte del Corvi Medium-lower part – Lower Pliocene Landslide | | | | |
| 3 | | Yellowish-ochre silty sand, sometimes arenaceous with organogenetic remains. | | | | | |
| 4 | | Yellowish-ochre silty sand mixed with layers and lenses of grey-yellowish clayey silt including calcarenite clasts. | | | | | |
| 5 | | Destructured and chaotic material. | | | | | |
| 6 | | | | | | | |
| 7 | | | | | | | |
| 8 | | Alternation of yellow sands and grey-yellowish sandy silt. | | | | | |
| 9 | | Destructured material, slightly chaotic. | | | | | |
| 10 | | | | | | | |
| 11 | | | | | | | |
| 12 | | | | | | | |
| 13 | | | | | | | |
| 14 | | | | | | | |
| 15 | | | | | | | |
| 16 | | | | | | | |
| 17 | | | | | | | |
| 18 | | | | | | | |
| 19 | | | | | | | |
| 20 | | Destructured yellowish sands-silts. | | | | | $2,7 \cdot 10^{-4}$ |
| 21 | | | | | | | |
| 22 | | Destructured, chaotic silty sandy clay | | | | | $7,3 \cdot 10^{-6}$ |
| 23 | | | | | | | $3,1 \cdot 10^{-7}$ |
| 24 | | | | | | | |
| 25 | | | | | | | |
| 26 | | | | $5,4 \cdot 10^{-8}$ | | | |
| 27 | | | Unit of Monte del Corvi – Lower Pliocene Sequence of intact layers with fractures of tectonic origin | | Dry Material | | |
| 28 | | Rhythmic sequence of marly clays and turbiditic sands. | | | | | |
| 29 | | Each layer has thickness variable between 60 cm e 2 m | | | | | |
| 30 | | | | | | | |
| 31 | | | | | | | |
| 32 | | | | | | | |
| 33 | | | | | | | |
| 34 | | | | | | | |
| 35 | | | | | | | |
| 36 | | | | | | | |
| 37 | | | | | | | |
| 38 | | | | | | | |
| 39 | | | | | | | |


Borehole n° 7
Level 50 m a.s.l. – Depth = 50 m

| Depth m. b.g.l. | Lithology | Stratigraphic description | Lithic horizon | Vertical permeability K=cm/s | Ground water | Depth to sliding surface |
|--------------------|--------------------------------------------------|-------------------------------------------------------------------------------------------------------------------------|------------------------------------------------------------------------------------|------------------------------------|-------------------------------------------------------------------------------------|--------------------------------|
| 1 | | Disturbed topsoil | Aggregato | | | |
| 2 | | Greyish-yellowish sandy silt with scarce clay fraction. | Alteration horizon of the Monte dei Corvi Unit – Lower Pliocene Landslide | |  | |
| 3 | | | | | | |
| 4 | | | | | | |
| 5 | | | | | | |
| 6 | | Light brown silty-clayey sand with fragments of plant material and calcitic concretions. | | | | |
| 7 | | | | | | |
| 8 | | Bioclastites fragments mixed to yellowish silty sand with sandstone fragments. | | 6,5 · 10 ⁻⁶ | | 8,60 m |
| 9 | | | | | | |
| 10 | | | | 3,4 · 10 ⁻⁷ | | |
| 11 | | | | | | |
| 12 | | Ochre organogenic calcarenite. | | | | |
| 13 | | | | | | |
| 14 | | Ochre silty sand. | | | | |
| 15 | | | | | | |
| 16 | | Organogenic calcarenite with abundant bioclastites. | Monte dei Corvi Unit – Lower Pliocene Intact lithic sequence | | | |
| 17 | | | | | | |
| 18 | | Yellowish sandy silt, destructured. | | | | |
| 19 | | | | | | |
| 20 | | | | | | |
| 21 | | | | | | |
| 22 | | Greyish-bluish marly clay interbedded with thin greyish-yellowish sandy layers. Wet and destructured material. | | | | |
| 23 | | | | | | |
| 24 | | | | | | |
| 25 | | | | | | |
| 26 | | Silty-sandy layer with no fabric, chaotic | | | | |
| 27 | | | | | | |
| 28 | | | | | | |
| 29 | | | | | | |
| 30 | | Greyish-yellowish marly clay with lenses of bluish silty sand. Chaotic material, very wet. | | 7,6 · 10 ⁻⁶ | | |
| 31 | | | | | | |
| 32 | | | | | | |
| 33 | | | | | | |
| 34 | | | | | | |
| 35 | | | | | | |
| 36 | | Rhythmic sequence of marly clay and turbiditic sand. Each layer has thickness variable between 60cm and 2m. | Monte dei Corvi Unit Lower Pliocene Lower sequence. | 1,8 · 10 ⁻⁷ |  | 35,3 m |
| 37 | Intact lithic sequence, lightly fractured. | | 4,3 · 10 ⁻⁸ | | | |
| 38 | | | | | | |
| 39 | | | | | | |
| 40 | | | | | | |
| ↓ 50 | | | | | | |

Borehole n° 8
Level 50 m a.s.l. – Depth = 40 m

| Depth m. b.g.l. | Lithology | Stratigraphic description | Lithic horizon | Vertical permeability K=cm/s | Ground water | Depth to sliding surface |
|--------------------|-----------|---------------------------------------------------------------------------------------------------------------------------------------------------------------|-------------------------------------------------------------------------------|------------------------------------|-----------------------------------------------------------------------------------|--------------------------------|
| 1 | | Disturbed topsoil | Aggregate | | | |
| 2 | | Sandy clay with arenaceous stony fragments and calcitic concretions | Alteration horizon of Monte dei Corvi Unit- Lower Pliocene Landslide | 6,5 · 10 ⁻⁶ |  | 8,60 m |
| 3 | | Greysandy silt with scarce greyish-yellowish clay fraction. | | | | |
| 4 | | Destructured grey sand and clay. | | | | |
| 5 | | Greyish-bluish marly clay with interbedments of thin sandy layers. Alternation of plastic clayey layers and chaotic and disturbed thin silty layers. | | | | |
| 6 | | | | | | |
| 7 | | | | | | |
| 8 | | | | | | |
| 9 | | | | 3,4 · 10 ⁻⁷ | | |
| 10 | | | | | | |
| 11 | | | | | | |
| 12 | | | | | | |
| 13 | | | | | | |
| 14 | | A-rhythmic sequence of clayey marly and silty sandy layers (30-60cm thick) | Monte dei Corvi Unit – Lower Pliocene Intact lithic sequence | 3,2 · 10 ⁻⁸ | | |
| 15 | | | | | | |
| 16 | | | | | | |
| 17 | | | | | | |
| 18 | | | | | | |
| 19 | | fissured, | | | | |
| 20 | | firm, | | | | |
| 21 | | dry. | | | | |
| 22 | | | | | | |
| 23 | | | | | | |
| 24 | | | | | | |
| 25 | | | | | | |
| 26 | | | | | | |
| 27 | | | | | | |
| 28 | | | | | | |
| 29 | | | | | | |
| 30 | | | | | | |
| 31 | | | | | | |
| 32 | | | | | | |
| 33 | | | | | | |
| 34 | | | | | | |
| 35 | | | | | | |
| 36 | | | | | | |
| 37 | | | | | | |
| 38 | | | | | | |
| 39 | | | | | | |

Borehole n° 9
Level 20 m a.s.l. – Depth = 31 m

| Depth m. b.g.l. | Lithology | Stratigraphic description | Lithic horizon | Vertical permeability K=cm/s | Ground water | Depth to sliding surface |
|--------------------|-----------|--------------------------------------------------------------------------------------------------------------------------------------------------------------------------------------------------------------------------|--------------------------------------------------------------------------------|------------------------------------|-----------------------------------------------------------------------------------|--------------------------------|
| 1 | | Topsoil and Made Ground | Aggregate | | | |
| 2 | | Clay and marly clay mixed with sand and silt; altered material, chaotic, discontinuous. Arhythmic boulders of sandstone, marl and clay at plastic state with hints of layering come out with depth. | Alteration horizon of Monte dei Corvi Unit - Lower Pliocene Landslide | $7,5 \cdot 10^{-6}$ |  | 7,60 m |
| 3 | | | | | | |
| 4 | | | | | | |
| 5 | | | | | | |
| 6 | | | | | | |
| 7 | | | | | | |
| 8 | | | | | | |
| 9 | | A-rhythmic sequence of clayey marly and silty sandy layers (30-60cm thick) fissured, firm, dry. | Monte dei Corvi Unit - Lower Pliocene Intact lithic sequence | $1,2 \cdot 10^{-7}$ | Dry material | |
| 10 | | | | | | |
| 11 | | | | | | |
| 12 | | | | | | |
| 13 | | | | | | |
| 14 | | | | | | |
| 15 | | | | | | |
| 16 | | | | | | |
| 17 | | | | | | |
| 18 | | | | | | |
| 19 | | | | | | |
| 20 | | | | | | |
| 21 | | | | | | |
| 22 | | | | | | |
| 23 | | | | | | |
| 24 | | | | | | |
| 25 | | | | | | |
| 26 | | | | | | |
| 27 | | | | | | |
| 28 | | | | | | |
| 29 | | | | | | |
| 30 | | | | | | |
| 31 | | | | | | |

7.4.6 Technical Analysis of the Slope

In situ permeability tests were performed during the drilling of the boreholes at the transition between the horizon of alteration and the intact unit made of well-stratified greyish-bluish marly clay (see borehole logs). The aim was to discover the value of K at failure. During the drilling of boreholes S4–S5–S6–S7 it has been observed that the sliding surface had permeability of between the values $K = E \times 10^{-6}$ cm/sec and $K = E \times 10^{-7}$ cm/sec. The latter is the value of the impermeable base where maximum is the hydraulic head along the vertical. It also represents the boundary to percolation waters in the subsoil and the lower boundary for the alteration process of the cohesive mass. Not always, however, the sliding surface is generated at the base of the horizon of alteration. Borehole S8 showed that the shearing surface of landslide mass 1 is at 15.2 m from ground level where the permeability is of about $E \times 10^{-4}$ cm/sec. It could not be otherwise. In fact, there “*the shear deformation in the ground is due to the progressive reduction of the limit state of the soil induced by viscous and softening processes in addition to alteration*” (see paragraph 7.2). In borehole S9 this surface is shallow, 7 m below ground level; this one also is located in altered soil and is induced by the hydraulic head of the submerged marine scarp underneath the railway line. Unlike the sliding section of masses 2 and 3, where the shear deformation is caused by the hydraulic head at the base of the horizon of alteration, in the one next to the coastline the deformation assumes a viscous-plastic character due to oscillations in piezometric level more frequent over time. There a water flow-path is created by the sea hydraulic head and facilitated by the permeability values that are progressively greater towards the coast line. This path is the same that is used by the sliding mass. At the base of mass 1, therefore, the shear resistance was certainly the residual one given that the mass was subjected to the active thrust of the upslope landslide mass No. 2.

Even prior to fail, however, Posatora slope showed deformational geometric conditions that suggested the presence of pre-failure phenomena taking place in the intermediate and upper section of the slope, where the maximum hydraulic head values were found, especially within boreholes S7 and S6. There, the largest thickness of altered soil was observed where also took place all the other deformational phenomena induced by variations in the effective stress as well as to those of creep and softening, which resulted in the reduction of the local stress status of the altered soil.

For a long time (~ 70 years), the marls and sands of Monte dei Corvi (Unit 12 on the Geological-Structural Map, Fig. 7.4) have undergone a degradation process due to meteoric water seeping through the ground undergoing variations in the hydrostatic head in undrained conditions that have induced, within the lithic mass, the rise and decrease of neutral pressures. The clay mass deformed and underwent small movements without having mobilised the downslope soil mass or that this one, in turn, made unstable the one further downslope. On Posatora slope, therefore, plastic swelling deformations took place within soil masses which were compressed at the front and extended orthogonally to the line of maximum steepness (Figs. 7.7 and 7.9). This plastic deformation was supported, to the front, by large sandy banks already intercalated in the turbiditic succession of the Unit of Monte dei Corvi.



Fig. 7.9 Landslide area corresponding to the development of Section S–N. Four main trenches can be identified, with their scarps, parallel to themselves and to the coastline, which are typical of the front of every landslide

In the most elevated part of the same lithic mass, instead, a relaxation occurred, whose effect was of producing a shallow main trench that was exalted at the time of collapse. Initially, the scarps were of 0.50–1 m.

From the point of view of the prediction, therefore, these lithic masses can be detected and mapped individually when they are still in place by means of an accurate morphological analysis. During the failure of the slope they constitute real landslides masses in regressive succession to the upslope. Their dimensions are given by the depth of the sliding surface, which however can also be detected before the disruption via the evaluation in situ of the permeability coefficient K , which indicates that the sliding surface will develop at the depth at which K assumes a value between 10^{-6} and 10^{-7} cm/s, i.e. at the lower boundary of the horizon of alteration.

These factors of morphological modification of the slope are unmistakable elements of an evolutionary state of the ground going towards a failure process that cannot be considered as deep since, as shown, the maximum depth of the sliding surface is 35.3 m below the ground level, with a minimum value to the downslope, in S9, of 7.60 m below ground level. The Great Ancona Landslide of 13th December 1982, therefore, cannot be considered as a deep and therefore unpredictable phenomenon, nor it can ever be in the future developments of this slope. Historical evidence informs us that this landslide is repetitive and of large spatial extension; maybe in further 70 years, when a new layer of altered ground is formed on the slope of Posatora–Torrette, underlying the one still existing, there will be a new Great Ancona Landslide, with a sliding surface at a depth greater than the current one. This is actually part of a natural process of renewal of the slopes that inevitably makes its course in the full respect of the evolutionary processes of the environment.

7.4.7 *Landslide Dynamics*

From a dynamic point of view, the Great Ancona Landslide had an origin and an end over time and, like all the landslides in cohesive soils, developed along a sliding surface whose depth resulted as variable due to the geological-structural conditions and to the hydraulic head applied to the surface itself. Whatever it was the genetic process of this landslide, the latter did not appear isotropically distributed across the slope and was subdivided into four landslide units with different potential kinetic energy, that dissipated along the path in order to get to a new equilibrium state.

To clarify, let us consider a mass of soil at plastic state sliding along a shearing surface. This mass brings within itself both kinetic energy (due to its motion) and potential energy (due to the height of the slope on which it moves). The higher the starting point of this mass, the greater its potential energy. During the sliding, the potential energy decreases as the kinetic rises. If the lithic mass was small and at the same time located at a low starting point on the slope its motion would have been

slow, with low kinetic energy with respect to potential energy. Landslide mass 1, at the base of the slope, thus has a potential energy greater than the kinetic one, and therefore in the distribution of shearing stresses would be the most resistant, enough to withstand the active thrust of landslide mass 2 until the whole system collapses. In fact, the entire slope stays in equilibrium until landslide mass 1 is not at the limit state on its sliding surface. Generally, this limit is reached when the piezometric level is at ground level, i.e. when the entire lithic mass at the base of the slope is saturated. At that point, the soil mass assumes physical meaning as the symbol of autonomous and generalized subsistence.

In this conditions, the deformation dynamics of the whole slope develop through a sequential regressive process, in the sense that upslope landslide units, n. 2 and n. 3, will only be activated once the lithostatic counterthrust of the downslope landslide unit will cease to be applied.

This type of dynamics of landslides are typical of all those cohesive soils that have a high index of porosity, like that of altered and/or destructured soils.

Side by side with the larger instability phenomena across the northern slope of the Ancona area, like the ones associated to the Great Landslide, further minor and shallow instability phenomena take place, which develop in a way different from what just described. The shallow mass movement, most common to the bottom of the slope, is caused by localized episodes of greater water seepage; in some areas flow lines are vertically oriented, with downward flow, but they quickly change direction, to become initially parallel to the slope and then pointing out of the surface. All this happens because of a sensible increase in density and, consequently, of the reduction of the permeability coefficient with depth. This type of behaviour, very often, occurs in a more complex geological context where lithological and structural discontinuities cause an increase in the thickness of the horizon of altered and decompressed material. The thickness of that horizon depends, in particular, on the possibility that the degradation process extends through preferential levels with poorer geotechnical characteristics, connected with structures inherited from the substrate.

Initially, the mass moves with movements of measurable amount, causing the opening of cracks at ground level; then a phase of material expansion takes place and the mass behaviour gradually changes from distension to compression due to increasing shear deformation. Along the entire path in plastic conditions the soil undergoes a progressive differentiation of stresses and deformations. Additional rainfalls induce a further increase in weight (due to imbibition of the soil mass, particularly in the portion subjected to dilation) as well as the development of hydrostatic stresses in cracks and fractures. The slope achieves a state where there is an increase in shear deformation velocity and a phase of pure compression begins, following the previous dilation in which the soil undergoes softening (Fig. 7.10).

At this stage a condition occurs in which the soil loses part of its intrinsic strength on one side and undergoes an increase in pore-water pressure on the other side. As a consequence, slope movement can rapidly change into mudflow, which can occur suddenly and involve discrete soil parts moving at a fluid state. This is the

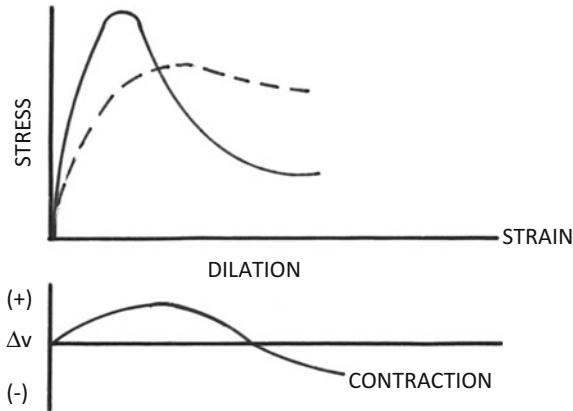


Fig. 7.10 Transition from dilation to contraction

reason for the overturning of the large fortress wall of Forte Scrima, bearing in unstable manner onto underlying buildings.

The morphological situation that emerges after the landslide is that of a mass of soil deposited at the foot of the cavity.

7.5 Conclusions

The Great Ancona Landslide has a cyclical behaviour, as it manifests itself over time with the same modes and with the same shapes as in the past. What has changed, is the dimensions of the sliding mass, which in a destabilization process of the slope result to be poor thing if compared to the timescale. This means that the northern slope of the Posatora hill will be affected again by processes of hydrogeological instability. Unfortunately, when this will happen is unknown. Anthropoc communities generally face the problem of hydrogeological instability only after tragic disasters hit some places. Problems arise when risk factors interact with those of urban expansion. Posatora slope, from this point of view, was well-known as being at risk; why was it urbanized? It is very ingenuous, perhaps pretestuous, to say that the Barducci–Montagnolo landslide, so complex and repetitive at the same time, may exist simply by fortuity.

If it is true that the date of the next mass movement cannot be determined, is it possible to imagine of getting forecasts for the prediction and the prevention of future events? In order to follow this guidance, it was certainly necessary to analyse with systematic caution, the physical and chemical aspects of the current mass movement in the context of a simpler analytical process aimed to the evaluation of the true causes influencing the destabilization of the slope, as it is.

In summary, what characterizes the triggering of landslides in altered silty-clayey soils is:

1. the destabilising action of cohesive soils is given by the oscillation of piezometric level, which at failure reaches its maximum with groundwater at ground level;
2. landslides in cohesive soils can be identified on the slope because of their shape, dimensions and succession even before of their movement at failure;
3. the pre-failure deformation in cohesive soils develops at the depth where the permeability coefficient K achieves a value of between 10^{-6} and 10^{-7} cm/s;
4. the maximum depth of the horizon of alteration is the same of water percolation, where permeability has a value of $K = E \times 10^{-7}$ cm/s. It identifies with the depth of the shearing surface;
5. the permeability coefficient K is the only parameter that determines the depth of the shearing surface;
6. the relation K -depth is not a linear function;
7. the mechanics of landslide in cohesive soils is influenced by the passive resistance produced by the landslide immediately downslope;
8. the pre-failure deformation in cohesive soils at the toe of the slope is of elastic-viscous-plastic type;
9. the deformation of a slope in cohesive soils is always of regressive-sequential type.

References

- Ambrosetti, P., Centamóre, E., Deiana, G., Dramis, F., & Pieruccini, U. (1981). *Schema di evoluzione neotettonica dell'area umbro-marchigiana tra il Tronto ed il Metauro. Convegno geodinamica, Udine, Rend. Soc. Geol. It.*
- Bertini, T., Cugusi, F., D'Elia, B., & Rossi-Doria, M. (1986). *Lenti movimenti di versante nell'Abruzzo Adriatico: caratteri e criteri di stabilizzazione* (Vol. 1, pp. 91–100). Atti del 16° Convegno Italiano di Geotecnica, Bologna.
- Bjerrum, L. (1967). *Progressive failure in slopes of overconsolidated plastic clays. International Journal of Soil mechanics Engineering Division, ASCE*, 1–49.
- Bromhead, E. N. (1986). *The stability of slopes*. Glasgow: Blachie & Son Ltd.
- Cancelli, A., & Pellegrini, M. (1987). Deep-seated gravitational deformations in the Northern Apennines, Italy. In *Proceedings of 5th International Conference and Field Workshop on Landslides, Christchurch* (pp. 171–178).
- Carlioni, G. C., & Ceretti, A. (1967). *Cenni geologici dei dintorni di Ancona*. Com. Neog. Medit. Comm. Strat. IV Congr. Guida alle escursioni, 136–145, Bologna.
- Cello, G., & Coppola, L. (1979). *Elementi neotettonici dell'area anconetana*. Foglio 118 (Ancona pp.). C.N.R. Urog. Final Geodinamica. Sotto- prog. Neotettonica.
- Colalongo, M. L., Cremonini, G., Fabbri, P., & Ricci, Lucchi F. (1975). Studio sediment ologico-bio- stratigrafico di alcune sezioni pleistoceniche nei dintorni di Offagna (Ancona). *Geologica Romana*, 14, 125–140.
- Colalongo, M. L., Manni, T., & Ricci, Lucchi F. (1979). Sedimentazione ciclica nel Pliocene anconetano. *Geologica Romana*, 8, 71–92.

- Console, R., Peronaci, F., & Sonaglia, A. (1973). Relazione sui fenomeni sismici dell'anconetano (1972). *Annali di Geof.*, 26.
- Crescenti, U., Coppola, L., & Tommassoni, D. (1974). Sul Mio-pliocene di Ancona: note stratigrafiche. *Boll. Serv. Geol. d'Italia*, n. 95.
- Di Maio, C. (1996a). Exposure of bentonite to salt solution: osmotic and mechanical effects. *Géotechnique*, 695–707.
- Di Maio, C. (1996b). *The influence of pure fluid composition on the residual shear strength of some natural clayey soils*. In VII International Symposium on Landslides, Trondheim (Vol. 2, pp. 1189–1194).
- Eigenbrod, K. D., Graham, J., & Burak, J. P. (1992). Influence of cycling porewater pressures and principal stress ratios on drained deformations in clay. *Canadian Geotechnical Journal*, 326–333.
- Fancelli, R., & Radrizzani, S. (1964). *Foglio 118 Ancona*. Note III. Carta Geologica d'Italia, 42, Roma.
- Fenelli, G. B., & Picarelli, L. (1990). The pore pressure field built up in a rapidly eroded soil mass. *Canadian Geotechnical Journal*, XXVII(3), 387–392.
- Fenelli, G. B., & Picarelli, L., & Silvestri, F. (1992). *Deformation process of a hill shaken by the Irpinia earthquake in 1980*. Atti del Conv. Italo-Francese «Stabilità dei Pendii in Zona Sismica», Bordighera.
- Gasparini, C., Ianaccone, G., & Scarpa, R. (1980). On the focal mechanism of Italian earthquakes. *Rock Mechanics*, 9, 85–91.
- Gasparini, C., & Praturlon, A. (1981). *Modelli sismo-tettonici e geologia classica a confronto nell'Italia centrale*. Relazione presentata al convegno annuale del progetto finalizzato geodinamica (Udine, 12–14 maggio 1981).
- Giese, P., Morelli, C., Nicolich, R., & Scarascia, S. (1979). *Crustal structure of the Italian Peninsula*. Pubbl. Ist. Geof. Min. Università di Trieste.
- Gillet, S. (1969). La faune messinienne des environs d'Ancona. *Giorn. Geol. s.*, 2(3), 69–100.
- Handin, J. (1969). Oil the Coulomb-Mohr failure criterion. *Journal of Geophysical Research*, 74, 5343–5348.
- Hoek, E., & Brown, C. T. (1980). Empirical strength criterion for rock masses. *Journal of Engineering Division, ASCE*, 1013–1035.
- Lambe, T. W., & Marr, W. A. (1979). *Stress path method* (2nd ed., pp. 724–738). JGED, ASCE.
- Lefebvre, G. (1987). *Slope instability and valley formation in Canadian soft clay deposits*. *Canadian Geotechnical Journal*, XXIV(3), 261–270.
- Leroueil, S., Vaunat, J., Picarelli, L., Locat, J., Lee, H. J., & Faure, R. (1996). *Geotechnical characterization of slope movements* (Vol. 1, pp. 53–74). In International Symposium on Landslides, Trondheim.
- Matheson, D., & Thomson, S. (1973). Geological implications of valley rebound. *Canadian Journal Earth Sciences*, X, 961–978.
- Mogi, K. (1974). On the pressure dependence of strength of rocks and the Coulomb fracture criterion. *Tectonophysics*, 21, 273–285.
- Moruzzi, G., & Follador, V. (1973). Il Miocene superiore ed il Pliocene inferiore della zona dello scoglio del Trave (tra Ancona ed il Monte Conero) e loro inquadramento geologico regionale. *Geol. Romana*, 12, 129–149.
- Pasek, J. (1974). Gravitational block-type slope movements. In *Proceedings of 2nd International Congress on I AEG, Sao Paulo*, V-PC-1 (Vol. II).
- Picarelli, L. (1991). *Resistenza e meccanismi di rottura nei pendii naturali* (Vol. II, pp. II-7/II-61). Convegno su “Deformazioni in prossimità della rottura e resistenza dei terreni naturali e delle rocce”, Ravello.
- Picarelli, L. (1993). *Structure and properties of clay shales involved in earthflows*. In Atti dell' International Symposium on The Geotechnical Engineering of Hard Soils-Soft Rocks, Atene (Vol. 3, pp. 2009–2019).
- Picarelli, L. (1999). *Alcune considerazioni sui meccanismi di innesco e di propagazione delle colate in terreni sciolti e detritici*. Convegno su Previsione e Prevenzione di Movimenti Franosi Rapidi, Trento (pp. 163–179).

- Picarelli, L., Di maio, C., Olivares, L., & Urcioli, G. (1998). Properties and behaviour of tectonized clay shales of Southern Apennines. In International Symposium on the Geotechnics of Hard Soils—Soft Rocks, Napoli (Vol. 3). (in corso di stampa).
- Picarelli, L., Di Maio, C., Olivares, L., & Urciuoli, G. (1998). *Properties and behaviour of tectonized clay shales of Southern Apennines*. In International Symposium on the Geotechnics of Hard Soils—Soft Rocks, Napoli (Vol. 3).
- Picarelli, L., Russo, C., & Mandolini, A. (1999). *Long-term movements of an earthflow in tectonized clay shales*. In Atti dell' International Symposium on Slope Stability Engineering: Geotechnical and Geoenvironmental Aspects, Matsuyama, Japan (Vol. 2, pp. 1151–1158).
- Picarelli, L., Russo, C., & Urciuoli, G. (1995). *Modelling earthflows based on experiences*. In Atti dell'11^{ma} European Conference on Soil Mechanics and Foundation Engineering, Copenhagen (Vol. 6, pp. 157–162).
- Riedel, W. (1929). *Zur mechanic geologischer bruchercheinungen*. Centralbl. f. Mineral Geol. u. Pal. (pp. 354–368).
- Russo, C. (1997). *Caratteri evolutivi dei movimenti traslativi e loro interpretazione meccanica attraverso l'analisi numerica. Tesi di Dottorato, Università di Napoli Federico II*.
- Selli, R. (1967). *Cenni sul Neogene dell'avanfossa marchigiana*. U.I.S.G. Comm. Strat. Comit. Neogene Medit., IV Congr. Guida alle escursioni, 126–135, Bologna 1967.
- Taylor, D. W. (1948). *Fundamentals of soil mechanics*. New York: Wiley.
- Terzaghi, K., & Peck, R. B. (1967). *Soil mechanics in engineering practice* (2nd ed.). New York: Wiley. (The first edition was published in 1948).
- Vaughan, P. R. (1994). Assumption, prediction and reality in geotechnical engineering. *Geotechnique*, 571–609.
- Vaunat, J., Leroueil, S., & Tavenas, F. (1992). *Hazard and risk analysis of slope stability*. In Canadian Symposium on Géotechnique and Natural Hazards, Vancouver (Vol. 1, pp. 397–404).
- Wood, D. M., Jendele, L., Chan, A. H. C., & Cooper, M. R. (1995). *Slope failure by pore pressure recharge: numerical analysis*. In Atti della 11^{ma} European Conference on Soil Mechanics and Foundation Engineering, Copenhagen (Vol. 6, pp. 1–8).
- Yoshida, N. (1990). *Time-dependent instability in fissured overconsolidated clays and mustones* (PhD Thesis, University of Alberta, Edmonton).

Chapter 8

The Prediction and Prevention of Landslides

8.1 Introduction

The prediction and prevention of landslides starts from the assumption: *the need for monitoring the soil Why?*

The answer to this question requires the introduction of a postulate able to provide Geological and Environmental Scientists with an objective basis for the evaluation of the developing physical processes.

It was previously written (Chap. 6) that “the timely identification of soil deformation at failure in areas subjected to high hydrogeological risk has, as fundamental assumption, the definition of the distinctive characteristic of the type of disruption that could develop within the slope”. For this purpose, site recognition for the definition of the method of identification of an area subjected to hydrogeological risk in predominantly cohesive soils, widely supported from the examples reported in Chap. 6, is based upon the traditional geomorphological and structural survey of the slopes through the subjective perception of the observer; therefore, the evaluation of the hydrogeological risk for a certain area is function of the experience of the latter and cannot be considered, epistemologically, as an aspect of scientific knowledge to be applied to a principle of quantum mechanics applied to the study of landslides. In fact, if considering a second observer studying the same slope, he could consider the same identical morphological and structural superficial effects as the results of a wave function within a quantum system of interactions. However, also in this case, the second observer develops a subjective cognitive process, even if based on an interpretation of quantum physics, that considers the wave function as the product of the most fundamental set theory, which combines *logics*, expression of the mind, to *shape*, expression of the matter. Actually, to gain scientific validity, the two postulates should be supported by the use of instruments that allow to overtake the theoretical view of soil behaviour, especially at depth, and use the experience in situ as a direct and objective proof, summarising in themselves all the variables not defined within the unsatisfactory *modelling*, which is

hardly able to define the linearity of the function of a physical phenomenon during the time. In fact, quantum mechanics is not valid when conscious beings, such as the two observers, are part of the system. In other words, quoting Odifreddi (2008), “the collapse of the wave function is a subjective phenomenon determined by the action of consciousness”. This position is made explicit by Eugene Wigner, Nobel Prize for Physics in 1963, who stated in “Symmetries and Reflections” that mathematical concepts in applications of physics do not always achieve reasonable efficiency, rather, very often, are reductive with respect to the multitude of phenomena ruling the reality. These evaluative difficulties are clearly expressed in Fig. 6.5, sketched by Prof. Luciano Picarelli, full professor at Seconda Università di Napoli, who operates in the sector of Geotechnical Engineering, where it can be observed that the mechanics of the failure of natural slopes is strongly influenced by pre-failure deformational phenomena “of which often there is no knowledge”.

In that figure, it is theorised the progressive reduction with time of the factor of safety of slopes “subjected to cyclic oscillations of the regime of pore-water pressures and to phenomena of strength decay due to softening”. The Author himself confirms that the diagram is qualitative and puts into evidence “the relationship existing among precursors of failure, such as the ones inducing a contraction of the limit state surface of the soil, and triggering factors, in this case linked to the oscillation of pore-water pressures”. From the same figure, moreover, further information can be derived on the difficulty to assign a value to a certain physical quantity:

1. Fig. 6.5 is not the representation of quantum calculations on the sum of all the elements contributing to failure;
2. the wave function is not limited by minimum and maximum numerical values of the real oscillations of rainfalls;
3. the failure of the rock mass takes place only when the wave function becomes linear;
4. the time needed for the identification of the phase of failure of the slope is variable from soil to soil and within the same soil as well.

The analytical procedure for achieving the prediction of landslides in cohesive soils, therefore, must be devoted to in situ testing in a manner equivalent to the physical processes under development by means of the long-term instrumental monitoring of the areas at risk.

8.2 Control of the Areas at Hydrogeological Risk

In cohesive soils, the triggering of landslides is mainly induced by water seepage, that produces changes in the effective stresses within the soil. A horizontal thrust (σ_{ho}) is generated at the base of the piezometric column which is greater than the

strength of the saturated soil (see Sect. 6.4.3). In that area, develop pre-failure deformations extending progressively with time until the failure of the slope is achieved. Such deformations are therefore prodromal of a landslide and are fundamental for setting up a predictive model related to its development. Therefore, the first question to ask is: “Does a landslide destroy or preserve the information acquired from the slope prior to failure?”. The answer to this question requires the introduction of the assessment of the interaction among the particles constituting the mass of the slope within the predictive analysis of hydrogeological instability of the slope itself.

It is already understood that all the interactions developing in the soil among soil and electrostatic forces, magnetic fields, attractive gravitational force, friction and adhesion forces, stress fields of local tectonic, chemical reactions, atomic decay nuclear processes, etc., are the demonstration of three fundamental types of interaction that can lead the slope to failure. In fact, all the chemical interactions taking place among soil particles are expression of the *electromagnetic interaction*; the hydraulic head leading the slope to pre-failure, is the effect of *gravitational interaction*; *frictional and adhesive interactions*, instead, are responsible of the links among protons and neutrons in the creation of stable cores within the soil mass. No atomic cores and no atoms constituting clay platelets could exist without them. Such interactions are extremely different among them and are not inter-dependant, not even follow the reversibility law ruling the events of quantum mechanics. They, however, are essential for the evolutionary modification of a slope. In fact, during its movement, the soil mass transports both kinetic energy (because of its motion) and both potential energy (because of the height of the slope along which it is moving): the greater the slope height, the greater its potential energy. During sliding, the potential energy reduces, whereas kinetic energy increases, involving in the movement all the three interaction factors within a process of accelerated expansion of the mass. What remains observable is solely the shape of the sliding surface, characterised by a depth reducing to the downslope and becoming zero at the intersection with the plain. It is because of the shape of the sliding surface that, nowadays, are developed the interpretative processes of quantum mechanics for setting up mathematical models for the back-analysis.

In the earlier chapters, considerable emphasis was given to the *time* as key physical factor for approaching the prediction and prevention of the landslides on natural slopes.

In order to understand what is the time in the current application, it is needed to relate to the concept of space-time, expressed by the Einstein’s equation (1917), where it is assimilated to the *gravitational field*.

$$R_{ab} - 1/2 R g_{ab} + \lambda g_{ab} = 8\pi G T_{ab}$$

where

R_{ab} Riemann’s curvature
 $R_{ab} e R g_{ab}$ represent the curvature in the space-time

| | |
|------------------|-----------------------------------|
| T_{ab} | energy of matter |
| G | Newton's gravity force (constant) |
| λg_{ab} | cosmological constant |

The space-time is proportional to the energy of the matter.

In effects, Einstein's equations take into account that quantum mechanics is at the base of atomic physics, which is the physics of elementary particles, while in the macroscopic world the interactions among the masses are ruled by the laws of general relativity. But quantum mechanics and general relativity are not coherent laws among themselves; notwithstanding this, they belong to the finite world, i.e. the natural one. Space-time is a real object in the physic field bending under the weight of matter and which flows from the quantum gravitational field. In the finite world, therefore, like on Earth, all the natural phenomena defining the development of the environment are not made from fields and particles, but from the same identical type of object, that is the quantum field. Einstein's vision implies that in nature there are no longer particles moving across the space during the course of time, but quantum fields where the elementary interactions develop in the space-time. Natural phenomena, therefore, result to be determined by four essential dimensional components and not from just three. From this, "the world of existing things is reduced to the world of possible interactions. The reality itself is reduced to interaction" (Rovelli 2014).

Velocity is the property of the motion of an object with respect to another one. This notion was extended by Einstein also to time. Relativity, therefore, has the maximum extension within quantum mechanics by grouping in itself all the natural processes concerning the Environment.

It is only in correlations that is possible to obtain the measure of time; and, in fact, the failure velocity of a natural slope is valued with respect to the speed of Earth. The genesis of a landslide can only be described if it is related to other physical systems; such as, for example, neutral stress (u). Quantum mechanics, therefore, do not describe objects (extension fractures, fissures, etc.) but describe events that are interactions among processes (e.g. pre-failure deformation) and, in that case, it cannot be avoided to evaluate the space-time factor for deriving a prediction of landslides.

The *method of global limit equilibrium* (Terzaghi 1943; Taylor 1948), surely better known in Geotechnics, is a method that responds to statistic laws able to define the moment of failure but does not describe what happens to a physical system during its development; it describes what happens to the *limit equilibrium*, i.e. in an infinitesimal fraction of time. But what does it mean? It means that the reality of a system that does not interact cannot be described from an evolutionary point of view. How can, thus, be developed the knowledge of a four-variables physical system? The interpretation by means of quantum mechanics is not suitable for the evaluation of a multi-variables physical field such as the Natural Environment, even if is undeniable its empirical success in defining the structure of the world, quantum fields, light and all the contents of the Universe.

Site researches noticed that any physical-environmental phenomenon is ruled by the time factor, therefore the analysis for the prediction and prevention of a landslide must be carried out not as a rationalization of the hypothetical properties of a physical event but as the result of experiments in situ obtained by the complementarity among measuring devices.

8.3 Notes on the State of the Art

At present, there are no reliable methods for predicting and preventing a landslide in a predetermined area, but rather it is trusted on mathematical models implemented by specific software whose reliability is rather lacking. The above modelling concerns the **Limit Equilibrium Method** that is based on differential mathematical equations trying to approximate the behaviour of the soils under investigation. It is evident, however, that such modelling, further to being extremely complex, is not very precise, as a multitude of factors are known only approximately.

First of all, the mechanical behaviour of the soil is compared to the one of a perfect plastic body and it is assumed that in the conditions of sliding the stress state is constant and independent from deformation and time. This approximation introduces into the calculation a series of non-negligible evaluation errors.

Furthermore, in the former methodology, it is not possible to know the depth of the failure surface, which is of utmost importance to set a predictive calculation on an eventual mass movement. In fact, without obtaining indications on the deformation state of the soil prior to collapsing, no modelling is possible with the purpose of the prediction of a mass movement if not after its occurrence. Even those methods of survey and investigation such as GPS, LASER, RADAR, etc., that contribute precisely to delineating surface movements and effects at the ground level, do not provide sufficient information on the causes of the landslide within the slope and on the factors influencing the triggering, which are at present often uncertain, questionable and certainly lately foreseeable.

It is not generally considered what are the mechanical processes leading to the failure of the slope, what are their implications on the failure itself and hence on the factor of safety; however, predominantly clayey soils are subjected to variations in the regime of pore-water pressures, due to oscillations of shallow groundwater, which significantly affect the frictional resistance; nor are expected pre-failure deformations as signals of an incipient instability of the slope.

Ultimately, with the use of current calculation methods, all these uncertainty factors are approximated with complex and unclear parameters for which the final outcome for landslide prediction is of scarce use.

8.4 Identification of Areas Subjected to Hydrogeological Risk

Before proceeding with analytical assessments for the prediction of landslides, it is logical and necessary to identify the areas at hydrogeological risk.

It was read in Chaps. 6 and 7 that *pre-failure phenomena are those that define the initial state of deformation at failure and develop in that part of the soils where the coefficient of permeability K tends to $E \times 10^{-7}$ cm/s and in rather prolonged periods, depending on the oscillations of the piezometric surface. Parameter E is a decimal number and therefore, apart from it, the triggering occurs where K has orders of magnitude ranging between 10^{-6} and 10^{-7} . In these areas, the piezometric pressure is maximum (Figs. 6.19 and 6.20—Chap. 6) and is the cause for the development of pre-failure processes along a band, dx , indicative of the area where the sliding surface develops at the time of slope failure.*

The sliding surface of a landslide always occurs along the same path as the previous pre-failure deformations, independently from the time passed between the two deformational manifestations.

Movements are due to sliding effects that are concentrated along extension surfaces or surfaces under tension. The latter develop into a variable time span, sometimes in many decades, especially for multiple landslides that are conditioned by a long process of soil alteration and by the creep and softening phenomena that characterize the landslides to the downslope. The knowledge of such kinematic aspect is fundamental for the implementation of analytical procedures for the prediction of mass movements. In fact, the pre-failure deformational effect is the one taking place at the initial stage of each hydrogeological slope instability process and is always located upslope of the area at risk, where σ_1 , induced by the hydraulic head, obtains a high value along band δx (Figs. 7.1 and 7.2).

Eigenbrod et al. (1992) carried out specific laboratory investigations on the behaviour of lightly overconsolidated, medium-plasticity clays subject to cyclical oscillations of **back pressure**, thus simulating fluctuations in the interstitial water pressure regime. They observed that the effects induced are similar to those due to creep caused by increases in deviatoric stress and consist in the accumulation of irreversible deformations depending on the number of cycles or time. In principle, therefore, the piezometric level excursions produce deformations and displacements of the soil, especially when considering the additional effect of time on the mechanical decay of the soil. **The pre-failure deformation, therefore, represents one of the most important predictors of landslides as it contributes to the definition of the incipient shearing zone in the ground under propagation even before the collapse.** Therefore, the analytical procedure for identifying the area subjected to hydrogeological risk in cohesive soils must first be directed to the detection of the effects at the surface of such pre-failure deformation in the soil. For the composite landslides (Sect. 7.3), it has been shown that the individual landslides are already visible on the slope even before their activation; “*this is due to the fact that, because of meteoric precipitations, the altered soil layer (which is the*

mass under deformation) was subjected in the short-term to load increase in undrained conditions and deforms slowly, differentiating itself into several potential units of landslides in succession on the slope without being mobilized (stress path—Fig. 6.16). The cohesive mass, in fact, implements different behaviours depending on the granulometric percentages of the aggregates, on the alteration state and on the soakage conditions, however it compresses to the front due to the behaviour imposed by the downslope part, whose swelling contributes to produce a convex surface profile, gibbous-like, of low-acclivity, while to the upslope part relaxation is obtained with consequent depression of the slope due to a mass tensile process. These morphological aspects of a slope are indicative of the process of development of the pre-failure band in the ground, to the depth at which K is between 10^{-6} and 10^{-7} cm/s. In that zone, the modification of the pore-water pressure regime in the soil, which influences considerably the deformation up to failure, must be monitored and, with it, the ground movements.

With regards to monotypic landslides (Sect. 7.2), the morphological examination is simpler. These landslides usually occur on low acclivity slopes, with slope angles $\alpha = 18^{\circ}$ – 25° , and are more common in overconsolidated cohesive soil, slightly fractured by local tectonics. Typically, they are small landslides, but can present large width phenomena, with discontinuous deformations. The depth to the sliding surface is always at the base of the alteration layer and is strictly dependent on the permeability coefficient K , which can reach the value of 10^{-7} cm/s already at depths of 6–13 m (Fig. 7.1). Surface effects, induced by the pre-failure mechanism, are typical of an undulated slope in a generalized manner, with swelling more evident to the upslope and less to the downslope. There, in fact, swelling is due to viscous-plastic movements of the superficial altered layer when this one is saturated (Fig. 7.9).

8.5 Analytical Procedure for Achieving the Prediction of Landslides in Cohesive Soils

Real-time monitoring of an area already identified at hydrogeological risk provides, in addition to the immediate knowledge of what is happening on a slope, the possibility to implement incoming information into decision-making processes using analytical models and territorial databases. The rapidity of analysis, joined with the results of instrumental monitoring, can allow for short and medium-term forecasts that, especially for hydrogeological protection, can mitigate the risk of vulnerable areas.

The prediction of the hydrogeological disruption of a slope can then be obtained through long-term *instrumental monitoring* of areas at risk. The advantage of this monitoring is to overcome a certain theoretical view of soil behaviour and to use in situ experience as a direct proof that sums up all the variables not defined by mathematical process.

Following to the identification of the hydrogeologically hazardous area, it is necessary to define the geological and geotechnical survey plan for underground exploration and the installation of monitoring equipment. The number of boreholes and their distribution will be dictated by the monitoring logic and by the extension of the risk area. The depth of each survey, on the other hand, is a function of the permeability coefficient K since the boreholes does not necessarily need to reach extreme depths for the search of a possible shearing surface, but it is sufficient that the drilling reaches the depth where $K = 10^{-7}$ cm/s and to stop a few meters underneath. As it is known, in fact, the extreme depth limit for the pre-failure deformation, where the sliding surface develops, is equal to the depth where $K = 10^{-7}$ cm/s. In order to identify this limit during the drilling, it is necessary the undertaking of in hole “Slug Tests”.

Slug tests have become one of the most commonly used methods for a quick estimate of the main hydrogeological parameters of aquifers, including first of all hydraulic conductivity. In particular, the rapidity and ease of execution of these hydrodynamic tests are of primary importance to meet the requirements of modern methods for assessing aquifers vulnerability and pollution risk. A slug test consists in causing an instantaneous variation of the piezometric level, in a borehole of “not large” diameter (e.g. in a piezometer) and to measure the time necessary for the subsequent restoration of initial conditions; this can be achieved in a number of ways, but the simplest is the introduction (or extraction) of a known volume of water or of a cylindrical solid in the borehole.

For the same volume of “slug” water used for the test, the recovery rate of the original level will be directly correlated to the hydraulic conductivity of the aquifer tested.

The test can be carried out either by increasing or decreasing the head, i.e. by first adding and then, once the original water level has been restored, by extracting from the test piezometer the volume of water which caused the original loss in level.

The success of the test depends onto the care used in the operative choices regarding the correct data acquisition technique and the achievement of a significant variation in the water level in the piezometer; the latter will depend on the volume of the solid slug, the borehole diameter and the permeability of the aquifer subject to the test (Fig. 8.1).

The benefits of using slug tests are numerous.

Slug tests affect the entire filtered length and therefore involve levels at different permeability within the same aquifer, providing different K values due to the more or less marked heterogeneity and anisotropy of the aquifer as a whole; therefore, the hydraulic conductivity of both aquifers and aquitards can be determined.

Hydraulic conductivity measurements are carried out in situ and this avoids errors that can occur in laboratory tests, when carried out on remoulded soil samples; it is not necessary to extract water from the aquifer and this is particularly important in case of contaminated groundwater.

Tests are quick and cheap, because no pumping and observation wells are needed.

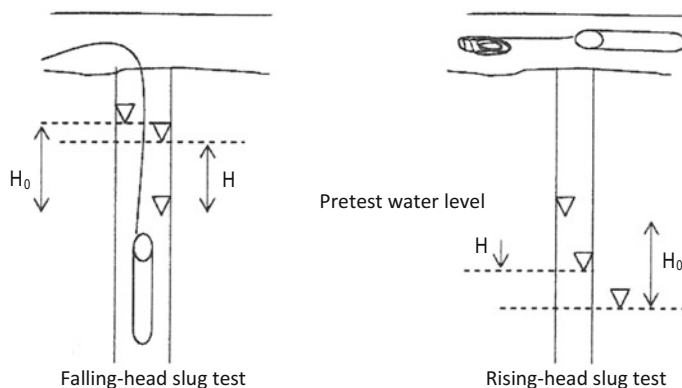


Fig. 8.1 Geometry of Slug-Tests. *Legend* H_0 : water head between the initial water level pre-testing and the highest level reached immediately after the insertion of the slug. H : water head between the initial level and the level reached at a period t after the insertion of the slug

The detection of the pre-failure δx band (Figs. 7.1 and 7.2) is therefore indicative of the area where it will develop the sliding surface for the slope failure. In that zone, multi-parametric columns will be inserted, in order to control the development of deformations indicative of the pre-shearing stage and thus allow for corrective action in useful time. The columns are continuous 2D/3D monitoring columns composed of a set of rigid modules, implementing suitable sensors, connected by special joints with 2–3 degrees of freedom, able to record whatever ground deformation, even if millimetric, while maintaining the azimuthal direction (Fig. 8.2).

The use of this instrumentation, named *DMS (Differential Monitoring of Stability)*, allows to obtain a complete view of ground deformations, both for the mechanical aspects of horizontal and vertical deformations as well as for pore-water pressures and groundwater conditions. Each DMS 3D column is able to perform continuous and contextual monitoring of inclinometers piezometers, temperature, assestimeters and acceleration within the same borehole, allowing for the needed correlation to geotechnical parameters (Figs. 8.3, 8.4 and 8.5). The system provides accurate and reliable measurement of inclinometric data as well as of micro-displacements for the assessment of the activation of a system dedicated to the undertaking of interventions of civil protection and rehabilitation.

The system is already covered by Italian and European industrial patents, dated 09.11.2007, and therefore well known to the State of the Art. However, the continuous monitoring system certainly does not satisfy the question of the acquisition of information regarding the interaction between the electromagnetic forces of cohesive soil particles and groundwater or that of the interaction between these forces and the quantum gravity of planet Earth before the collapse of a slope.

The continuous and contextual detection of inclinometric, piezometric, temperature, assestimetric and acceleration data in the same borehole, however,

DMS 3D (Patents)**Fig. 8.2** 3D continuous monitoring columns

provides a fairly simple approach to the theory of prediction and prevention of hydrogeological disruption in cohesive soils, because otherwise it would be necessary to carry out precise calculations that are impossible to be done. In fact, in the environmental sector, the ability of prediction is affected by the number and complexity of the interactions among soil particles, by stress fields, and by the presence of water. This complexity often keeps a large part of the Scientific Community particularly anchored to preconceived solutions such as accepting a theory only if it is supported by mathematical calculations. In this context, however, the models merely present a description that is only superficial of reality and force the designer to use retaining structures with the function of resisting to the thrust of lithic masses under motion; nor are valid calculations devoted to the search for

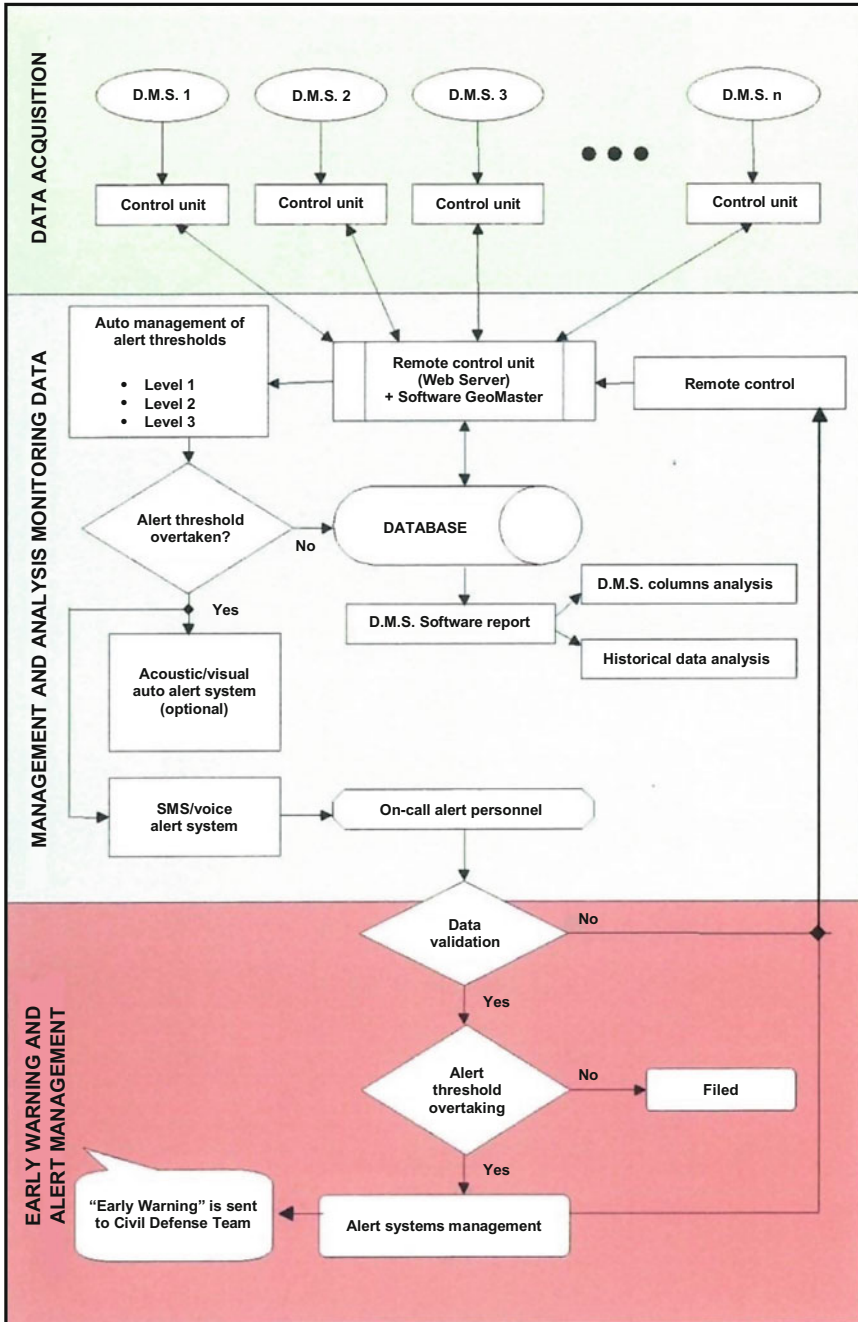


Fig. 8.3 Early warning management by means of DMS columns



Fig. 8.4 DMS system equipped with automatic acoustic/visual alerting devices

coefficients that can be directly applied to shearing resistance parameters. Such an approach equals to ignore that a landslide is a living body which explicates, with its motion, a power able to overcome whatever value of induced passive resistance. It is, therefore, also a very empirical way of searching for reliable parameters for the safety of natural slopes, because the analytical process inevitably does not take into account the various sources of uncertainty, neither the designer can realize that the safety margins adopted are effectively comparable to the uncertainties resulting from the adoption of certain geotechnical parameters (Taylor 1948). From the point of view of safety and environmental respect, it is preferable to attribute to the clayey soils elements of stimulus to ensure that the slope naturally consolidates itself before the “fetus” of the landslide develops into it. In gynaecological terms, this would mean inducing an abortion.

In the view of predicting and preventing hydrogeological disruption, therefore, the analysis cannot be carried out by means of a mathematical calculation model, but must be performed on site, by assessing the objective hydrogeological risk elements of a natural slope.

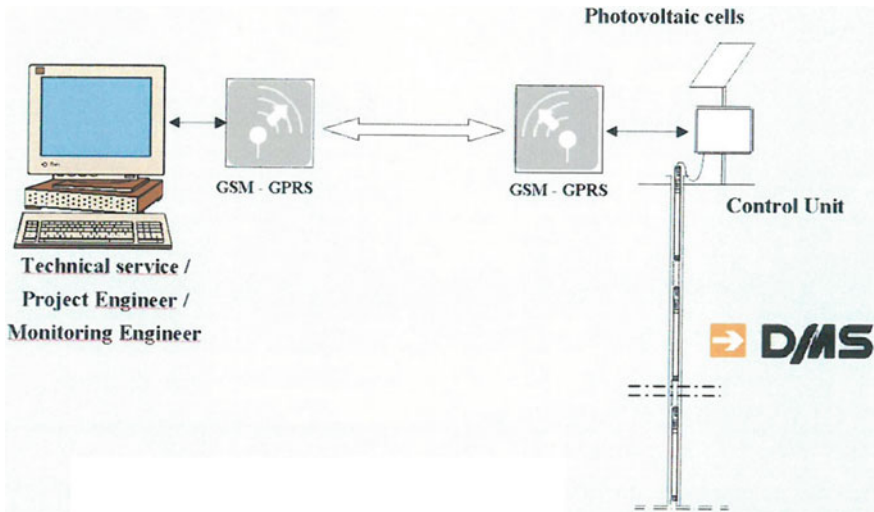


Fig. 8.5 DMS system in remote control

The DMS system was presented at the 6th International Conference on Field Measurements in Geomechanics (FMGM), held in Oslo (Norway) on 15th–18th September 2003. The proceedings of the conference were published in the volume “Field Measurements in Geomechanics”, Frank Myzvoll publisher, Balkema publishing house, in the “Measurement Technology” and “Case Histories” sections. It is worth to point out that a DMS monitoring station is neither a theory, nor a model, it is simply an effect detector.

Through the properties of its sensors, digitally managed, it controls ground kinematics and monitors the geostatic behaviour in relation to the different stresses induced by groundwater. In other words, the 2D/3D DMS inclinometric and piezometric columns for continuous monitoring introduced into the soil to the depth where $K = 10^{-7}$ cm/s, provide data on the development of the pre-failure that foregoes of years the landslide in relation to the hydraulic head of groundwater. For the purpose of predicting and preventing the hydrogeological instability the values of these two parameters, i.e. displacements in millimetres and piezometric head, are the ones that better represent the substantial change in the effective stresses field. In this way, it is possible monitoring in continuous ground movements that are indicative of the initial state of a future failure of the slope. Known the failure load, it is therefore easy to act with appropriate drainages that keep the piezometric level well below the value recorded by the device at the time of failure. This results in a reduction of the hydraulic head (σ_1) so that the influence of the confining pressure (σ_3) on the brittle deformation is very low, unable to induce the collapse.

This non-invasive system allows the soils to consolidate themselves over time in full respect of the surrounding natural environment, thus exerting an action able to protect urbanized slopes.

This book ends here but not before reminding that the study of the physics of natural systems and of the development of the environment has not yet become history. Regarding to that, there is still a lot of Science to be developed that certainly cannot be confined to the sole study of the surface or of the ground using DMS columns. However, when the interacting bodies are more than three the problem becomes mathematically unsolvable and the models useless. At the moment, any attempt to solve the problem of slope stability in terms of quanta continues to be very far to be achieved.

It should also be reminded that a landslide is life and that it is part of a natural process for the development and conservation of the Environment. Among the numerous strategies for the prevention and defence from hydrogeological disasters, long-term instrumental monitoring and real-time data processing are the most effective and qualifying elements of the new methodology for the preservation and conservation of building, archaeological, historical, architectural, monumental and superstructural heritage as well as for the protection of human life. However, such operational possibilities require a relevant clarification of the use of the Device for the Prediction and Prevention of landslides in cohesive soils. *The achievement of the prediction of plastic-rotational landslides cannot and must not be used indiscriminately, neither extended to all the areas of a region subjected to hydrogeological risk.* Such a procedure would inevitably lead to prejudice the local environment of the region itself. Areas free from the presence of man-made goods but subjected to hydrogeological disruption should not be reclaimed even if this can affect the agricultural productivity.

The processes and events giving life to inorganic matter are neither casual nor, even less, accidental. A mutation in them often leads to a change in the overall structure of the organism that owns them in its genome. Almost always, this change is deleterious and has no future. In fact, the debris moving along a slope are ultimately carried by the waters washing away in a riverbed and then deposited in the sea for beaches nourishment. The debris themselves are the ones forming alluvial deposits, such as coastal or foothill plains, which are generally fertile for the development of agriculture. The deposition of river terraces often constitutes large water tanks; the study of river terraces allows the reconstruction of ancient morphological situations determined by the action of watercourses and also to trace their dynamics back over time.

References

- Eigenbrod K. D., Graham J. E., & Burak J. P. (1992). Influence of cycling porewater pressures and principal stress ratios on drained deformations in clay. *Canadian Geotechnical Journal*, 326–333.
- Einstein A. (1916). Die Grundlage der allgemeinen Relativitätstheorie. *Annals*, 10, 15, 28, 29, 31, 35, 53, 61–76, 79–83, 85, 89–92–95, 98–101, 103, 105, 106.
- Odifreddi, P. (2008). *Il Vangelo secondo la Scienza*. Torino: Einaudi Editore.
- Picarelli, L. (2000). *Meccanismi di deformazione e rottura dei pendii*. Hevelius Edizioni, Benevento (Italy): Argomenti di Ingegneria Geotecnica.

- Rovelli, C. (2014). *La realtà non è come ci appare*. Milano: Raffaello Cortina Editore.
- Skempton A. W. (1948). *The $\phi = 0$ analysis of stability and its theoretical basis*. In *2nd ICSM* Rotterdam.
- Taylor D. W. (1948). *Fundamentals of soil mechanics*. Wiley.
- Terzaghi, K. (1943). *Theoretical soil mechanics*. N.Y.: Wiley.
- Wigner E. P. (1967). *Symmetries and reflections*, Indiana University Press, Bloomington, London.

Index

A

Absorbed water, 21
Active thrust coefficient, 39
Adriatic Foreland, 91
Aerial photographs, 59
Alluvial clays, 8
Alteration, 5, 7, 68, 148, 154, 167, 169–171, 192–195, 198, 202, 203, 216, 221, 226, 228, 230, 231, 234, 238, 240–242, 252, 254, 257, 266, 267
Alteration process, 22, 252
Alumina, 5, 7
Amphiboles, 7
Analytical models, 267
Angle of shearing resistance, 34
Anions, 7, 19, 20
Anisotropy, 31, 92, 177, 179, 187, 197, 201, 268
Anthropic activities, 28
Anti-dip slope, 74, 75, 84
Apennines, 66, 71, 77, 86, 91, 139, 171, 180, 199, 215, 223
Applied geology, 101
Aquifer, 30, 242, 268
Argentina, 172, 203
Atomic physics, 2644
Attractive forces, 19, 23
Axial compression, 91

B

Basal space, 5, 9, 11, 14, 19
Basento, 71, 73–75, 77, 78, 80, 83–88, 141, 146
Basin, 8, 29, 68, 74, 75, 80, 87, 140, 149, 153–155, 157, 159, 162, 195, 197, 203, 204

Behaviour, 27, 28, 34, 42, 43, 47, 52, 54–56, 69, 91, 92, 94, 98, 100, 101, 109, 110, 129, 132–134, 139, 162, 171, 174, 175, 177, 179, 187, 198, 203, 218, 220, 225, 226, 229, 240, 242, 255, 256, 261, 265–267
Bentonite, 9
Biotite, 14
Boundary, 28, 31, 32, 39, 65, 78, 91, 141, 169, 195, 204, 215, 225–227, 232, 252, 254
Bradanic Foredeep, 80, 140, 204
Brittle deformation, 42, 95, 98, 273
Brucite, 14, 16
Building heritage, 29

C

Calabrian, 74, 76, 80, 140, 204
Calcite, 8, 101, 102, 109, 116
Calilegua Formation, 163, 164, 166, 167, 170
Capillarity, 25, 34
¹⁴C carbon, 60
Carbonates, 6, 8, 158
Cation, 10, 11, 14, 19–22
Chalk, 8
Chifente, 149, 151, 153, 155–157, 159, 162
Chlorides, 7
Chlorite, 14, 16, 17, 155–157
Chronological units, 64
Civil engineering, 101
Clay, 5–9, 14, 16, 18, 19, 21–25, 29, 31, 32, 64, 80, 84, 94, 140, 147, 155, 161, 162, 164, 168, 171, 172, 192, 193, 198, 208, 212, 219, 221, 227, 238, 240, 252, 263
Clay activity, 25
Climatic oscillations, 60
Climatic variations, 60
Clinographic correlations, 159, 161

- Coefficient of permeability, 30, 170, 171, 191, 220, 230, 231, 242, 266
 Coefficient of thrust at rest, 33–36, 168
 Comarca de Aquas Negras Calilegua, 163
 Composite landslides, 221, 225, 226, 229, 231, 266
 Compression test, 42, 50, 172, 173, 176, 178
 Compressive strength, 45, 54
 Conjugated planes, 102
 Consolidation, 28, 68, 87, 88, 118, 147, 169, 197, 198, 203
 Consolidation stress, 28, 36
 Coulomb's equation, 55
 Cracks, 28, 35, 44, 45, 64, 65, 75, 77, 80, 84, 86, 92, 95, 100, 103, 107–109, 115, 141, 169, 214, 218, 220, 221, 226, 227, 255
 Crystal, 5, 9, 14, 16, 19
 Crystalline lattice, 9
 Crystalline structure, 7, 18
 Crystallisation, 25, 107, 109
 Crystallised fibres, 107
 Cultural heritage, 145, 148
 Curve of Dupuit, 196
- D**
- Darcy's Law, 30, 195, 242
 Dating, 59–61, 64–67, 76, 184, 187
 Deconstruction, 91
 Deep hydromorphism, 193
 Deformability, 55, 94
 Deformation, 28, 30, 34, 35, 37, 50, 54–56, 61, 66, 80, 91, 94, 97, 98, 100, 105–107, 111, 117, 118, 121, 131, 132, 139, 141, 150, 151, 167, 171, 173–176, 179, 180, 186, 187, 195, 198, 199, 207, 213–216, 219, 221, 223, 225–227, 229, 231, 252, 255, 257, 261, 263–269
 Deformation at failure, 118, 171, 225
 Dendritic pattern, 164
 Deposition, 34, 60, 65, 69, 70, 76, 84–88, 155, 185, 204, 237, 274
 Deviatoric stresses, 150, 218
 Diaclases, 100, 101, 106, 109, 113
 Dilatancy, 116
 Disarticulation, 143
 Discontinuities, 56, 64, 65, 75, 76, 91, 94, 95, 101, 105, 106, 108, 110, 111, 113–115, 134, 180, 184, 187, 192, 197, 225, 236, 255
 Dispersion, 94, 157
 Domains, 19, 53, 175
 Double layer, 19
- E**
- Earthquakes, 60, 88, 237
 Effective cohesion, 32, 50, 55, 132
 Effective stress, 29, 30, 32, 215, 218, 227
 Einstein, 264
 Elastic-brittle, 42
 Elastic domain, 42
 Elastic-plastic, 42, 198
 Electric dipoles, 23
 Electric environment, 23, 24
 Electrostatic forces, 192, 263
 Elementary particles, 264
 Elongation, 104, 106, 107, 111, 131, 173
En echelon, 102
 Entropy, 5
 Erosion, 25, 27, 28, 65, 68–70, 78, 80, 84, 86, 87, 132, 146, 148, 150, 151, 154, 159, 162, 164, 169, 180, 197–200
 Erosional action, 28
 Erosional scarps, 28
 Erosive effect, 85, 148
 Erosive process, 87, 159
 Evolutionary processes, 60, 80, 86, 254
 Extensional cracks, 77, 95, 221
 Extension cracks, 77, 95, 97
 Extension fractures, 66, 100, 102, 107, 108, 197, 264
- F**
- Fabric, 8, 9, 18, 23, 60, 78, 162, 191, 193, 197
 Failure, 32, 35, 37, 42, 43, 45–48, 50, 51, 53–55, 60, 64, 71, 86, 91, 94–98, 102, 107, 111, 113–115, 126, 128, 130, 132–134, 140, 145, 169, 171, 172, 174–180, 187, 193, 195, 199, 203, 211, 213, 214, 220, 221, 225, 227, 228, 230–232, 237, 238, 254, 257, 262–265, 273
 Failure surface, 32, 95, 102, 114, 126, 128–130, 169, 172, 265
 Fault, 28, 80, 83, 84, 86, 98, 100, 102, 104–106, 109, 111, 114, 116, 118, 120, 126, 128, 148, 234, 236
 Fauna, 61
 Feldspars, 6
Fentes, 77, 100, 107, 108
 Fibrous structure, 107, 116
 Fissured, 56, 92, 94, 228
 Fissures, 94, 228, 264
 Flocculated, 19, 23, 24
 Flora, 61
 Flow, 23, 29–31, 68, 69, 76, 84, 87, 100, 158, 164, 171, 180, 193, 196, 197, 199, 200, 203, 212, 216, 218, 229, 230, 232

Flow lines, 197, 201, 216, 218, 226, 255
 Flow net technique, 200
 Fluorides, 7
 Fluorosilicates, 7
 Foreland, 80, 91
 Fracturing, 64, 92, 94, 98, 105, 106, 111, 116,
 132, 159, 171, 187, 226, 236, 237, 240
 Free energy, 5
 Friction angle, 29, 34, 50, 53, 55, 111, 114,
 134, 229

G

General relativity, 264
 Geological survey, 94
 Geomorphological survey, 94, 184
 Gibbsite, 9, 11, 14
 Glacial clays, 8
 Glaciations, 60
 GPS, 27, 265
 Grain size distribution, 8, 85, 155, 157, 159,
 161
 Grassano, 71, 74, 75, 78, 83–88, 184
 Great Ancona Landslide, 223, 231, 254, 256
 Ground deformation, 139, 269
 Groundwater level, 34, 35, 145
 Gypsum, 6

H

Halloysite, 9, 10
 Heritage, 29, 145, 148, 274
 Historical evidences, 59
 Holocene, 59, 86, 87
 Honeycomb, 23
 Hydration, 7, 11, 19
 Hydraulic gradient, 28, 31, 147, 195, 242
 Hydraulic head, 30, 191, 195, 213, 216, 220,
 221, 226, 230, 231, 242, 252, 254, 263,
 266, 273
 Hydrogeological disruption, 21, 60, 64, 65, 70,
 140, 141, 163, 180, 181, 233, 238, 240,
 241, 267, 270, 272, 274
 Hydrogeological hazard, 64, 71
 Hydrogeological instability, 5, 27–29, 78, 88,
 91, 93, 118, 139, 145, 159, 165, 170,
 184, 193, 203, 210, 219, 225, 230, 256,
 263, 273
 Hydrographic network, 27, 65, 67, 76, 80, 84,
 85, 87, 164, 238
 Hydrographic system, 28, 84
 Hydromicas, 11, 14, 19
 Hydromorphic horizon, 193
 Hydromorphism, 192, 193, 195, 221
 Hysteresis, 19

I

Illite, 6, 8, 14, 18, 155, 156, 162
 Illitic clay, 23
 Impermeability, 192
 Initial conditions, 91, 268
 In-situ tests, 94
 Instability, 5, 28, 29, 75, 78, 91, 93, 95, 118,
 134, 139, 145, 159, 168, 170, 171, 184,
 187, 193, 195, 198, 203, 219, 225, 226,
 230, 231, 241, 255, 256, 263, 266
 Instrumental monitoring, 213, 215, 227, 262,
 267, 274
 Interaction, 5, 18, 19, 21, 31, 197, 240, 261,
 263, 264, 269
 Inter-basal spaces, 5
 Interbedments, 60, 74, 78, 163, 204
 Inter-layer, 19, 20
 Interstitial fluid, 31, 177
 Intra-crystal swelling, 19
 Ionic sheets, 5
 Ions, 5, 7, 11, 13, 14, 16, 18, 19, 23
 Isopach, 98
 Isopach folds, 100
 Isotropic, 23, 55, 92, 105, 111, 119, 120, 197,
 200, 221

J

Jaky, 34
 Joints, 56, 100, 101, 106, 109, 117, 199, 203,
 269
 Jujuy, 64, 203

K

Kaolinite, 6–11, 19, 20, 155, 156
 Kinematic interpretation, 94
 Kinetic energy, 254, 255, 263

L

Laboratory testing, 92
 Lacustrine clays, 8, 24
 Lagoon clays, 8
 Lamellae, 5, 6, 10, 14
 Landslide, 27–29, 31, 56, 59–61, 63–66, 68,
 70, 71, 75, 76, 78, 80, 84–88, 91, 92,
 118, 134, 139, 140, 142, 145–148, 163,
 168, 170–172, 174, 179, 180, 183–188,
 191, 193, 195, 197, 203, 212–215,
 225–227, 229–233, 235, 240, 241,
 252–255, 257, 261–267, 272–274
 LASER, 27, 265
 Limit Equilibrium Method, 132, 134, 145, 265
 Limit state surface, 262

- Lithostatic, 32, 54, 106, 120, 170, 176, 203, 212, 214, 215, 220, 221, 225–227, 231, 255
- Lithostratigraphic, 59
- Lower Clayey Member, 204, 205
- M**
- Macrostructure, 94
- Maps, 59, 64
- Marbling, 192, 194
- Marine clays, 8, 23
- Marine oscillations, 60
- Mass movements, 87, 94, 132, 148, 154, 168, 170, 208, 211, 240, 266
- Mechanical behaviour, 27, 55, 56, 92, 101, 134, 242, 265
- Mechanical properties, 22, 28, 91, 97, 218
- Mechanism of interaction, 28
- Mesostructure, 132, 134, 150
- Metamorphic actions, 25
- Metamorphic phenomena, 25
- Mica, 6, 7, 14, 17, 19, 106
- Mica-schist, 25
- Micro-fault, 107
- Mineralogic characteristics, 5
- Miocene, 91
- Molecular arrangement, 7
- Molecular ratio, 7, 11
- Monitoring, 92, 94, 134, 145, 200, 213, 216, 219, 242, 268–270
- Monoaxial compression, 95, 96
- Monoclinical, 70, 74, 84, 154
- Monotype landslides, 226, 230
- Montmorillonite, 6, 7, 11, 12, 19
- Morpho-evolutionary process, 146
- Morphology, 65, 76, 78, 101, 103, 107, 111, 148
- Multi-parametric columns, 215, 269
- Muscovite, 13, 14, 16
- Mylonitised, 118
- N**
- Natufian, 61
- Natural environment, 59, 264, 273
- Natural slopes, 21, 28, 55, 60, 187, 192, 197, 200, 223, 226, 262, 263, 272
- Neogenic Basin of Siena, 140
- Neolithic, 61
- Neotectonics, 27
- Neutral pressure, 28, 30, 31, 87, 118, 132, 150, 169, 171, 179, 186, 197, 200, 201, 203, 204, 213, 218, 229, 252
- Neutral stress, 31, 32, 218, 264
- Normal faults, 102, 104, 128
- Normally consolidated soils, 34
- Normal stress, 32, 47, 50, 52, 53, 168, 220
- Noutronites, 11
- O**
- Oedometric test, 36
- Organogenic, 8, 204
- Orogenetic arrangement, 91, 170
- Outcrop, 74, 106, 114, 162, 199, 226
- Overconsolidated, 25, 36, 88, 92, 132, 140, 198, 203, 218, 266, 267
- Overconsolidation, 25
- Overconsolidation ratio, 25
- Overpressures, 151
- P**
- Palaeolithic, 61
- Passive thrust coefficient, 39
- Pelitic facies, 74
- Permeability, 30, 64, 86, 151, 169–171, 191, 192, 195, 197, 199–201, 203, 216, 221, 225, 228, 230, 252, 254, 267, 268
- Phyllosilicate, 5, 7, 18
- Piezometric head, 28, 231, 242, 273
- Piezometric level, 31, 145, 168, 198, 203, 214, 215, 227, 252, 255, 266, 268, 273
- Piezometric monitoring, 145, 213, 215
- Piezometric surface, 31, 141, 167, 169, 171, 186, 193, 196, 225, 242, 266
- Planar surfaces, 113
- Plastic deformation, 42, 100, 107, 174, 179, 214, 252
- Plasticity, 18, 34, 36, 198, 228, 240, 241, 266
- Platelets, 5, 7, 18, 22, 23, 192, 193, 221, 263
- Plate loading tests, 94
- Pleistocene, 59, 60, 74, 154, 180, 198, 236
- Pliocene, 67, 151, 153, 154, 234
- Plio-Pleistocenic, 77, 215
- Pollinic zones, 60
- Pore-water pressure, 29, 35, 54, 139, 145, 169, 171, 195, 201, 212, 215, 225, 229, 255, 262, 267, 269
- Porosity, 117, 118, 191, 193, 201, 228, 255
- Porous medium, 31
- Potential energy, 28, 31, 195, 229, 254, 255, 263
- Precipitation, 20, 28, 132, 145, 163, 212, 231, 266
- Precursors of failure, 262
- Prediction, 27, 56, 60, 66, 91, 118, 219, 256, 261, 262, 264–266, 270, 274
- Pre-existing landslides, 66, 78, 174, 186, 187, 203
- Pre-failure phase, 141

- Prevention, 27, 56, 66, 91, 118, 256, 261, 263, 270, 274
- Principal stress, 37, 53, 220
- Principle of effective stresses, 28, 30, 55
- Progressive failure, 134, 214, 223, 229, 231
- Pyrite, 6
- Pyroclastic deposits, 163
- Pyroxenes, 7
- Q**
- Quantum gravitational field, 264
- Quantum mechanics, 261–264
- Quartzite, 6
- Quasi-crystals, 19
- Quaternary subdivisions, 65
- Quebrada de Humahuaca, 163
- Quick method, 131
- R**
- Radar, 27, 265
- Radial cracks, 141
- Radioactive, 60
- Rainfall, 28, 67, 68, 86, 141, 145, 146, 159, 167, 211, 215, 222, 232, 240, 255, 262
- Real-time monitoring, 267, 274
- Recent landslides, 139, 172, 174
- Red Flysch, 140–142, 203
- Regoliths, 80
- Regressive erosion, 146, 148, 164
- Residual shear strength, 51
- Resistance, 30, 47, 56, 94, 97, 158, 159, 172, 215, 218, 225, 230, 240, 252, 265, 272
- Reverse fault, 102, 104, 105
- River terrace, 60, 64, 68, 76, 274
- Rock salt, 6
- Rotational-plastic deformation, 139
- Rotational sliding, 141, 154
- Roughness, 97, 108–110, 114, 116, 161
- Runoff, 20, 148, 158, 159, 161, 162, 207
- S**
- San Lorenzo, 163
- Saponites, 11
- Saturation, 31, 32, 34, 36, 80, 141, 169, 192, 193, 195, 215, 242
- Scanning Electron Microscope (SEM), 9
- Scanning electron microscope, 6
- Scarps, 28, 64, 65, 76, 141, 188, 253, 254
- Secondary extensional cracks, 95
- Sediment, 8, 22–24, 61, 80, 99, 154, 155, 159, 162, 204
- Sedimentary basin, 8
- Sedimentary cycles, 59
- Sedimentary environment, 22
- Sedimentation process, 77, 87, 197
- Seepage, 28, 30, 31, 66, 147, 168, 180, 191, 200, 203, 211, 215, 226, 228, 240, 242, 262
- Seepage motion, 28, 60, 147, 215
- Seismic activity, 80, 86, 141
- Sequential movement, 140
- Serrania Calilegua, 163, 170
- Shaley clays, 25
- Shearing, 32, 88, 97, 98, 108, 109, 114, 118, 134, 141, 170, 171, 191, 213, 219, 220, 225, 227, 229, 231, 254, 257, 268, 272
- Shear resistance, 30, 97, 230, 252
- Shear strain, 32, 172, 187, 218, 221, 231
- Shear stress, 32, 46, 47, 50, 51, 105, 108, 220
- Shear surface, 65, 97, 121, 186–188
- Shortening faults, 117
- Side valleys, 148, 149
- Silica, 5, 7, 9, 11
- Silicate, 7, 9
- Sliding plane, 51, 173
- Slope, 5, 27, 28, 31, 59–61, 65, 66, 68–70, 74–78, 80, 84–88, 91, 95, 118, 132, 134, 139, 141, 145, 147, 148, 154, 159, 162, 165, 171, 172, 180, 184–188, 191, 193, 195, 197, 198, 200, 203, 204, 207, 212–214, 216, 221–223, 226, 229, 231, 233, 237, 238, 240, 252, 254, 256, 261–263, 265, 267, 269, 272, 274
- Slug tests, 268
- Smectite, 9, 11, 155–158, 162
- Softening, 43, 188, 198, 211, 223, 228, 231, 252, 262, 266
- Soil matrix, 92
- Soil stiffness, 219
- Soil strength, 132, 134, 229
- Soil-water retention curves, 19
- Solid skeleton, 22–24
- Square mesh flow nets, 201
- Stability, 29, 69, 94, 132, 134, 145, 147, 151, 197, 200, 236, 269
- Stability of slopes, 94, 200
- Steepness, 76, 85, 146, 231, 238, 241, 252
- Stepped fault, 116
- Stepped surfaces, 113
- Strength, 21, 29, 38, 39, 44, 45, 50, 52, 109, 132, 134, 159, 171, 174, 187, 193, 198, 220, 228, 262
- Stress-strain curve, 42, 174, 176, 177
- Striations, 80, 102, 104, 116, 118, 120, 126, 128, 129, 131
- Strike-slip fault, 80, 83, 84, 102–104, 207
- Structural survey, 261
- Stylolitic, 117, 131

- Subtropical, 163
 Suction, 19, 191
 Sulphides, 7
 Surface hydromorphism, 192, 203
 Swelling, 10, 14, 19, 25, 148, 162, 171, 198, 231, 252
 Swelling potential, 14, 150
- T**
 Tectonic, 25, 34, 42, 64, 65, 69, 77, 78, 83–85, 98, 100, 108, 113, 118, 126, 148, 164, 177, 179, 180, 187, 203, 236, 238, 263
 Tectonic actions, 25, 98
 Tensile strength, 45, 54
 Tensile stresses, 35, 95, 109, 211
 Tensile tests, 42, 54, 133, 175
 Tension crack, 44, 64, 95, 108, 218
 Terrace, 10, 60, 65, 76–78, 80, 85, 86, 88, 171, 185
 Territorial databases, 267
 Thrust tectonics, 91
 Time factor, 42, 60, 69, 132, 169, 264, 265
 Time history, 94
 Total stress, 29, 30, 132, 169, 227
 Transpressive, 126, 128
 Transtensive, 126, 128
 Transverse ridges, 64, 141
 Triaxial compression, 45, 47, 97, 173, 220, 231
 Triaxial stress, 45, 95, 131
 Triaxial tests, 111
- Triggering, 27, 64, 71, 86, 139, 159, 179, 197, 212, 215, 225, 231, 257, 265, 266
 Triggering factors, 225, 262
- U**
 Unconfined compressive test, 45
 Undrained behaviour, 94
 Undrained cohesion, 32, 132, 134
 Undrained conditions, 31, 32, 50, 171, 204, 215, 231, 267
 Upper Clayey Member, 204
- V**
 Valle Grande, 163, 166
 Varicoloured Clay, 140, 203
 Vermiculite, 13, 14
 Viscous deformation, 151
 Viscous elastic properties, 28
 Viscous-plastic movements, 168, 169, 267
 Voids index, 31, 34, 226
- W**
 Würm, 60, 66, 78, 83, 85–88, 172, 183
- X**
 X-ray diffractometry, 5, 158
- Z**
 Zeolitic water, 18, 198